NORTHWESTERN UNIVERSITY

Inverse Analysis of a Supported Excavation through Chicago Glacial Clays

A DISSERTATION

SUBMITTED TO THE GRADUATE SCHOOL

IN PARTIAL FULFILLMENT OF THE REQUIREMENTS

for the degree

DOCTOR OF PHILOSOPHY

Field of Civil Engineering

By

Michele Calvello

EVANSTON, ILLINOIS

December 2002

Volume I

ABSTRACT

Inverse Analysis of a Supported Excavation through Chicago Glacial Clays

Michele Calvello

In inverse modeling, a model is calibrated by iteratively changing the estimates of its input parameters until the value of an objective function, which quantifies the errors between observed data and computed results, is minimized. The major advantage of an inverse analysis approach is the automatic and objective calculation of the parameter values that produce the best fit between observations and computed results. In this work model calibration is conducted using the optimization algorithm UCODE to update the design predictions of a supported excavation in soft clays using monitoring data collected during construction.

Results of triaxial compression tests on Chicago clay specimens are initially used to calibrate, by inverse analysis, four soil models: the Duncan-Chang, Modified Cam-Clay, Anisotropic Modified Cam-Clay and Hardening-Soil models. Parametric studies conducted for the MCC model on a number of regression variables show that the variables to which results are more "sensitive" are: (i) number and type of triaxial tests used as observations, (ii) number of input parameters estimated simultaneously and (iii) weighting of observations.

A numerical procedure that improves the state-of-the-practice of controlling ground movements associated with supported excavations is presented. The methodology, developed and tested using data from a 39 ft deep excavation through Chicago glacial clays, shows that: (i) inverse analysis based on field monitoring data can be effectively used to update the predicted performance of the supported excavation system, and (ii) successful recalibration of the model at an early construction stage positively affects subsequent "predictions" of the soil behavior. Results of a number of studies, conducted to evaluate the effect of modeling assumptions on the inverse analysis of the supported excavation, indicate that the three main characteristics of a "well-posed" inverse analysis problem are: effective numerical modeling, acceptable parameterization and appropriate choice of observations.

ACKNOWLEDGMENTS

First and foremost, I would like to thank Professor Richard J. Finno, my advisor, for his guidance and support throughout this research. I also want to acknowledge Professors Charles H. Dowding and Raymond J. Krizek, members of my dissertation committee, for their valuable suggestions and comments.

Then, I want to acknowledge everybody I know with a collective and comprehensive THANK YOU. In Italian it would sound like: "GRAZIE A TUTTI!" By being a friend of mine during these years, whether you were distant or close, whether I was discussing about my work with you or not, you helped me "grow". Every discussion, every advise, every experience, every moment with you has been valuable. Without you, I would not be who I am and I would not be where I am. Therefore, I sincerely thank you.

Finally, I want to thank three people who, above all others, helped me in this effort: my Mother, my Father and my brother Heriberto. Without their encouragement and (distant but) continuous support I would not have been able to complete this work.

TABLE OF CONTENTS

LIST OF FIGURES

LIST OF TABLES

CHAPTER 1

1 INTRODUCTION

Almost all engineers would agree that engineering judgment, the non-quantifiable knowledge used for designing and/or analyzing an engineering system, is indispensable to the successful practice of engineering. In geotechnical engineering, the role of judgment has become even more important over the past decades as a result of theoretical developments in soil mechanics and growing availability of more powerful and less expensive computers. Finite element (FE) methods are now used for analyzing a variety of geotechnical engineering problems. However, to effectively use FE methods for the analysis of a geotechnical problem, an engineer must recognize the assumptions and approximations involved in any numerical analysis and be aware of the uncertainties associated with the computed results. The reliability of the numerical predictions depends on these uncertainties. Engineering judgment alone cannot quantify the "amount of uncertainty" of a FE analysis.

In FE methods, soil behavior is represented by constitutive models. Various constitutive models have been developed that capture many of the important features of the real soil

behavior. The response of a model to geotechnical "actions" (i.e. loads, prescribed displacements, excavation) is defined by the characteristics of the model and the values of its input parameters. Significant challenges are involved in estimating a model's input parameters. Generally, soil models are calibrated using trial-and-error methods and the "accuracy" of the fit between the experimental data and the numerically computed results is rarely quantitatively evaluated. Inverse models rarely are used for this purpose.

In inverse modeling, a model is calibrated by iteratively changing the estimates of the model input parameters until the value of an objective function, which quantifies the match between observed and computed results, is minimized. The major advantage of an inverse analysis is the automatic and objective calculation of the parameter values that produce the best fit between measured data (often called observations) and computed results. The main difficulties are related to the complexity of most numerical models, which sometimes cause problems of non-uniqueness and instability of the solution or insensitivity of the results to changes in the values of the parameters.

This work evaluates the use of inverse analysis techniques for different geotechnical engineering tasks. In particular, inverse modeling is herein used to (i) calibrate soil models from results of laboratory experiments, and (ii) update the design predictions of a supported excavation system using monitoring data collected during construction.

Chapter 2 discusses the advantages and limitations of inverse analysis as a tool for geotechnical engineers dealing with problems involving the calibration of numerical

models, and presents the optimization algorithm UCODE (Poeter and Hill 1998), a computer code designed to allow inverse modeling posed as a parameter estimation problem.

In Chapter 3 the Modified Cam-Clay soil model is calibrated from results of triaxial laboratory tests using UCODE, which minimizes the errors between the experimental data and the numerically computed stress-strain response. A series of parametric studies is conducted to evaluate the effect of a number of "regression variables" on the optimization results.

In Chapter 4 the results of triaxial tests conducted on four layers of compressible Chicago glacial clays (locally known as the Upper Blodgett, Lower Blodgett, Deerfield and Park Ridge layers) are used to calibrate, by inverse analysis, four different soil models: the Duncan-Chang model, the Modified Cam-Clay model, the Anisotropic Modified Cam-Clay model, and the Hardening-Soil model.

Chapter 5 presents a numerical procedure that uses construction monitoring data to effectively update design predictions of deformations for supported excavation systems. The inverse analysis methodology is developed and tested using field performance data from a 39 ft deep excavation through Chicago glacial clays (Finno et al. 2002). The procedure is used to optimize the plane-strain finite element model of the supported excavation. Five clay layers, modeled using the Hardening-Soil model, are "recalibrated" using inclinometer data that measured, at different construction stages, lateral movements

of the soil behind the supporting walls on both sides of the excavation. The estimates of the H-S parameters that best fit the triaxial test data presented in Chapter 4 are used as starting point of the analysis.

Chapter 6 deals with the "modeling assumptions" used to set up the inverse analysis of the supported excavation described in Chapter 5. A number of studies is presented that evaluates the effect on the results of: (i) the soil model used and the parameterization of the inverse problem, (ii) the stress history of the soil at the excavation site, and (iii) the observations used in the regression. Results of the various simulations are compared with the results of the analysis discussed in Chapter 5.

Chapter 7 summarizes the thesis and presents its conclusions.

CHAPTER 2

2 INVERSE ANALYSIS

2.1 INTRODUCTION

In the last few years the use of finite element (FE) modeling to analyze and solve practical geotechnical engineering problems has increased steadily. Enhancements in computer performances, affordable prices for powerful hardware solutions and increasing availability of technical software have made it easier to perform complex numerical analyses with relatively little effort. Finite element methods, when properly used, can produce realistic results, very useful to the analysis of practical geotechnical problems. To perform useful numerical analyses, however, an engineer must have a good understanding of both soil mechanics and finite element theory. It is important to recognize the assumptions and approximations involved in FE analyses, to be aware of the uncertainties related to the estimation of the input parameters, and to wisely exercise the engineering judgment necessary for the interpretation of the numerical results.

Unfortunately many engineers who carry out numerical analyses are not fully aware of the potential restrictions and drawbacks associated with inappropriate use of the numerical results. Thus, the reliability of finite element predictions can vary greatly. Furthermore, formal uncertainties analyses of the numerical results rarely are conducted.

The design of an engineering system based on numerical modeling simulations will always have a certain amount of uncertainty associated with it. Uncertainties arise from approximations made in the conversion of a physical system into a numerical model, assumptions made in the analysis procedure, and subjectivity of the final heuristic judgment of the results of the analysis. In geotechnical engineering, further uncertainties are present, arising from: (i) inevitable varability of soil strata and material properties, (ii) interpretations of the geometry of the subsurface conditions based on a limited number of observations, and (iii) inferred nature of the depositional environment and stress history of a soil.

In conventional design procedures, these uncertainties are not quantified, but recognized and accounted for through safety factors. However, a number of investigators recently have recognized the importance of organizing and evaluating uncertainty in engineering, and different ways of quantitatively dealing with uncertainties are presented in literature.

Schweiger (1998) studied the reliability on numerical model predictions by specifying two simple geotechnical benchmark problems and comparing the results obtained by various users to which the problems were sent for analysis. One of the problems was a plane strain analysis of a 12m deep supported excavation. A Mohr-Coulomb model was specified for

the 3 soil layers involved. The study showed how slightly different user-dependant modeling assumptions, within rather tight problem specifications, significantly affected the computed results. For instance, only 50% of the analyses predicted displacements toward the excavation after the first excavation step (a 4m deep cantilever situation).

Whitman (1996) stated that probabilistic methods are tools that can effectively supplement traditional methods for geotechnical projects. The methods can provide better insights into the uncertainties and an improved basis for interaction between engineers and decision-makers. A way to use probabilistic methods in civil engineering was proposed by Carino (1998). He developed a methodology in which non-deterministic analyses are used, in conjunction with a mechanical model, to predict allowable probabilistic excursions in system response. First, a finite element model is made of the problem, as if it were treated by a pure deterministic approach. Secondly, a statistical analysis of planned finite element runs is performed, with respect to a generated set of input parameters provided by the concepts of central composite design. Auvinet et al. (2000) propose the use of a stochastic finite element method (SFEM), a generalization of the deterministic method in which material properties, geometry and loading are described by random variables or random fields. They state that SFEM, complementing standard finite element analysis, makes it possible to evaluate the uncertainty induced by random soil parameters on computed displacements, strains and stresses.

The work described herein focuses on the uncertainties associated with the mechanical properties of the materials used in numerical analyses and with the characteristics and approximations of selected soil models.

2.2 MODEL CALIBRATION BY INVERSE ANALYSIS

In model calibration, various parts of the model are changed so that the measured values are matched by equivalent computed values until, hopefully, the resulting calibrated model accurately represents the main aspects of the actual system. Despite their apparent utility, inverse models are used for this purpose much less than one would expect. In practice, numerical models typically are calibrated using trial-and-error methods because, perhaps, of the difficulties of implementing an inverse analysis, the complexity of the simulated systems, and/or the engineers' perception that automated estimation of model parameters without "engineering judgment" is impossible. One outcome of this work is to show that these concerns are, in most cases, unjustified and inverse modeling represents a valuable tool for geotechnical engineers.

With an inverse modeling approach, a given model is calibrated by iteratively changing model input values until the simulated output values match the observed data (i.e. observations). Figure 2-1 shows a schematic of an inverse analysis procedure. The input parameters are initially estimated by conventional means (e.g. using available laboratory and field test results). Next a numerical simulation of the problem is run and the results are stored in a file (generally in ASCII text format). The simulated results are then compared to

the field observations and a regression analysis is performed to minimize an objective function. The objective function quantifies the fit between computed results and observations and its minimization is reached by updating the set of input parameters needed to perform the numerical simulation. If the model fit is not "optimal", the procedure is repeated until the model is optimized.

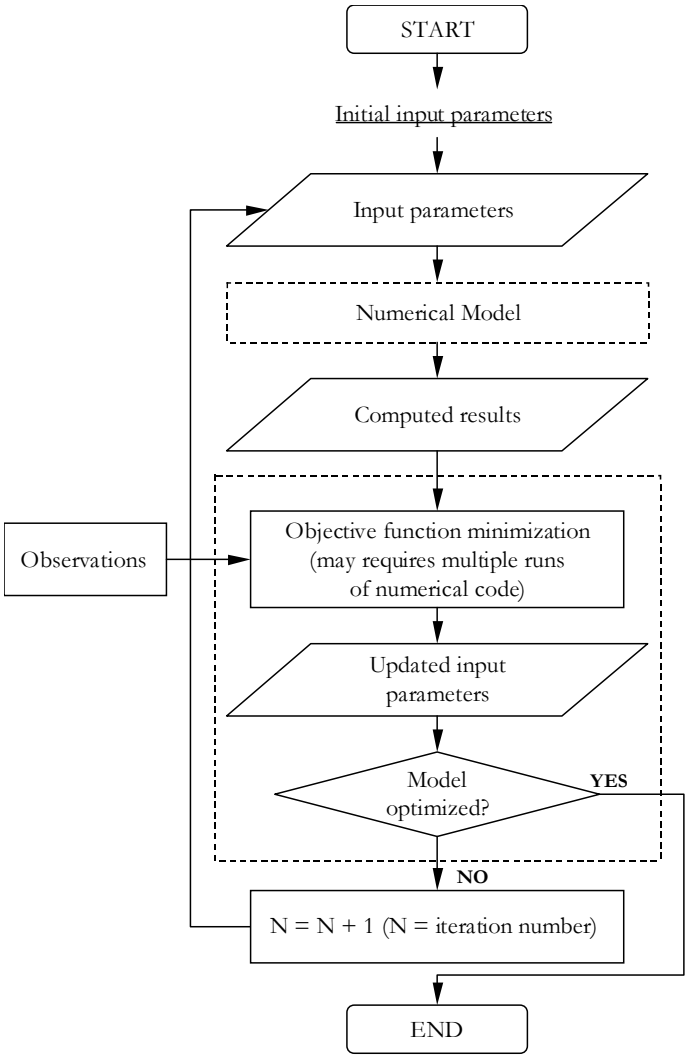

Figure 2-1 Schematic of inverse analysis procedure

2.2.1 Advantages and disadvantages

Inverse analysis works in the same way as a non-automated calibration approach: parameter values and other aspects of the model are adjusted until the model's computed results match the observed behavior of the system. However use of an inverse model provides additional results and statistics that offer numerous advantages in model analysis and, in many instances, expedites the process of adjusting parameter values.

The fundamental benefit of inverse modeling is its ability to automatically calculate parameter values that produce the best fit between observed and computed results. In addition other benefits are derived, including: (i) substantial time saving over traditional trial-and-error calibration methods; (ii) statistics that quantify quality of calibration, data shortcomings and reliability of parameter estimates and predictions; and (iii) identifications of issues that are easily overlooked during non-automated calibration.

The main difficulties inherent to inverse modeling algorithms are related to the complexity of real systems, almost always modeled non-linearly, which sometimes leads to problems of: (i) insensitivity, when the observations do not contain enough information to support estimation of the parameters; (ii) non-uniqueness, when different combination of parameter values match the observations equally well; and (iii) instability, when slight changes in model variables radically change inverse model results.

Although these potential difficulties make inverse models imperfect tools, recent work in various civil engineering fields (Poeter and Hill 1997, Jahangir 1997, Keidser et al. 1991) clearly demonstrated that inverse modeling provides capabilities that help modelers significantly, even when the simulated systems are very complex.

2.2.2 Possible geotechnical uses of inverse analysis

An engineer undertakes a number of steps to solve a typical geotechnical problem, including:

1) Define the problem (e.g., bearing capacity of foundation, surface settlements associated with tunneling, movements around excavations)

2) Choose a model to analyze the problem (e.g., formula, empirical method, numerical method)

3) Acquire information on soil characteristics of the site (e.g., past experience, laboratory or field tests, literature)

4) Calibrate the model based on soil characteristics (e.g., assign values to formula constants or numerical model parameters)

5) Use the calibrated model to solve the problem (e.g., design load of a foundation, differential settlement of structures affected by tunnel's construction or excavations)

6) Evaluate the design predictions and estimate the confidence in the results provided by the chosen model (e.g., experience, engineering judgment, reliability statistics)

7) Check for validity of predictions during project construction or after project completion (compare computed results and field observations)

If the model used to simulate the project (step 2) is numerical, then inverse modeling can be used to reduce the time and costs associated with some of the other steps. In particular, inverse analysis can help the practitioner in calibrating the model based on the soil characteristics (step 4) and in evaluating critical inputs to performance predictions (step 6). If a monitoring program is included during construction of the project, then inverse analysis can also be used to update predictions during construction or analyze the validity of the predictions at the end of the project (step 7).

The objective of this work is to demonstrate the effectiveness of inverse analysis techniques for these different geotechnical engineering tasks, and to show that the information obtained during model calibration by inverse analysis is extremely valuable for geotechnical practitioners and researchers. In geotechnical engineering the research on the subject is limited, yet it shows promising results.

Zentar et al. (2001) developed an inverse method, by associating a finite element code with an optimization code, to identify soil parameters from pressuremeter test results. The method was applied to solve the inverse problem of a cylindrical cavity expansion in a

Modified Cam-Clay type medium. The method, although unable to estimate all the model parameters because of the nature of the test, was able to identify the shear modulus, G, and the failure parameter, M. The study revealed some of the difficulties of parameter identification when strong coupling exists among the parameters and when changes to them do not influence the test results significantly. Yet inverse modeling, when used for estimating the two parameters, produced a very close agreement between calculated and experimental curves.

Ou and Tang (1994) presented an optimization method for determining soil parameters for finite element analysis of deep excavations. Non-linear optimization techniques were employed to calibrate soil constants by minimizing the difference between measured and calculated values of wall deflections. The pseudo-elastic hyperbolic Duncan-Chang model, which requires the calibration of nine input parameters, was used to model the soil behavior. The authors decided to use inverse analysis to estimate two parameters (K and K_b). The remaining seven parameters were not included in the optimization either because their estimate can be achieved fairly accurately by conventional laboratory testing or because their changes had negligible influence on the analysis results. The convergence and the stability of the proposed techniques were verified using three well-known mathematical functions, a hypothetical excavation case and an actual excavation project.

2.2.3 On implementing the "observational method"

For many geotechnical engineering projects, especially in urban environments, it is critically important to predict the magnitude and distribution of the ground movements caused by the construction procedures. Given the uncertainties with the movement predictions, it is usual to include a monitoring program to record the ground movements and, in some cases, adjacent building movements developed during construction. These movements can be used to evaluate how well the actual construction process is proceeding in relation to the predicted movements. Ideally, these recorded movements can also be used to control the construction process and update predictions of movements given the measured deformations at early stages of constructions.

The procedure to accomplish this task is usually referred to as the "observational method" (Peck 1969, Morgestern 1995, Whitman 1996), a framework wherein construction procedures and details are adjusted based upon observations and measurements made as construction proceeds. It is quite difficult, however, to currently use observed movements for these purposes in a timely enough fashion to be of use in a typical project where time is of the essence to a contractor. To obtain inclinometer or optical survey data, process it, and use it to "calibrate" the results of a finite element model is a time-consuming process. For instance, an analyst has to modify the input soil parameters until a match is obtained with the important performance parameter (e.g., the lateral displacement distribution measured by an inclinometer of the soil surrounding an excavation). This updating process can be

done in a timely fashion only with the commitment of a significant number of personnel. In this process, there are no quantitative measures of the goodness of the fit and the appropriateness of the "optimized" parameters. Consequently there is much judgment involved, requiring detailed knowledge of the finite element procedures and constitutive model. Furthermore, while conceptually this idea of updating predictions based on observed data is an excellent one, the current practices and reality of budget constraints make its execution beyond the capabilities of most teams assembled for a project.

This work proposes the use of inverse analysis procedures, wherein a given model is automatically and objectively calibrated until the simulated output values match the measured data, to improve the state-of-the-art of predicting and controlling ground movements associated with geotechnical engineering projects (e.g., supported excavations, tunnels).

2.3 AN INVERSE ANALYSIS ALGORITHM: UCODE

In the work described herein model calibration by inverse analysis was conducted using UCODE (Poeter and Hill 1998), a computer code designed to allow inverse modeling posed as a parameter estimation problem. UCODE has been developed for ground-water models, but it can be effectively used in geotechnical modeling because it works with any application software that can be executed in batch mode. Its model-independency allows the chosen numerical code to be used as a "closed box" in which modifications only involve model input values. This is an important feature of UCODE, in that it allows one

to develop a procedure that can be easily employed in practice and in which the engineer will not be asked to use a particular finite element code or inversion algorithm. Figure 2-2 shows a detailed flowchart of the parameter optimization algorithm used in UCODE. Note that the minimization requires multiple runs of the finite element code. Details on the structure of the program and examples of batch input files are given in Appendix A.

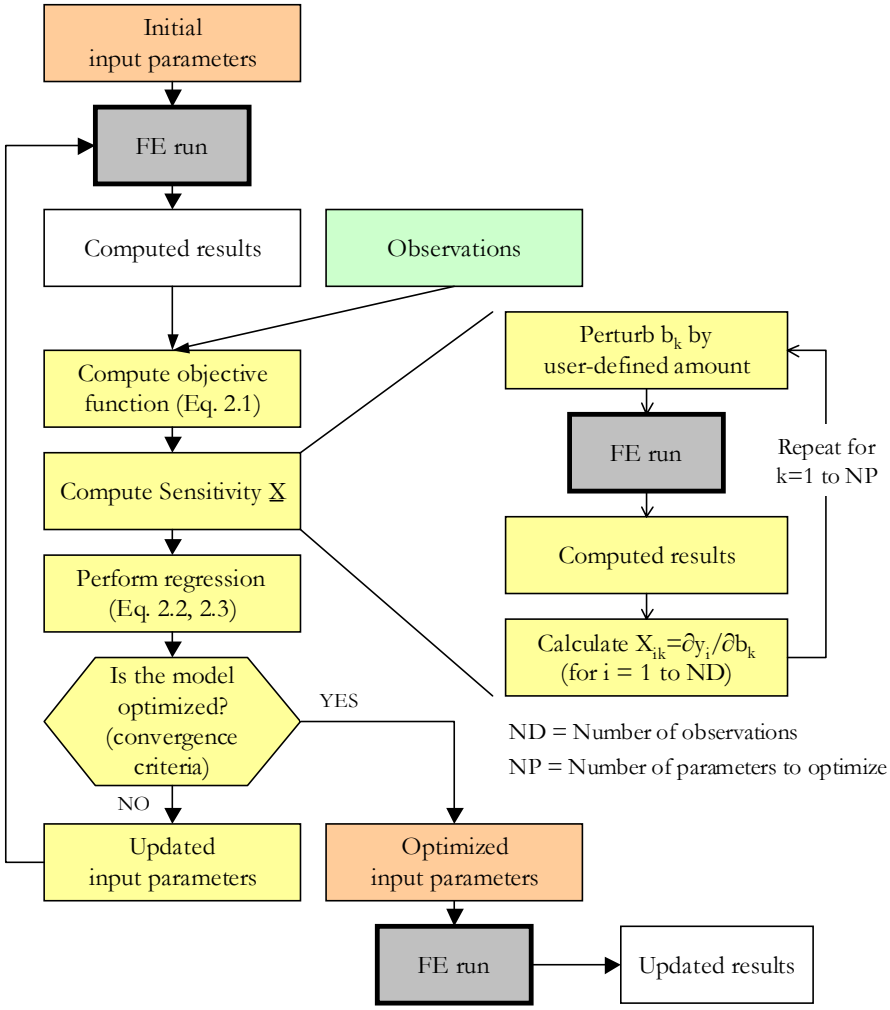

Figure 2-2 Parameter optimization algorithm flowchart

In UCODE the weighted least-squares objective function S($\underline{b}$) is expressed by:

$$S(\underline{b}) = \left[\underline{y} - \underline{y}'(\underline{b})\right]^T \underline{\omega}\left[\underline{y} - \underline{y}'(\underline{b})\right] = \underline{e}^T \underline{\omega e} \tag{2.1}$$

where $\underline{b}$ is a vector containing values of the number of parameters to be estimated; $\underline{y}$ is the vector of the observations being matched by the regression; $\underline{y}'(\underline{b})$ is the vector of the computed values which correspond to observations; $\underline{\omega}$ is the weight matrix; and $\underline{e}$ is the vectors of residuals.

Non-linear regression is an iterative process. The modified Gauss-Newton method used by UCODE to update the input parameters is expressed as:

$$\left(\underline{C}^T \underline{X}^T{}_r \underline{\omega} \underline{X}_r \underline{C} + \underline{I} m_r\right)\underline{C}^{-1}\underline{d}_r = \underline{C}^T \underline{X}^T{}_r \underline{\omega}\left(\underline{y} - \underline{y}'(\underline{b}_r)\right) \tag{2.2}$$

$$\underline{b}_{r+1} = \rho_r \underline{d}_r + \underline{b}_r \tag{2.3}$$

where $\underline{d}_r$ is the vector used to update the parameter estimates $\underline{b}$; r is the parameter estimation iteration number; $\underline{X}_r$ is the sensitivity matrix ($X_{ij}=\partial y_i/\partial b_j$) evaluated at parameter estimate $\underline{b}_r$; $\underline{C}$ is a diagonal scaling matrix with elements c_{jj} equal to $1/\sqrt{(\underline{X}^T \underline{\omega}\ \underline{X})_{jj}}$; $\underline{I}$ is the identity matrix; m_r is a parameter used to improve regression performance; and ρ_r is a damping parameter.

For problems with large residuals and a large degree of nonlinearity, the term $\underline{X}_r^T \underline{\omega}\, \underline{X}_r$ is replaced by $\underline{X}_r^T \underline{\omega}\, \underline{X}_r + \underline{R}_r$ (Dennis et al. 1981) to help convergence when the objective function changes less than 0.01 over three regression iterations.

Multiple runs of the FE model are required to update the input parameters at a given iteration because the sensitivity matrix $\underline{X}_r$ is computed using a perturbation method. At any iteration every input parameter b_k is independently perturbed by a fractional amount to compute the results' response to its change. Sensitivities are calculated by forward or central differences approximations. For these approximations each iteration requires (NP+1) and (2NP+1) runs, respectively, to estimate a new set of updated parameters, where NP is the number of parameters optimized simultaneously. Computation time may become an issue for very complicated finite element models, depending on how much time is needed for a single model run.

At a given iteration, after performing the modified Gauss-Newton optimization (Eq. 2.2 and 2.3), UCODE decides whether the updated model is optimized according to two convergence criteria. The parameter estimation is said to converge if either:

i. the maximum parameter change of a given iteration is less than a user-defined percentage of the value of the parameter at the previous iteration;

ii. the objective function, $S(\underline{b})$, changes less than a user-defined amount for three consecutive iterations.

When the model is optimized the final set of input parameters is used to run the model one last time and produce final "updated" results.

2.3.1 Model fit statistics

Different quantities can be used to evaluate the model fit. At first, one can consider the magnitude of the weighted and unweighted residuals and their distribution both statistically and relative to independent variable values such as location and time. In initial model runs large residuals and weighted residuals can indicate gross errors in the model, in the data, in how the observed quantity is simulated, or in the weighting. In subsequent model runs, after the gross errors have been corrected, other statistics become increasingly important.

A commonly used indicator of the overall magnitude of the weighted residuals is the model error variance, s^2, which equals:

$$s^2 = \frac{S(\underline{b})}{ND - NP} \tag{2.4}$$

where S($\underline{b}$) is the objective function; ND is the number of observations; and NP is the number of estimated parameters.

The value of the objective function (Eq. 2.1) is also used to indicate model fit informally, because its variation indicates by how much an optimized model improves with respect to the initial simulation of a problem. The objective function changes can be expressed through a new statistic, the fit improvement (FI), which indicates by what percentage the

optimized results improved compared to the initial fit between experimental data and computed results. The fit improvement is defined as:

$$FI = \frac{S(\underline{b})_{initial} - S(\underline{b})_{optimized}}{S(\underline{b})_{initial}} \tag{2.5}$$

where $S(\underline{b})_{initial}$ is the initial value of the objective function; and $S(\underline{b})_{optimized}$ is the value of the objective function for the optimized set of parameters.

Graphical analyses are also useful to assess the validity of the model optimization. Ideally, weighted residuals are scattered evenly about 0.0, and their size is not related to the simulated values. Weighted residuals plotted on maps or time graphs should not show any discernible patterns and should appear random. When weighted observations are plotted against weighted simulated values, the hope is that the points fall close to a line with slope equal to 1.0 and an intercept of zero. The associated summary statistic is R_N^2, the correlation coefficient between the weighted residuals ordered from smallest to largest and the order statistics from a N(0,1) probability distribution function (Brockwell and Davis, 1987). The correlation coefficient is calculated as:

$$R_N^{\ 2} = \frac{\left[\left(\underline{e}_0 - \underline{m}\right)^T \underline{\tau}\right]^2}{\left[\left(\underline{e}_0 - \underline{m}\right)^T \left(\underline{e}_0 - \underline{m}\right)\right]\left(\underline{\tau}^T \underline{\tau}\right)} \tag{2.6}$$

where all vectors are of length ND; $\underline{m}$ is a vector with all components equal to the average of the weighted residuals; $\underline{e}_0$ is a vector of weighted residuals ordered from smallest to largest; and $\underline{\tau}$ is a vector with the i^{th} element equal to the ordinate value of a N(0,1) probability distribution function.

2.3.2 Input parameters statistics

The relative importance of the input parameters being simultaneously estimated can be defined using parameter statistics, including the sensitivity of the predictions to changes in parameters values, the variance-covariance matrix, confidence intervals and coefficients of variation.

Different quantities can be used to evaluate the sensitivity of the predictions to parameters changes. One percent sensitivities, dss_{ij}, scaled sensitivities, ss_{ij}, and composite scaled sensitivities, css_j, can be used for the purpose. These sensitivities are defined in Eq. (2.7), (2.8) and (2.9), respectively.

$$dss_{ij} = \frac{\partial y'_i}{\partial b_j}\frac{b_j}{100} \tag{2.7}$$

$$ss_{ij} = \left(\frac{\partial y'_i}{\partial b_j}\right) b_j \omega_{ii}^{1/2} \tag{2.8}$$

$$css_j = \left[\sum_{j=1}^{ND} \left(\left(\frac{\partial y'_i}{\partial b_j} \right) b_j \omega_{ii}^{1/2} \right)^2 \Bigg|_{\underline{b}} \Big/ ND \right]^{1/2} \tag{2.9}$$

where y'_i is the i^{th} simulated value; y_i/b_j is the sensitivity of the i^{th} simulated value with respect to the j^{th} parameter; b_j is the j^{th} estimated parameter; ω_{jj} is the weight of the i^{th} observation

One percent scaled sensitivities represent the amount that the simulated value would change if the parameter value increased by one percent. Scaled sensitivities are dimensionless quantities that can be used to compare the importance of different observations to the estimation of a single parameter or the importance of different parameters to the calculation of a simulated value. Composite scaled sensitivities indicate the total amount of information provided by the observations for the estimation of one parameter.

The reliability and correlation of parameter estimates can be analyzed by using the variance-covariance matrix, $\underline{V}(\underline{b}')$, for the final estimated parameters, $\underline{b}'$, calculated as:

$$\underline{V}(\underline{b}') = s^2 \left(\underline{X}^T \, \underline{\omega} \underline{X} \right)^{-1} \tag{2.10}$$

where s^2 is the error variance; $\underline{X}$ is the sensitivity matrix; and $\underline{\omega}$ is the weight matrix.

The diagonal elements of matrix $\underline{V}(\underline{b}')$ equal the parameter variances, the off-diagonal elements equal the parameter covariances. Parameter variances are most useful when used to calculate two other statistics: confidence intervals for parameter values and coefficients of variation. Parameter covariances can be used to calculate correlation coefficients.

A linear confidence interval for each parameter b_j can be calculated as follows (Hill 1994):

$$b_j \pm t\left(n, 1.0 - \frac{\alpha}{2}\right)\sigma_{b_j} \tag{2.11}$$

where $t(n,1.0-\alpha/2)$ is the student-t statistic for n degrees of freedom and a significant level of α; and σ_{bj} is the standard deviation of the j^{th} parameter.

Coefficients of variation, cov_i, are equal to:

$$\mathrm{cov}_i = \frac{\sigma_i}{b_i} \tag{2.12}$$

where σ_i is the standard deviation of parameter b_i.

Correlation coefficients are calculated by:

$$cor(i,j) = \frac{\mathrm{cov}(i,j)}{\mathrm{var}(i)^{1/2}\ \mathrm{var}(j)^{1/2}} \tag{2.13}$$

where cor(i,j) indicate the correlation between the i^{th} and j^{th} parameter; cov(i,j) equal the off-diagonal elements of $\underline{V}(\underline{b}')$; and var(i) and var(j) refer to the diagonal elements of $\underline{V}(\underline{b}')$.

A confidence interval is a range that has a stated probability of containing the true value of the estimated variable. The width of the confidence interval can be thought of as a measure of the likely precision of the estimate, with narrow intervals indicating greater precision. The coefficients of variation provide dimensionless numbers with which the relative accuracy of different parameter estimates can be compared. Correlation coefficients close to –1.0 and 1.0 are indicative of parameters that cannot be uniquely estimated with the observations used in the regression.

2.3.3 Observations' weighting

The weights assigned to the observations are an important part of the regression analysis because they influence the value of the objective function, and thus the regression results. UCODE uses a diagonal weight matrix. Weighting is used to reduce the influence of observations that are less accurate and increase the influence of observations that are more accurate. For problems with more than one kind of observation, weighting also produces weighted residuals that have the same units, so that they can be squared and summed. In UCODE the weight of every observation, ω_{ii}, is equal to the inverse of its error variance, σ^2:

$$\omega_{ii} = 1 / \sigma_i^2 \qquad (2.14)$$

Users assign the weight of an observation by specifying a value for its variance, standard deviation or coefficients of variation. Assigning appropriate weight values to the observations can be problematic. For regression methods to produce parameter estimates with the smallest possible variance Hill (1998) suggests that weighting needs to be proportional to the inverse of the variance of the measurement errors. At the end of the regression analysis, the value of the model error variance, s^2 (Eq. 2.4), can be used to evaluate the consistency between the model fit and the measurement errors, as expressed by the observations' weights. Values larger than 1.0 indicate that the model fits the data less well than would be accounted for by expected measurement errors.

2.4 ON CONSTRAINING PARAMETERS DURING OPTIMIZATION

While limiting constraints on parameter values may, at times, appear to be necessary, UCODE users are not allowed to set upper or lower limits on parameters to be estimated. Hill et al. (1998) demonstrated that this practice might disguise model inaccuracies. Indeed, unrealistic optimized input parameter values are likely to indicate either (i) that there is a more fundamental model error (thus, users are prompted to find and correct the error), or (ii) that the observations do not contain enough information to estimate the parameters.

Responses to the second circumstance could be either the exclusion of the parameter from the optimization or the use of prior information on the parameter value. Using prior information allows direct measurements of model input parameters to be included in the regression and tends to produce estimates that are close to specified parameter values. The

effect that the prior information has, in "forcing" an estimated parameter to remain close to a specified value, depends from its weight. Users must treat the prior information like an extra observation point. Its influence in conditioning the response of the regression analysis depends on both the number of observations included and the weight of the prior information relative to the weight of the other observations.

One problem with the "unconstrained approach" used by UCODE is that many geotechnical parameters have natural constrains. Many soil models' input parameters, for instance, admit only positive values (e.g. Young's modulus, cohesion), and some of them are bounded by upper and lower physical limits (e.g. Poisson's ratio, friction angle). To address the first problem UCODE allows the user to optimize the log-transformed value of the native parameter. This produces an inverse problem that prevents the actual parameter value from becoming negative. Nothing is directly implemented in UCODE to address the second problem. However, users can specify functions of the parameter values to be used as input to the application model.

Users can relate the input parameter to a bounded "mapping function." For example, the input parameter to be constrained, x, can be mapped by a hyperbolic function expressed in terms of e^x. Figure 2-3 shows such a function. Its expression is given by:

$$f(x) = y_1 + \frac{e^x}{\frac{e^x}{(y_2 - y_1)} + \frac{1}{Tan}} \tag{2.15}$$

where x is the native parameter, y_1 is the lower limit of x, y_2 is the upper limit of x, and Tan is the initial tangent in the y-e^x space.

Note that, in order to "center" the mapping function around a specific value y_0, the variable Tan must be equal to:

$$Tan = \frac{(y_0 - y_1)(y_2 - y_1)}{y_2 - y_0} \tag{2.16}$$

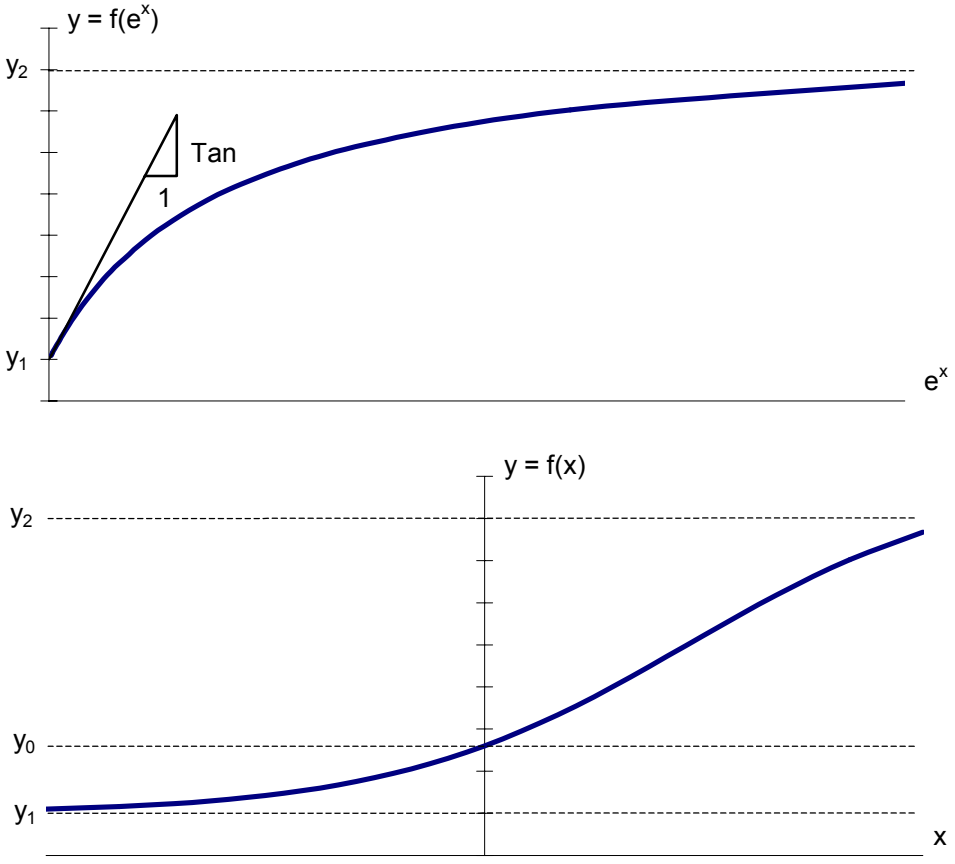

Figure 2-3 Hyperbolic mapping function to constrain the value of an input parameter

2.5 SUMMARY

In this chapter inverse analysis has been introduced as a tool for geotechnical engineers dealing with problems involving the calibration of numerical models. In the first part of the chapter the basics of inverse analysis have been introduced and advantages and limitations of the method have been discussed. In the second part of the chapter and the inverse modeling algorithm UCODE has been presented.

3 CALIBRATION OF SOIL MODELS BY INVERSE ANALYSIS

3.1 INTRODUCTION

Developing soil parameters for use in constitutive models is a procedure that involves much judgment and usually is best accomplished by experienced users of a particular model. The fit of the model based on the selected parameters is rarely quantitatively evaluated. Inverse analysis techniques can be used effectively to calibrate soil parameters in a more objective fashion by minimizing the difference between experimental results and numerical simulations of geotechnical tests.

3.2 CALIBRATION OF MODIFIED CAM-CLAY MODEL FROM TRIAXIAL TEST RESULTS

The calibration of a finite element soil model, based on results from triaxial laboratory experiments, is presented in this section. Inverse analysis is used to calibrate Modified Cam-Clay (MCC) parameters from results of one drained and one undrained triaxial compression

tests on specimens of compressible Chicago glacial clays. This approach couples the finite element code JFEST (e.g. Finno & Harahap 1991) and the inverse analysis algorithm UCODE to minimize the differences between computations of stress-strain response and experimental data. The two programs' input and output files used herein are presented in Appendix A.

The soil specimens used for the laboratory tests considered are undisturbed samples of Chicago clay from a location in downtown Chicago (Finno et al. 2002). The clay samples are compressible, lightly overconsolidated, low-to-medium plastic clays, typical of many deposits in the Great Lakes area.

3.2.1 Modified Cam-Clay representation of Chicago glacial clays

A Modified Cam-Clay model (Roscoe et al. 1958) was chosen to represent the soil response. The MCC model is an isotropic, work hardening, non-linear, elasto-plastic model. The responses are defined in terms of three state variables: the mean normal stress p', the deviatoric stress q, and the void ratio e. The first two variables are defined as:

$$p' = \frac{I_1}{3} \tag{3.1}$$

$$q = \sqrt{3J_2} \tag{3.2}$$

where $I_1=\sigma_{11}+\sigma_{22}+\sigma_{33}$ is the first Cauchy stress invariant, and $J_2=1/6[(\sigma_{11}-\sigma_{22})^2+(\sigma_{11}-\sigma_{33})^2+(\sigma_{22}-\sigma_{33})^2+6\sigma_{12}+6\sigma_{13}+6\sigma_{23}]$ is the second deviatoric stress invariant.

The four MCC input parameters are: λ, κ, M and G. Table 3-1 shows their meaning and the conventional way of estimating them. Parameters λ and κ define the model hardening law, M locates the Critical State Line (CSL) in the p'-q space, and G, along with κ, define the elastic behavior inside the yield surface. Beside the initial values of the state variables, the initial conditions include a parameter expressing the stress history of the soil, p_c*, and the critical state void ratio, e_{cs}, defining the position of the CSL in the e-p' space.

Parameter	Explanation	Initial estimates
κ	Slope of rebound isotropic consolidation curve	Cr / 2.303
λ	Slope of virgin isotropic consolidation curve	Cc / 2.303
M	Slope of the failure line in q-p' space	6 sin ϕ / (3 – sin ϕ)
G	Shear modulus (kPa)	q/γ at 50% $q_{failure}$

Table 3-1 Modified Cam Clay input soil parameters to optimize

The initial estimates of κ and λ are based herein on results from consolidation tests conducted on samples coming from the same Shelby tube, whereas M and G are estimated from the stress-strain response of the triaxial tests. M is estimated assuming a straight failure line passing through zero in p'-q space. G is estimated by averaging the secant shear

stiffness at a shear stress level of 50% of the failure value. The initial value of p_c*, assuming the soil OCR ≅ 1, is set equal to the consolidation stress of the test modeled, and e_{cs} is estimated as the value of the CSL at p'=1 kPa.

3.2.2 Procedures

Two triaxial compression tests form the basis of the optimization: one performed in drained conditions (D1) and one in undrained conditions (U1). Both specimens were isotropically consolidated and then sheared by increasing the vertical principal stress to failure. The finite element code JFEST was used to simulate the triaxial tests. The behavior of the samples was considered elemental, thus one single 8-noded isoparametric element was used to model the specimen. A penalty formulation was used to simulate the undrained tests.

To evaluate the match between the soil response and the FE predictions, two curves were used to calibrate the objective function for each type of test: the changes in principal stress difference (q-ε_a) and the volumetric changes (ε_v-ε_a) with axial strain for the drained test D1; the changes in principal stress difference (q-ε_a) and pore pressures (u-ε_a) with axial strains for the undrained test U1.

Figures 3-1 and 3-2 show the experimental results and the observation points used for the drained and undrained stress-strain curves respectively. The stress-strain curves of the drained test were discretized by considering one observation point every 0.5% axial strain

up to ε_a = 12%. Curves for the undrained test were discretized using one observation point every 0.15% axial strain up to ε_a = 4.5%. Therefore, UCODE used a total of 108 observations to calibrate the MCC model. The weight of the observations was assigned through coefficients of variation.

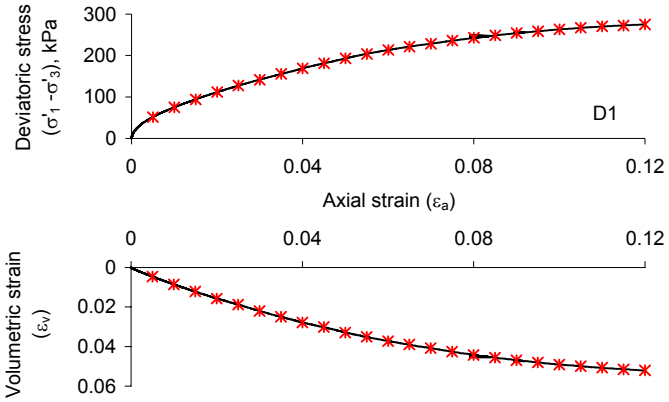

Figure 3-1 Discretization of experimental results for drained test D1

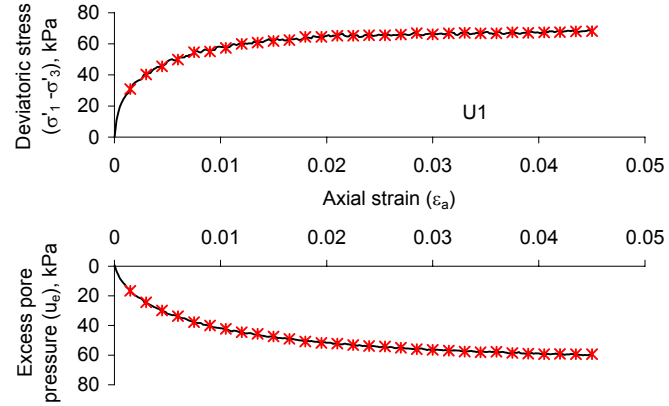

Figure 3-2 Discretization of experimental results for undrained test U1

3.2.3 Results

Visual examination of the stress-strain plots provides the simplest way to evaluate the fit between experimental and modeled response and thus evaluate the effectiveness of the inverse analysis.

Figure 3-3 shows a comparison between experimental data and computed results when the initial estimates of soil parameters are used to simulate the model response. The computed results match the overall test results relatively well. However, they slightly underpredict the deviatoric stress response of the drained test, and they are not able to capture the initial response of the undrained test. The computed results show that the behavior of the soil as predicted by the numerical simulation is softer that the real behavior of the clay sample.

Figure 3-4 shows a comparison between experimental data and computed results when the optimized estimates of soil parameters are used to simulate the model response. The computed results match the overall test results extremely well for both tests at either small or large strain levels.

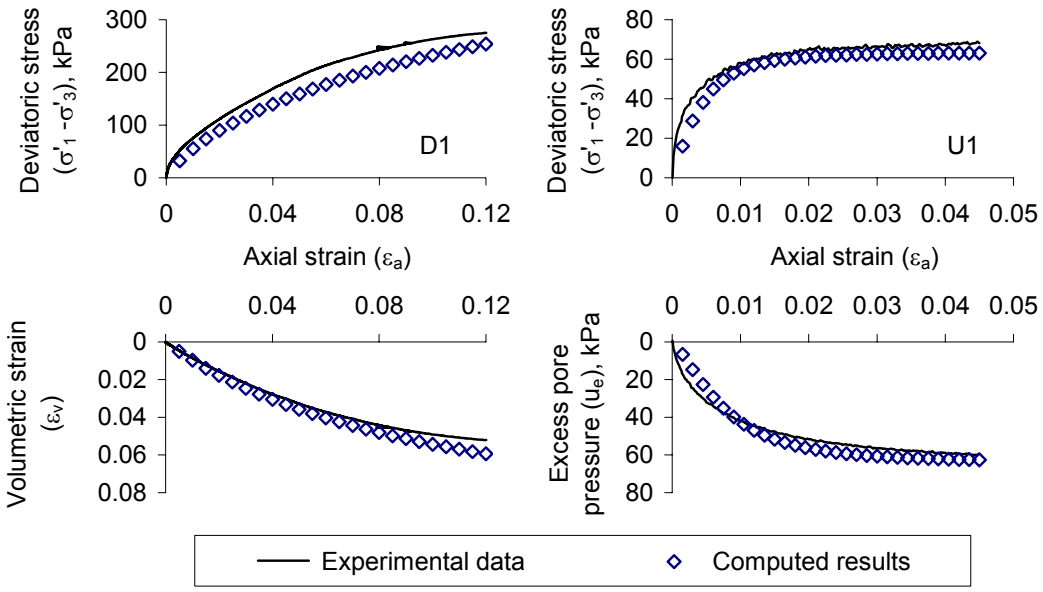

Figure 3-3 Visual fit between experimental data and computed results for initial estimates of soil parameters

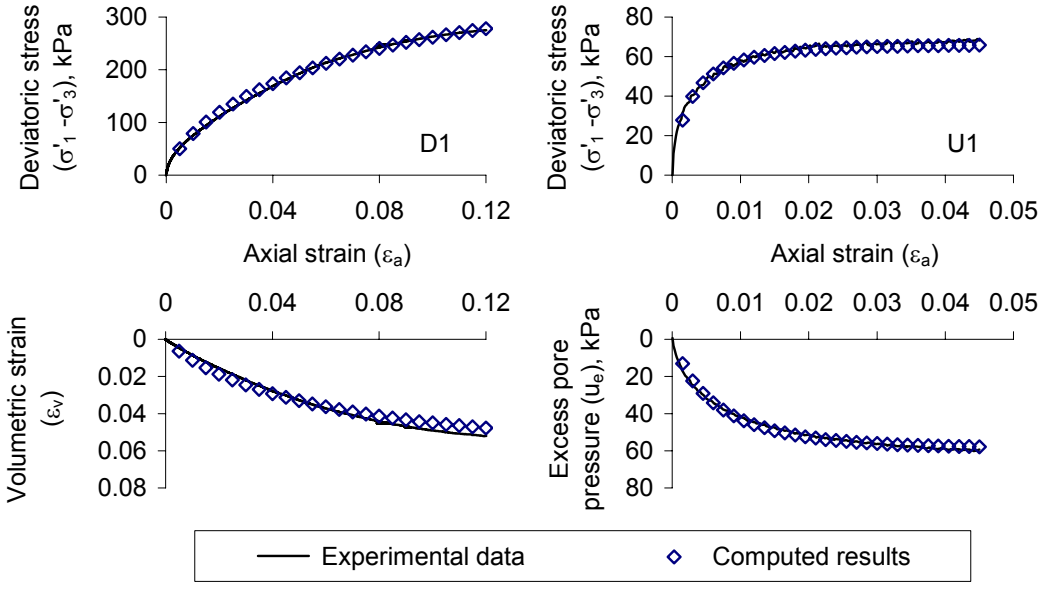

Figure 3-4 Visual fit between experimental data and computed results for optimized estimates of soil parameters

Table 3-2 shows the values of the four MCC input parameters before and after the optimization. Only small changes in values of κ, λ and M are needed to obtain the best-fit values, whereas the optimized value of the stiffness parameter G is almost 3 times larger than the initial one. Note that four MCC input parameters are not optimized independently and that the same set of parameters is used to simulate the two tests.

	Input parameter				Visual fit	
	κ	λ	M	G (kPa)	D1 (q-ε_v)	U1 (q-u)
Initial	0.017	0.130	1.09	4000	marginal good	marginal marginal
After optimization	0.021	0.096	1.04	11054	good good	good good

Table 3-2 Input parameter values before and after optimization

Results of the optimization are consistent with what a "knowledgeable" geotechnical engineer would have guessed by looking at the fit illustrated in Figure 3-3. The initial set of input parameters underestimates the stiffness of the soil samples, which in the MCC model is mainly (but not uniquely) expressed by parameter G. And indeed G was the parameter that varied the most. However, one could not say *a priori* by how much the value of G was underestimated in the initial predictions. Moreover, it is very doubtful that one could have estimated by trial-and-error the small fractional change of the first three parameters to arrive at the fit illustrated in Figure 3-4. Note that if one tries to optimize the value of the stiffness parameter only, keeping the other parameters to their initial value, the fit between

experimental data and computed results never become as good as the one in Figure 3-4. Results relative to this case, for which only parameter G was optimized, are shown in Table 3-3 and Figure 3-5.

	Input parameter				Visual fit	
	κ	λ	M	G (kPa)	D1 (q/ε_v)	U1 (q/u)
Initial	0.017	0.130	1.09	4000	marginal good	marginal marginal
After optimization	0.017	0.130	1.09	8693	marginal marginal	good marginal

Table 3-3 Input parameter values before and after optimization (optimize parameter G only)

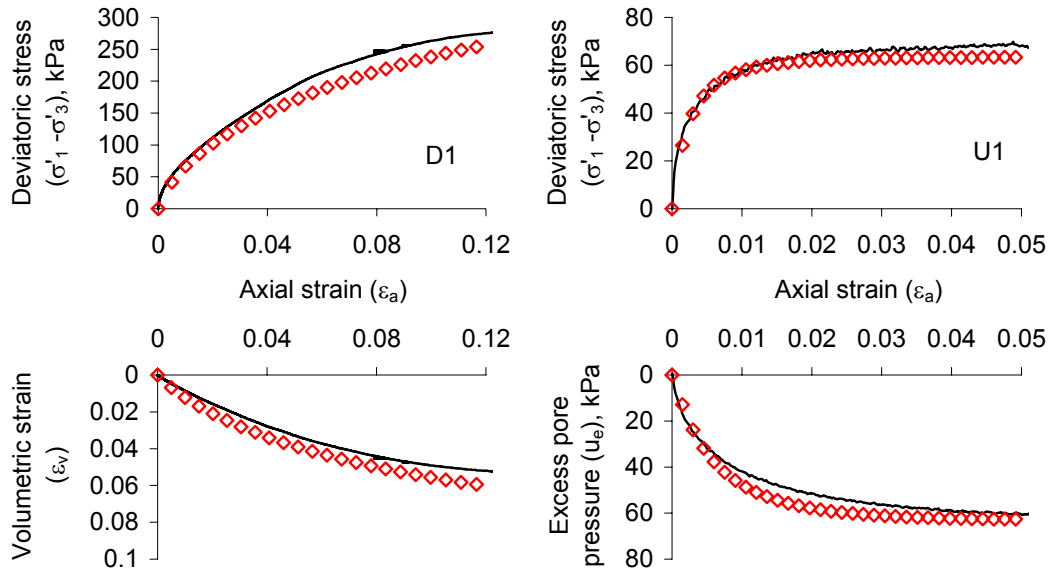

Figure 3-5 Visual fit between experimental data and computed results for optimized estimates of soil parameters (optimize parameter G only)

3.2.3.1 Model fit statistics

Table 3-4 shows a summary of the values of statistics indicating model fit. The objective function, model variance, correlation coefficient and fit improvement are computed according to Eq. 2.1, 2.4, 2.6 and 2.5, respectively.

	Visual fit		Model fit statistics				
	D1 (q/ε_v)	U1 (q/u)	Objective function	Model variance	Correlation coefficient	Fit Improvement (FI)	Number of iterations
Initial	marginal good	marginal marginal	789	7.59	80.1%		
After optimization	good good	good good	93.8	0.90	97.5%	88.1%	5

Table 3-4 Model fit statistics for initial and final set of parameters

The model fit statistics clearly show that the optimization of the input parameters improves the fit significantly. Indeed, the objective function value decreased by almost 90% (i.e. FI=88.1%), the model variance is less than 1.0, indicating that the fit is consistent with the error of the observations as expressed by the weighting, and the correlation coefficient is very close to its ideal value of 100%. Before the optimization the same statistics were showing that the fit between experimental data and simulated response was inadequate.

3.2.3.2 Input parameters statistics

Figure 3-6 shows, in a graphical format, the values of the four MCC input parameters before and after the optimization. The figure also shows the composite scaled sensitivities,

css_j (Eq. 2.8), of the input parameters on the secondary y-axis, whose scale was kept constant in the four charts to allow the reader to easily compare the sensitivity values.

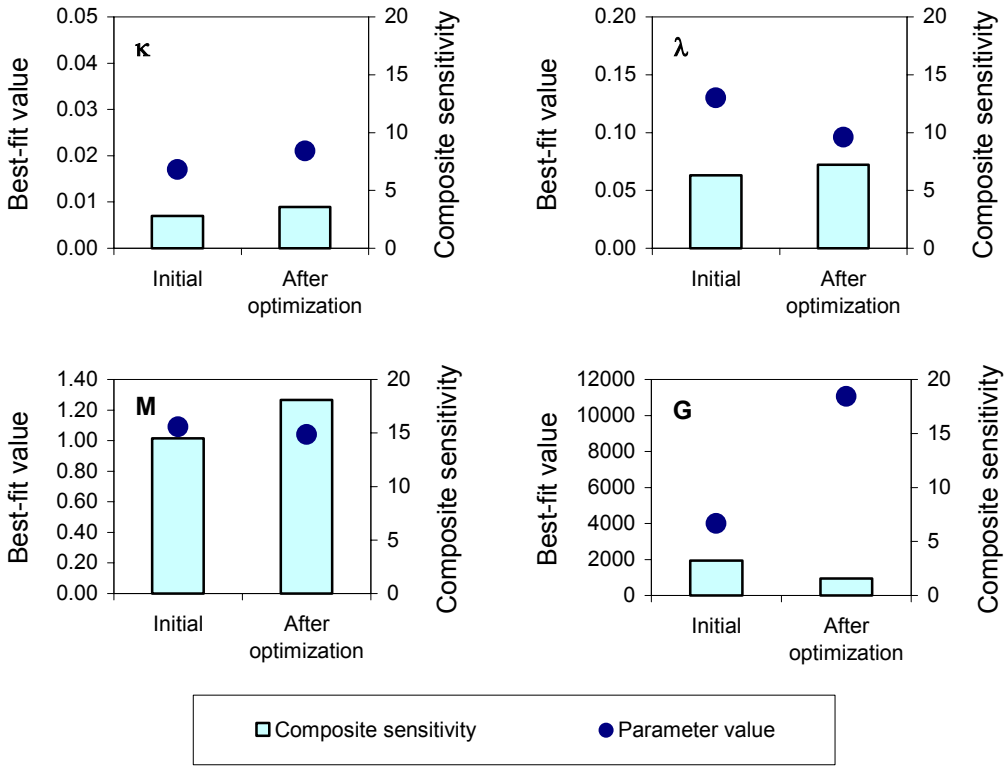

Figure 3-6 Input parameters value and their composite scaled sensitivity before and after optimization

For nonlinear problems, the sensitivity is different for different input values, thus css_j are plotted for the initial and the optimized parameters values. Results, however, show that the difference between sensitivity values at the beginning and at the end of the regression analysis is not significant. This indicates that, despite the non-linearity of the model, the influence of a given parameter on the results is relatively constant. If, during the iterative regression analysis, the sensitivities were to vary too much from iteration to iteration it is

doubtful that the modified Gauss-Newton optimization method used in UCODE (Eq. 2.2 and 2.3) would have been so efficient.

Composite scaled sensitivities vary from values smaller than 4 for parameters κ and G, to values larger than 7 for parameter λ and 15 for parameter M. These values indicate that changes of M have the largest impact on the computed values (recall that the higher the sensitivity value, the more impact in that parameter has on the computed results). This was to be expected since the compression tests were conducted on specimens of lightly overconsolidated clays reconsolidated in the laboratory to stresses greater than or equal to the field value of vertical effective stress. This loading history establishes the stress at the start of the shearing portion of the test very close to or at yield, and hence the parameters associated with plastic hardening and failure (M and λ) would have the most effect on the computed results.

However, this does not mean that one can exclude the least sensitive parameters from the regression analysis. Indeed, results show that the sensitivities relative to different parameters are all within the same order of magnitude. This indicates that all parameters have a quantifiable effect on the modeled results. Indeed, the least sensitive parameters, G, is the one that changes the most to reach its optimal value.

In Figure 3-7 the composite scaled sensitivities are grouped by stress-strain curve type. The parameters that most affect the stress-strain response of the drained test are clearly M and

λ. However, if one considers the undrained test response, particularly the pore water pressure response, the parameter κ becomes more "important" than the parameter λ. This occurs because in the Cam-Clay model the hardening law, which controls the volumetric plastic strain, depends from both λ and κ and, for undrained compression stress-paths in the p-q-e space, contrary to what happens for drained compression loads, the contribution of κ is predominant over the contribution of λ, even after yield. These results illustrate the validity of this statistical measure to detect the parameters that are most important in affecting the test results.

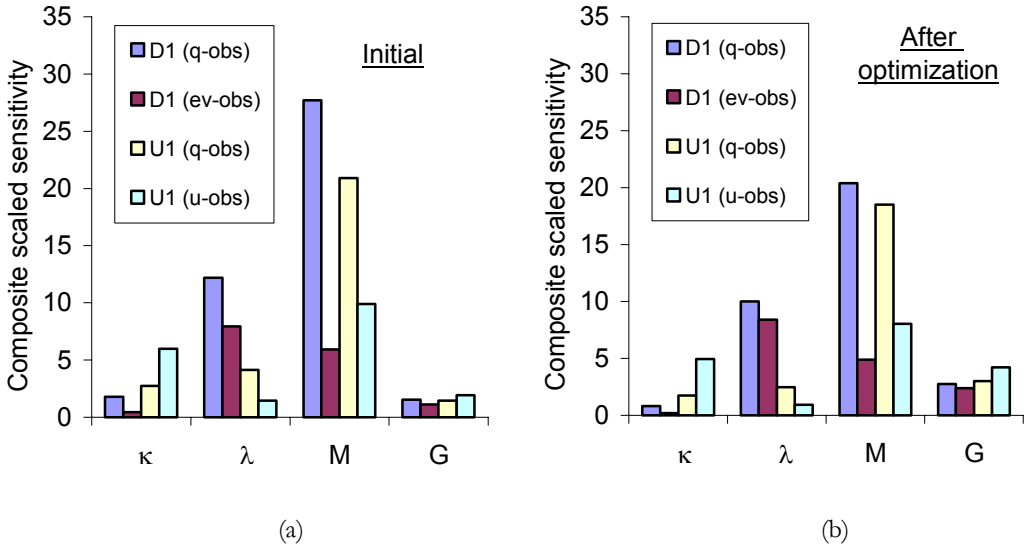

Figure 3-7 Composite scaled sensitivities, grouped by stress-strain curve type, of (a) initial set of input parameters (b) optimized set of input parameters

Figures 3-8 and 3-9 show, respectively, the 1% sensitivities, dss_{ij}, and the scaled sensitivities, ss_{ij}, plotted for every observation point. Both statistics (respectively defined in Eq. 2.7 and

2.8) can be used to compare the importance of different parameters to the calculation of a simulated value. 1% sensitivities do not take into account the weight of the observations, thus their values for observations with different units (i.e. stress vs. strain responses) cannot be compared. In contrast, scaled sensitivities depend on the weight of the observations. Note that, given that the weight of the observations is assigned through a constant coefficient of variation, higher valued observations are weighted less than lower valued ones and their dimensionless sensitivity results reflect this trend.

Figure 3-8 shows, as one would expect, that: (i) positive changes in M produce higher deviatoric stresses, higher volumetric strains and higher excess pore pressures; (ii) positive changes in λ produces lower deviatoric stresses, higher volumetric strains and negligible changes in pore pressures; (iii) changes in κ significantly affect only the undrained test response; and (iv) changes in G only affect the initial stress-strain response.

Figure 3-9 shows, for parameters M and G, two distinct behaviors between the first few initials observations (i.e. small strains) and the subsequent ones. The ss_{ij} values for M increase at first, but then remain almost constant for the final part of the tests. The ss_{ij} for G decrease from relatively high values to almost zero within very few observation points. Both behaviors were to be expected because the failure parameter M becomes more important as the tests move toward failure, whereas the elastic stiffness parameter G only affects results at small strain levels.

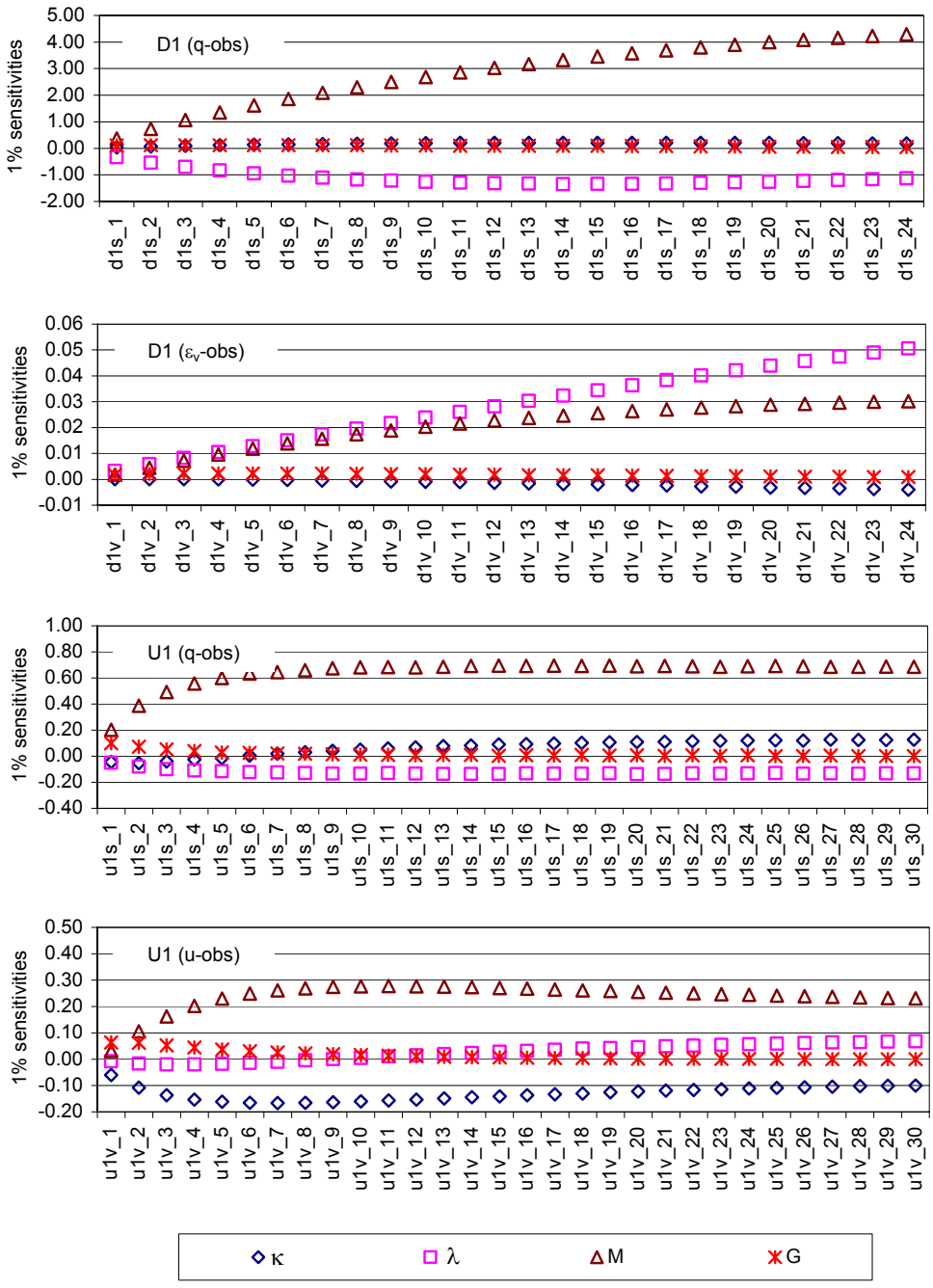

Figure 3-8 1% scaled sensitivities of input parameters to stress-strain observations: (a) q-observations for D1, (b) ε_v-observations for D1, (c) q-observations for U1, (b) u-observations for U1

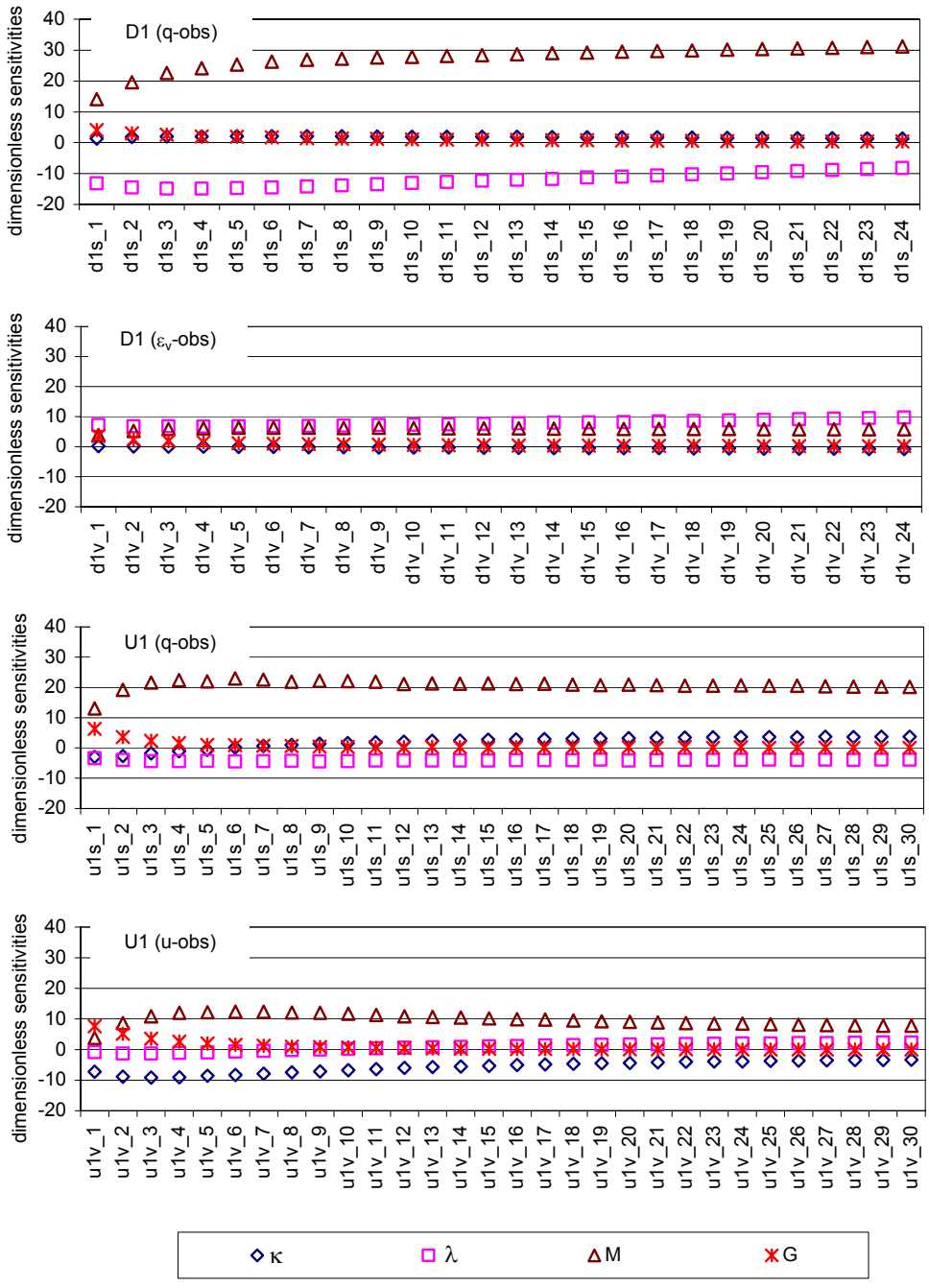

Figure 3-9 Dimensionless scaled sensitivities of input parameters to stress-strain observations: (a) q-observations for D1, (b) ε_v-observations for D1, (c) q-observations for U1, (b) u-observations for U1

Table 3-5 shows the values of some of the parameter statistics derived from the variance-covariance matrix (computed according to Eq. 2.10). Parameter G, the least sensitive of the four input parameters, shows the greatest coefficient of variation (7.5%).

	Initial value	Optimized value	Lower 95% Confidence Interval	Upper 95% Confidence Interval	Coefficient of variation
κ	0.017	0.021	0.0196	0.0222	3.1%
λ	0.13	0.096	0.0932	0.1	1.8%
M	1.09	1.04	1.03	1.05	0.7%
G (kPa)	4000	11054	9410	12700	7.5%

Table 3-5 Parameter statistics derived from variance-covariance matrix

Figure 3-10 shows a graphical representation of these statistics. A bar chart is used to indicate by what percentage the optimized parameter values changed compared to their initial estimate. The plot also shows the parameters' 95% confidence intervals (computed according to Eq. 2.11). Confidence intervals results indicate that estimates of the κ, λ and M values calculated by the regression algorithm are accurate.

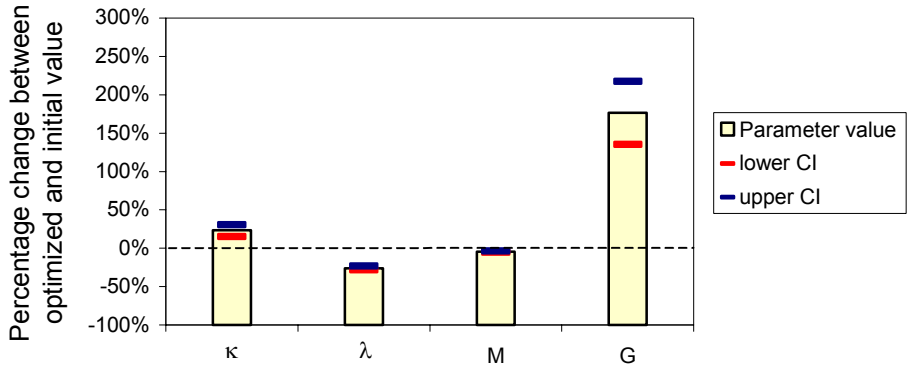

Figure 3-10 Percentage change between optimized and initial parameter values and confidence intervals

Table 3-6 shows the values of the correlation coefficients for the four input parameters (computed using Eq. 2.12). All the values are very far from either 1.0 or –1.0, indicating that none of the parameters is correlated to any other one. This trend suggests that the observations used in the regression provide enough information for the four parameters to be simultaneously estimated.

	Correlation coefficients			
	κ	λ	M	G
κ	1.000	0.374	-0.035	0.451
λ	0.374	1.000	0.539	0.150
M	-0.035	0.539	1.000	-0.372
G	0.451	0.150	-0.372	1.000

Table 3-6 Parameter correlation coefficients

3.2.4 Comments

In this section the inverse analysis algorithm UCODE was used to calibrate, from triaxial test results, the four input parameters of the MCC soil model. Inverse analysis calibration proved to be more effective in defining these model parameters than conventional estimation methods. Indeed, the use of an optimization algorithm to calibrate the MCC model yielded:

1. almost perfect fit between experimental results and the response computed from the finite element simulation of the tests;

2. objective estimation of the model input parameters;

3. useful model fit statistics, which can be used to evaluate the adequacy of the soil model to simulate the experimental soil response;

4. very valuable parameter statistics, which can help geotechnical engineers in interpreting the features of a soil model.

The most important parameter statistic is probably the composite scaled sensitivity, a powerful statistical measure to detect the parameters that most affect the test results.

3.3 PARAMETRIC STUDY ON "GEOTECHNICAL VARIABLES"

The previous section showed how inverse analysis can effectively calibrate a soil model from triaxial test results by matching the experimental response of soil samples with the results of finite element simulations of the tests. Inverse problems can be posed many different ways because the variables that play a role in "conditioning" the results of the regression analysis are numerous. For example, the number of laboratory tests that form the basis of the optimization or how the data set is discretized may have an effect on the results of the analysis. A parametric study on a number of these variables has been conducted to evaluate their effects on the optimized results. The term "geotechnical variables" is herein used to indicate variables that relate to choices that a geotechnical engineer needs to make to setup the inverse analysis to calibrate a soil model.

In this section, inverse analysis optimized results are compared with experimental results of five triaxial tests performed on Chicago clay samples coming from the same Shelby tube. The five samples were isotropically consolidated and then sheared in compression or reduced extension. All specimens were either normally or lightly overconsolidated, "wet of critical" in Cam-Clay parlance, prior to shearing. Table 3-7 shows the type of test, consolidation pressure and maximum deviatoric stress reached during the shearing portion of the test. Tests D1 and U1 are the same tests considered for the calibration of the MCC model in section 3.2. Tests D2 and D3 are two additional drained compression tests. Test E1 is a reduced triaxial extension test.

	D1	D2	D3	U1	E1
Test type	CID TXC	CID TXC	CID TXC	CIU TXC	CID RTXE
σ'_c (kPa)	200	400	107	100	85
Max deviatoric stress (kPa)	280	~450	180	70	-70

Table 3-7 Triaxial tests consolidation pressures

Figure 3-11 shows the four "geotechnical variables" considered for this parametric study and the simulations run to evaluate the variables' effect on the regression results. The four "geotechnical variables" are: (i) the number and type of triaxial tests used as observations; (ii) the number of input parameters estimated simultaneously; (iii) the initial value of the input parameters; and (iv) the number of observations used to discretize the triaxial results (i.e. stress-strain curves).

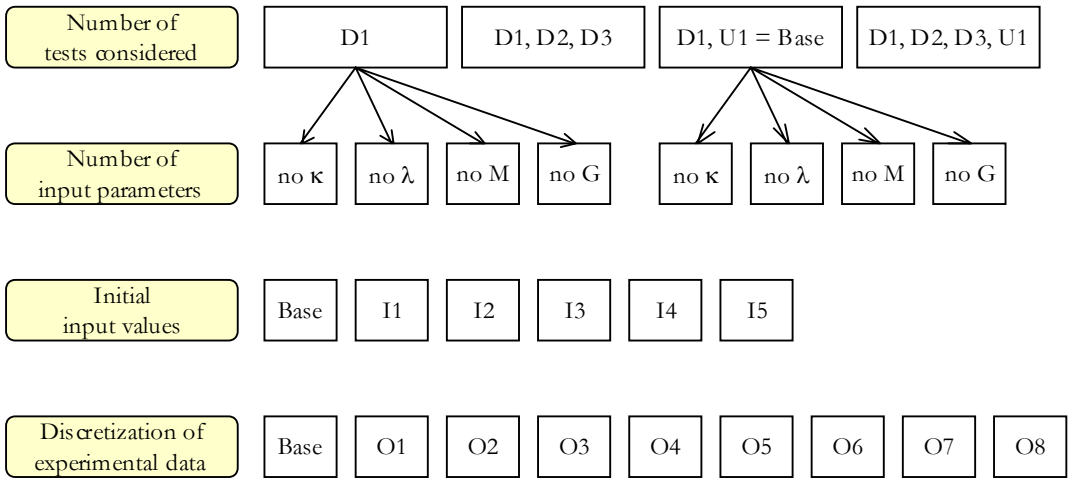

Figure 3-11 Summary of simulations for parametric study on "geotechnical variables"

The simulation discussed in section 3.2, for which results from tests D1 and U1 were used, is herein called "Base." Tables with detailed results of the four parametric studies discussed in this section can be found in Appendix B. Note that the extension test (E1) was never included among the results used to optimize the input parameters because the MCC model, given its characteristics, cannot simulate the strain response recorded during the test. The MCC model features an isotropic yield surface and an associative hardening law. A "wet-of-critical" sample subjected to a reduced extension test undergoes a stress path that, for any value of the input parameters, always produces plastic compression once the stresses reach the yield surface. Experimental results, instead, show dilative strains. This is an example of how optimization by inverse analysis will never work if results computed by the model do not reflect experimental data.

3.3.1 Number and type of triaxial tests used as observations

Four simulations were run for this parametric study. Table 3-8 shows the number of observations and the triaxial tests used to perform the inverse analysis. Simulation ET1 only employs observations relative to D1 test results, simulation ET1b takes into account all three drained tests, simulation ET2 is equivalent to the case discussed in section 3.2 (i.e. uses one drained and one undrained test), and simulation ET3 considers all compression tests. Table 3-9 shows a summary of the results of this parametric study. The fit between experimental and computed results was estimated visually, using Figures 3-12 to 3-16.

	File name	ET1	ET1b	ET2	ET3
Observations used for regression analysis	D1	stress: 24 strains: 24	stress: 24 strains: 24	stress: 24 strains: 24	stress: 24 strains: 24
	D2		stress: 12 strains: 6		stress: 12 strains: 6
	D3		stress: 24 strains: 24		stress: 24 strains: 24
	U1			stress: 30 pressure: 30	stress: 30 pressure: 30

Table 3-8 Observations used for regression analysis

	File name	Initial	ET1	ET1b	ET2	ET3
Visual fit	D1	marginal marginal	good good	good marginal	good good	good marginal
	D2	marginal bad	good marginal	good marginal	good marginal	good marginal
	D3	bad bad	marginal marginal	good good	marginal marginal	good good
	U1	marginal marginal	bad bad	bad bad	good good	good good
	E1	bad bad	marginal bad	marginal bad	marginal bad	marginal bad
Parameters' best-fit values	κ	0.017	0.000	0.000	0.021	0.018
	λ	0.130	0.089	0.065	0.096	0.074
	M	1.09	1.10	1.05	1.04	1.02
	G	4000	6686	9054	11054	9685

Table 3-9 Summary of results for study on number and type of triaxial tests used as observations

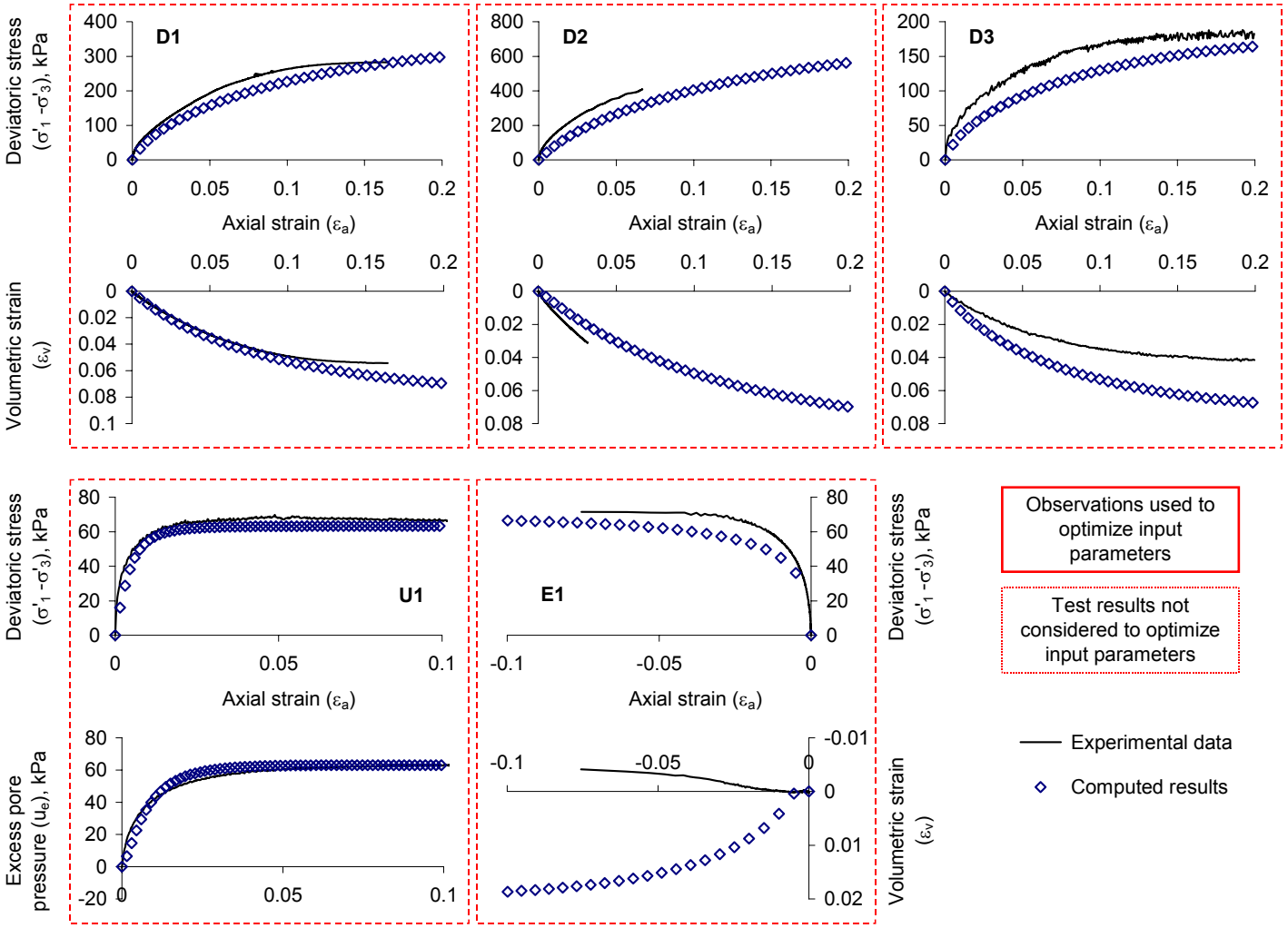

Figure 3-12 Comparison between experimental and computed results for initial estimate of input parameters

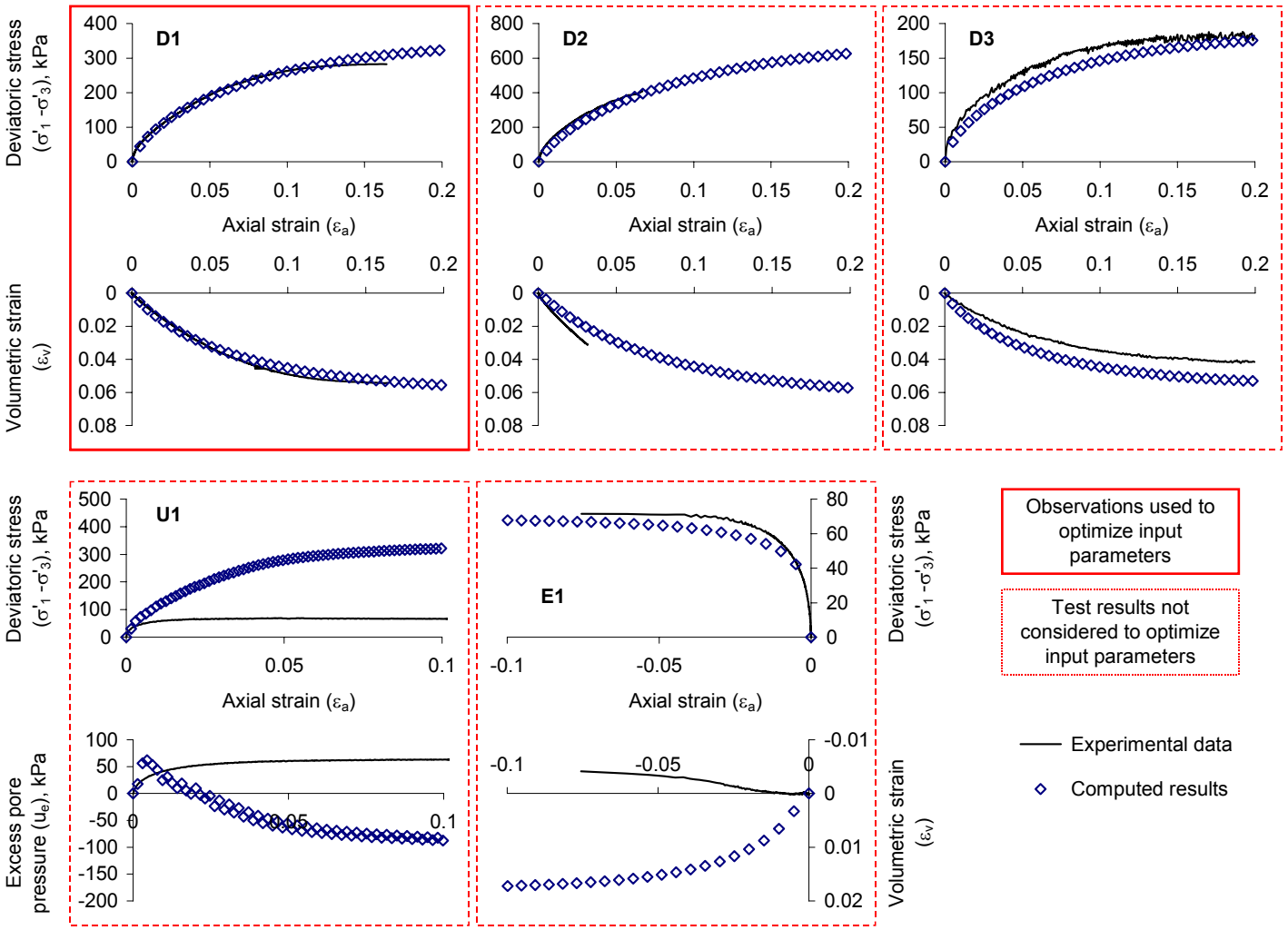

Figure 3-13 Comparison between experimental and computed results for simulation ET1

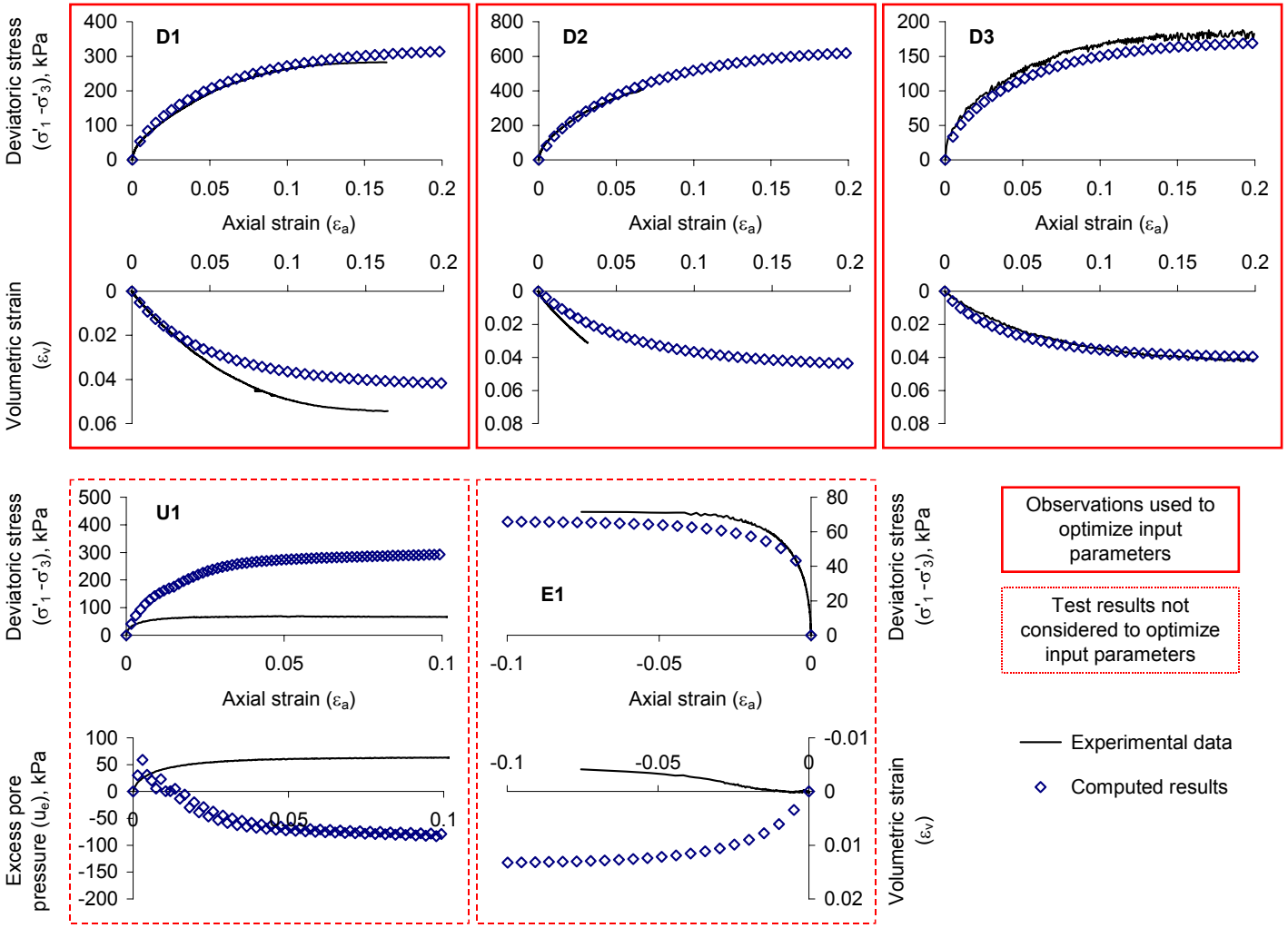

Figure 3-14 Comparison between experimental and computed results for simulation ET1b

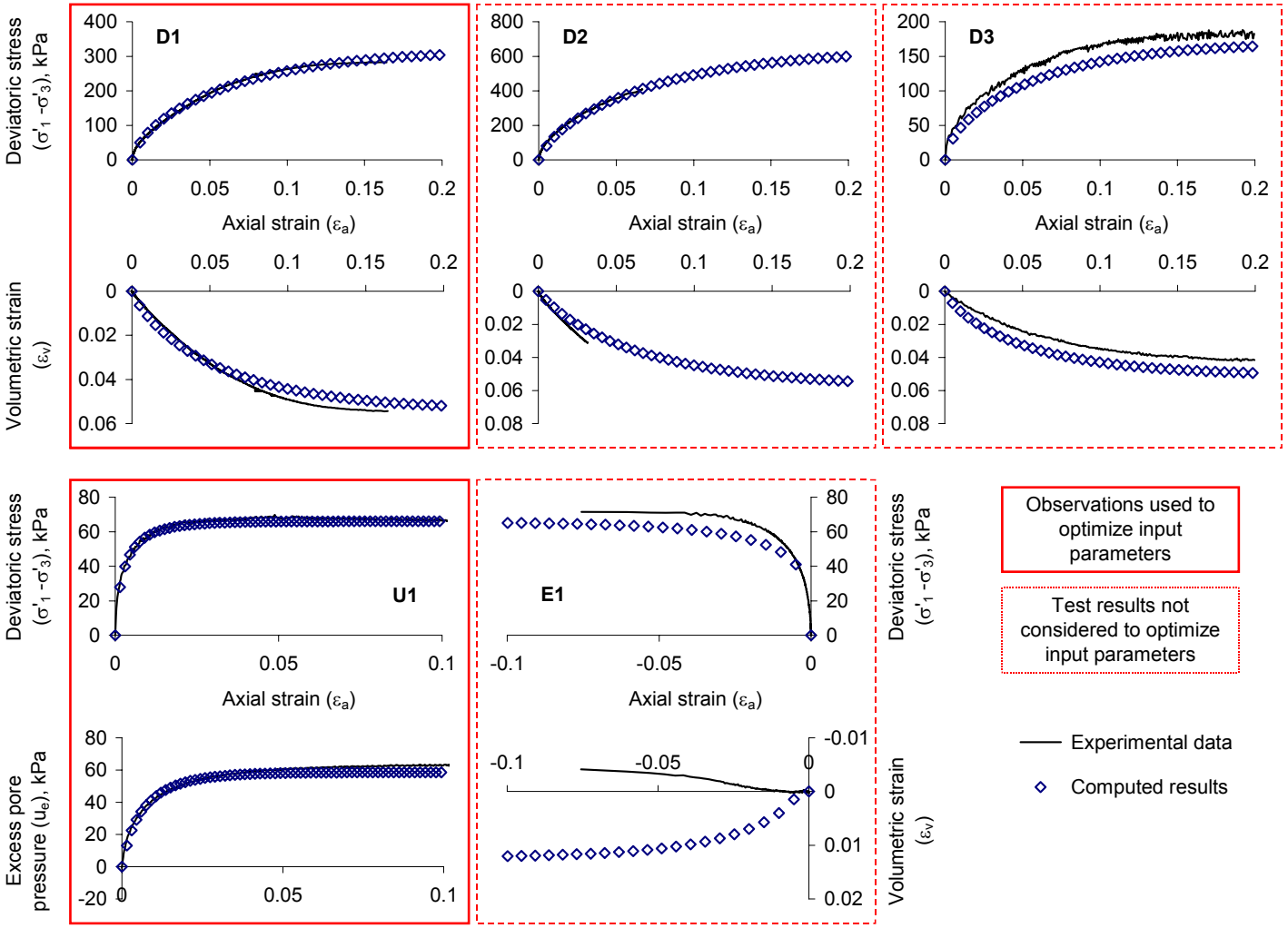

Figure 3-15 Comparison between experimental and computed results for simulation ET2

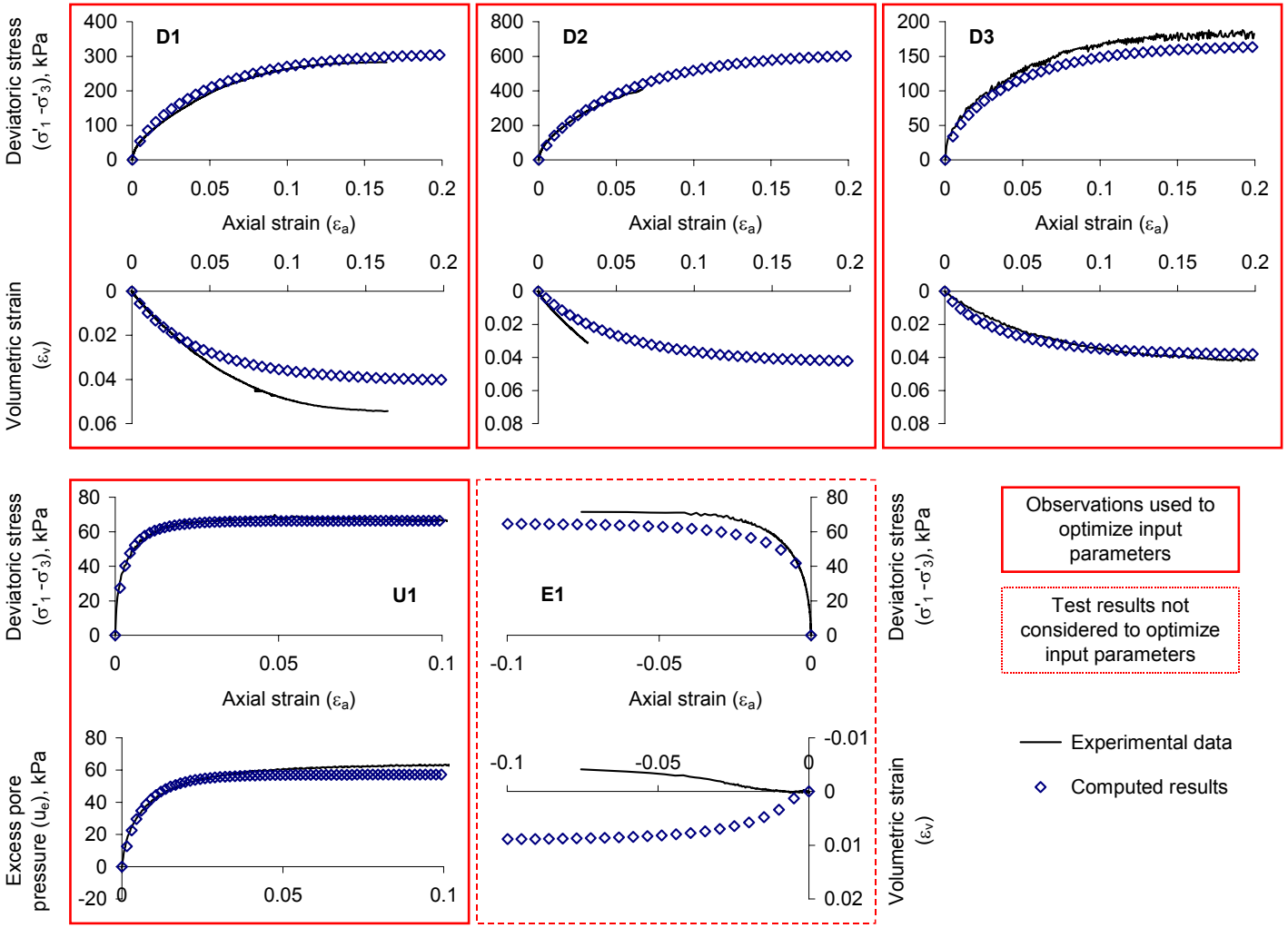

Figure 3-16 Comparison between experimental and computed results for simulation ET3

Figure 3-12 refers to results based on the initial estimates of the input parameters. For all five tests, computed results consistently underestimate the deviatoric stress response. The fit between experimental and computed volumetric strain results is more erratic: the drained computed response matches the data fairly well for test D1, underestimates the experimental response for test D2, overestimates it for test D3, and does not capture the reduction in ε_v recorded for test E1. The undrained test U1 is simulated fairly accurately, except at low strains when the experimental soil response is stiffer than the computed one.

Figure 3-13 refers to results of simulation ET1, where the optimized parameters are based on results of test D1. The fit between experimental and computed data for test D1 is almost perfect. The other two drained tests, D2 and D3, also show a relatively good fit. Computed results for the undrained test U1, however, are much worse that the initial ones and are "illogical" from a geotechnical point of view. This behavior results from an unrealistic estimate of the input parameter κ (the optimal κ is approximately zero), which occurs because of the lack of information in the observations used to condition the optimization. Indeed the optimization is based on results of one drained test performed on a normally consolidated clay sample. It is reasonable to expect that, for this type of test, the value of κ does not have a significant effect on the computed results. Therefore, its optimal value is simply the result of numerical approximations in the computation of the parameter's sensitivities.

Figure 3-14 refers to results of simulation ET1b, where the optimized parameters are based on results of tests D1, D2 and D3. The optimized input parameters values are close to the ones estimated for ET1 and, indeed, the computed response is very similar to ET1. The same comments made for ET1 about the unrealistic estimate of κ hold true. The extra observation points used in the regression (i.e. tests D2 and D3) do not add any extra information about κ to the inverse analysis problem. The simply allow the computed results to better fit the experimental data of all three drained tests simultaneously. Figure 3-15 refers to results of simulation ET2, where both drained and undrained test responses were explicitly considered in the optimization process. The visual fit between experimental and computed results is satisfactory for both the drained and the undrained tests. The behavior of the soil is captured extremely well at both small and large strain levels. Results from this simulation prove that the MCC model, accurately calibrated, is able to model both drained and undrained behavior of a given soil with the same set of input parameters. Figure 3-16 refers to results of simulation ET3, where all four compression tests were used as observations. Results are very similar to ET2, suggesting that adding more observations of the same kind (i.e. results from tests D2 and D3) to a well-posed problem is not strictly necessary. New observations result in an averaging that accounts for the natural variability of the soil samples.

Figure 3-17 graphically summarizes the results of the optimization for the four cases considered in this parametric study. The input parameters' optimized values and their composite scaled sensitivities are plotted on the primary and secondary y-axis, respectively.

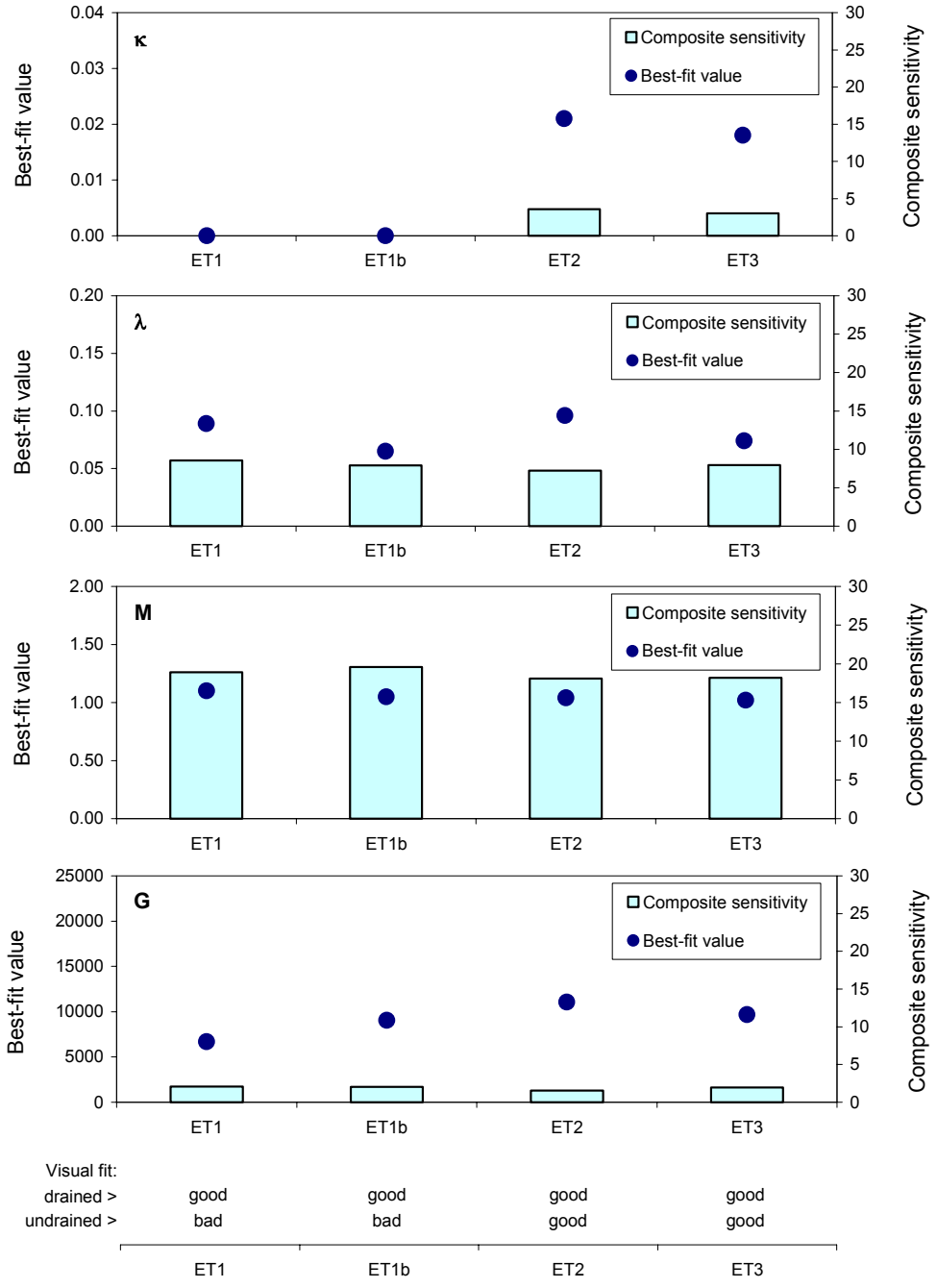

Figure 3-17 Input parameters' optimized values and sensitivities

Results show that the composite scaled sensitivities of parameter κ for cases ET1 and ET1b are negligible. This means that the observations used in the optimization process in these two cases do not bear sufficient information to estimate the parameter. Thus, for the optimization analysis to produce reasonable results, parameter κ should not have been included among the parameters to optimize. Results also show that the sensitivities of parameter G are small for all four cases, yet they are not negligible. Indeed, variations of the value of the stiffness parameter G are important for successfully calibrating the MCC model. The small sensitivity values explain why these variations need to be quite large to improve the fit between computed and experimental results. The larger values of composite scaled sensitivities for M and λ correctly indicate that these two parameters have the largest influence on the MCC predictions of drained and undrained compression responses of "wet-of-critical" clays.

Figure 3-18 shows the values of two statistics indicating model fit: the model error variance, s^2, and the fit improvement, FI. The interpretation of these graphs is not straightforward because the model fit statistics produced by the inverse analysis only refer to the observations used. For instance the values of s^2 and FI for case ET1 seem to indicate a very good fit. And indeed, if we consider test D1 only, the fit between experimental data and computed results is almost perfect. However, if we use the same set of optimized input parameters to model the undrained test, results are extremely unsatisfactory (see Figure 3-13). Obviously the regression algorithm does not "know" anything about tests not

explicitly included in the inverse analysis, thus these model fit statistics cannot be used to judge the ability of a calibrated model to simulate other tests.

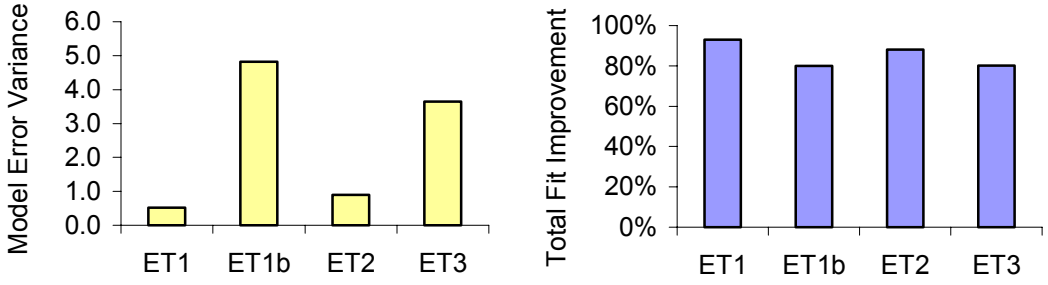

Figure 3-18 Model fit statistics s^2 and FI

Figure 3-19 shows the values of a model statistic, the global objective function (OF), which can be used to assess the "predictive" nature of the calibration of the MCC model by inverse analysis. The global objective function was computed according to Eq. 2.1 using all the observations available (i.e. results from tests D1, D2, D3 and U1), even if they were not used during the regression analysis of the simulation:

$$OF = \left[\underline{y}^{*} - \underline{y}'^{*}\right]^{T} \underline{\omega} \left[\underline{y}^{*} - \underline{y}'^{*}\right] \tag{3.3}$$

where $\underline{y}^{*}$ is the vector of all available observations; $\underline{y}'^{*}$ is the vector of the computed values which correspond to the observations; and $\underline{\omega}$ is the weight matrix used in the regression.

Note that ET3 is the only simulation for which OF is equal to the objective function minimized by the optimization algorithm (i.e. S($\underline{b}$) of Eq. 2.1). Figure 3-20 shows, in pie-

chart format, the contribution of the observations from the various tests to the global objective function values.

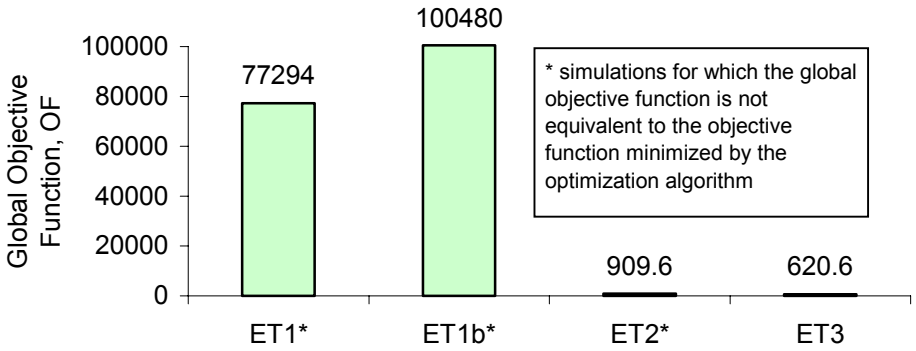

Figure 3-19 Global objective function values

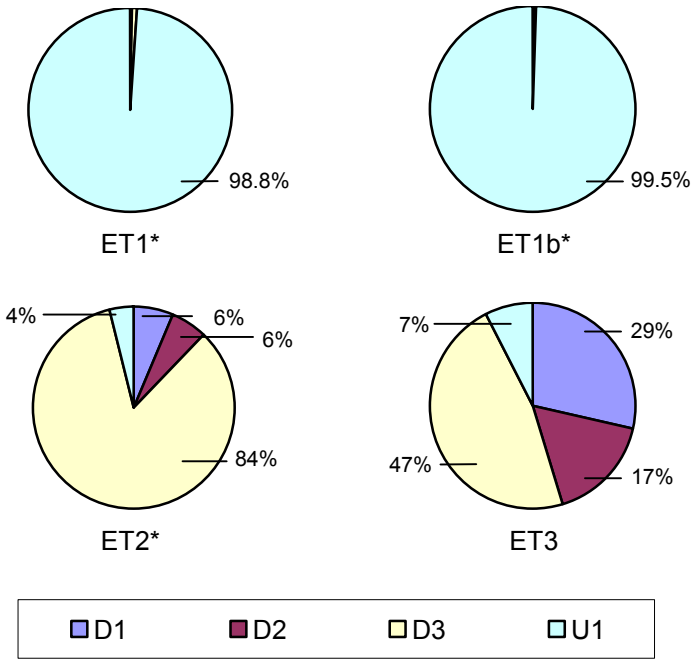

Figure 3-20 Contribution of observations from the various tests to the global objective function values (i.e. "distribution of errors" of the four simulations)

Results show that the global objective function values for ET1 and ET1b, where the optimized parameters are only based on results of drained tests only, are about two orders of magnitudes higher than values relative to ET2 and ET3, where the optimized parameters are based on results that include the undrained test U1. Simulations ET1 and ET1b are able to fit the experimental data of the drained compression tests (i.e. the contribution to the value of global objective function of tests D1, D2 and D3 is negligible), yet they are unable to "predict" the experimental results of the undrained test, U1. On the contrary, the "distribution of errors" for simulations ET2 and ET3 is relatively even among the four tests. Note that the value of OF for ET2, where the optimized parameters are based on results from D1 and U1, is very close to the value of OF for ET3, where the optimized parameters are based on results from all four tests. This confirms that the problem for case ET2 is well-posed, and that one drained test and one undrained tests are sufficient to predict the behavior of clay samples sheared in triaxial compression conditions. When more tests are available (ET3), however, the calibration of the MCC model implicitly takes into account the natural variability of a soil, which causes results from different soil samples to be always slightly different even if tested in the same conditions.

3.3.2 Number of input parameters considered

Eight simulations were made to evaluate the effects of the number of parameters on the optimized results. For any given simulation only three of the four MCC input parameters were optimized simultaneously. Simulations P1 to P4 only use observations from D1, and

their results are therefore compared to results from ET1. Simulations P5 to P8 use results from D1 and U1, and are therefore compared to ET2. When a parameter was not optimized its value was kept constant at its initial estimate.

Table 3-10 shows results relative to simulations P1 to P4. For case P1 parameter κ was not optimized, for cases P2, P3 and P4 the parameters excluded from the optimization were λ, M and G, respectively. The visual fit was evaluated, as for the previous parametric study, from stress-strain plots. Figure 3-21 graphically summarizes the results of the optimization. The input parameters' optimized values and their composite scaled sensitivities are plotted on the primary and secondary y-axis, respectively.

	File name	ET1	P1	P2	P3	P4
Parameters optimized		κ, λ, M, G	λ, M, G	κ, M, G	κ, λ, G	κ, λ, M
Visual fit top line q-ε_a bottom line ε_v-ε_a (drained) u-ε_a (undrained)	D1	good good	good good	good good	good good	good good
	D2	good marginal	good marginal	good marginal	good marginal	marginal marginal
	D3	marginal marginal	marginal marginal	marginal marginal	marginal marginal	marginal marginal
	U1	bad bad	good good	bad bad	bad bad	bad bad
	E1	marginal bad	marginal bad	bad bad	marginal bad	marginal bad
Parameters' best-fit values	κ	0.000	0.017*	0.078	0.000	0.000
	λ	0.087	0.096	0.13*	0.087	0.108
	M	1.10	1.07	1.00	1.09*	1.15
	G	6686	6279	4978	6827	4000*

* parameter kept constant and not optimized

Table 3-10 Summary of results for study on number of input parameters considered (compare with ET1)

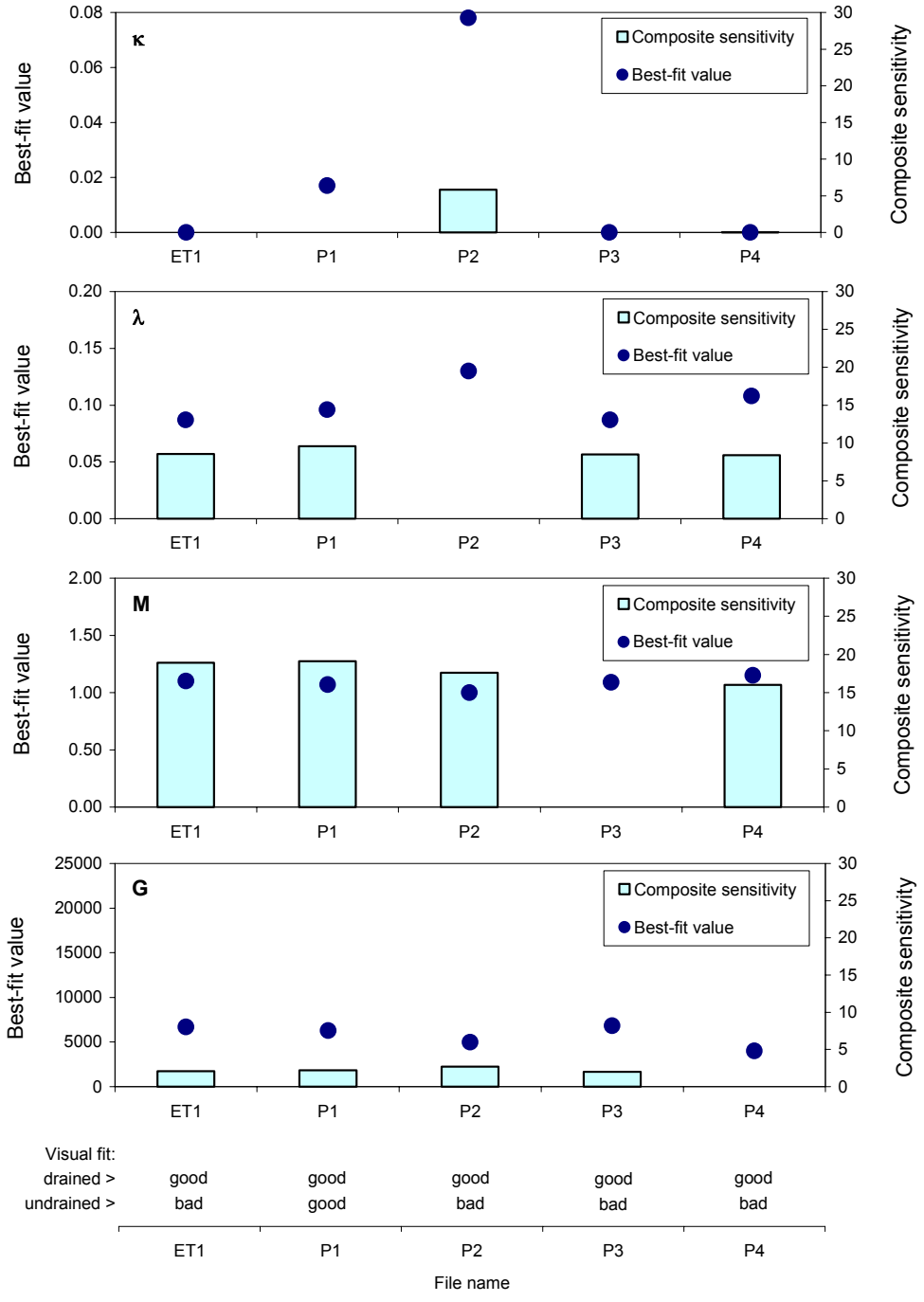

Figure 3-21 Input parameters' optimized values and sensitivities (compare with ET1)

Results show that every simulation successfully matched D1 test results. However, cases P2, P3 and P4 yield unreasonable optimized values of parameter κ, and only P1 produces a good fit for the undrained as well as for the drained tests. The unreasonable results derive, for cases P3 and P4, from the very low sensitivity value of parameter κ and, for case P2, from the fact that the high estimate of κ compensates for the high value of λ (not optimized in this simulation). These results confirm what was proved in the previous parametric study, namely that a parameter cannot be estimated by regression analysis if the observations used are not influenced by its changes. Results also show that the initial estimate of κ is reasonably good because when κ is kept constant (e.g. case P1), and only λ, M and G are optimized, results improve the fit for both drained and undrained tests. For the same reasons results indicate that the initial estimate of λ is not accurate enough.

Table 3-11 shows a summary of results of simulations P5 to P8. For case P5 parameter κ was not optimized, for cases P6, P7 and P8 the parameters excluded from the optimization were λ, M and G, respectively. Results show that simulations P5, P6 and P7 all produce a good fit between computed and experimental data and only simulation P8 does not successfully match the test results. This demonstrates that more than one set of "optimal parameter values" is able to model the test results correctly. The non-uniqueness of the parameters' estimates, however, was to be expected. In the MCC model, the constitutive equations are non-linear and depend from more than one input parameter. For instance, the hardening law depends from both κ and λ; thus, the same results can be produced by

more than one combination of these parameters' values. Moreover the MCC model has an associative flow rule; therefore plastic strains are also influenced by the position of the yield surface, which in turn depends from the value of parameter M. Note that, when parameter G was kept constant to its initial value (P8), the optimization did not converge to a good set of optimized results, mainly because the initial estimate of G is much lower than any of its optimized values. This illustrates that if the initial estimate of a parameter is not "reasonable," changes in other parameters' values cannot compensate for the incorrect estimate. Figure 3-22 graphically shows the input parameters' optimized values and their composite scaled sensitivities.

	File name	ET2	P5	P6	P7	P8
Parameters optimized		κ, λ, M, G	λ, M, G	κ, M, G	κ, λ, G	κ, λ, M
Visual fit top line q-ε_a bottom line ε_v-ε_a (drained) u-ε_a (undrained)	D1	good good	good good	good marginal	good good	good marginal
	D2	good marginal	good marginal	good good	good marginal	marginal marginal
	D3	marginal marginal	marginal marginal	marginal marginal	marginal marginal	marginal marginal
	U1	good good	good good	good good	good good	marginal marginal
	E1	marginal bad	marginal bad	marginal bad	marginal bad	marginal bad
Parameters' best-fit values	κ	0.021	0.017*	0.025	0.021	0.016
	λ	0.096	0.092	0.13*	0.105	0.093
	M	1.04	1.04	1.10	1.09*	1.10
	G	11054	9237	11711	9269	4000*

* parameter kept constant and not optimized

Table 3-11 Summary of results for study on number of input parameters considered (compare with ET2)

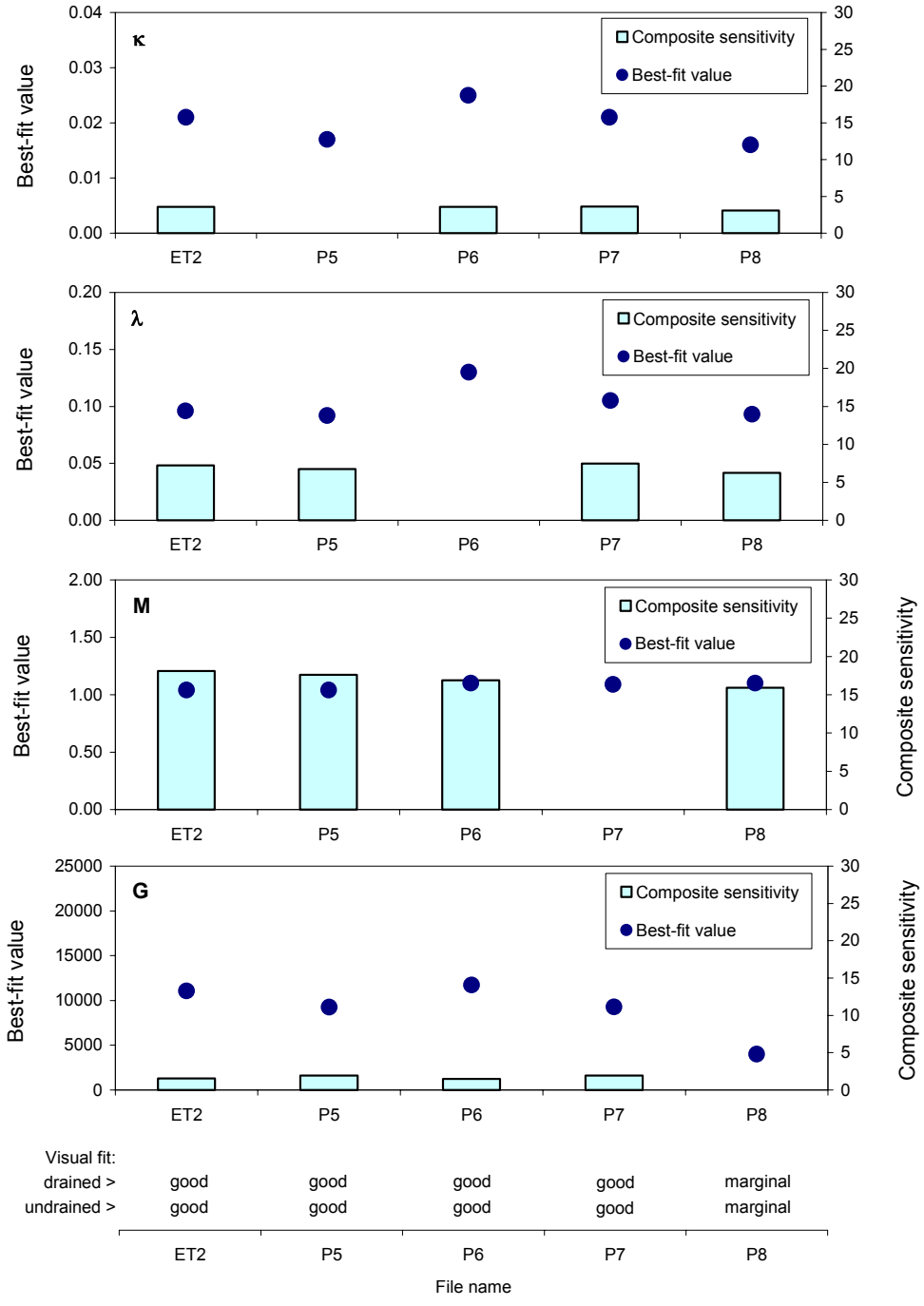

Figure 3-22 Input parameters' optimized values and sensitivities (compare with ET2)

Results show that the composite scaled sensitivity values of a given parameter do not change significantly for the four simulations, indicating that all parameters are important in the regression analysis. Yet, the results of the optimized simulations indicate that the MCC model can be successfully calibrated even when a parameter is excluded from the optimization, provided that the initial parameter estimate is "reasonable." Therefore, for larger problems (e.g., excavations) with a large number of input parameters, if most of the parameters are reasonably estimated, one can still effectively optimize the simulation by focusing on the most sensitive ones.

3.3.3 Initial values of input parameters

Six simulations were made to evaluate the effects that initial values of parameters have on the optimized results. Observations refer to results from tests D1 and U1, thus the base case of this parametric study is equivalent to simulation ET2. Table 3-12 shows the initial parameter values for the six cases.

	File name	Base	I 1	I 2	I 3	I 4	I 5
Initial parameters' values	κ	0.017	0.0085	0.0255	0.0017	0.034	0.17
	λ	0.13	0.065	0.195	0.013	0.26	1.3
	M	1.09	0.545	1.635	0.109	2.18	10.9
	G	4000	2000	6000	400	8000	40000

Table 3-12 Initial parameter values

The values of the input parameters were varied within two orders of magnitudes around their initial estimates. For case I1 the values of the input parameters were equal to half the values they had in the Base case. For cases I2 and I4 their base values are multiplied by 1.5 and 2.0 respectively. For case I3 and I5 the base values are respectively divided and multiplied by 10.

Table 3-13 shows a summary of the results of this parametric study. The fit between experimental data and results simulated using the initial sets of parameters' values is always unsatisfactory because most of these values are clearly unreasonable from a geotechnical point of view. Yet they were used to test the ability of the regression algorithm to converge to a reasonable set of parameters' values. Results show that, for every simulation, the optimization successfully converged to the essentially same optimized set of parameters' values.

	File name	Base	I 1	I 2	I 3	I 4	I 5
Initial model fit	Visual (D1): q-ε_a and ε_v-ε_a	marginal marginal	bad bad	bad bad	bad bad	bad bad	bad bad
	Visual (U1): q-ε_a and u-ε_a	marginal marginal	bad bad	bad bad	bad bad	bad bad	bad bad
	Initial S(b)	789.5	7853.8	4486.3	21275	17151	361050
Parameters' best-fit values	κ	0.021	0.021	0.021	0.021	0.021	0.021
	λ	0.096	0.097	0.097	0.096	0.097	0.097
	M	1.04	1.04	1.04	1.04	1.04	1.04
	G	11054	11127	11018	10975	11075	11088
Final model fit	Visual (D1): q-ε_a and ε_v-ε_a	good good	good good	good good	good good	good good	good good
	Visual (U1): q-ε_a and u-ε_a	good good	good good	good good	good good	good good	good good
	Final S(b)	93.8	93.8	93.8	93.8	93.8	93.8
	# iterations	5	6	5	7	6	11

Table 3-13 Results for study on initial values of input parameters

Results from the six different simulations differ only in the number of iterations the regression analysis needs to converge to the optimal solution. The further the initial parameters are from their optimal values, the more iterations the optimization algorithm needs to converge.

Figure 3-23 shows the variation of the objective function from its initial values to the final optimized value during the regression iterations. The y-axis is plot in logarithmic scale for graphical purposes. The point indicating the final iteration for a given simulation is plotted

with a larger symbol. The results show that the value of the objective function gradually decreases until it converges, for all simulations, to a common value of 93.8.

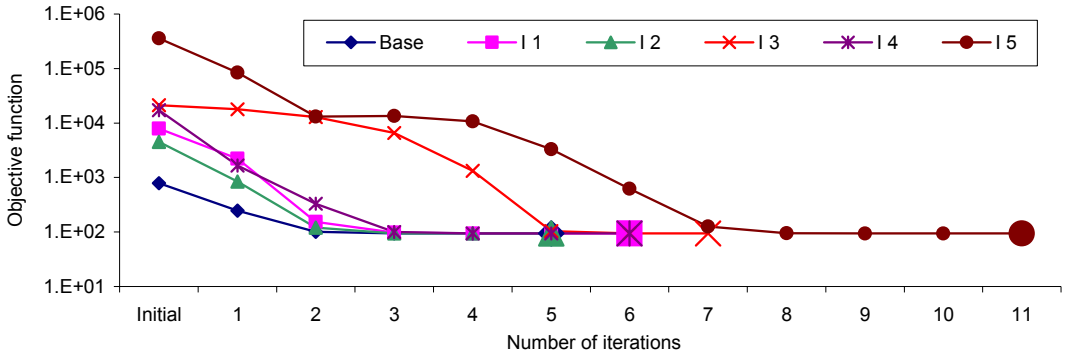

Figure 3-23 Variation of objective function during regression iterations

Figure 3-24 show the variation of input parameters' values during the regression iterations. All four parameters, for almost all cases, converge univocally from their initial values towards their final optimal values. I5 is the only simulation for which values of parameters κ and G fluctuate around the optimal solution before reaching it.

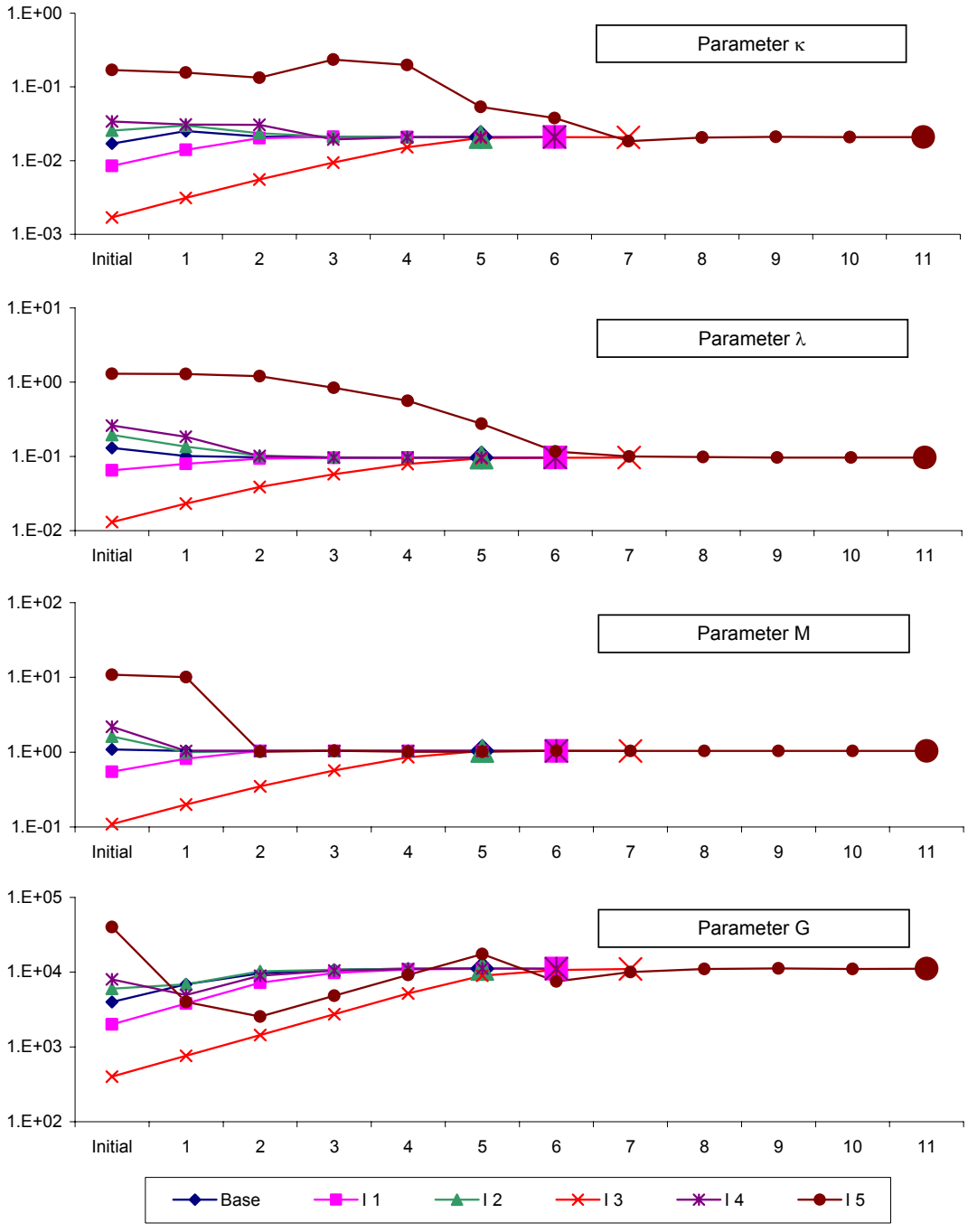

Figure 3-24 Variation of input parameters' values during regression iterations

The surprisingly good results prove that a well-posed problem (i.e. correct soil model, appropriate choice of parameters to estimate simultaneously, observations bearing appropriate information to estimate parameters) is able to converge to a unique solution, even if the initial estimates of the input parameters are far from their optimal values. However, if one of the parameters is excluded from the optimization scheme, then the excluded parameter must be close to the actual value or, as shown in last section, the other parameters will converge to different optimized values.

3.3.4 Discretization of experimental data

Nine simulations were conducted to evaluate the effects of the number of observations on the optimized parameters. Observations, as for the previous parametric study, refer to results from tests D1 and U1, thus the base case is equivalent to simulation ET2. Four "observation curves" were used for each simulation: two for the drained test (i.e. the stress-strain and volume change responses) and two for the undrained test (i.e. the stress-strain and pore pressure responses). Table 3-14 shows the criteria used to discretize the curves, and total number of observations used in the regression. In simulations O1 to O5, the number of observations was progressively reduced by half. Simulation O6 only considers observations relative to small strains while O7 uses small strain observations and a final failure point. Simulation O8 only uses two "failure" observations per curve.

File name	Drained curves	Undrained curves	Total # of observations
Base	$\Delta\varepsilon_a$ = 0.5%	$\Delta\varepsilon_a$ = 0.15%	108
O 1	$\Delta\varepsilon_a$ = 1%	$\Delta\varepsilon_a$ = 0.3%	54
O 2	$\Delta\varepsilon_a$ = 2%	$\Delta\varepsilon_a$ = 0.6%	26
O 3	$\Delta\varepsilon_a$ = 4%	$\Delta\varepsilon_a$ = 1.2%	12
O 4	ε_a = 6%, 12%	ε_a = 2.1%, 4.5%	8
O 5	ε_a = 12%	ε_a = 4.5%	4
O 6	ε_a up to 3% ($\Delta\varepsilon_a$ = 0.5%)	ε_a up to 0.9% ($\Delta\varepsilon_a$ = 0.15%)	24
O 7	ε_a up to 3% + ε_a = 12%	ε_a up to 0.9% + ε_a = 4.5%	28
O 8	ε_a = 11%, 12%	ε_a = 4.2%, 4.5%	8

Table 3-14 Criteria used to discretize the stress-strain curves

Table 3-15 shows the results of this parametric study in terms of visual fit between experimental and computed results. For the first five cases (Base, O1 to O4) the number of observations does not influence the model fit significantly. For the remaining four cases the overall fit is not satisfactory. When small strain data (O6, O7) were considered as observations the model results match the experimental data at those strain level but fail to reproduce the soil response up to failure. Results show that, provided that the observations are "properly" chosen (i.e. they are representative of the response variation over the range of strains of interest), a relatively low number of them produces the same results as does a large number. For these triaxial tests, as little as 2 data points per curve (O4) produced a good fit of the data.

Figure 3-25 shows the fit improvement plotted as a function of the number of observations used in the regression. The graph is presented to highlight the risk of interpreting model fit

statistics incorrectly. Results seem to show that the fit improves as the number of observations decreases. This conclusion should not be inferred by the plot, whose results reflect the fact that model fit statistics produced by the inverse analysis only refer to the observations used.

File name	Visual fit (overall)	Visual fit (small strains)
Base	good	good
O 1	good	good
O 2	good	good
O 3	good	good
O 4	good	good
O 5	bad	bad
O 6	bad	good
O 7	bad	good
O 8	bad	bad

Table 3-15 Summary of visual fit between experimental and computed results

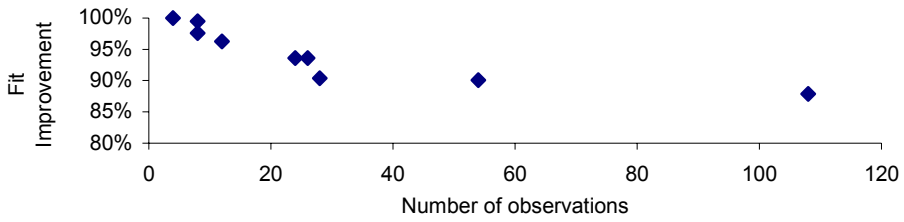

Figure 3-25 Fit improvement vs. number of observations used in regression analysis

Figure 3-26 graphically summarize the results of the optimization for the nine cases considered in this parametric study. Once again, the plots show that λ and M are the

parameters to which the results are most sensitive and that G (i.e. the least sensitive parameter) is the parameter that exhibits the largest variation throughout the study.

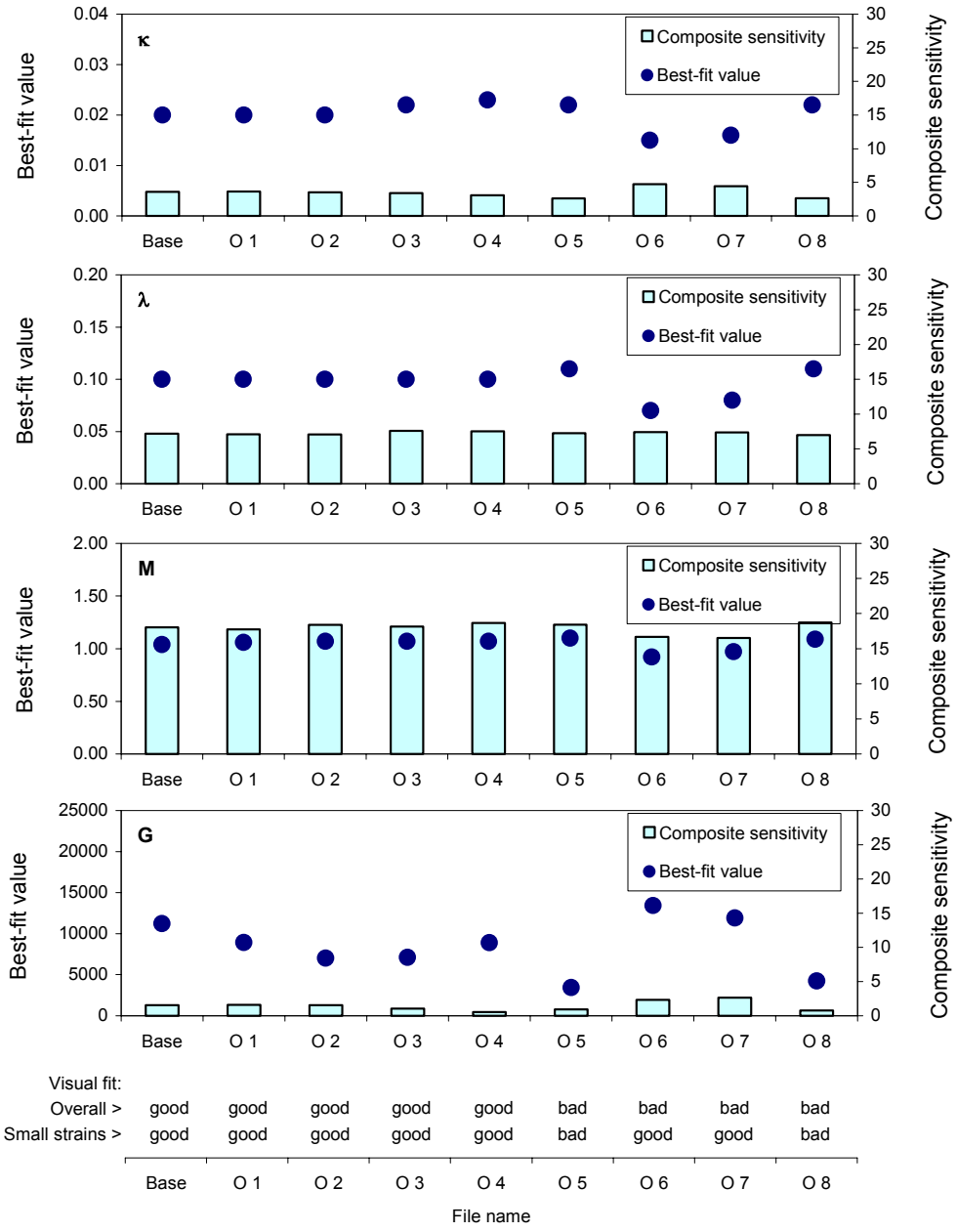

Figure 3-26 Input parameters' optimized values and sensitivities

3.3.5 Comments on parametric study results

A parametric study on the regression variables related to "geotechnical" issues has been conducted to evaluate their influence on the calibration of a soil model by inverse analysis. The geotechnical variables studied were:

1. the number and type of triaxial tests used as observations,
2. the number of input parameters estimated simultaneously,
3. the initial value of the input parameters, and
4. the number of observations used to discretize the triaxial results.

From the results of the parametric study the following conclusions can be drawn.

1. Observations for both drained and undrained tests need to be used to successfully calibrate the four MCC input parameters simultaneously. Adding more observations of the same kind to a well-posed problem serves to take into account and average the natural variability of the soil samples. Model fit statistics can only be used to evaluate the fit between computed results and experimental data whose observations are included in the regression analysis. These statistics cannot be used to forecast the goodness of simulations for tests not included in the regression.

2. Input parameters cannot be estimated by regression analysis if the observations used are not influenced by its changes. More than one set of parameter values is able to "appropriately" model the test results if not all model parameters are optimized. If the initial estimate of one parameter is not "appropriate", changes in values of other parameters cannot compensate for the incorrect estimate.

3. Well-posed problems are able to converge to a unique solution, even if the initial estimates of the input parameters are far from their optimal values.

4. When observations are "properly" chosen a relatively low number of them produces the same results of a large number of them.

3.4 PARAMETRIC STUDY ON "OPTIMIZATION VARIABLES"

In the previous section the effects of the "geotechnical variables" on the inverse analysis' results have been evaluated. Those variables are not the only ones that affect the results of a regression analysis. In UCODE, users need to input values for a series of internal "optimizazion variables." This section describes the parametric study conducted on these variables. The "optimization variables" have been grouped in four categories, according to the way in which their changes affect the regression algorithm:

8) Weighting of observations. Users can assign weights of observations in terms of variance, σ_i^2, standard deviation, σ_i, or coefficient of variation, cov_i.

9) Convergence criteria. Users define the convergence criteria in terms percentage of maximum parameter change, TOL, and percentage of objective function change over three consecutive iterations, SOSR.

10) Regression control. Users specify the maximum fractional parameter change per iteration, MAX-CHANGE.

11) Sensitivity calculation. Users specify the fractional amount, PERTURBATION, by which a parameter is perturbed to calculate the sensitivity matrix and whether a forward or central difference approximation is used (variable DIFFERENCING).

Note that all the simulations conducted for this study use observations from tests D1, D2, D3 and U1. Tables with detailed results of the four parametric studies discussed in this section can be found in Appendix B.

3.4.1 Weighting of observations

In UCODE, the weight of every observation (Eq. 2.14) is equal to the inverse of its error variance. The error variances are either directly input by the users or computed from specified values of standard deviations or coefficients of variation (Eq. 2.12). Figure 3-27 shows the shape of two typical "error envelopes." In the first chart the errors of the observations are specified using a constant value of standard deviation, σ_i, and in the second chart the errors are specified through a constant coefficient of variation, cov_i.

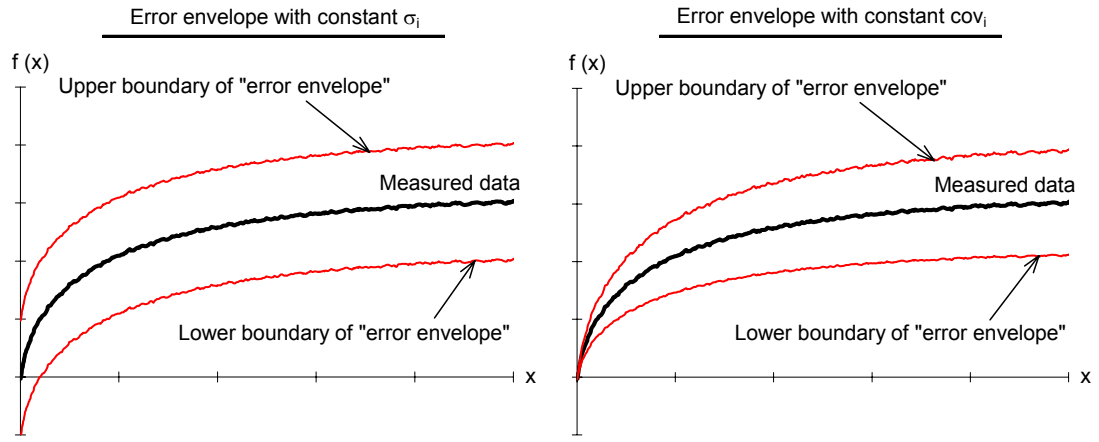

Figure 3-27 "Error envelopes" for observation errors specified trough constant σ_i and cov_i

Table 3-16 shows the weights used for this parametric study. The first row of the table shows the statistic used to specify the weights, the following two rows show the value of that statistic used for the drained tests data, the final two rows refer to the statistic's value for the undrained test results. Six different weighting scenarios have been considered. Note that simulation W1 is equivalent to simulation ET3 (section 3.3.1).

		W1	W2	W3	W4	W5	W6
Weighting expressed using…	Statistic	cov	cov	σ	σ	σ	σ
	Value for q (drained)	0.05	0.05	0.5kPa	0.5kPa	5kPa	5kPa
	Value for ε_v	0.1	0.05	0.05%	0.05%	0.50%	0.50%
	Value for q (undrained)	0.05	0.05	0.5kPa	3.5kPa	5kPa	35kPa
	Value for u	0.05	0.05	3.5kPa	3.5kPa	5kPa	35kPa

Table 3-16 Weights used for observations

In the first two simulations (W1 and W2) weights are assigned using coefficients of variation (Eq. 2.12). This means that the error associated with an observation increases as the value of the observation increases. For instance, for cov=0.05 and a deviatoric stress of 100kPa, the standard deviation of that observation is equal to 5kPa. The purpose of this choice is to provide more weight to the initial readings of the stress-strain response (the weight of an observation is inversely proportional to its error). Indeed, initial observation points are very important in "characterizing" the computed results because, for a given model (e.g. MCC), the shape of the stress-strain curves is strongly influenced by its initial response.

In the last four simulations (W3, W4, W5 and W6) weights are assigned based on measurement errors (see Appendix B for details on computations). For W4 the coefficient of variations are directly computed from measurement device's errors ($\pm E_i$) assuming that the measurement errors have a normal distribution around the correct value and that $\pm 2E_i$ represents the 95% confidence interval of the distribution. To get the standard deviation, σ_i, the following formula has been used:

$$\sigma_i = \frac{2E_i}{1.96} \tag{3.4}$$

For W3 the weight of the deviatoric stress q for the undrained case is assumed to be the same of that of the drained tests. For W5 and W6 the errors of the drained tests

observations are assumed to be 10 times larger than those used for cases W3 and W4, respectively.

Table 3-17 shows the initial and optimized input parameters' values for all cases. Results indicate that weighting has little effect on the estimation of parameters λ and M (i.e. the most sensitive parameters), and that parameters κ and G (i.e. the least sensitive parameters) show the greatest changes. Indeed, since κ and G have the least effect on the computed results, they have to change the most to affect the solution.

	Initial	W1	W2	W3	W4	W5	W6
κ	0.018	0.019	0.019	0.023	0.029	0.02	0.029
λ	0.11	0.082	0.08	0.091	0.095	0.089	0.095
M	0.95	1.02	1.01	1.04	1.03	1.04	1.03
G	6670	12950	12390	8991	8557	9027	8593

Table 3-17 Initial and optimized values of input parameters

Figure 3-28 shows the optimized parameters in terms of percentage change from their initial value. The percentage change of parameter p from its initial estimate, PC_p, is defined as:

$$PC_p = \frac{p_{opt} - p_{init}}{p_{init}} \quad \text{for p=1, NP} \tag{3.5}$$

where p_{init} is the values of the input parameter before the optimization, and p_{opt} is the values of the input parameter after the optimization.

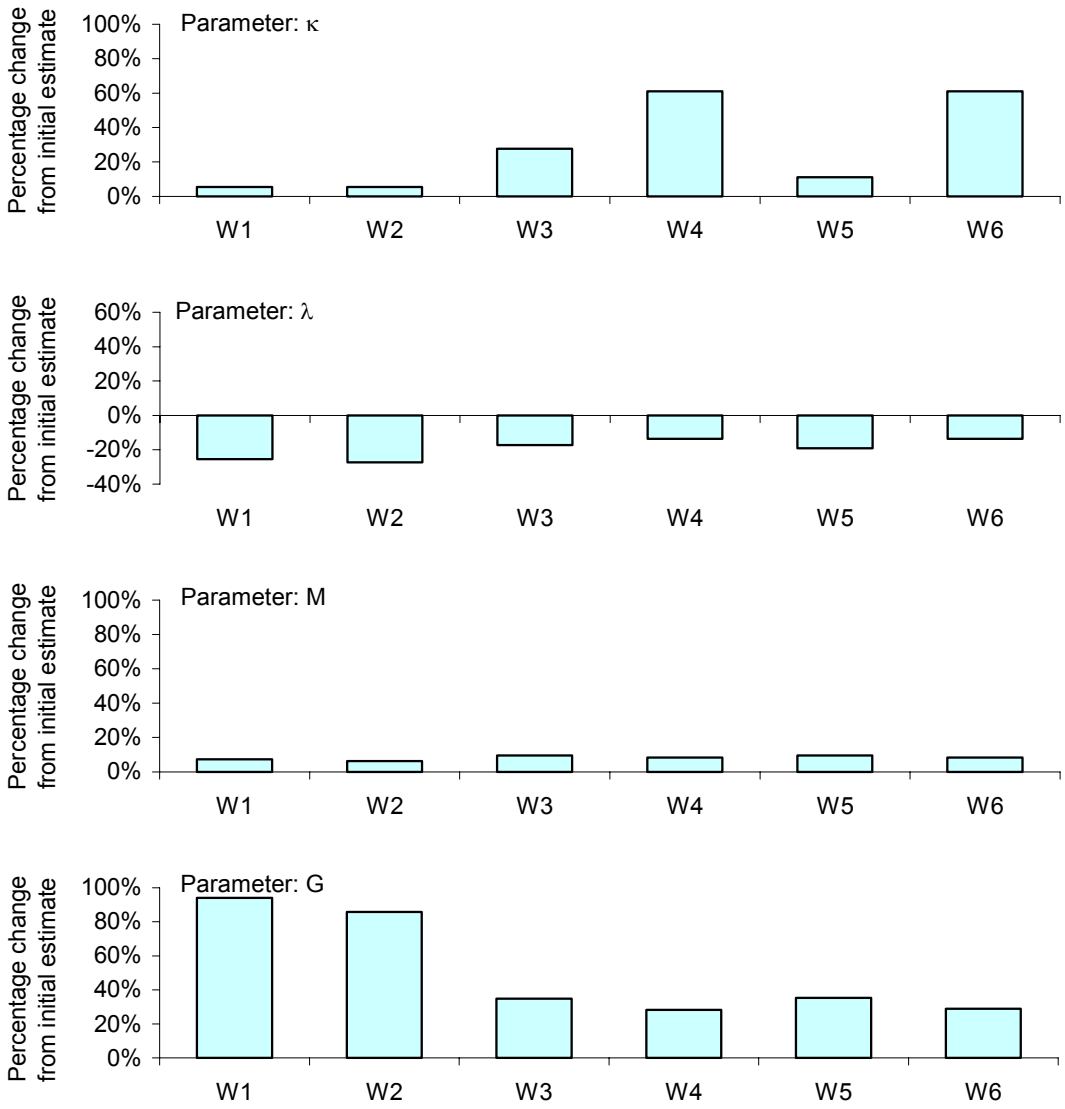

Figure 3-28 Optimized parameters' percentage change from initial estimates

Results show that the weighting influences the optimized values of κ and G greatly. W5 yields the set of optimized input parameters with the smallest change from the initial set of parameters.

In Figure 3-29 results are shown in term of three statistics representing model fit and in terms of visual fit (satisfactory for all six simulations).

1. The model error variance, s^2, is plotted in the first chart. The relatively low values of s^2 for W1 and W2 indicate that the weighting defines an error envelope around the experimental data consistent with the computed results. The extremely high values of s^2 for W3 and W4, where the weights reflect the uncertainty of the measurement errors, suggest that this uncertainty contribution is very low compared to the uncertainty related to the natural variability of the material, which is implicitly considered in the visual estimate of the fit. When 10-times larger errors are used to assign the weights (e.g. W5, W6), the computed results match the experimental data within the accuracy of the errors.

2. The fit improvement, FI, is plotted in the second chart. FI values tell one what percentage the optimized results improved as compared to the initial fit. The highest FI values are obtained for cases W3, W4, W5 and W6, which do not necessarily reflect the best fit in the data.

3. The third chart shows the number of iterations needed for the regression analysis to converge. For the first five cases relatively few iterations were needed to get to the optimal solution, while W6 needs 9 iterations to converge. The tolerance criterion ending the regression is shown at the bottom of this chart.

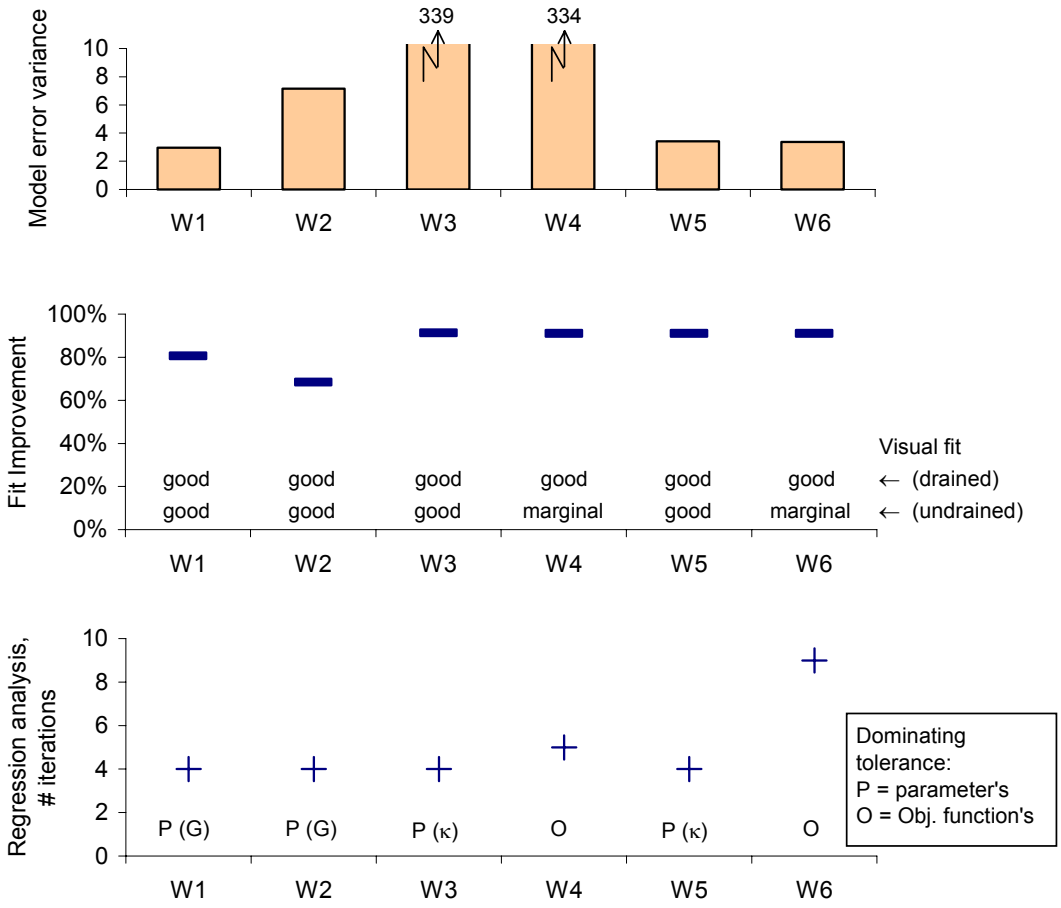

Figure 3-29 Statistics indicating model fit

Overall, model fit statistics show that the best results do not occur when weighting takes into account measurement errors only (e.g. W3, W4). Instead they seem to show the

importance of considering other uncertainty contribution (i.e. sampling, sample preparation and natural variability of the clay) to the discrepancy between measured data and computed results.

3.4.2 Tolerance on convergence criteria

Convergence criteria are needed for the modified Gauss-Newton iterative process used in UCODE. This parametric study aims at evaluating the effect on the optimization results of the values of the tolerance parameters of the convergence criteria. The parameter estimation converges if either one of two following convergence criteria are satisfied:

$$\max\left|\frac{d_j^{\,r}}{b_j^{\,r}}\right| < TOL \quad \text{for j=1,NP} \tag{3.6}$$

$$\Delta S\left(\underline{b}\right) < SOSR \quad \text{for three sequential iterations} \tag{3.7}$$

where b_j^r is the value of parameter j at iteration r, d_j^r is the parameter change at iteration r, and $\Delta S(\underline{b})$ is the change in value of the objective function between two iterations.

The convergence criteria user-defined quantities are two: TOL and SOSR. They control the end of the iterative process, but they do not influence the results of the analysis at a given iteration. Thus, it is possible to analyze their effect by performing one single optimization analysis, assigning very low values to the two tolerance parameters and looking at the

regression results at each iteration. The simulation used for this purpose is equivalent to simulation ET3 except for the very low value used for TOL=SOSR=0.1%.

Figure 3-30 shows the objective function's variation at each iteration in terms of absolute value and percentage change from the previous iteration. Figure 3-31 shows the input parameters' maximum percentage change at each iteration.

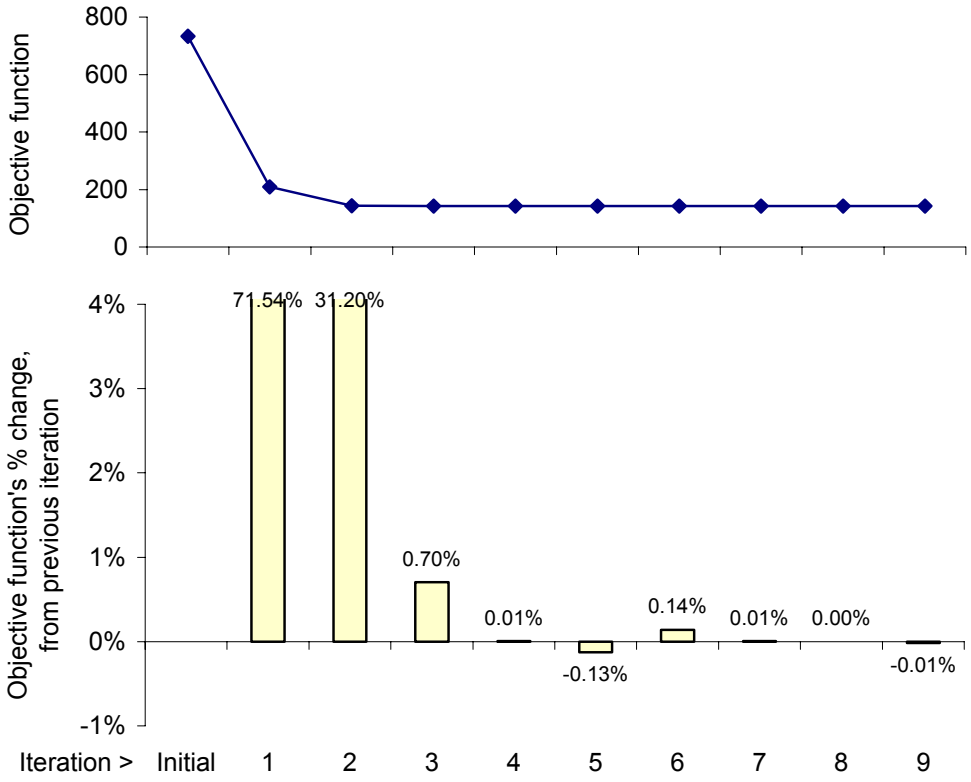

Figure 3-30 Objective function change at each iteration

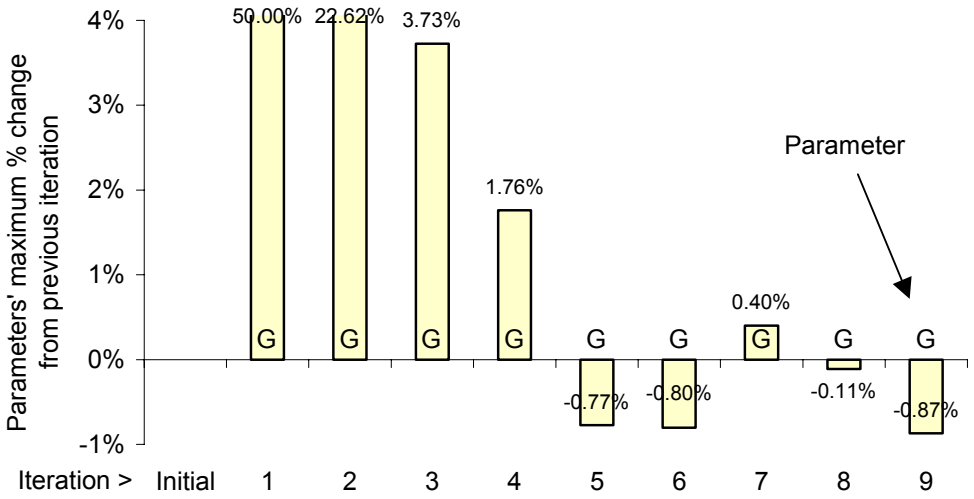

Figure 3-31 Input parameters' maximum percentage change at each iteration

Figure 3-32 shows the variation of the four input parameters at each iteration. Note that changes in parameters' values after iteration #3 are negligible, yet the regression takes 9 iterations to converge because of the very low tolerance values specified.

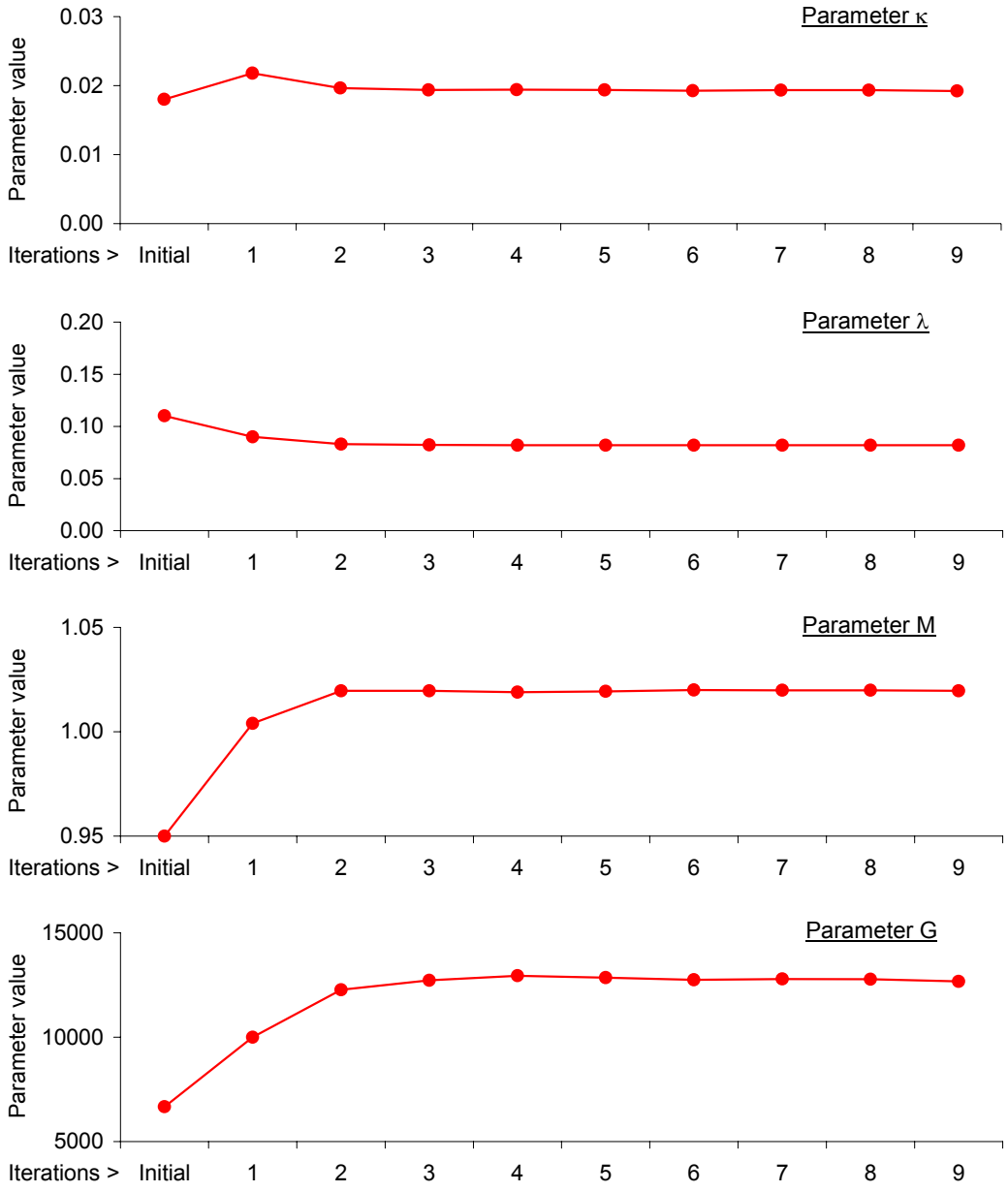

Figure 3-32 Variation of input parameters' estimates at each iteration

Results show that it takes 9 iterations for the non-linear regression to converge with the specified tolerance values. However, the figures show that after iteration #3 the changes in

objective function and parameters' values are not significant. For instance, if TOL=SOSR is set to 5% the regression converges after 3 iterations. If TOL=SOSR is set to 2% the regression converges after 4 iterations. If TOL is set to 2% and SOSR is set to 1% the regression converges after 5 iteration. If TOL=SOSR is set to 0.5% the regression converges after 6 iterations.

Results of this parametric study suggest that the variables TOL and SOSR should be set to values that express the magnitude of changes considered "negligible" by the engineer who is performing the inverse analysis. For instance, for the calibration of a soil model by conventional means, estimates of the input parameters with precisions lower than 2-5% are unrealistic. Thus, TOL=SOSR=2% would adequately represent, for a model calibration by inverse analysis, the accuracy sought for the estimates of the parameters.

3.4.3 Regression control

The regression algorithm used in UCODE is a Gauss-Newton optimization method modified by the addition of three terms (Eq. 2.2 and 2.3): a Marquardt parameter, m_r; a quasi-Newton term, $\underline{R}_r$; and a damping parameter, ρ_r. The damping parameter, ρ_r, is the only "variable" among the three terms because m_r is not a user-defined quantity and $\underline{R}_r$ is never engaged in this study (SOSR is larger than 0.01). The damping parameter, ρ_r, (Eq. 2.3) which can vary in value between 0.0 and 1.0, is calculated from a user-defined quantity, MAX-CHANGE, to ensure that the maximum fractional parameter changes at each iteration do not exceed MAX-CHANGE:

$$\frac{\left(b_j^{\,r+1} - b_j^{\,r}\right)}{\left|b_j^{\,r}\right|} < MAX - CHANGE \quad \text{for j=1,NP} \tag{3.8}$$

where b_j^r is the value of parameter j at iteration r, and b_j^r is the value of j at iteration r+1.

Note that the main advantage of an "undamped" regression analysis is that the number of iterations necessary to converge is always the lowest possible number for the problem under study. The main advantage of a "damped" regression analysis is that it reduces the risk of converging toward an unrealistic solution (i.e. optimized parameters very different from their initial estimates). Indeed, ρ_r is used as a precaution against local non-linearities that may cause high and unrealistic changes in parameters' value between two sequential iterations.

This parametric study evaluates the effects of the value of MAX-CHANGE on the regression results. Five simulations were run, for which MAX-CHANGE was varied within 2 orders of magnitude, from 5 to 0.05. Table 3-1 shows the parameters' maximum fractional change for the five cases.

	R1	R2	R3	R4	R5
Parameters' max fractional change	5	1	0.5	0.1	0.05

Table 3-18 Value of maximum parameter change (i.e variable MAX-CHANGE) for the five simulations

Table 3-19 shows a summary of the results of this parametric study. The regression analysis converges to almost exactly the same results for all five cases. Note that the values of TOL and SOSR were both set to 2% for all five simulations.

		Initial	R1	R2	R3	R4	R5
Model fit	Objective function	733.5	142.6	142.6	142.6	142.6	142.6
Optimized parameters	κ	0.018	0.019	0.019	0.019	0.019	0.019
	λ	0.11	0.082	0.082	0.082	0.082	0.082
	M	0.95	1.02	1.02	1.02	1.02	1.02
	G	6670	12720	12720	12950	12560	12680

Table 3-19 Optimization results

Figure 3-33 shows the number of iterations needed for the regression algorithm to converge and highlights whether damping was necessary at any given iteration. Results show that the lower the value of MAX-CHANGE (e.g., from R1 to R5), the more iterations are needed to get to the optimal solution. However, there is a certain value of MAX-CHANGE (e.g., 0.5) from which the number of iterations starts to increase. Note that: (i) damping is not "engaged" in the first two simulations (i.e. ρ_r=1.0 during the regression), an that is why results of simulations R1 and R2 are identical, (ii) a minimum number of iterations is needed for the "undamped" regression to converge (e.g., three iterations), and (iii) simulation R3 "requires" damping at the first iteration, yet still converges in the lowest possible number of iterations.

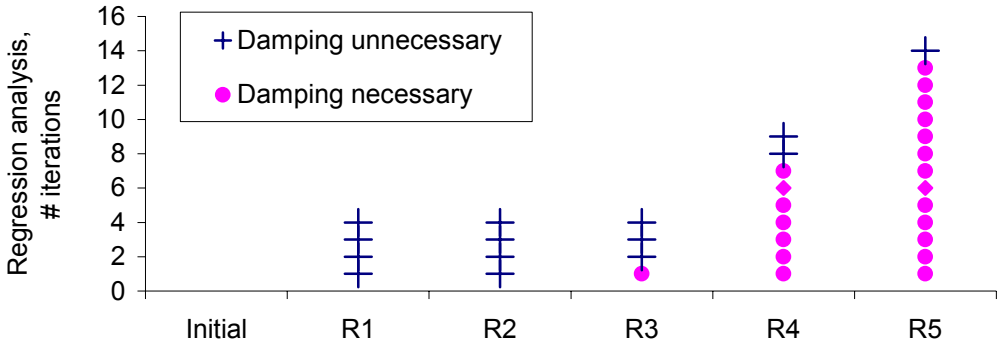

Figure 3-33 Objective function values for different runs

The results of this parametric study suggest that the value of MAX-CHANGE that best combines the advantages of an undamped regression (i.e. lower number of iterations) and a damped regression (i.e. regression convergence to the "real" solution) is 0.5.

3.4.4 Sensitivity calculation

For each iteration of the Gauss-Newton method used in UCODE, the model is linearized about the parameter values estimated at the last iteration. Therefore the sensitivity matrix, $\underline{X}_r$, used in the regression equations needs to be recomputed at the beginning of each iteration. To calculate $\underline{X}_r$ the model (i.e. FE simulation) is executed once for each parameter, and each time the values of that parameter is perturbed by a fractional amount. The differences between perturbed simulated values and unperturbed simulated values (i.e. computed results at previous iteration) are used to calculate the sensitivities. In UCODE sensitivities are calculated using either a forward or central difference approximation according to the following formulas:

$$\frac{\Delta y_i'}{\Delta b_j} = \frac{y_i'\left(b_j + \Delta b_j\right) - y_i'\left(b_j\right)}{\left(b_j + \Delta b_j\right) - \left(b_j\right)} \quad \text{(forward difference)} \tag{3.9}$$

$$\frac{\Delta_2 y_i'}{\Delta_2 b_j} = \frac{y_i'\left(b_j + \Delta b_j\right) - y_i'\left(b_j - \Delta b_j\right)}{\left(b_j + \Delta b_j\right) - \left(b_j - \Delta b_j\right)} \quad \text{(central difference)} \tag{3.10}$$

where y_i' is the value of the i^{th} computed result at iteration r; b_j is the value of the j^{th} parameter at iteration r; Δb_j is the perturbation of b_j; and Δ_2 is used to denote central difference.

The UCODE variables controlling the value of $\underline{X}_r$, and therefore the optimization algorithm, are: the fractional amounts by which each parameter is perturbed, $PERTURBATION_j$ (for j=1,NP), and the use of forward or central difference approximation.

This parametric study aims at evaluating the effect of the value of $PERTURBATION_j$ on the regression results. Six simulations were run, S1 to S5 and S3_CD. In the first five cases each one of the four input parameters was perturbed by the same fractional amount, PERTURBATION = $PERTURBATION_j$ (j=1,4), and PERTURBATION was varied within 2 orders of magnitude, from 0.1 to 0.001. Case S3_CD has the same PERTURBATION value of case S3, but central differences were used instead of forward differences (used for S1 to S5). Table 3-20 shows the value of PERTURBATION for the

six cases. Note that the values of TOL and SOSR were both set to 2% for all five simulations.

	S1	S2	S3	S4	S5	S3_CD
%change of parameters for computing X	0.1	0.05	0.01	0.005	0.001	0.01

Table 3-20 Value of PERTURBATION for the six simulations

Table 3-21 show the optimization results for this parametric study. The regression analysis converges to almost exactly the same results for all six cases.

		S1	S2	S3	S4	S5	S3_CD
Model fit	Objective function	142.6	142.6	142.6	142.6	142.4	142.6
Optimized parameters	κ	0.019	0.019	0.019	0.019	0.019	0.019
	λ	0.082	0.082	0.082	0.082	0.082	0.082
	M	1.02	1.02	1.02	1.02	1.02	1.02
	G	12720	12750	12950	12900	12440	12740

Table 3-21 Optimization results

The value of PERTURBATION directly influences the computed sensitivities at each iteration. Figure 3-34 shows the initial value of the composite scaled sensitivity of every parameter for the six simulations. Results do not vary significantly for perturbations less than 10%.

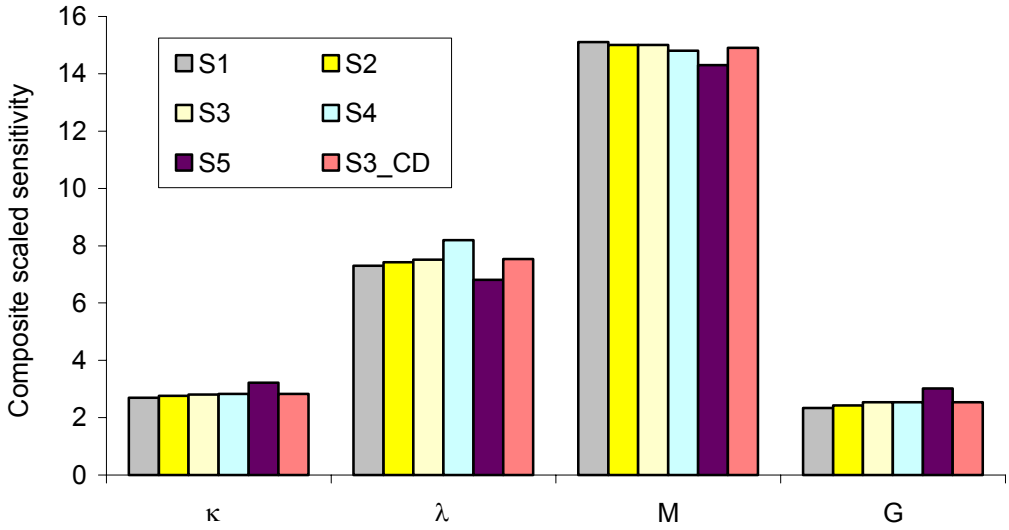

Figure 3-34 Initial value of composite scaled sensitivity for the four input parameters

3.4.5 Comments on parametric study results

A parametric study on the regression variables related to the "optimization" algorithm (modified Gauss-Newton method) has been conducted to evaluate their influence on the calibration of a soil model by inverse analysis. The optimization variables were grouped in four categories:

1. Weighting of observations
2. Tolerance on convergence criteria
3. Regression control
4. Sensitivity calculation

From the results of the parametric study the following conclusions can be drawn.

1. Observation weights assigned based only on measurement errors define very narrow "error envelopes" around the experimental data, much smaller than wider geotechnically admissible error envelopes which consider the natural variability of the material. Weighting should include all the observations' uncertainty contributions (i.e. measurement errors, sampling disturbance, sample preparation and natural variability). Weighting greatly influences the results of the optimization. More than one set of parameter values is able to "appropriately" model the test results.

2. Convergence criteria values should be set equal to what the user perceives as a "negligible change" of parameter values or model fit results (expressed by the objective function). For the calibration of the MCC model 2% proved to be an adequately small value for the two tolerance variables.

3. Very small values of the variable controlling the damping parameter increase the optimization computational time without improving the results of the analysis.

4. The variable used to specify the parameters' perturbation from which the sensitivity matrix is computed, does not influence the optimization results significantly when its value is less than 10%.

3.5 SUMMARY

Inverse analysis was used to successfully calibrate the MCC parameters from results of two compression tests on clay specimens. The approach coupled a finite element code JFEST and the inverse analysis algorithm UCODE to minimize the differences between computations of stress-strain response and experimental data. Results showed that inverse analysis did an excellent job in matching the observations and that the "objectively" optimized input parameters were realistic from a geotechnical point of view.

Parametric studies were conducted on regression variables (geotechnical and optimization variables) to evaluate their effect on the optimization results. The variables to which results proved to be more "sensitive" are:

- number and type of triaxial tests used as observations;
- number of input parameters estimated simultaneously;
- weighting of observations.

4 SOIL PARAMETERS FOR CONSTITUTIVE MODELS OF CHICAGO CLAYS

4.1 INTRODUCTION

In a finite element simulation of a geotechnical problem, the calibration of the models used to reproduce the soil behavior often poses significant challenges. This chapter will use the results of triaxial tests on Chicago clay specimens to calibrate, by inverse analysis, four different soil models: the Duncan-Chang model, the Modified Cam-Clay model, the Anisotropic Modified Cam-Clay model, and the Hardening-Soil model. The laboratory data used for the calibration of the models refer to samples from four layers of compressible Chicago glacial clays, locally known as the Upper Blodgett, Lower Blodgett, Deerfield and Park Ridge layers.

4.2 CONSTITUTIVE SOIL MODELS

Real soil is a highly nonlinear material, with both strength and stiffness depending on stress and strain levels. A single constitutive model that can describe every aspect of the soil behavior does not exist. Yet, many constitutive models have been developed that can capture many of the important features of the soil behavior. This section presents an overview of the four soil models chosen to represent the behavior of Chicago glacial clays: Duncan-Chang (D-C), Modified Cam-Clay (MCC), Anisotropic Modified Cam-Clay (AMCC), and Hardening-Soil (H-S). The D-C is a nonlinear pseudo-elastic model in which the material parameters vary with stress and strain levels. The remaining are elasto-plastic models in which a yield surface defines the boundary between elastic and plastic behavior. The four models were chosen because they represent a diverse range of constitutive modeling solutions for numerical analyses in geotechnical engineering and their response is defined by relatively few parameters.

4.2.1 Duncan-Chang model

The Duncan-Chang (D-C) model is a non-linear pseudo-elastic model. Details about the mathematical formulation of the model can be found in Duncan and Chang (1970). The stiffness matrix, that relates stresses to strains, has the same expression of the elastic stiffness matrix but the two elastic parameters (e.g., stiffness modulus E and bulk modulus B) are not constants in this model. Eight parameters are needed to define their variation. Table 4-1 shows the input parameters, their meaning and the conventional way of

estimating their value. Parameters ϕ, c, R_f, K and n are used to define a hyperbolic representation of the stress-strain response, with failure determined by the Mohr-Coulomb failure criteria. Parameters K_{UR} and n define the elastic unload-reload stiffness modulus dependency upon the minor principal stress. Parameters K_b and m define the bulk modulus dependency upon the minor principal stress, and therefore allows for non-linear volume changes during shear. At least three triaxial tests are needed to estimate the input parameters.

Parameter	Explanation	Initial estimates
ϕ	Friction angle	Slope of faillure line in σ_n-τ stress space
c	Cohesion	y-axis intercept in σ_n-τ stress space
R_f	Ratio of deviatoric stress at failure vs. ultimate deviatoric stress	$(\sigma_1 - \sigma_3)_f$ / $(\sigma_1 - \sigma_3)_{ult}$
K	Modulus number	y-axis intercept in $\log(\sigma_3/p_a)$-$\log(E_i/p_a)$ space
n	Modulus exponent	Slope of trendline line in $\log(\sigma_3/p_a)$-$\log(E_i/p_a)$ space
K_{ur}	Unload-reload modulus number	y-axis intercept in $\log(\sigma_3/p_a)$-$\log(E_{ur}/p_a)$ space
K_b	Bulk modulus number	y-axis intercept in $\log(\sigma_3/p_a)$-$\log(B/p_a)$ space
m	Bulk modulus exponent	Slope of trendline in $\log(\sigma_3/p_a)$-$\log(B/p_a)$ space

Table 4-1 Duncan-Chung input parameters

4.2.2 Modified Cam-Clay

The Modified Cam-Clay (MCC) model is an isotropic, work hardening, non-linear, elasto-plastic model (Roscoe et al. 1958). The characteristics of this model were presented in detail in paragraph 3.2.1. The input parameters are four: κ, λ, M and G. Figure 4-1 shows the shape of the MCC yield surface, an ellipse centered about the p-axis.

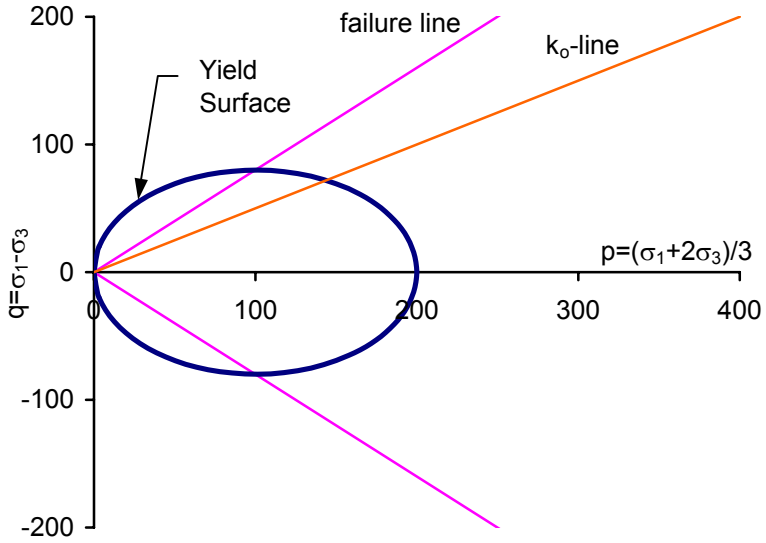

Figure 4-1 Yield surface of MCC model

4.2.3 Anisotropic Modified Cam-Clay

The Anisotropic Modified Cam-Clay (AMCC) model is equivalent to the MCC model except for the shape of the yield surface, which is a rotated and distorted ellipse. The ellipse is, for a normally consolidated clay, initially centered about the k_0-line. Details about the mathematical formulation of the model can be found in Dafalias (1986). The degree of

rotation and distortion of the yield surface in a p-q space is determined by the value of the variable α. Figure 4-2 shows the ellipse in a p-q stress space.

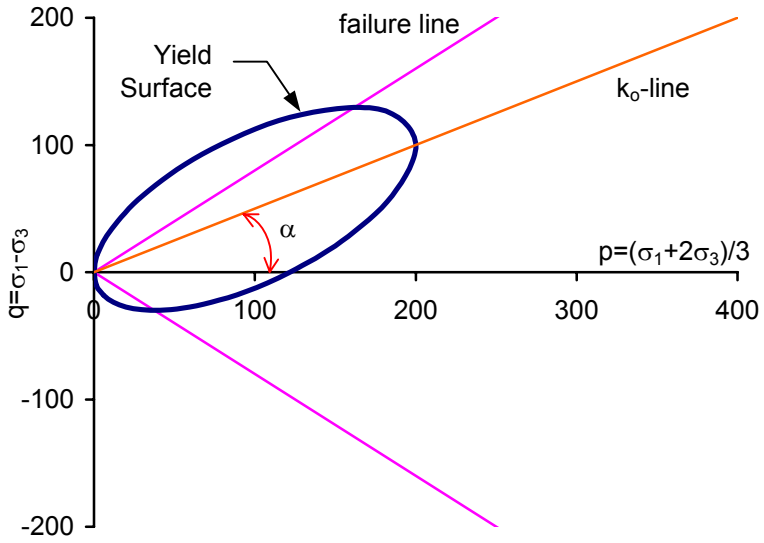

Figure 4-2 AMCC yield surface

In a general stress space σ_1-σ_2-σ_3 a second hardening law, which depends from two new model parameters x and c, controls the "evolution" of the anisotropic variables α_{ij},. The initial value of α_{ij}, and thus the initial position of the yield surface, can be computed from k_{in}, the initial ratio between horizontal and vertical effective stresses, according to the following formulas (*x*, *y* and *z* are assumed to be principal directions):

$$\alpha_x = \alpha_z = \frac{k_{in} - 1}{1 + 2k_{in}} \tag{1.1}$$

$$\alpha_y = \frac{2\left(1-k_{in}\right)}{1+2k_{in}} \tag{1.2}$$

$$\alpha = \sqrt{3\left(\alpha_x{}^2 + 0.5\alpha_y{}^2\right)} \tag{1.3}$$

Table 4-2 shows the input parameters of the AMCC model, their meaning and the conventional way of estimating them. The model parameters are six: λ, κ, M, G, x and c. The first 4 parameters are the same parameters used by the MCC model, x controls the degree of anisotropy which develops under a constant η=q/p loading, and c controls the pace at which such anisotropy develops or demises.

Parameter	Explanation	Initial estimates
κ	Slope of rebound isotropic consolidation curve	Cr / 2.303
λ	Slope of virgin isotropic consolidation curve	Cc / 2.303
M	Slope of the failure line in q-p' space	6 sin ϕ / (3 – sin ϕ)
G	Shear modulus (kPa)	E_{50} / 2 (1 + ν)
x	Degree of anisotropy developing under constant η loading	-
c	Pace of anisotropy development	-

Table 4-2 AMCC input parameters

The initial estimates of the last two parameters are difficult to obtain from results of standard geotechnical tests. Dafalias (1986) showed that, if the yield surface is assumed to remain similar to itself under constant k_0 load conditions, then x is equal to the slope of the k_0-line divided by the value of α. Thus, if one assumes that the initial yield surface is centered around the k_0-line, the initial value of x can be set to 1.0. Parameter c is generally calibrated by trial-and-error to obtain best fit from experimental data.

4.2.4 Hardening-Soil model

The Hardening Soil (HS) model is an elasto-plastic multi-yield surface model. Details about the mathematical formulation of the model can be found in Schanz et al. (1999). Failure is defined by the Mohr-Coulomb failure criteria. Two families of yield surfaces are considered to account for both volumetric and shear plastic strains. Figure 4-3 shows the yield surfaces of the model in p-q stress space. A yield cap surface controls the volumetric plastic strains. On this cap, the flow rule is associative. On the shearing yield surfaces, increments of plastic strain are non-associative and the plastic potential is defined to assure a hyperbolic stress-strain response for triaxial compression load conditions.

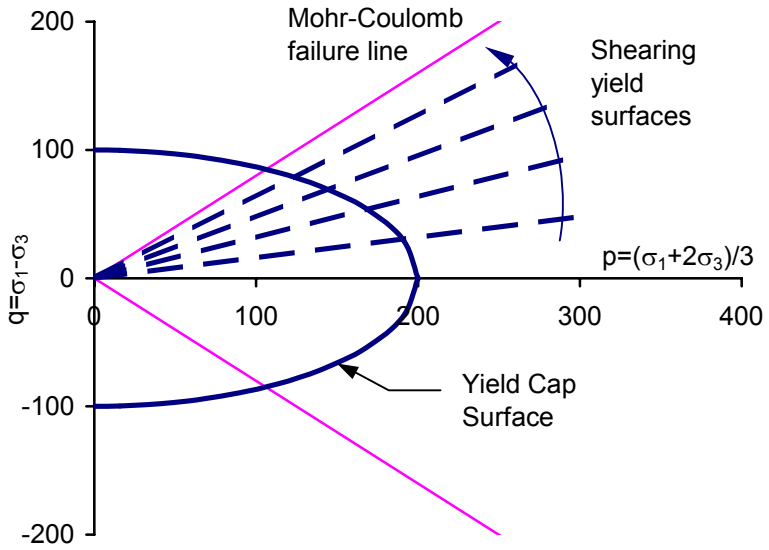

Figure 4-3 H-S yield surfaces

The H-S model input parameters are ten: ϕ, c, R_f, ψ, E_{50}^{ref}, E_{oed}^{ref}, m, E_{ur}^{ref}, ν_{ur} and k_0. Table 4-3 shows their meaning and the conventional way of estimating them. The failure parameters ϕ, c and R_f are estimated assuming a Mohr-Coulomb failure criteria. The parameter ψ is a function of the post-peak stress response of overconsolidated soils (ψ is zero for normally consolidated soils). Parameters E_{50}^{ref}, m, E_{oed}^{ref} and E_{ur}^{ref} are estimated assuming the values of E_{50}, E_{oed} and E_{ur} are stress dependent (p^{ref}=100kPa). Parameter ν_{ur} is usually set between 0.15 and 0.3. Parameter k_0 is estimated using Jaky's empirical relationship with the peak friction angle.

Parameter	Explanation	Initial estimates
ϕ	Friction angle	Slope of faillure line in σ_n-τ stress space
c	Cohesion	y-axis intercept in σ_n-τ stress space
R_f	Failure ratio q_f/q_a	$(\sigma_1 - \sigma_3)_f$ / $(\sigma_1 - \sigma_3)_{ult}$
ψ	Dilatancy angle	Function of ϕ_{peak} anf $\phi_{failure}$
E_{50}^{ref}	Secant stiffness in standard drained triaxial test	y-axis intercept in $\log(\sigma_3/p^{ref})$-$\log(E_{50})$ space
m	Power for stress-level dependency of stiffness	Slope of trendline in $\log(\sigma_3/p^{ref})$-$\log(E_{50})$ space
E_{oed}^{ref}	Tangent stiffness for primary oedometer loading	y-axis intercept in $\log(\sigma_v/p^{ref})$-$\log(E_{50})$ space
E_{ur}^{ref}	Unloading-reloading stiffness	y-axis intercept in $\log(\sigma_3/p^{ref})$-$\log(E_{ur})$ space
ν_{ur}	Poisson's ratio	0.15 - 0.3
k_0	k_0 value for normally consolidated soil conditions	1 - sinϕ

Table 4-3 Hardening-Soil input parameters

4.3 PARAMETER IDENTIFICATION BY INVERSE ANALYSIS

A set of triaxial compression tests was performed on samples from four different layers of compressible Chicago glacial clays. The triaxial testing program was part of an extensive experimental laboratory program established to adequately define the soil properties of the main geologic strata on the site of the Chicago & State excavation project (Finno et al.

2002). Four soil models were calibrated based on triaxial results using the inverse analysis procedure presented in chapters 2 and 3.

4.3.1 Chicago glacial clays

The site laboratory samples were obtained from the location of the excavation/renovation of the Chicago & State subway station. Figure 4-4 shows the subsurface conditions at the site. All elevations refer to the Chicago City Datum (CCD), which corresponds to the average level of Lake Michigan. For the purposes of the laboratory experimental program, four main layers were identified in order of increasing depth: the Upper Blodgett, the Lower Blodgett, the Deerfield, and the Park Ridge. The laboratory experiments concentrated on the top four clay layers because they are more compressible than the lower Tinley stratum clays and thus they are the most important in characterizing the soil mass response to the excavation at the site.

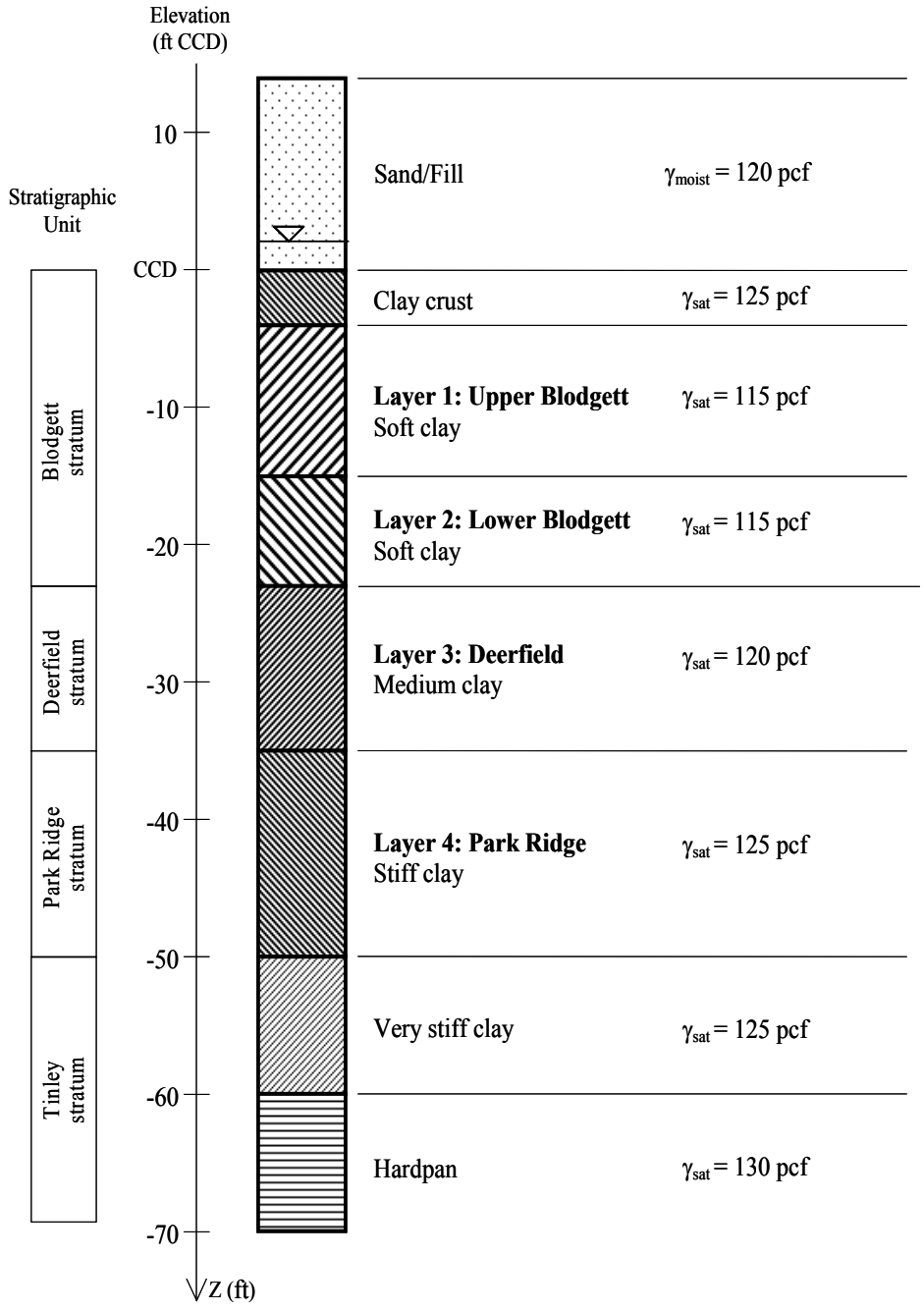

Figure 4-4 Subsurface profile

The stratigraphic units at the site are derived from four major geologic events that impacted the subsurface conditions of the Chicago area: (i) marine sediment deposition, (ii) a long period of erosion, (iii) successive advances and retreats of a continental glacier, and (iv) the variation of elevation of the glacial Lake Chicago (Chung and Finno 1992). Much of the subsoil in the Chicago area is called the Wadsworth Till of the Wedron formation. This till is debris that is aggregated and deposited directly by glacier ice without disaggregation by other agents, such as melt water. Bretz (1939) and Otto (1942) suggested the Wadsworth Till was deposited in six fairly distinct till sheets due to local glacier advances and retreats during the Wisconsin Stage. The advance and retreat process was marked by terminal moraines, which created easily identifiable strata. In order of deposition they are the Valparaiso, Tinley, Park Ridge, Deerfield, Blodgett, and Highland Park tills.

The ice margin deposits subject of the experimental program presented in this chapter (i.e. the Park Ridge, Deerfield, and Blodgett strata) define the Lake Border morainic system. Deposition of these strata occurred under water, when Lake Chicago was at its highest elevation. Each stratum can be identified by its sediment properties that resulted from deposition in a particular subenvironment. The depositional environment determined the fundamental geotechnical properties of the glacial deposits including: texture, particle shape, fabric, density and stress history.

The Blodgett stratum was deposited in a complicated glacial environment and includes glaciolacustrine clays and melt-out and flow tills, and, as a result, exhibits variable

geotechnical characteristics. The Deerfield and Tinley Park strata were probably deposited as basal melt-out tills or waterlain paratills and, as a result, have relatively uniform geotechnical characteristics (Chung and Finno, 1992). The Blodgett and Deerfiled tills, termed "compressible" by Peck and Reed (1954), have higher water contents and lower stiffnesses and compression strengths than the Park Ridge and older strata.

4.3.2 Experimental program

An extensive experimental laboratory program was conducted to adequately define the effective stress soil properties in each of the four main geologic strata of the glacial clays at the excavation site. This laboratory program included index property, consolidation and triaxial testing (Roboski 2001). The inverse analysis approach described in chapter 3 will be only applied to results of drained and undrained triaxial compression tests. Table 4-4 shows a summary of the triaxial experimental program. Three consolidated drained compression tests and one consolidated undrained compression test were performed on soil samples from each of the four clay layers. The test samples were first consolidated to different isotropic effective stresses (the in-situ vertical effective stress and two significantly higher stresses) and then sheared until failure. The principal stress difference, the volumetric and axial strains and the excess pore pressures were recorded.

Stratum	Depth of sample (ft)	Test type	Test name	Consoildation pressure (kPa)	Void ratio after consolidation
Upper Blodgett	17-20	CID TXC	UB_1	107	0.85
			UB_2	200	0.77
			UB_3	400	0.7
		CIU TXC	UB_U	100	0.89
Lower Blodgett	35-37	CID TXC	LB_1	134	0.53
			LB_2	220	0.54
			LB_3	400	0.51
		CIU TXC	LB_U	130	0.61
Deerfield	40-42	CID TXC	D_1	175	0.54
			D_2	350	0.5
			D_3	450	0.49
		CIU TXC	D_U	168	0.54
Park Ridge	54-57	CID TXC	PR_1	200	0.39
			PR_2	350	0.38
			PR_3	450	0.37
		CIU TXC	PR_U	204	0.53

Table 4-4 Triaxial experimental program

Figure 4-5 shows the results of the three drained tests for each layer. Some of the experimental results are not plotted at large strains because, due to experimental difficulties, not every sample could be sheared to failure. As expected, results show that the deviatoric stresses at failure increase with depth (i.e. upper-strata clay samples are "weaker" than lower-strata ones) and, for a given layer, with increasing consolidation pressure. The volumetric strain response shows the same trend, although less noticeable. Figure 4-6 shows the results of the undrained tests performed. Both the deviatoric stress and the excess pore pressures at failure increase with increasing depth, and thus increasing effective consolidation pressure.

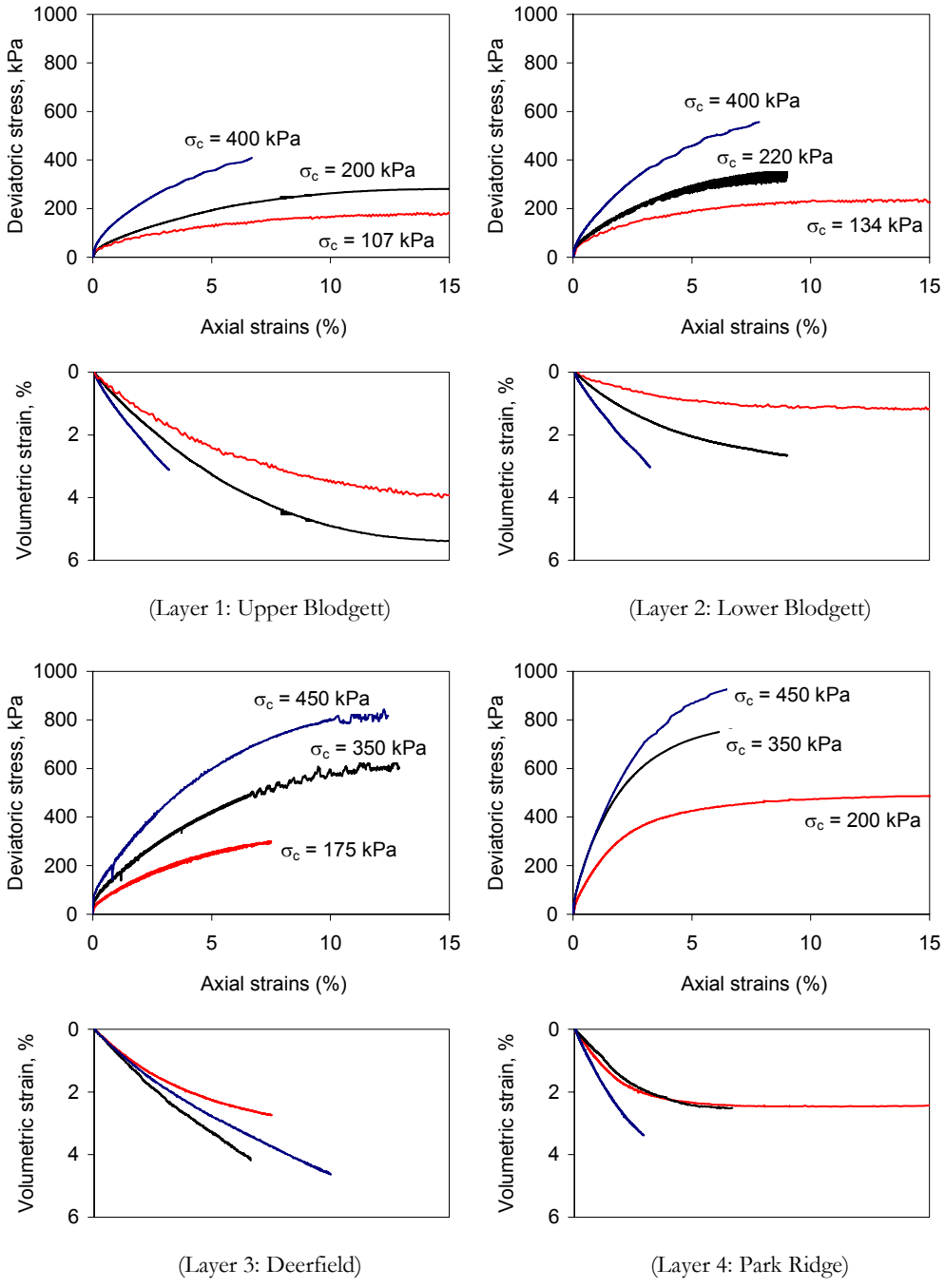

Figure 4-5 Experimental results of drained compression tests (CID TXC) for Layers 1, 2, 3, and 4

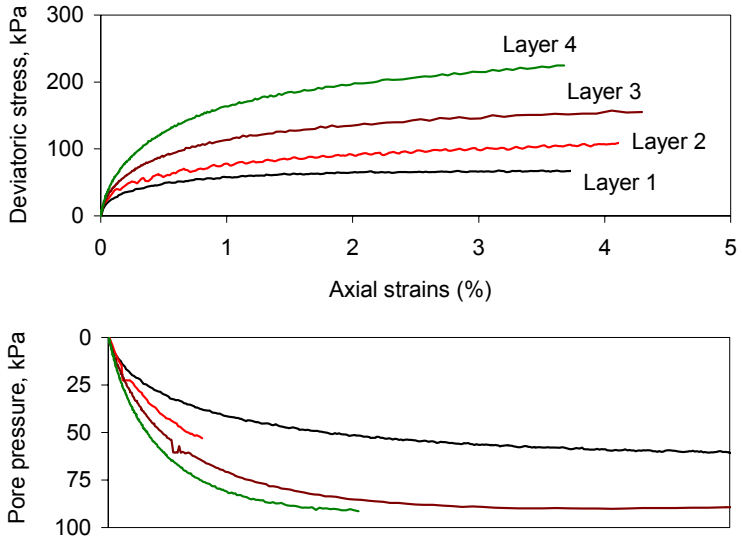

Figure 4-6 Experimental results of undrained compression tests (CIU TXC)

4.3.3 Numerical implementation

Model calibration by inverse analysis was conducted using the parameter optimization algorithm UCODE, which provides means to "extract" the modeled results from specified software output files (provided they are in ASCII format), to compare them with given observations and to "export" the calculated optimized input parameters into the software input files (see section 2.3 for details about UCODE). Different finite element codes were used to simulate the triaxial tests with the four constitutive soil models presented in section 4.2. The code JFEST (Finno and Hararap 1991) was used to model the soil response with the D-C, MCC, and AMCC models; the commercial software PLAXIS (developed by PLAXIS BV) was used to simulate the tests with the H-S model.

The code JFEST is a finite element program, written in Fortran77, able to analyze the soil response to tunneling, excavation and embankment loadings. JFEST input and output files are in ASCII format, thus perfectly compatible with UCODE. In its original version (Finno 1983) JFEST included, among others, the Duncan-Chang and the Modified Cam-Clay soil models. For the work described herein the Anisotropic Modified Cam-Clay model was added to the material models library. The basic structure of JFEST and the Fortran subroutines written to include the AMCC model in the code can be found in Appendix C.

PLAXIS is a finite element package developed for the analysis of deformation and stability in geotechnical engineering projects. PLAXIS offers different soil models to choose from; the model used for this work is the Hardening-Soil model. The many pre- and post-processing features available in PLAXIS make this code relatively easy to use. The software, however, does not have any option to save input or output files in ASCII format. PLAXIS is therefore unsuitable for direct coupling with UCODE. In order to overcome this limitation, windows-macros were written, using the software package MacroExpress 2.1e (developed by Insight software solutions), to convert the PLAXIS I/O into text files. The UCODE, PLAXIS and MacroExpress input files used to calibrate the H-S model can be found in Appendix A.

Figure 4-7 show a schematic of the interaction between UCODE and PLAXIS during the inverse analysis. Figure 4-8 shows a flowchart of the tasks that the macro needs to perform to convert the PLAXIS I/O into ASCII format files.

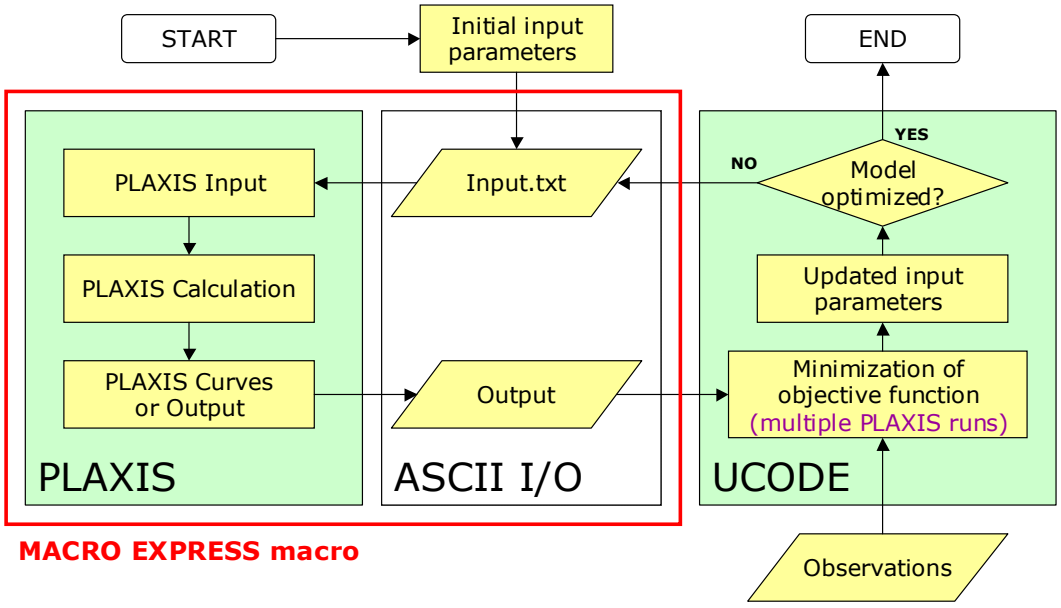

Figure 4-7 Inverse analysis with UCODE and PLAXIS

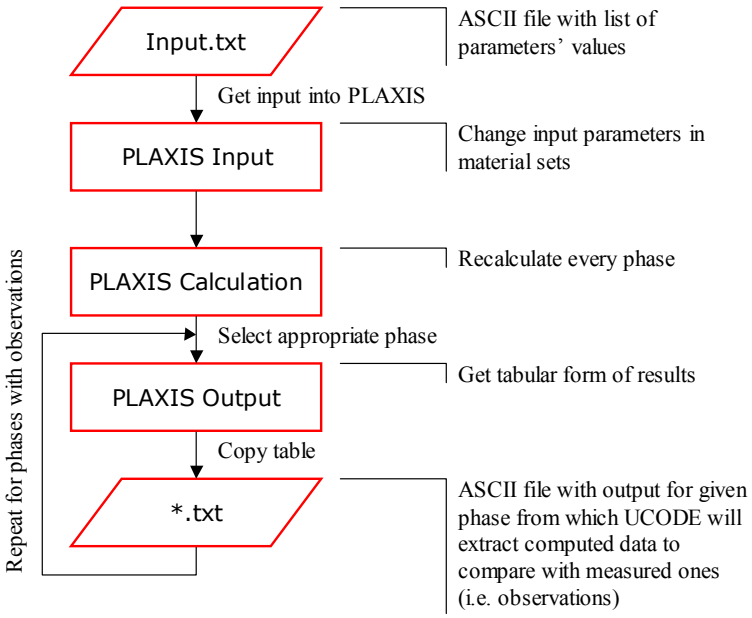

Figure 4-8 Creating a macro to convert PLAXIS I/O into ASCII format files

PLAXIS is composed of four modules: Input, Calculation, Output and Curves. The mesh and the model characteristics are specified in the first module (Input), the second module (Calculation) "computes" the simulation and the last two modules (Output and Curves) present the computed results. A macro is needed to (i) produce model changes in PLAXIS-Input from an input text file, (ii) switch between PLAXIS modules, (iii) calculate the simulated model in PLAXIS-Calculation, and (iv) generate an output text file from the PLAXIS-Output.

Table 4-5 shows the values of the geotechnical and optimization variables used to define the inverse analysis problem for the calibration of the four soil models. They were chosen based on the results of the parametric studies discussed in sections 3.3 and 3.4. The number of input parameters to optimize will be chosen based on the model parameters' sensitivity to the observations.

Geotechnical variables	Tests used as observations	3 CID TXC and 1 CIU TXC
	Number of input parameters	model dependent
	Initial values	Roboski (2001)
	Discretization (drained tests)	every 2% axial strain
	Discretization (undrained tests)	8 obs, more frequent at small strains
Optimization variables	Observations' weighting (stress data)	cov = 0.05
	Observations' weighting (strain data)	cov = 0.10
	Tolerance on convergence criteria	TOL = SOSR = 2%
	Regression variables	MAX-CHANGE = 0.5
	Sensitivity calculation	PERTURBATION = 0.01

Table 4-5 Values of regression variables used for the calibration of soil models

4.4 MODEL CALIBRATION RESULTS

This section presents the results of the calibration of the four models presented in section 4.2. The initial estimates of the input parameters of the models were computed by Roboski (2001) according to conventional calibration procedures. The best-fit values were obtained by inverse analysis. The stress-strain plots with the comparison between the experimental data and the computed results (initial and best-fit) can be found in Appendix D. Note that:

- The tests on samples from layer 1 are the same tests used in chapter 3 to calibrate the MCC model and run the parametric studies on the regression variables.

- For the calibration of the different models at layer 2 (see Table 4-4), the observations only refer to tests LB_D2 and LB_U, because volumetric strain results from LB_D1 and LB_D3 were "inconsistent" with the rest of the results. Possibly because of air in the triaxial lines and because specimen LB_D1 was taken from a Shelby tube extracted from a different boring.

4.4.1 D-C model

Table 4-6 shows the initial values of the 8 D-C input parameters for the four layers. The strength parameter ϕ and the stiffness parameters K, K_b and K_{ur} tend to increase with depth, whereas the failure ratio R_f and parameters n and m do not show any specific trend.

	Initial estimate			
Parameter	Layer 1	Layer 2	Layer 3	Layer 4
ϕ	24.1	27.0	28.9	31.4
c (kPa)	0	0	0	0
R_f	0.70	0.77	0.71	0.83
K	46.0	66.1	68.7	276.0
n	0.87	0.80	0.80	0.42
K_b	17.5	27.8	27.8	53
m	0.16	0.40	0.53	0.31
K_{ur}	180.0	213.0	222.0	n.a.

Table 4-6 Initial values of input parameters

Figure 4-9 shows the composite scaled sensitivities (see Eq. 2.9) of the 8 parameters. The sensitivities were computed at the initial estimated values of the parameters. Note that the

observations used in the regression did not include the pore pressure response of the undrained compression tests. This choice was dictated by the characteristics of the pseudo-elastic D-C model, which does not have any parameter that controls the generation of excess pore pressures in undrained conditions. For undrained triaxial compression loads ($\Delta\sigma=\Delta\sigma_1$) the D-C model, when the water is assumed to be incompressible, always yields excess pore pressures Δu_e equal to:

$$\Delta u_e = \frac{1}{3}\Delta\sigma_1 \tag{1.4}$$

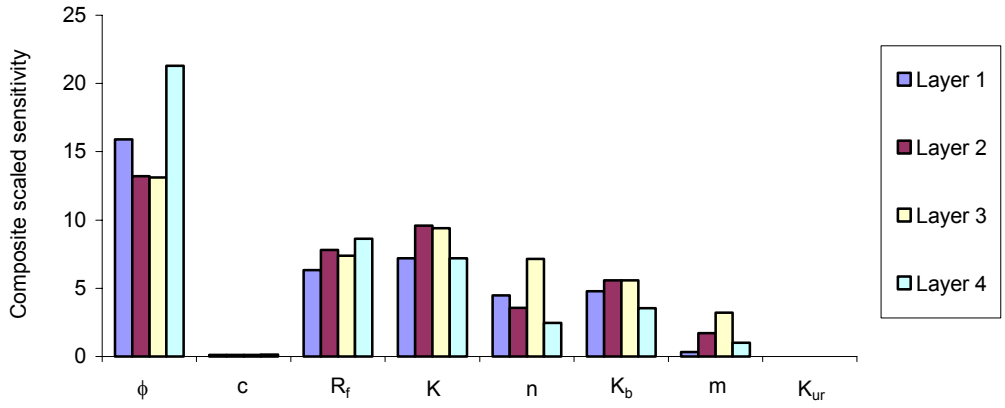

Figure 4-9 Composite scaled sensitivity of H-S input parameters

Figure 4-9 shows that: (i) the parameter to which results are most sensitive is the friction angle ϕ, (ii) the effects on the computed results of parameters R_f, K, n, K_b, and m are noticeable, and (iii) changes in parameters c and K_{ur} do not affect the result of the simulations. These results were to be expected given the characteristics of the model and

the data used as observations (e.g., triaxial compression tests). Test results were conducted on normally consolidated clays, thus c is not expected to be important in defining the Morh-Coulomb failure criterion. The data used as observations do not include any unload-reload cycle, thus E_{ur} is never "used" to simulate the test results.

The sensitivities in Figure 4-9 indicate that 6 input parameters significantly affect the computed results. However, when all 6 parameters are estimated simultaneously, the regression results are "unreasonable". Table 4-7 shows the best-fit values of the six parameters and the final values of the highest correlation coefficients (Eq. 2.12) for analyses conducted on layers 1 and 2. The unreasonable estimates of the parameters are underlined in the table. These results indicate that the inverse analysis problem is not "well-posed" when 6 parameters are optimized simultaneously.

	Best-fit values*		Correlation coefficients higher than 0.9	
Parameter	Layer 1	Layer 2	Layer 1	Layer 2
ϕ	<u>35.3</u>	<u>17.1</u>	0.99	0.91
R_f	<u>1.70</u>	0.92		
K	93.20	209.40		
n	0.36	<u>0.005</u>		
K_b	13.8	<u>3.5</u>		-1
m	<u>0.008</u>	<u>1.80</u>		

* Underlined values are "unreasonable"

Table 4-7 Results of regression when 6 parameters are estimated simultaneously (e.g., layers 1 and 2)

The unreasonable results may be explained considering that during the optimization iterations, parameters R_f and m, which were not correlated to any other parameter at the beginning of the regression became correlated to parameters ϕ and K_b, respectively. Indeed, when parameters R_f and m were kept constant at their initial estimated values and only ϕ, K, n and K_b were optimized by inverse analysis, the calibration of the D-C model was successful.

Table 4-8 shows the values of the input parameters after the optimization and their coefficients of variation (Eq. 2.11), which measure the accuracy of the inverse analysis estimates. In Figure 4-10 the optimized parameter values are compared, in a bar chart, with the initial estimates of the parameters. The error bars refer to the 95% confidence interval for the estimated parameters.

	Best-fit value				Coefficient of variation			
Parameter	Layer 1	Layer 2	Layer 3	Layer 4	Layer 1	Layer 2	Layer 3	Layer 4
ϕ	23.7	21.3	24.1	32.4	0.037	0.067	0.049	0.022
K	68.70	137.20	150.00	141.50	0.101	0.192	0.156	0.134
n	0.44	0.45	0.36	0.96	0.310	1.170	0.451	0.168
K_b	15.8	29.6	26.2	49.7	0.145	0.253	0.147	0.096

Table 4-8 Best-fit values of input parameters

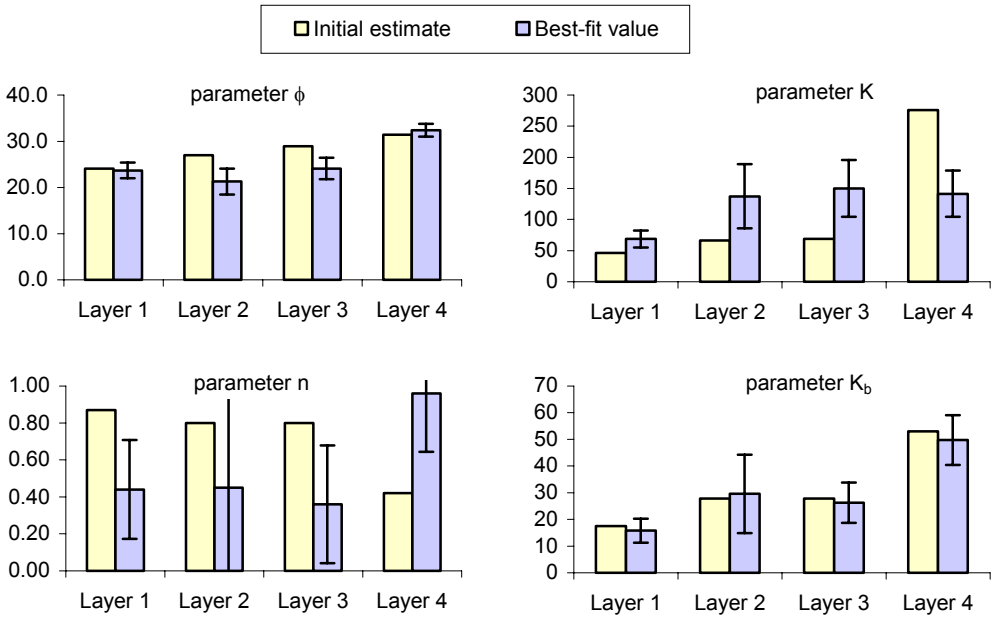

Figure 4-10 Initial and optimized input parameters

Results in Figure 4-10 show that significant differences between the initial and the best-fit values occur for parameters K and n. These two parameters also show high coefficients of variation values, which indicate that the reliability of both parameter estimates is relatively low. This suggests that, despite the correlation coefficients not showing any correlation between the two parameters, the simultaneous estimate of K and n is "difficult." Note that, in the D-C model, both parameters are used in the same equation that defines the stress dependence of E_i, the initial stiffness of the hyperbolic stress strain curve in a q-ε_a space:

$$E_i = Kp_a\left(\frac{\sigma_3}{p_a}\right)^n \tag{1.5}$$

where K is the modulus number, n is the modulus exponent, p_a is the atmospheric pressure, and σ_3 is the minor principal stress invariant.

Figure 4-11 shows the values, for the four layers, of two model statistics: the error variance, s^2, which indicate the overall magnitude of the weighted residuals (Eq. 2.4), and the fit improvement, FI, which indicate by what percentage the optimized results improved compared to the initial ones (Eq. 2.5). For the first three layers the error variance values are much higher than the ideal value of 1.0 (see section 2.3.3). This suggests that the fit between the computed results and the experimental data is not "optimal". However, positive FI values indicate that the calibration of the D-C model by inverse analysis yields better results than conventional calibration methods.

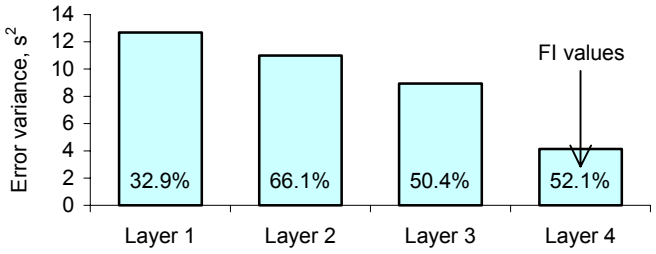

Figure 4-11 Model fit statistics of inverse analysis at four layers

The results of the calibration by inverse analysis were strongly influenced by the fact that the Duncan-Chang model is a pseudo-elastic model, thus it is not able to predict the pore pressure response of tests conducted in undrained conditions.

4.4.2 MCC model

Table 4-9 shows the initial values of the input parameters of the MCC model for the four layers. These values were estimated by conventional means using triaxial and oedometric test results. Note that the initial values of the input parameters for layer 1 are slightly different from the ones used in chapter 3 (see Table 3.2). This difference is due to the fact that the values were computed by different users (i.e. the author, for chapter 3, and Roboski, for this chapter). These different estimates show that, despite the test results and the (conventional) procedure used to calibrate the MCC model were the same, different engineers can come up with different calibrated values of input parameters.

	Initial estimate			
Parameter	Layer 1	Layer 2	Layer 3	Layer 4
κ	0.018	0.008	0.009	0.007
λ	0.110	0.070	0.065	0.040
M	0.95	1.07	1.15	1.26
G (kPa)	6670	15580	30000	56300

Table 4-9 Initial values of input parameters

Figure 4-12 shows the composite scaled sensitivity of the four input parameters. Only minor differences exist among results relative to different clay layers. The graph shows that M is the most sensitive input parameter, yet all four parameters have a quantifiable effect on the computed results. Based on these results it was decided to optimize all 4 parameters by inverse analysis.

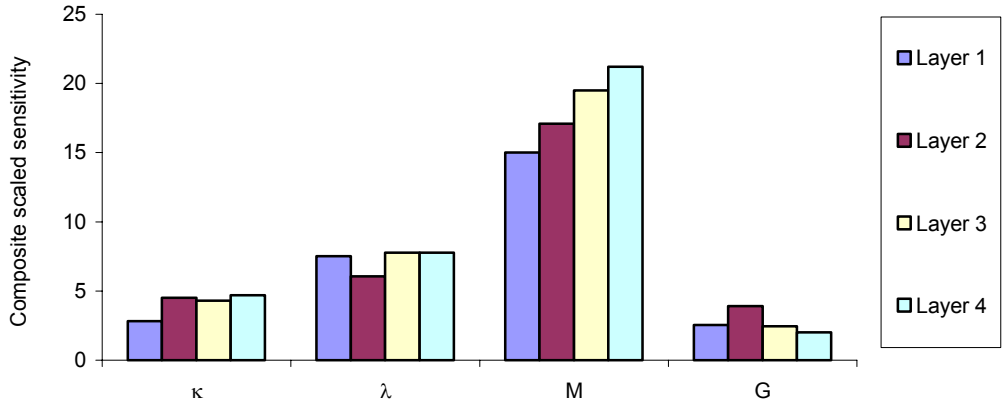

Figure 4-12 Composite scaled sensitivity of MCC input parameters

Table 4-10 shows the optimized values of the input parameters and their coefficients of variation (see Eq. 2.12). In Figure 4-13 the initial and optimized parameter values are plotted in a bar chart. The error bars refer to the 95% confidence interval for the estimated parameters. The main differences between initial and best-fit parameters occur for parameters κ and G, which also show the largest coefficients of variation. Results show clear trends for parameters M and G (both increasing with increasing depth) and a more irregular response of hardening parameters κ and λ (which should be decreasing with increasing depth). The variability of the optimized values of κ and λ for the first two layers may be attributed to the inherent variability of the Blodgett stratum clays.

	Best-fit value				Coefficient of variation			
Parameter	Layer 1	Layer 2	Layer 3	Layer 4	Layer 1	Layer 2	Layer 3	Layer 4
κ	0.019	0.010	0.015	0.018	0.096	0.116	0.095	0.104
λ	0.082	0.042	0.053	0.038	0.039	0.084	0.050	0.054
M	1.02	1.00	1.10	1.28	0.016	0.028	0.023	0.019
G (kPa)	12950	12850	19920	25160	0.197	0.148	0.160	0.134

Table 4-10 Best-fit values of input parameters

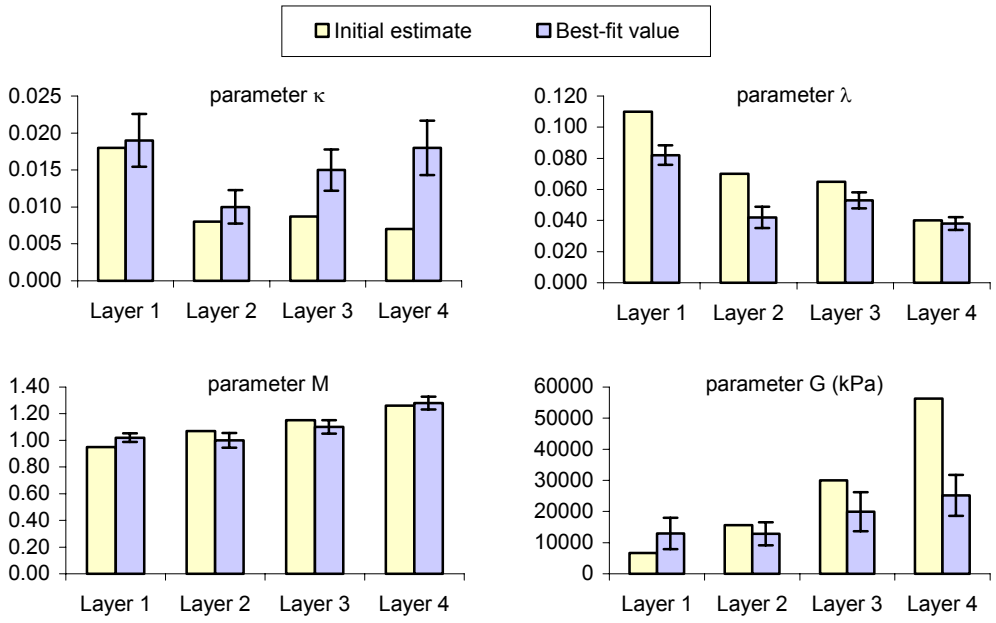

Figure 4-13 Initial and optimized input parameters

Figure 4-14 shows the values of error variance, s^2, and fit improvement, FI, for the four layers. Results demonstrate that the calibration by inverse analysis, compared to the initial conventional calibration, significantly improves the fit between experimental and computed

results (e.g., FI > 80%). Results also show that the simulation error variances are not far from their ideal value of 1.0.

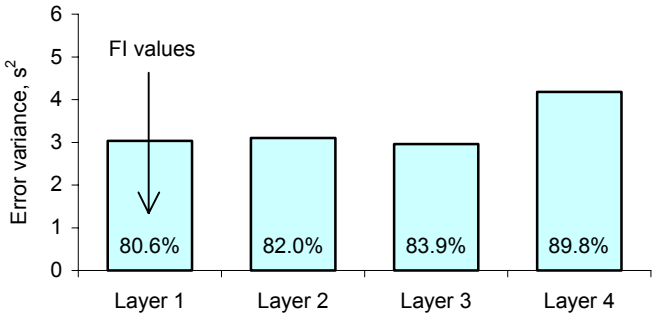

Figure 4-14 Model fit statistics of inverse analysis at four layers

Results showed in this section illustrated that inverse analysis can be used successfully to estimate the MCC parameters of compressible Chicago Clays.

4.4.3 AMCC model

In the AMCC model the anisotropic yield surface rotates due to plastic deformations. The evolution of the yield surface depends on the value of the two model parameters x and c. Figure 4-15 shows the evolution of the AMCC yield surface of a normally consolidated soil specimen sampled at about 20ft below ground surface and consolidated isotropically to 400 kPa (i.e. specimen UB_3). Results were computed assuming the values of both x and c were 1.00, and the values of κ, λ, M and G were the same as the best-fit values found for the MCC model in section 4.4.2.

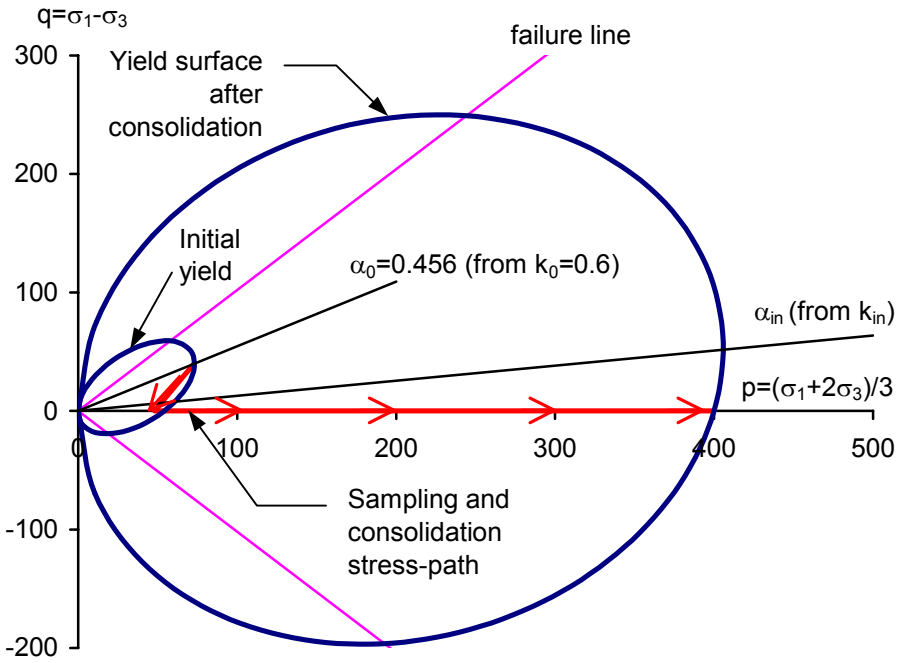

Figure 4-15 Yield surface evolution due to sampling and consolidation

For the calibration of the AMCC model by inverse analysis the sampling and consolidation stages were not modeled, and conditions at the end of the consolidation stage were used as initial conditions of the finite element simulations of the triaxial tests. This choice was dictated by the lack of experimental data relative to the sampling stage and by the numerical difficulties encountered to model the consolidation and the shearing stages sequentially. Figure 4-15, however, clearly shows that the yield surface at the end of the consolidation stage is significantly different from the initial one. Given that the estimate of the initial yield surface position is controlled by the value of k_{in}, this parameter was included among the AMCC parameters estimated by inverse analysis.

Table 4-11 shows the initial values of the seven input parameters for the four layers. The initial values of the first four parameters (κ, λ, M and G) were assumed to be the same as the best-fit values of the calibrated MCC model. The initial values of the last three parameters (x, c and k_{in}) were all set to 1.00, based on the assumption that the initial yield surface is centered around the mean-stress axis.

	Initial estimate			
Parameter	Layer 1	Layer 2	Layer 3	Layer 4
κ	0.019	0.010	0.015	0.018
λ	0.082	0.042	0.053	0.038
M	1.02	1.00	1.10	1.28
G (kPa)	12950	12850	19920	25160
x	1.00	1.00	1.00	1.00
c	1.00	1.00	1.00	1.00
k_{in}	1.00	1.00	1.00	1.00

Table 4-11 Initial values of input parameters

Figure 4-16 shows the composite scaled sensitivity of the seven parameters. Only minor differences exist among results relative to the four layers. The graph shows that M is the most sensitive input parameter. Parameters κ, λ, G and k_{in} also have non-negligible sensitivity values. The triaxial experimental results available, however, do not provide enough information for the estimation of parameters x and c.

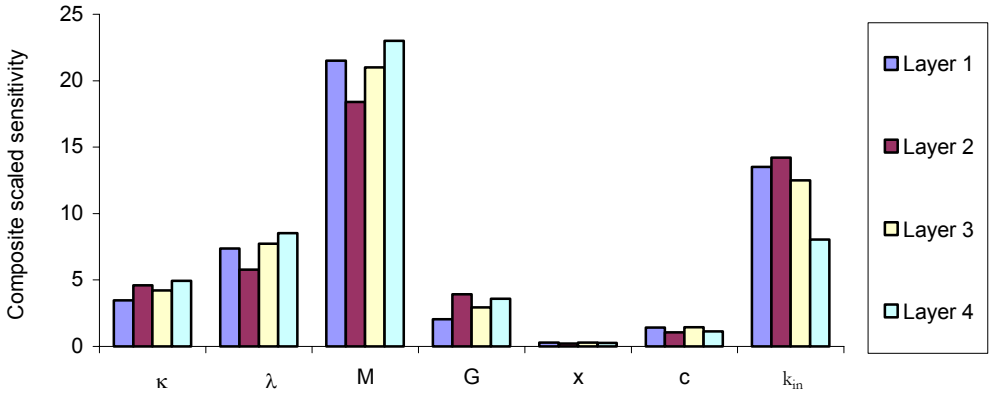

Figure 4-16 Composite scaled sensitivity of AMCC input parameters

For a triaxial test to "engage" the anisotropic parameters x and c, it would have to be an undrained extension type test. The experimental program used for this work, however, did not include any such test. Nevertheless, trial simulations were conducted for which parameter c was included among the parameters to optimize. Results of those simulations, however, produced values of x and k_{in} of about 0.0 and 1.0 respectively, for which the AMCC model becomes equivalent to the MCC model. Therefore, c was not included among the parameters to optimize and only 5 parameters (κ, λ, M, G and k_{in}) were estimated by inverse analysis. Note that the advantages of employing an anisotropic model to simulate the clay behavior are not fully exploited herein.

Table 4-12 shows the values of the input parameters after the optimization and their coefficients of variation. In Figure 4-17 these results are plotted and compared to the initial estimates of the parameters.

	Best-fit value				Coefficient of variation			
Parameter	Layer 1	Layer 2	Layer 3	Layer 4	Layer 1	Layer 2	Layer 3	Layer 4
κ	0.018	0.011	0.014	0.019	0.123	0.126	0.127	0.080
λ	0.096	0.048	0.061	0.044	0.052	0.080	0.063	0.043
M	0.98	1.01	1.06	1.27	0.018	0.025	0.024	0.013
G (kPa)	13100	16230	19990	71910	0.326	0.241	0.259	0.456
k_{in}	1.02	1.1	1.02	1.3	0.042	0.031	0.053	0.025

Table 4-12 Best-fit values of input parameters

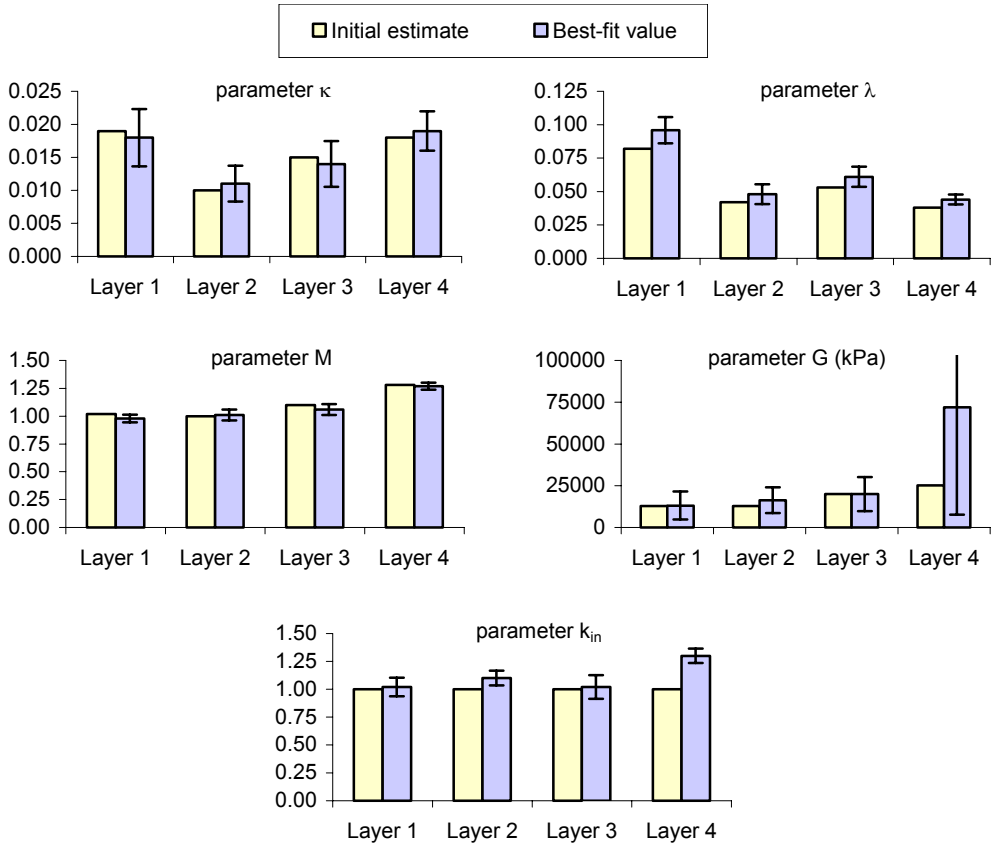

Figure 4-17 Initial and optimized input parameters

Results show that the trends of the best-fit parameter values over the four soil layers are similar to those observed for the MCC model. Note that the high estimate of G for layer 4 corresponds to a high coefficient of variation, an indication that the regression algorithm had difficulties converging to the best-fit value (thus the high uncertainty associated with the estimated value).

Figure 4-18 shows the values of error variance, s^2, and fit improvement, FI, for the four layers. The improvement obtained in calibrating the AMCC model by inverse analysis is less significant that the one shown for the MCC model. Indeed FI values are always < 70%. One has to consider, however, that the initial values of four AMCC parameters were equal to the best-fit values of the calibrated MCC model. Thus, the initial fit between experimental and computed results was already relatively good before the optimization.

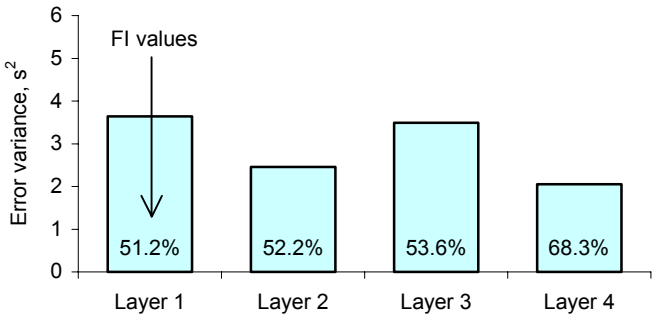

Figure 4-18 Model fit statistics of inverse analysis at four layers

This section's results showed, overall, that the calibrated AMCC model fit the experimental data well but the capabilities of the model were not exercised by the types of tests and data used to calibrate the model.

4.4.4 H-S model

Table 4-13 shows the initial values of the 10 input parameters of the Hardening-Soil model. Figure 4-19 shows the composite scaled sensitivities of the 10 input parameters.

	Initial estimate			
Parameter	Layer 1	Layer 2	Layer 3	Layer 4
ϕ	24.1	27.0	28.9	31.4
c (kPa)	0	0	0	0
R_f	0.70	0.77	0.71	0.83
ψ	0	0	0	0
E_{50}^{ref} (kPa)	2350	3700	4000	11700
m	1.00	0.91	1.00	0.94
E_{oed}^{ref} (kPa)	1600	2300	2440	4090
E_{ur}^{ref} (kPa)	10000	29100	30500	35000
ν_{ur}	0.20	0.20	0.20	0.20
k_o	0.59	0.55	0.52	0.48

Table 4-13 Initial values of input parameters

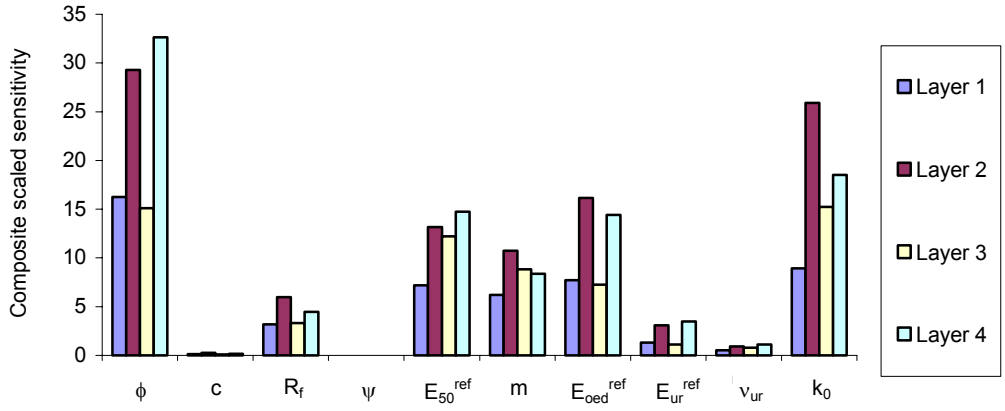

Figure 4-19 Composite scaled sensitivity of H-S input parameters

Results show that the sensitivities of the same parameters relative to the different layers vary significantly. The main parameters affecting the observations, however, are always ϕ, R_f, E_{50}^{ref}, m, E_{oed}^{ref}, and k_0. These six parameters were updated during the calibration of the H-S model. Not all six parameters, however, were estimated by inverse analysis. Only ϕ, E_{50}^{ref} and m were, whereas the best-fit values of parameters R_f, E_{oed}^{ref}, and k_0 were the result of calibration choices determined by the following characteristics of the H-S model (as implemented in PLAXIS):

1. There is a certain range of "valid" E_{oed}^{ref} values which is a function of the values of parameters E_{50}^{ref}, E_{ur}^{ref}, ν_{ur} and k_0. If a value of E_{oed}^{ref} outside this range is specified, PLAXIS rejects it and the nearest possible valid value is suggested for use. Parameter E_{oed}^{ref}, therefore, cannot be included in the optimization because the

regression algorithm would compute wrong sensitivities every time E_{oed}^{ref} is "corrected" by PLAXIS.

2. PLAXIS has an internal optimization algorithm that runs every time a new set of input parameters is specified. This algorithm considers the deviatoric stress response of an internally modeled compression-type load test and "adjusts" the values of parameters k_0 and E_{oed}^{ref} to produce a hyperbolic curve in a triaxial stress-strain space. The regression algorithm cannot possibly estimate values of parameters that are automatically corrected.

3. Users are advised to use the default setting for the advanced parameters (i.e. $E_{ur}^{ref}=3E_{50}^{ref}$, $\nu_{ur}=0.2$, $k_0=(1-\sin\phi)$ and $R_f=0.9$).

Because of the above-described model limitations only the failure parameter ϕ, and the stiffness parameters m and E_{50}^{ref} were optimized by inverse analysis. The value of E_{oed}^{ref} was kept constant during the optimization or, if outside the valid range, set to the PLAXIS-suggested value (function of the values of parameters E_{50}^{ref}, E_{ur}^{ref}, ν_{ur} and k_0). The default values were used for parameters k_0 and R_f.

Table 4-14 shows the best-fit values of the 6 parameters and the values of the coefficients of variation for the 3 parameters estimated by inverse analysis. Figure 4-20 shows a graphical representation of parameters ϕ, m and E_{50}^{ref} and compares their optimized values with their initial estimates. Note that during the calibration of the H-S model, differently

from what happened for the other soil models, the composite scaled sensitivities of the parameters varied notably during the regression iterations. This produced updated parameter estimates that fluctuated significantly before converging to their best-fit values.

	Best-fit value				Coefficient of variation			
Parameter	Layer 1	Layer 2	Layer 3	Layer 4	Layer 1	Layer 2	Layer 3	Layer 4
ϕ	23.40	23.50	25.60	32.80	0.019	0.041	0.038	0.013
E_{50}^{ref} (kPa)	4700	7250	6000	8580	0.053	0.095	0.029	0.018
m	0.74	0.68	0.85	0.84	0.111	0.315	0.044	0.035
E_{oed}^{ref} (kPa)	2330	4180	2680	4660	-	-	-	-
k_o	0.603	0.601	0.568	0.458	-	-	-	-
R_f	0.90	0.90	0.90	0.90	-	-	-	-

Table 4-14 Best-fit values of input parameters

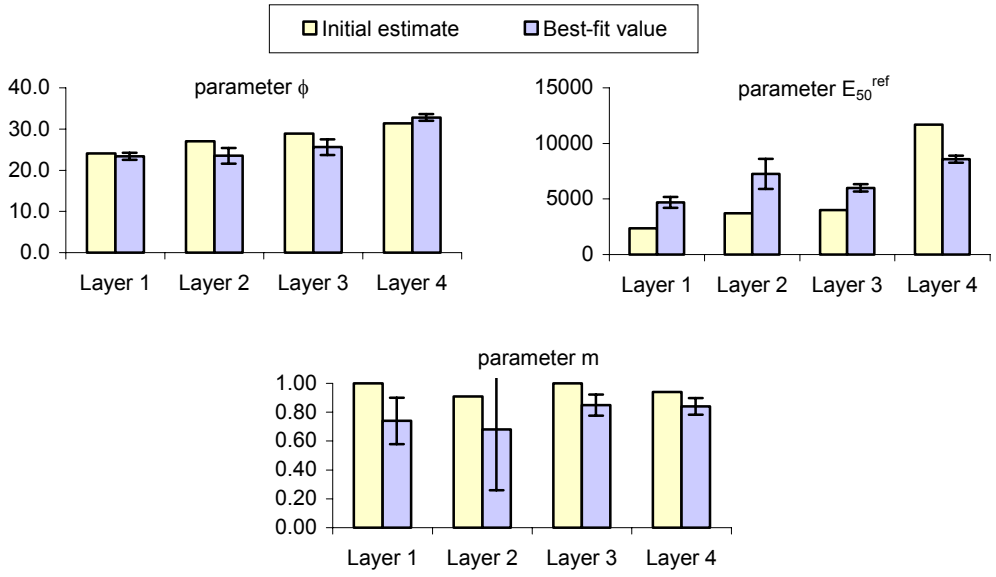

Figure 4-20 Initial and optimized input parameters

All estimates of parameters, except the ones relative to layer 2, seem to show expected trends (i.e. increasing values of strength and stiffness parameters with increasing depth). Parameters relative to layer 2 also show unusually high values of coefficients of variation. Both anomalies could depend on the fact that the calibration of the soil models for layer 2 is based on results from two triaxial tests only (LB_02 and LB_U). Possibly the observations used in the regression analysis for layer 2 were not "adequate" for an accurate estimation of the H-S parameters, despite the fact that composite scaled sensitivity values do not differ significantly from values relative to other layers.

Figure 4-21 shows the values of s^2 and FI for the calibrated model at the four layers. FI values are always larger than 70%, thus a significant improvement over the initial calibration was achieved by the inverse analysis. The error variance values, however, are generally larger than the ones computed for the other models.

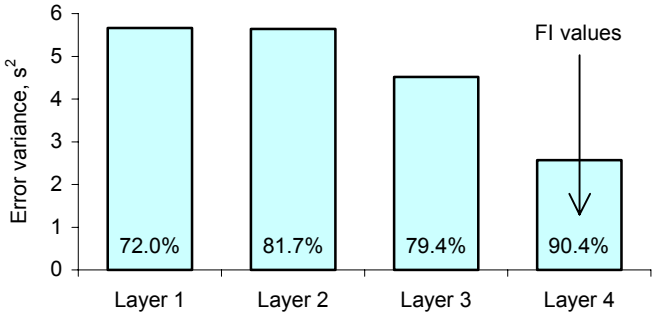

Figure 4-21 Model fit statistics of inverse analysis at four layers

4.4.5 Comparison of results

The objective function (see Eq. 2.1) of the different models can be used to compare the fit between the experimental data and the FE computed results. Figure 4-22 shows the values of the objective function for the four models calibrated in this chapter. The term "initial" refers to models calibrated by conventional means, the term "optimized" refers to models calibrated by inverse analysis. Objective function values can be directly compared, at a given layer, because the observations and weights used are the same. For the same reason, however, objective function values relative to different layers cannot be evaluated against one another. Note that the objective function values of the D-C model include the pore pressure observations of the undrained test (they were not included in the calibration of the model by inverse analysis).

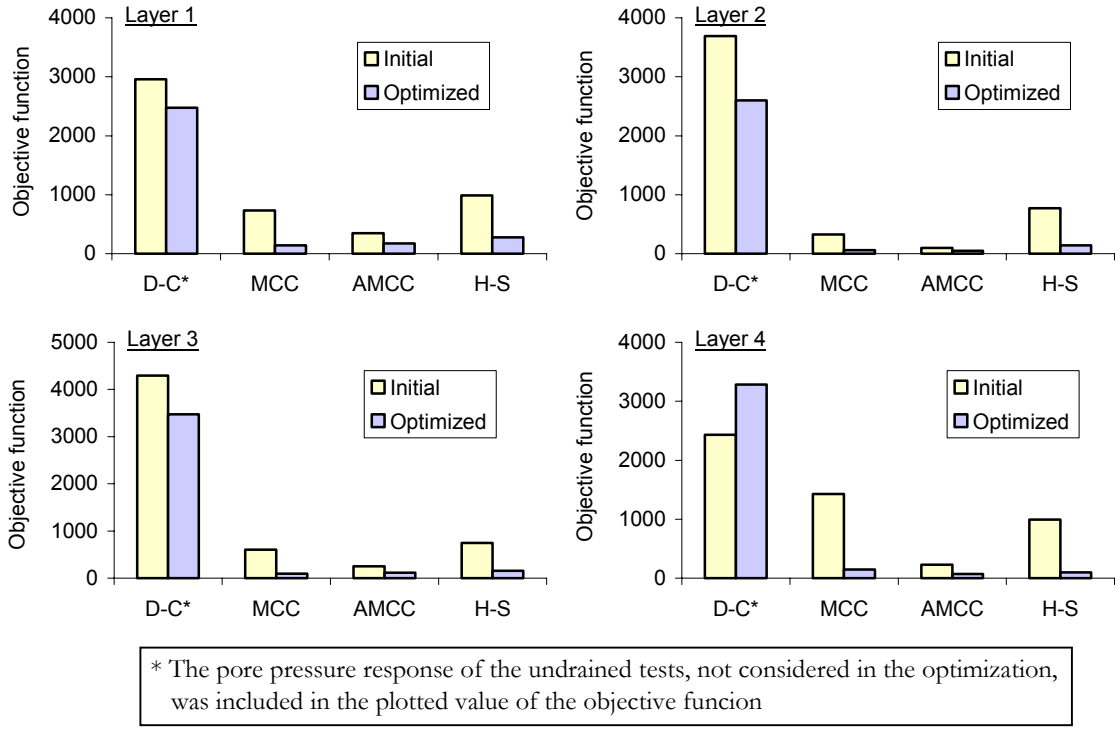

Figure 4-22 Objective function values before and after calibration by inverse analysis

Results show that: (i) the D-C model optimized results are significantly worse than the results of the other three models, (ii) the optimized MCC model yields, overall, the best results, (iii) the fit obtained using the AMCC model is always very close to the fit obtained by the isotropic version of the Cam-Clay model, (iv) the optimized H-S model simulates the behavior of the stiffer clays (i.e. layers 3 and 4) better than the behavior of the softer ones, and (v) optimized models always fit the experimental data better that "initial" models.

Note that these comparisons are valid for the compression tests described herein, which do not necessarily exercise all aspects of each of the models. Overall results would change if

the calibration of the models were based on different triaxial test results (e.g., k_0-consolidated and/or extension tests).

4.5 SUMMARY

In this chapter four soil models (i.e. Duncan-Chang, Modified Cam-Clay, Anisotropic Modified Cam-Clay and Hardening soil) were calibrated by inverse analysis. The calibration of the models was based on results from compression triaxial tests on four layers of compressible Chicago clays. (i.e. Upper Blodgett, Lower Blodgett, Deerfield and Park Ridge). Results show that:

- Inverse analysis can be used effectively to calibrate soil models based on drained and undrained compression triaxial test results.

- When inverse analysis is used to calibrate a soil model the optimization should never include observations that the model cannot "reproduce" (e.g., pressure response in undrained condition for D-C model) and parameters that the available observations cannot estimate (e.g., parameters x and c for AMCC model).

- The pseudo-elastic Duncan-Chang model cannot adequately model the effective stress-strain behavior of clays in undrained conditions.

- The Modified Cam-Clay model, when calibrated by inverse analysis, is the model that best simulates the triaxial compression tests that constituted this data set.

- The Anisotropic Modified Cam-Clay model does not have significant benefits over the isotropic version of the model (i.e. MCC) for the simulation of compression triaxial tests.

- The Hardening-Soil model yields better results for relatively stiff clays.

5 DEEP EXCAVATIONS: THE OBSERVATIONAL METHOD AND INVERSE ANALYSIS

5.1 INTRODUCTION

A major concern when performing deep excavations in urban environments is the impact of construction-related ground movements on adjacent buildings and utilities. The ground movements cause any structures supported by the affected ground to deform and possibly sustain damage. Therefore, predicting the magnitude and distribution of these movements is critically important. These predictions can then be used to estimate the tolerance of the structures and utilities to the deformations sustained as a result of the ground displacements.

Many factors affect movements associated with excavations, including soil properties (soil type, presence of water), support system properties (wall stiffness, support stiffness, preload) and construction activities or workmanship (construction sequence, installation of support, surcharge loads). In practice, when designers are faced with an excavation where

ground movements are a critical issue, they can base their estimate of movements on semi-empirical methods based in part on past performance data or on results of finite element analyses. The main limitation of the first approach is the variety of construction techniques of the case studies used in developing them. These activities can contribute significantly to the movements reported. Therefore design approaches developed from these data should be considered biased towards average construction practices. The only way to explicitly include the effects of the construction activities in the analysis is to perform numerical simulations of the problem. Indeed, if the exact construction procedure is known, a finite element analysis conceptually allows an engineer to model all aspects of excavation that cause stress change in soil: wall installation, dewatering, cycles of excavation, bracing and brace removal, and preloading of anchors.

In recent years numerical simulations have become much more common for the analysis of excavations in urban environments. Finno and Harahap (1991) performed a series of finite element analyses for an excavation in soft clays in Chicago. They concluded that the horizontal deflection of a supported wall during excavation could be predicted using the finite element method with good accuracy if a representative soil model and proper consideration of construction procedures were included in the analysis. Finite element predictions, however, contain uncertainties related to soil properties, support system details and construction procedures. If one wants to predict and evaluate the overall performance of a design, a procedure that incorporates an evaluation of the results of the analyses must be defined.

The procedure to accomplish this task is usually referred to as the "observational method" (see section 2.2.3). Morgenstern (1995), in his Casagrande Lecture, emphasizes the importance of the observational method and stresses the need to have plans to cope with possible eventualities. In practice, however, it is very difficult to quantitatively judge how well the work is proceeding especially considering the time constraints associated with construction. Ad-hoc mathematical tools are needed to compare observations and predictions.

To improve the state-of-the-practice of controlling ground movements associated with supported excavations, this chapter presents a procedure that "objectively" updates design predictions of deformations for supported excavations in clay. Monitoring data are used as observations in an inverse analysis that calibrates the numerical model of the excavation and thus supports, in an objective way, the engineering judgments made during the construction of the excavation system. The inverse analysis methodology was developed and tested using data from a 39 ft deep excavation through soft clays in Chicago (Finno et al. 2002).

5.2 UPDATE DESIGN PREDICTIONS USING MONITORING DATA BY INVERSE ANALYSIS

This section shows how inverse analysis based on field monitoring data can be used to objectively update the predicted performance of supported excavation systems. Movements of the soil surrounding an excavation, measured to evaluate how well the actual

construction process is proceeding in relation to the predicted behavior, can be recorded by inclinometers, which measure lateral deformations at various depths at discrete locations around the construction site, and survey points, which record ground movements and/or displacements of structures adjacent to the excavation. With an inverse analysis procedure (see Chapter 2), these recorded displacements can be used to control the construction process and update predictions of movements at early stages of construction. Any time a new set of construction monitoring data are available, the finite element model of an excavation can be "recalibrated" to provide the best fit to the field observations.

In the work described herein, inverse analysis is used to optimize the soil models that characterize the soil layers in finite element simulations of supported excavations. Inverse analysis algorithms allow the simultaneous calibration of multiple input parameters. However, identifying the important parameters to include in the inverse analysis can be problematic. Indeed, it is not possible to use the regression analysis to estimate every parameter of every soil model used in the simulation. The number and type of input parameters that one can expect to estimate simultaneously depend from many factors, among which:

- Soil models used. The characteristics of the soil models and the number and type of observations used in the simulation determine the input parameters that are expected to be successfully calibrated. Some model parameters may be correlated to one another and thus not likely to be estimated simultaneously.

- Aspects of the simulated system represented by estimated parameters. In many instances, supported excavations generally generate only small deformations in the soil surrounding the excavation. In these instances, stiffness parameters are expected to be more important than failure parameters in defining the behavior of the soil mass. Sensitivity analyses can be used to determine the input parameters of a soil model that are most relevant to the computed system response.

- Available observations. The number of observation points used in the inverse analysis is related to the maximum number of parameters that one can expect to estimate by regression analysis. Their spatial distribution influences the number of soil layers whose parameters can be calibrated.

- Finite element implementation. Computational time may constitute an important variable for very complex simulations. The number of finite element runs at any given iteration and the number of iterations needed for the convergence of the regression analysis are proportional to the number of estimated parameters, NP.

Figure 5-1 shows a procedural flowchart that can be used for the identification of the soil parameters to optimize by inverse analysis. As subsequently described, the total number of input parameters can be reduced, in four steps, to the number of parameters that are likely to be successfully optimized by inverse analysis.

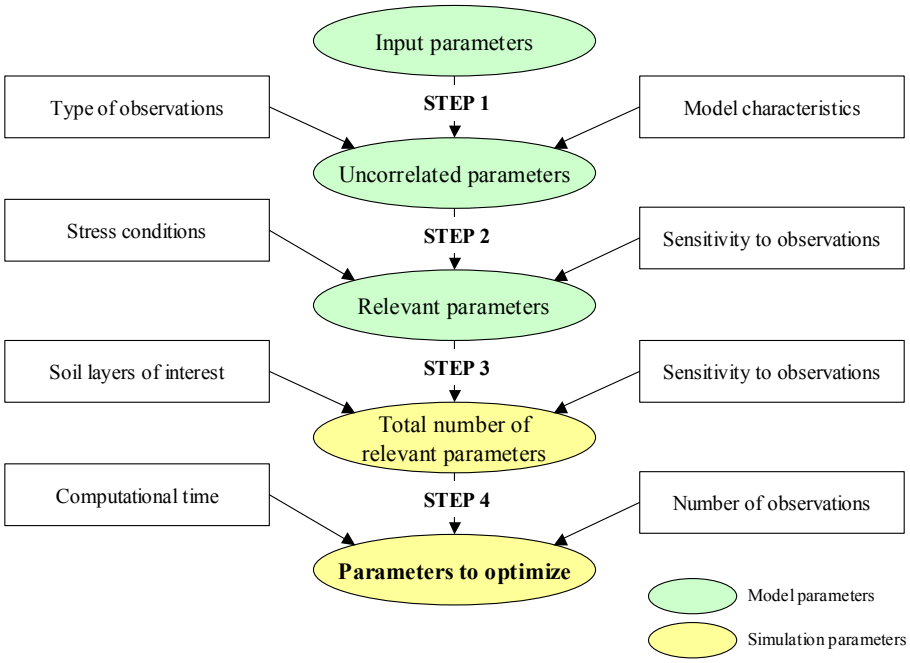

Figure 5-1 Flowchart for the identification of soil parameters to optimize by inverse analysis

Step 1: Model's input parameters ⇒ Model's uncorrelated parameters. The soil model chosen to simulate the soil behavior determines the total number of input parameters to estimate (e.g., the H-S model has 10 input parameters). The number of parameters that can be estimated by inverse analysis depends from the characteristics of the model and from the type of observations available. Parameter correlation coefficients (Eq. 2.13) can be used to evaluate which parameters are correlated and are, therefore, not likely to be estimated simultaneously by inverse analysis.

Step 2: Model's uncorrelated parameters ⇒ Model's relevant parameters. The parameters that most affect the computed results are determined by the stress conditions in the soil around the excavation. Composite scaled sensitivity values (Eq. 2.9) can provide valuable information on the relative importance of the different input parameters of a given model.

Step 3: Model's relevant parameters ⇒ Total relevant parameters. The number of soil layers to calibrate and the type of soil model used to simulate the layers determines the total number of relevant parameters of the simulation. A new sensitivity analysis may be necessary to check for correlations between parameters relative to different layers.

Step 4: Total relevant parameters ⇒ Parameters to optimize. The total number of observations available and computational time considerations may prompt a final reduction of the number of parameters to optimize simultaneously.

Figure 5-1 showed the key role that sensitivity analyses have in determining the parameters that are important for the finite element simulation of an excavation. Once the parameters to optimize have been chosen, sensitivity results continue to play an integral part in the regression analysis. Indeed, a sensitivity matrix is computed at every regression iteration. This is necessary because the simulation of an excavation system by finite element methods is a highly non-linear problem. Thus, the sensitivity of the results to changes in parameter values is not constant but depends on the particular values at which the sensitivity matrix is computed.

The design chart (Clough et al. 1989) given in Figure 5-2 will be used to explain the importance of this approach. The graph is generally used to design retention systems for supported excavations in soft to medium clays. The curves show how the ratio between the maximum horizontal movement of the wall and the height of excavation (δ_H/H) is a function of the factor of safety against basal heave (FS_{BS}) and of the retaining system stiffness ($EI/h^4\gamma_w$), a combination of wall stiffness and strut spacing.

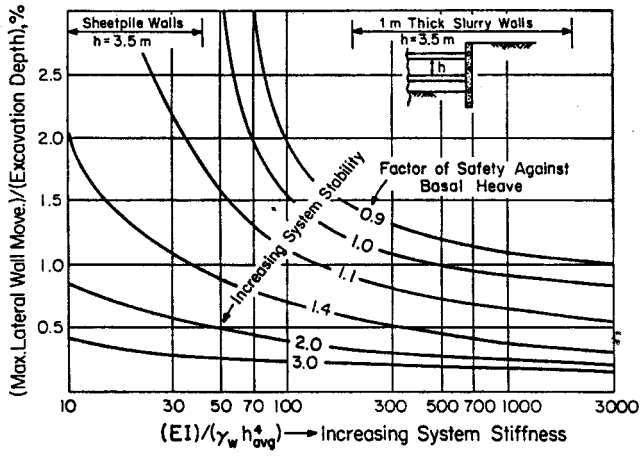

Figure 5-2 Design Curves for Maximum Lateral Movement in Soft to Medium Clay [after Clough et al. (1989)]

The chart can be considered a model of the excavation problem, where FS_{BS} and $EI/h^4\gamma_w$ are the input parameters and δ_H/H is a measure of the design performance. The tangent of the design curves expresses the sensitivity of the movements with respect to the system stiffness, the distance between the curves is related to the sensitivity of the movements with respect to FS_{BS}. The graph shows that, if the system is stiff or the factor of safety against

basal heave is high, the performance is less sensitive to either parameter (i.e. a small value of the tangent to the curve) than would be the case if the system is flexible or has a low FS_{BS} (i.e. a higher value of the tangent to the curve).

5.3 PROCEDURE VALIDATION: THE CHICAGO & STATE CASE STUDY

The proposed methodology was developed and tested using data from a project in downtown Chicago (Finno et al. 2002), the excavation/renovation of the Chicago & State CTA subway station.

5.3.1 Problem specifications

The renovation project included the excavation of 39 ft of soft to medium clay within 7 ft of a school (Frances Xavier Warde School) supported on shallow foundations. Figure 5-3 shows a section of the excavation support system. The support system consisted of a secant pile wall with three levels of support, which included pipe struts (1st level) and tieback anchors (2nd and 3rd levels). The design was made knowing some damage to the adjacent school would occur, and the support system was selected to minimize the damage. Ground and structural movements of the school building were recorded during construction to monitor and assess the damage to the school.

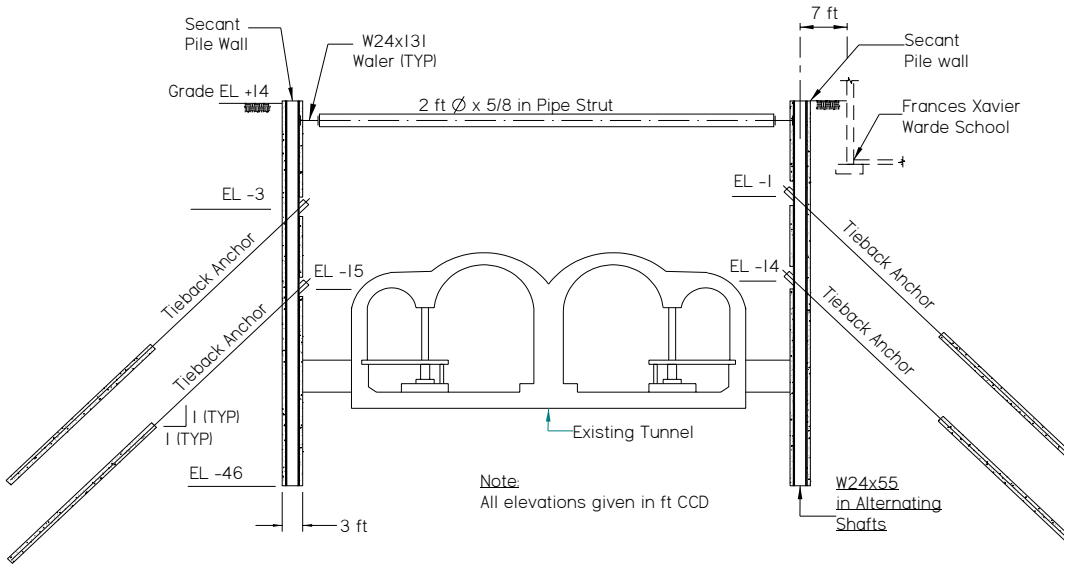

Figure 5-3 Section view of excavation support system

Figures 5.4 and 5.5 show pictures of the excavation site. Figure 5-4 was shot at the end of the excavation from the roof of the Warde school (looking north). It shows the excavation site, the three levels of support and the exposed tunnel tubes. Figure 5-5 shows a detailed view of the secant pile wall with the two levels of tiebacks installed. Note that, because of the presence of the tunnel tubes, the final depth of the excavation was only reached in a 8-ft-wide trench beside the wall. The secant pile wall was "chipped" to install the walers supporting the tiebacks.

Figure 5-4 Excavation site (view from roof of adjacent school)

Figure 5-5 Secant pile wall and tiebacks

A comprehensive monitoring program was employed to monitor the ground deformations around the excavation and the structural response of the adjacent school. As shown in Figure 5-6, lateral movements of the soil behind the secant pile wall were recorded using five inclinometers located around the site. Vertical movements were obtained from optical survey points located along the outside walls of the school, on the roof, and on eight interior columns. Measurements of the different instruments were taken before the installation of the wall, and at frequent intervals during construction. The observations for the inverse analysis described in this chapter are derived from inclinometer data (incl. 1 and incl.4) at various construction stages.

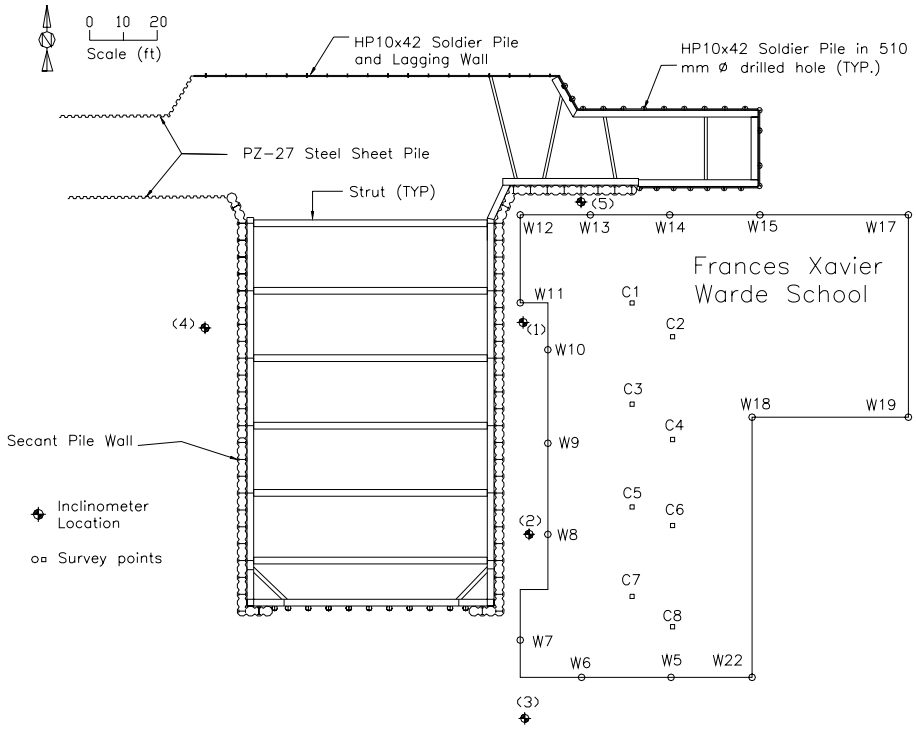

Figure 5-6 Plan view of excavation site

The retaining system was selected to limit the settlement of the school foundations to values that would avoid structural damage of the building and would produce only minor architectural damage. The design specifications set two settlement thresholds for the monitored building: a warning limit of 0.75 in and a maximum allowable movement of 1.25 in. The specifications also dictated that design reviews had to be considered had the settlement overcome the second threshold. During construction the vertical settlements of the school foundations exceeded 1.25 in. However, the construction activities went on, as designed, for two reasons: (i) there were no signs of structural damage in the building, (ii) at that stage the excavation had almost reached the final depth, thus there was very little room for design changes. The latter confirms the importance and the utility of a quantitative analysis of the monitoring data during the early stages of construction.

During the work at the Chicago & State project, field data were obtained and processed on a daily basis. Predictions of response to additional excavation were updated by trial-and-error adjustments of the finite element parameters that best fit the observed field data. The updating was done on the basis of comparisons between the maximum observed and computed lateral soil movement. Within the time constraints imposed by construction, neither the deflected shape of the inclinometer nor the distribution of the settlements behind the wall were matched. The results presented in this section will show that a inverse analysis procedure can instead perform those tasks effectively and in a timely fashion.

5.3.2 Finite element simulation of the problem

The finite element software PLAXIS was used to compute the response of the soil around the excavation. Figure 5-7 shows a schematic of the PLAXIS input. Details about the definition of the finite element problem, the calculation phases and the model parameters used in the simulation described herein can be found in Appendix E.

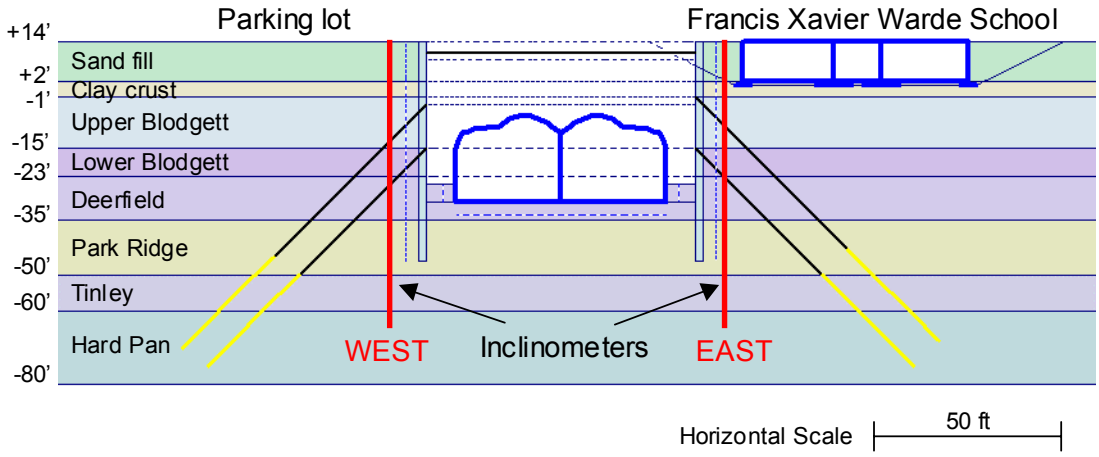

Figure 5-7 Schematic of PLAXIS input

The problem was simulated in plane-strain conditions. The soil stratigraphy was assumed to be uniform across the site (see Figure 4.4). The soil layers considered were 8: a fill layer overlaying a clay crust, a compressible clay deposit (in which 4 distinct clay layers were modeled) and two relative incompressible stiff silty clay strata. All elevations in the figure refer to the Chicago City Datum (CCD). Note that the figure, for display purposes, does not show the side boundaries of the mesh (600 ft x 94 ft), which was extended beyond the zone of influence of the settlements induced by the excavation (Hsien and Ou 1998 and

Caspe 1966). The finite element mesh boundary conditions were set using horizontal fixities, for the left and right boundaries, and total fixities, for the bottom boundary.

5.3.2.1 Calculation phases

The tunnel tubes and the school adjacent to the excavation were explicitly included in the finite element simulation of the problem to take into account the effect of their construction on the soil surrounding the excavation. Table 5-1 shows the PLAXIS calculation phases of the simulation described herein. The second column of the table shows the calculation phase number, the third column explains the purpose of the calculation phase, the fourth column indicates the calculation type, and the last column specifies the loading input condition. A plastic calculation indicates that an elasto-plastic deformation analysis is carried out in either fully drained or fully undrained conditions. For the simulation described herein, plastic calculations are always associated with staged construction loading conditions, which indicate changes in the geometric configuration of the FE mesh, and clay layers are always assumed to be in undrained conditions. Consolidation calculations are used to analyze the development and dissipation of excess pore pressures in the water-saturated soil layers as a function of time. An "ultimate time" (loading input condition) is specified to terminate a consolidation calculation. Note than in PLAXIS it is not possible to perform a staged construction calculation with simultaneous consolidation. More details about calculation types and loading input conditions can be found in the PLAXIS manual (Brinkgreve and Vermeer, 1998).

	Phase	Identification	Calculation	Loading input
	0	initial phase	N/A	N/A
Tunnel construction (late '30s)	1	mine tunnel and put ribs	Plastic	Staged construction
	2	put permanent liner	Plastic	Staged construction
	3	NIL step	Plastic	Staged construction
	4	change water table	Plastic	Staged construction
	5	consolidation (19 years)	Consolidation	Ultimate time
School construction (late '50s)	6	RESET DISPL. (NIL step)	Plastic	Staged construction
	7	excavate for school	Plastic	Staged construction
	8	place footings	Plastic	Staged construction
	9	load footings	Plastic	Total multipliers
	10	NIL step	Plastic	Staged construction
	11	consolidation (40 years)	Consolidation	Ultimate time
Wall installation (1999)	12	RESET DISPL. (NIL step)	Plastic	Staged construction
	13	drill piles (raise w.t 5' a.g.s.)	Plastic	Staged construction
	14	put concrete in piles	Plastic	Staged construction
	15	consolidation (20 days)	Consolidation	Ultimate time
Excavation (1999)	16	excavate [+9'] and put strut	Plastic	Staged construction
	17	excavate [-3']	Plastic	Staged construction
	18	prestress 1st tiebacks	Plastic	Staged construction
	19	excavate [-16']	Plastic	Staged construction
	20	prestress 2nd tiebacks	Plastic	Staged construction
	21	excavate [-25']	Plastic	Staged construction

Table 5-1 PLAXIS calculation phases

5.3.2.2 Hardening-Soil model initial calibration

The soil model used to characterize the clays in the PLAXIS simulation of the excavation is the Hardening-Soil model (see section 4.2.4). Table 5-2 shows the initial values of the H-S model parameters for the five clay layers that will be calibrated by inverse analysis. Layers 1 to 5 refer to the Upper Blodgett, Lower Blodgett, Deerfield, Park Ridge and Tinley layers, respectively. The model parameters of the soil layers that were not calibrated by inverse analysis can be found in Appendix E.

	Upper Blodgett	Lower Blodgett	Deerfield	Park Ridge	Tinley
Parameter	Layer 1	Layer 2	Layer 3	Layer 4	Layer 5
ϕ	23.4	23.4	25.6	32.8	32.8
c (psf)	1	1	1	1	1
R_f	0.9	0.9	0.9	0.9	0.9
ψ	0	0	0	0	0
E_{50}^{ref} (psf)	4700	6000	6000	8600	12900
m	0.8	0.8	0.85	0.85	0.85
E_{oed}^{ref} (psf)	3290	4200	4200	6020	9030
E_{ur}^{ref} (psf)	14100	18000	18000	25800	38700
ν_{ur}	0.2	0.2	0.2	0.2	0.2
k_0	0.603	0.603	0.568	0.458	0.458

Table 5-2 Initial values of H-S parameters for the 5 clay layers calibrated by inverse analysis

The initial estimates of the input parameters for layers 1 to 4 are based on the results of the model calibration by inverse analysis presented in section 4.4.4. Note that the values of parameter m, for layers 1 and 2, and parameter E_{50}^{ref}, for layer 2, are slightly different from the best fit-values presented in Table 4.13. Indeed, they were adjusted to produce values, for all layers, "consistently" increasing with depth. Because little laboratory data exists for the layer 5 soil, the initial values of the parameters for layer 5 are based on the following considerations: (i) layer 5 failure parameters are assumed to have the same values of layer 4 failure parameters, and (ii) layer 5 stiffness modules are assumed to be 1.5 times larger than layer 4 stiffness modules. For all layers, the value of parameter E_{oed}^{ref} is assumed to be equal to 70% E_{50}^{ref}.

The H-S stiffness parameters are defined with respect to a reference pressure (p_{ref}=100 stress units). Thus, it is difficult to relate the values of E_{50}^{ref}, E_{oed}^{ref}, and E_{ur}^{ref} to "typical" geotechnical estimates of stiffness moduli. The following equations define the stress dependent stiffness moduli used in the H-S model:

$$E_{50} = E_{50}^{ref} \left(\frac{c\cot\varphi + \sigma_3'}{c\cot\varphi + p^{ref}} \right)^m \tag{5.1}$$

$$E_{oed} = E_{oed}^{ref} \left(\frac{c\cot\varphi + \sigma_1'}{c\cot\varphi + p^{ref}} \right)^m \tag{5.2}$$

$$E_{ur} = E_{ur}^{ref} \left(\frac{c \cot \varphi + \sigma_3'}{c \cot \varphi + p^{ref}} \right)^m \tag{5.3}$$

where E_{50} is the secant Young modulus, E_{oed} is the oedometric modulus, E_{ur} is the unload-reload elastic modulus, σ_1' is the major principal stress, σ_3' is the minor principal stress, ϕ is the friction angle and c is the cohesion.

Figures 5-8, 5-9 and 5-10 show the variation with the vertical stress of E_{50}, E_{oed} and E_{ur}. The curves were computed, using the initial values of parameters c, ϕ and m (see Table 5-2), according to Equations 5.1, 5.2 and 5.3, respectively. The vertical and horizontal directions were assumed to be principal directions (i.e. $\sigma_v' = \sigma_1'$ and $\sigma_h' = \sigma_3' = k_0 \sigma_v'$).

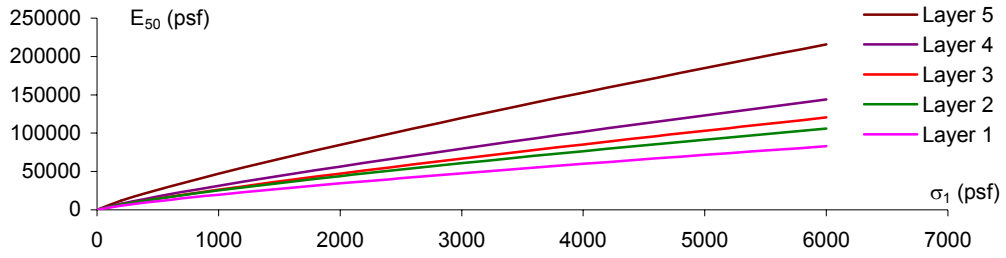

Figure 5-8 Variation of stiffness parameter E_{50} with vertical stress σ_v' (initial parameter estimates)

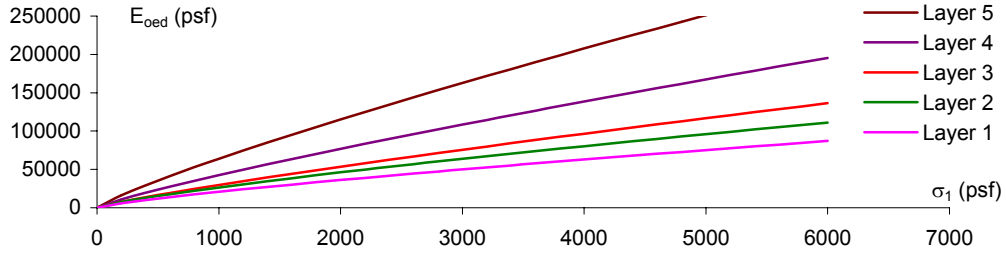

Figure 5-9 Variation of stiffness parameter E_{oed} with vertical stress σ_v' (initial parameter estimates)

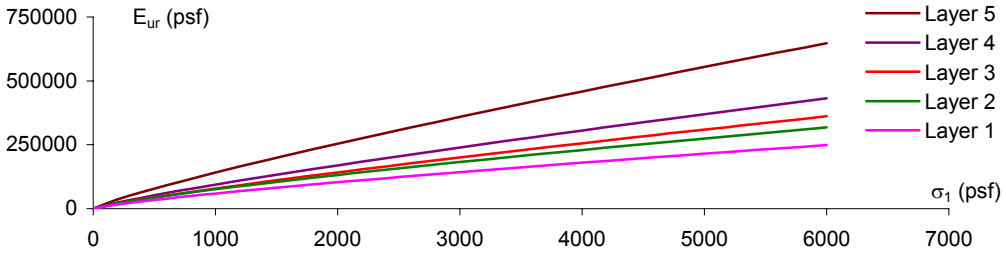

Figure 5-10 Variation of stiffness parameter E_{ur} with vertical stress σ_v' (initial parameter estimates)

To compare the stiffnesses of different layers, one has to consider the effective stresses of the soil. Table 5-3 shows the initial vertical effective stress in the middle of the five soil layers. These values can be used to compute, using Eq. 5.1 or Figure 5-8, the values of the secant stiffness modulus at 50% shear strength, E_{50}, at the beginning of the simulation.

Soil layer	Till layer	Elevation (ft CCD)		γ_{sat} (pcf)	σ_1' average (psf)
Layer 1	*Blodgett*	-1	-15	115	1939
Layer 2		-15	-23	115	2517
Layer 3	*Deerfield*	-23	-35	120	3073
Layer 4	*Park ridge*	-35	-50	125	3888
Layer 5	*Tinley*	-50	-60	125	4671

Table 5-3 Initial vertical effective stress of clay layers

Table 5-4 shows, for all five layers, the initial E_{50}^{ref} values, the computed E_{50} values, the estimated undrained shear strength S_u and the ratio between E_{50} and S_u. Note that the S_u values were estimated from field vane results and correlations based on water content data (Chung and Finno, 1992).

Soil layer	E_{50}^{ref} (psf)	E_{50} (psf)	S_u (psf)	E_{50}/S_u
Layer 1	4700	33594	360	93
Layer 2	6000	52851	520	102
Layer 3	6000	68194	870	78
Layer 4	8600	99487	2000	50
Layer 5	12900	174399	3000	58

Table 5-4 Initial E_{50} / S_u ratios of clay layers

Note that E_{50} represents a drained modulus. Nonetheless the ratio E_{50}/S_u can be used to judge the "relative inherent stiffness" of the various soil layers in undrained conditions. The initial E_{50}/S_u ratios used in this simulation show that: (i) the Blodgett layers (1 and 2) are

assumed to have about the same relative stiffness, and (ii) the other layers (3, 4 and 5) become, relative to their undrained shear strength, progressively more deformable with depth.

"Typical" values of E_u/S_u ratios are often presented in literature to evaluate the stress-strain undrained response of clays. Lambe and Whitman (1969) report E_u/S_u values of about 500 and 1000 for soft and stiff clays, respectively. E_{50}/S_u values are not generally quoted in literature. However, E_{50}/S_u ratios can be related to typical E_u/S_u ratios if the initial undrained stiffness modulus E_u is converted into an equivalent E_{50}. The following three steps describe a way of computing E_{50} from a given value of E_u.

Step 1 ($E_u \Rightarrow G_{in}$)

The following relationship between elastic moduli can be used to convert E_u (initial undrained stiffness modulus) into an equivalent G_{in} (initial shear stiffness modulus):

$$G_{in} = \frac{E_u}{3} \tag{5.4}$$

Step 2 ($G_{in} \Rightarrow G_{50}$)

The value of the shear stiffness modulus of clays, G, decreases with increasing shear strains:

$$G_{50} < G_{in} < G_0 \tag{5.5}$$

The maximum stiffness, G_0, only occurs at extremely small strains (ε_{sh}<0.001%). The initial undrained stiffness modulus E_u is generally computed at higher strain levels (ε_{sh}=0.05-0.1%). Thus, the initial shear stiffness modulus, G_{in}, is smaller than G_0. Based on published results (Viggiani and Atkinson, 1995) the value of G_{in} is assumed to be 0.5-0.75 times G_0 and G_{50} is assumed to be 0.25-0.50 times G_{in} (i.e. G_{50} = 0.15-0.35 G_0).

Step 3 ($G_{50} \Rightarrow E_{50}$)

The following relationship between elastic modules can be used to convert G_{50} (50% shear stiffness modulus) into an equivalent E_{50} (50% secant stiffness modulus):

$$E_{50} = 2(1+\nu)G_{50} \tag{5.6}$$

Finno and Chung (1992) reported E_u/S_u values of 400-600 for normally consolidated compressible Chicago clays (Blodgett and Deerfield layers) sheared in triaxial compression. Following the procedure outlined previously, an equivalent E_{50}/S_u ratio can be computed. Assuming E_u/S_u=500, $G_{50}=G_{in}/3$ and ν=0.2, the ratio E_{50}/S_u equals 133. This value is slightly higher than the initial values used in this simulation (see Table 5-4), suggesting that the initial estimates of the H-S parameters defining the soil stiffness may be conservative.

5.3.3 Inverse analysis set-up

The optimization algorithm UCODE was used to calibrate, by inverse analysis, the PLAXIS finite element simulation of the excavation. A schematic of the interaction

between PLAXIS and UCODE was presented in Figure 4-7. Examples of input and output files of the inverse problem analyzed in this section can be found in Appendix E.

5.3.3.1 Observations and weighting

Table 5-5 shows the construction stages for which the model predictions are updated. Lateral movements of the soil behind the secant pile wall were recorded using five inclinometers. The excavation, however, was modeled in plane strain conditions. Thus, only two of them (incl. 1 on the east and incl. 4 on the west) were used to compare field data and computed displacements. The measured settlements were not used as observations because the finite element predictions of the ground settlement induced by excavation are generally not as good as those of the horizontal movements of the soil.

		Construction day	
Stage	Plaxis phase	East (incl. 1)	West (incl. 4)
Initial	Beginning of project	0	0
Stage 1	Drill piles	11	18
Stage 2	Excavate [+9'] and put strut	60	73
Stage 3	Excavate [-3'] and prestress tiebacks (1st level)	88	95
Stage 4	Excavate [-16'] and prestress tiebacks (2nd level)	105	109
Stage 5	Excavate [-25']	112	123

Table 5-5 Excavation stages considered for updating model predictions

Figure 5-11 shows the observation points retrieved from the field readings of inclinometers 1 and 4 (the data in the plot refer to stage 1). The soil profile and a schematic of the

support system are also shown in the figure. Inclinometer readings were taken in the field every two feet. Not every reading, however, could be used as an observation for the inverse analysis because the finite element displacements were computed only at the intersection between the finite element mesh and the inclinometer location. Thus, 13 observation points were used for the east side and 11 observation points for the west side.

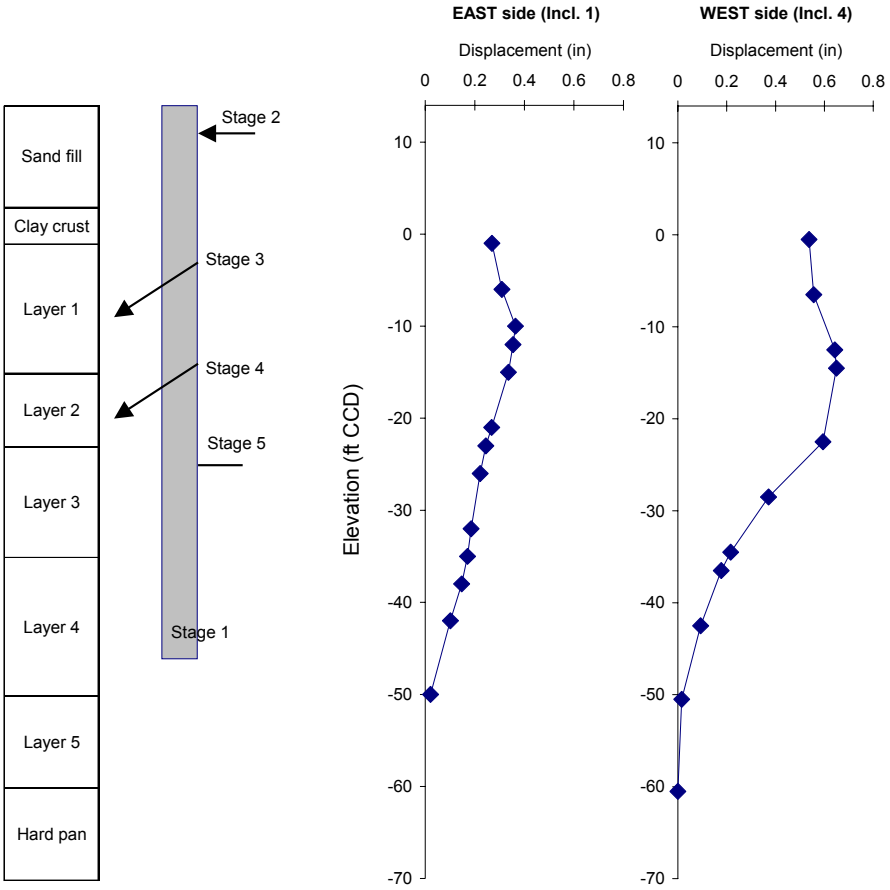

Figure 5-11 Schematic of retaining system and observation points used from inclinometer readings (e.g., stage 1 data)

The inverse of the variance of the measurement errors was used to assign weights to the observations (i.e. inclinometer data). Table 5-6 shows the values of the observation points used for the five construction stages and their measurement errors. See Appendix E for details about the inclinometer probe used to monitor the movements at the excavation site, its accuracy and the computed measurement errors. The measurement error of the horizontal displacement inclinometer data is not constant. Its value increases as one moves further away from the bottom of the casing because the inclinometer probe measures tilt and not displacements, thus errors become larger as one gets closer to the ground surface. Note that inclinometer data are available, for the east side, at all 5 construction stages considered. On the west side, however, the inclinometer was damaged by construction activities after stage 3. That is why the west side inclinometer readings are not shown, in subsequent figures, for the last two stages of construction.

	Elevation (ft CCD)	Horizontal diplacement (ft)					Measurement error, σ (ft)
		Stage 1	Stage 2	Stage 3	Stage 4	Stage 5	
EAST (incl.1)	-1	0.0225	0.0264	0.0340	0.0495	0.0579	0.0073
	-6	0.0258	0.0297	0.0371	0.0562	0.0670	0.0066
	-10	0.0304	0.0341	0.0455	0.0720	0.0869	0.0061
	-12	0.0296	0.0332	0.0455	0.0724	0.0886	0.0059
	-15	0.0280	0.0311	0.0412	0.0665	0.0836	0.0055
	-21	0.0224	0.0244	0.0307	0.0511	0.0680	0.0047
	-23	0.0204	0.0220	0.0275	0.0471	0.0635	0.0045
	-26	0.0185	0.0197	0.0241	0.0417	0.0564	0.0041
	-32	0.0155	0.0163	0.0194	0.0304	0.0402	0.0033
	-35	0.0142	0.0150	0.0175	0.0259	0.0336	0.0029
	-38	0.0123	0.0131	0.0152	0.0216	0.0270	0.0026
	-42	0.0085	0.0083	0.0099	0.0140	0.0168	0.0020
	-50	0.0018	0.0013	0.0024	0.0038	0.0043	0.0010
WEST (incl.4)	-0.5	0.0448	0.0551	0.0830			0.0084
	-6.5	0.0464	0.0535	0.0799			0.0076
	-12.5	0.0536	0.0579	0.0768			0.0068
	-14.5	0.0541	0.0582	0.0756			0.0066
	-22.5	0.0495	0.0505	0.0749			0.0055
	-28.5	0.0310	0.0298	0.0459			0.0048
	-34.5	0.0180	0.0160	0.0265			0.0040
	-36.5	0.0148	0.0126	0.0218			0.0038
	-42.5	0.0078	0.0052	0.0106			0.0030
	-50.5	0.0013	-0.0001	0.0025			0.0020
	-60.5	0.0000	0.0001	0.0009			0.0007

Table 5-6 Values of observations on the east side and west side and their measurement errors

5.3.3.2 Parameterization

The soil layers calibrated by inverse analysis are the upper Blodgett, lower Blodgett, Deerfield, Park Ridge and Tinley strata. In the analysis described herein they are referred to as layer 1, 2, 3, 4 and 5, respectively. All the layers are modeled using the Hardening-Soil model. The initial estimates of the H-S input parameters were presented in section 5.3.2.2. The input parameters optimized by inverse analysis were chosen following the procedure described in section 5.2. Note that the first two steps of the procedure (see Figure 5-1) refer to the selection of the "model parameters" (e.g., H-S model) that are relevant to the problem under study, the last two steps refer to the selection of the total number of "simulation parameters" (e.g., 5 soil layers calibrated simultaneously) to optimize by inverse analysis.

The H-S model features 10 input parameters. The characteristics of the model determine the number of uncorrelated parameters that one can expect to successfully optimize by inverse analysis. Results from section 4.4.4 showed that the H-S parameters that can be effectively estimated from laboratory data using an automated optimization algorithm are E_{50}^{ref}, m and ϕ. For the simulation discussed herein the values of the other model parameters, similarly to what was done for the calibration of the H-S model in section 4.4.4, are either kept constant at their initial value (parameters c, ψ, ν and R_f), or are assumed to be related to one of the other parameters ($E_{oed}^{ref} = 0.7\ E_{50}^{ref}$, $E_{ur}^{ref} = 3.0\ E_{50}^{ref}$ and $k_0 = 1 - \sin\phi$)

The sensitivity of the observations to changes in values of E_{50}^{ref}, m and ϕ determines the parameters that are relevant to the problem simulated herein. Figures 5.12 and 5.13 show the composite scaled sensitivities of the three parameters for layers 1 to 5. In the first figure the bar chart refers to sensitivities computed using all the observations, and the line charts refer to sensitivities computed from the observations of the different layers. In the second figure the sensitivities are grouped by construction stages. Both figures show that all three parameters (i.e. E_{50}^{ref}, m and ϕ) are important, from a model perspective, in affecting the outcome of the analysis. From a simulation perspective, results show that the parameters that most influence the simulation are the ones relative to layers 1 and 4. Layer 1 is the softest soil layer, thus its major influence on the displacement results is expected. Layer 4 is the stiff clay layer below the bottom of the excavation, into which the wall is tipped. The high sensitivity values relative to this layer indicate that the strength and the stiffness of the clay below the excavation have significant impact on movements. As one would expect Figure 5-12 also shows that the observations relative to a soil layer are mainly influenced by changes in that soil layer's parameters. For instance, the values of the sensitivities from layer 4 and layer 5 observations show a clear "peak", respectively, at layer 4 and layer 5 input parameters. Likewise, Figure 5-13 shows that the parameters of the deeper layers become more important at later construction stages (i.e. deeper excavation depths).

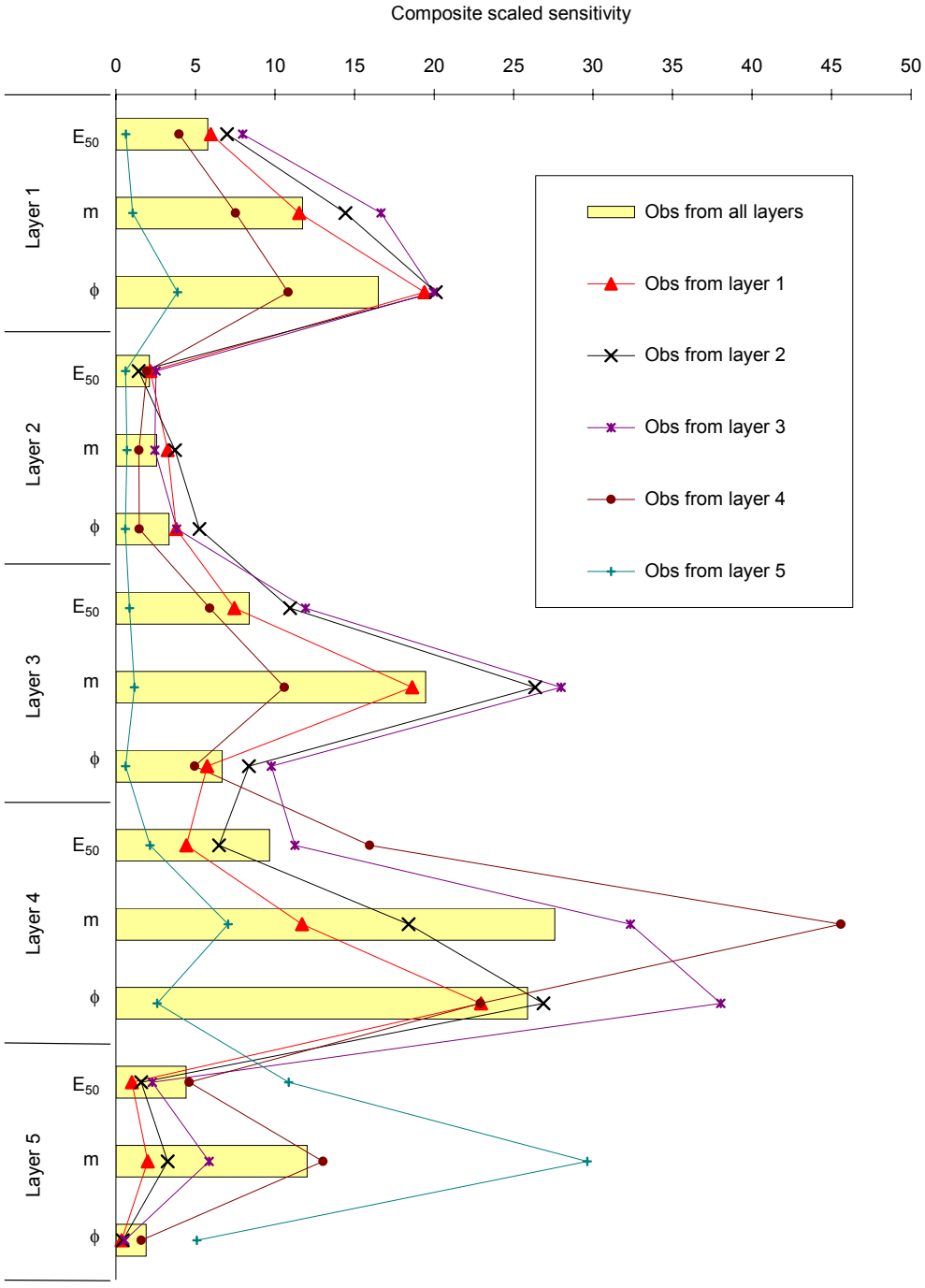

Figure 5-12 Composite scaled sensitivities of parameters E_{50}^{ref}, m and ϕ for layers 1 to 5.

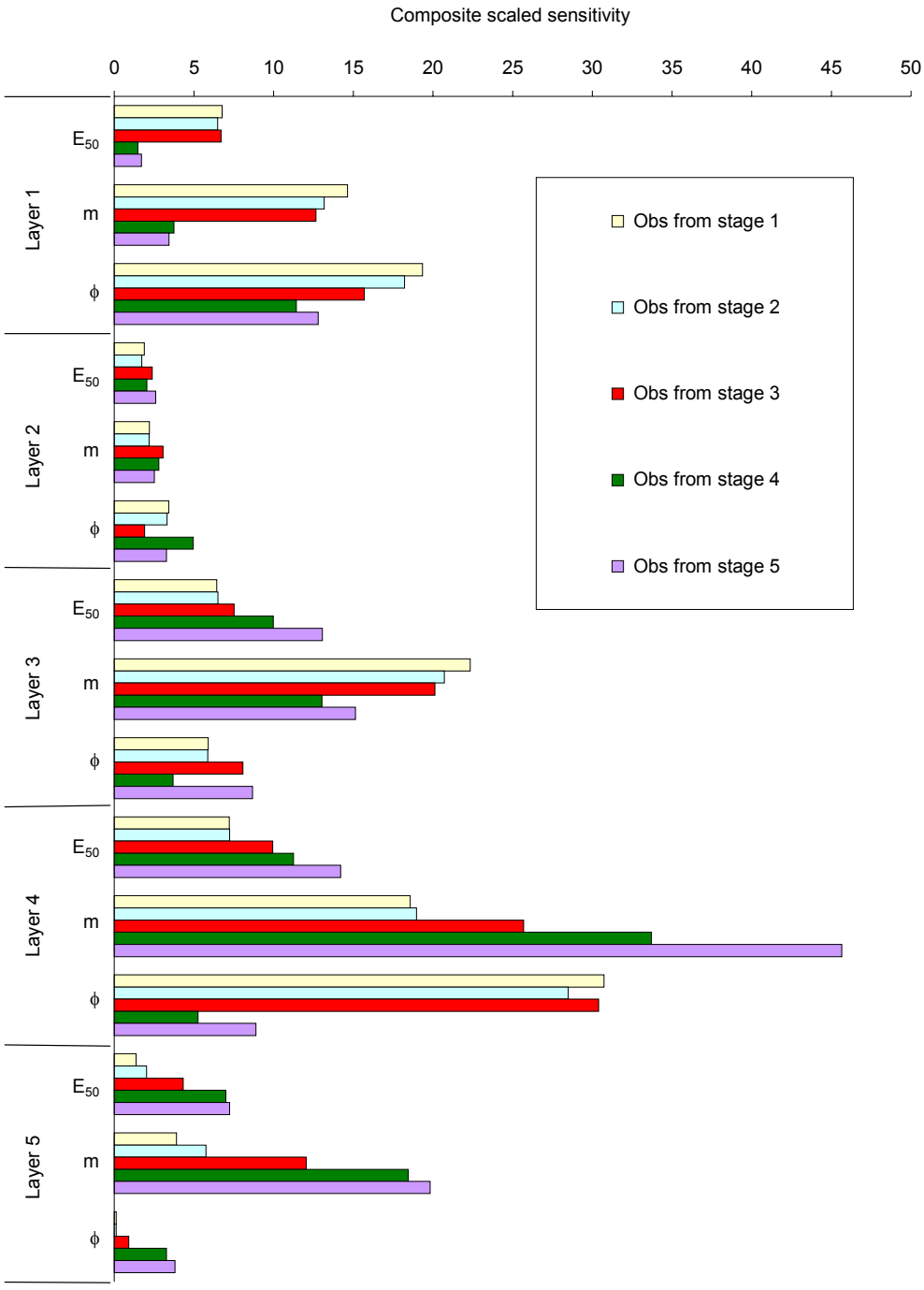

Figure 5-13 Composite scaled sensitivities of parameters E_{50}^{ref}, m and ϕ for layers 1 to 5 grouped by construction stages

Other important parameter statistics resulting from a sensitivity analysis are the correlation coefficients. The sensitivity analysis performed on E_{50}^{ref}, m and ϕ for layers 1 to 5 indicated that high correlation values occur between parameters E_{50}^{ref} and m. Table 5-7 shows the correlation coefficients between the three parameters at every layer. Results indicate that the two stiffness parameters (i.e. E_{50}^{ref} and m) cannot be simultaneously and uniquely optimized, even though the results of the analysis are sensitive to both parameters. Parameter E_{50}^{ref}, rather than parameter m, was chosen to "represent" the stiffness of the H-S model. The reasons behind this choice are: (i) m values are bounded between 0 and 1.0, thus they would require the use of a "mapping function" (see section 2.4) to avoid possible problems with unreasonable updated values during the regression iterations, and (ii) changes in E_{50}^{ref} values also produce changes in the values of parameters E_{oed}^{ref} (equal to 0.7 times E_{50}^{ref}) and E_{ur}^{ref} (equal to 3 times E_{50}^{ref}), thus their calibration can be considered as "representative" of the calibration all three H-S stiffness parameters.

Correlation coefficients					
between parameters	value	between parameters	value	between parameters	value
$m_{(1)}$ and $E_{50\,(1)}$	-0.70	$\phi_{(1)}$ and $E_{50\,(1)}$	-0.42	$m_{(1)}$ and $\phi_{(1)}$	0.33
$m_{(2)}$ and $E_{50\,(2)}$	-0.85	$\phi_{(2)}$ and $E_{50\,(2)}$	-0.59	$m_{(2)}$ and $\phi_{(2)}$	0.41
$m_{(3)}$ and $E_{50\,(3)}$	-0.87	$\phi_{(3)}$ and $E_{50\,(3)}$	-0.58	$m_{(3)}$ and $\phi_{(3)}$	0.25
$m_{(4)}$ and $E_{50\,(4)}$	-0.99	$\phi_{(4)}$ and $E_{50\,(4)}$	-0.07	$m_{(4)}$ and $\phi_{(4)}$	-0.14
$m_{(5)}$ and $E_{50\,(5)}$	-0.95	$\phi_{(5)}$ and $E_{50\,(5)}$	0.39	$m_{(5)}$ and $\phi_{(5)}$	-0.56

Table 5-7 Highest values of correlation coefficients

The results of the sensitivity analysis seem to indicate that the total number of relevant parameters is 10 (i.e. E_{50}^{ref} and ϕ for layers 1 to 5). However a final reduction of the parameters to optimize was necessary to establish a "well-posed" problem. Table 5-8 shows the parameters that are optimized by inverse analysis for the simulation described herein.

Layer	Parameter optimized	Related parameters
1	E1 = E_{50}^{ref}	E_{oed}^{ref} and E_{ur}^{ref}
2	E2 = E_{50}^{ref}	E_{oed}^{ref} and E_{ur}^{ref}
3	E3 = E_{50}^{ref}	E_{oed}^{ref} and E_{ur}^{ref}
4	E4 = E_{50}^{ref}	E_{oed}^{ref} and E_{ur}^{ref}
5	E5 = E_{50}^{ref}	E_{oed}^{ref} and E_{ur}^{ref}

Table 5-8 Parameters optimized by inverse analysis

The parameters to optimize were chosen based on the following considerations:

1. Hill (1998) suggests applying the "principle of parsimony." Thus, to begin calibration estimating very few parameters that together represent most of the features of interest and to increase the complexity of the parameterization slowly.

2. Poeter and Hill (1997) warn against "spreading the data too thin." If all 10 relevant parameters were to be optimized simultaneously, the ratio between the number of observations available at the first construction stage (24 displacement observation points) and the number of parameters estimated (NP=10) would be too low.

3. The first construction stage, which refers to the excavation of the 60'-deep secant pile wall, causes movements in all 5 clay layers. Thus, at least one parameter per layer had to be considered for optimization.

4. The stiffness parameters (E_{50}^{ref}) were chosen over the failure parameters (ϕ) because the excavation-induced stress conditions in the soil around the excavation were, for the most part, far from failure. Thus, the stiffness parameters were perceived to be more relevant to the simulated problem.

5. Results of the parametric study conducted on the number of input parameters considered for optimization by inverse analysis (section 3.3.2) suggest that a model can be successfully calibrated even if some "relevant" parameters are excluded from the optimization, provided that their initial estimate is "reasonable."

A comparison between the results obtained by the current parameterization of the inverse analysis and alternative parameterizations, in which the failure parameters will also be optimized by the regression algorithm, will be presented in Chapter 6.

5.3.3.3 Regression variables

A summary of the inverse analysis setup is presented in Table 5-9. The table shows the values of the variables used to define the Chicago & State regression analysis.

Geotechnical variables	Observations	readings from inclinometers 1 (east) and 4 (west)
	Number of input parameters	1 parameter (E_{50}^{ref}) per layer (5 layers considered)
	Initial values	calibration by inverse analysis from triaxial results
	Discretization (east)	13 readings per construction stage
	Discretization (west)	11 readings per construction stage
Optimization variables	Observations' weighting	σ^2 = measurement error variance
	Tolerance on convergence criteria	TOL = SOSR = 5%
	Regression variables	MAX-CHANGE = 0.5
	Sensitivity calculation	PERTURBATION = 0.01

Table 5-9 Values of regression variables used for the Chicago & State inverse analysis

5.3.4 Results

This section presents the results of the inverse analysis performed on the finite element simulation of the Chicago & State excavation project. Visual examination of the horizontal displacement distributions at the inclinometer locations plots provides the simplest way to evaluate the fit between computed and measured field response. Figure 5-14 shows the comparison between the measured field data and the computed horizontal displacements when the initial estimates of the parameters are used (see Table 5-2). The comparison shows that the finite element model computes significantly larger displacements at every construction stage. The maximum computed horizontal displacements are about two times the measured ones and the computed displacement profiles result in significant and unrealistic movements in the lower clay layers (Deerfield and Park Ridge). Results indicate that the stiffness properties for the clay layers have been underpredicted, as was suggested in 5.3.2.2.

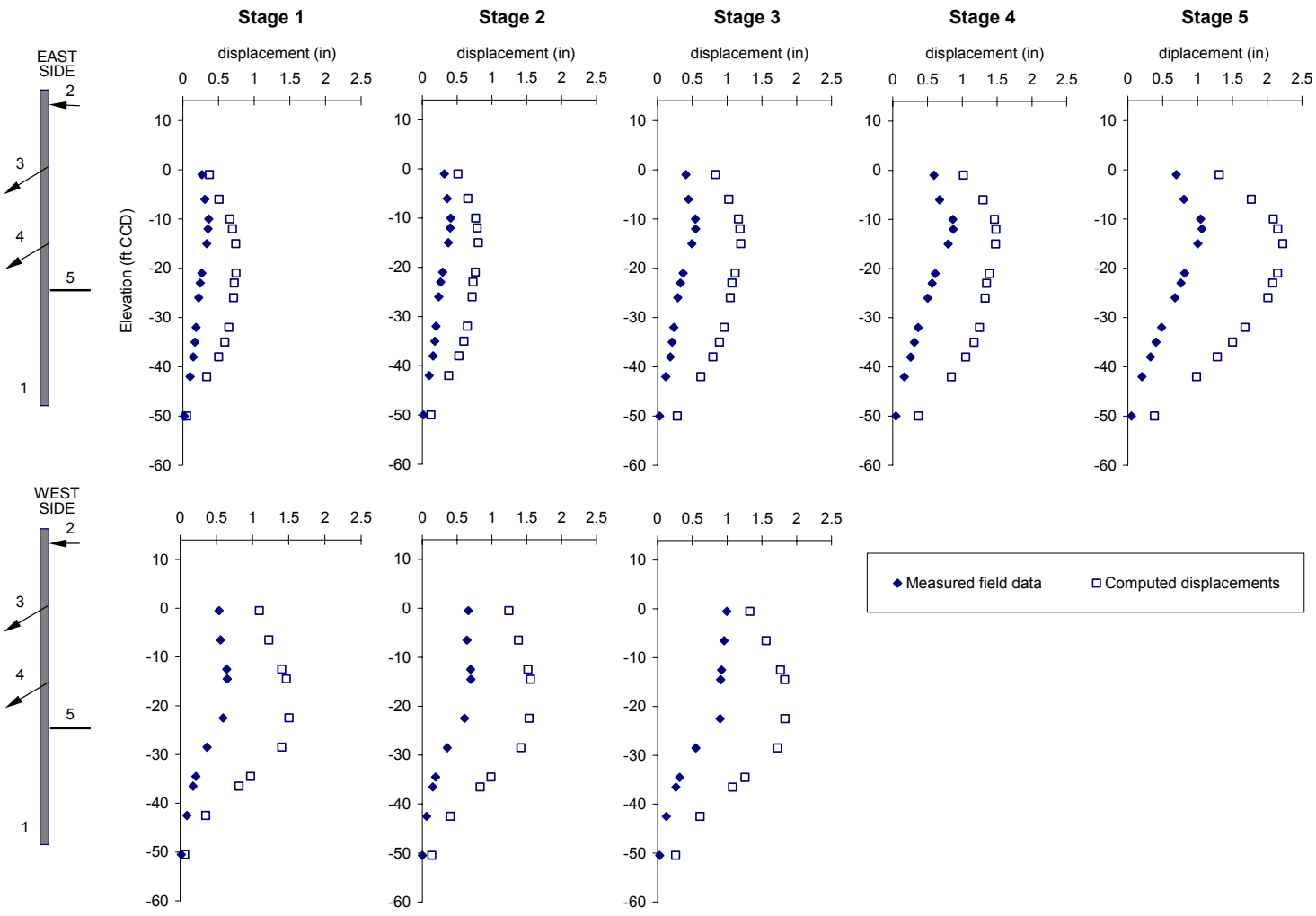

Figure 5-14 Measured vs. computed horizontal displacements: initial estimate of parameters

5.3.4.1 Optimization based on observations from construction stage 1

Table 5-10 shows the initial values of the 5 input parameters considered in the analysis and the values of the parameters that best fit the observations relative to stage 1. Results show that the optimized values of the parameters are, at all layers, higher than their initial estimates.

	E_1 (psf)	E_2 (psf)	E_3 (psf)	E_4 (psf)	E_5 (psf)
Initial	4700	6000	6000	8600	12900
Stage 1	6370		17960	42310	63465*

* Parameter not optimized indipendently

Table 5-10 Initial and optimized input parameters at stage 1

Note that: (i) parameters E_1 and E_2 were optimized together (i.e. layer 1 and layer 2 were considered as a single layer) and converged to a value slightly higher that the initial estimate of parameter E_2, and (ii) parameter E_5 was not optimized by inverse analysis, instead its changes were "tied" to changes in the value of E_4 (at every iteration E_5 was set equal to 1.5 times E_4). This approach was employed after various unsuccessful attempts at optimizing all five parameters simultaneously and independently. The exclusion of parameters E_2 and E_5 from the regression was based on the results of the sensitivity analysis presented in section 5.3.3.2, which showed that the parameters relative to layer 2 and layer 5 did not affect the computed results as "significantly" as the parameters relative to layers 1, 3 and 4.

Figure 5-15 shows the comparison between the measured field data and the computed horizontal displacements when parameters are optimized based on stage 1 observations. The improvement on the fit between the computed and measured response is significant. Despite the fact that the optimized set of parameters is calculated using only stage 1 observations, the positive influence on the calculated response is substantial for all construction stages. At the end of the construction (i.e. stage 5) the maximum computed displacement exceeds the measured data by only about 15%. These results are significant in that a successful recalibration of the model at an early construction stage positively affects subsequent "predictions" of the soil behavior throughout construction.

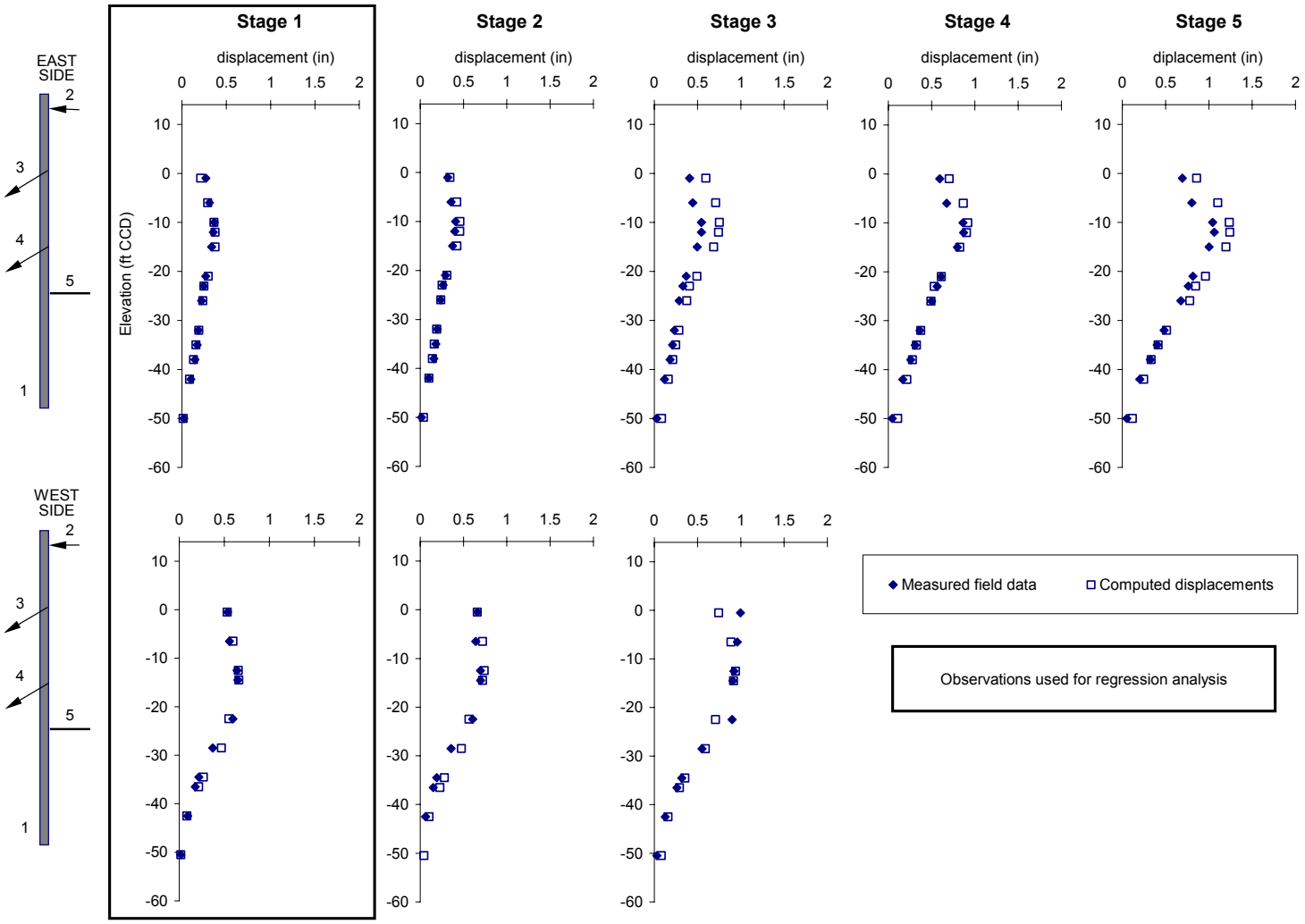

Figure 5-15 Measured vs. computed horizontal displacements: parameters optimized based on stage 1 observations

Table 5-11 shows the value of the following statistics that indicate the model fit to the field observations: $S(\underline{b})_{in}$ (initial objective function), $S(\underline{b})_{fin}$ (final objective function), s^2_{fin} (final error variance), CC_{fin} (final correlation coefficient) and FI (fit improvement). The values of these statistics prove that the calibration of the finite element simulation by inverse analysis based on stage 1 observations was extremely effective. The improvement over the initial predicted response is considerable (FI = 99.6%) and the final computed response fits the observations better than one would expect if the inclinometer measurement errors are taken into account ($s^2_{fin} < 1.0$).

Initial objective function	Final objective function	Final error variance	Final correlation coefficient	Fit improvement
$S(\underline{b})_{in}$	$S(\underline{b})_{fin}$	s^2_{fin}	CC_{fin}	FI
2132	7.57	0.40	0.97	99.6%

Table 5-11 Model fit statistics at optimization stage 1

Note that the statistics presented in Table 5-11 refer to stage 1 observations only. Thus, they cannot be used to assess how the calibrated simulation improves the fit between measured and computed response for the other construction stages. To quantify the "predictive" improvement of the calibration shown in Figure 5-15, one needs to consider the global objective function OF (Eq. 3.3), which takes into account all the observations available (from stage 1 to stage 5). A new model statistic, the predictive fit improvement

PFI, can be computed using the value of OF after the optimization and the value of OF relative to the initial estimates of the parameters:

$$PFI = \frac{OF_{base} - OF}{OF_{base}} \tag{5.7}$$

where PFI is the predictive fit improvement at the end of stage 1, OF_{base} is the global objective function relative the initial estimates of the parameters and OF is global objective function relative to the parameters based on stage 1 optimization.

Table 5-12 shows the values of the initial global objective function, the global objective function at the end of stage 1 and the predictive fit improvement at the end of stage 1.

Initial global objective function	Stage1 global objective function	Predictive fit improvement
OF_{base}	OF	PFI
21177	267.6	98.7%

Table 5-12 Model statistics quantifying the predictive improvement achieved by the calibration

5.3.4.2 Model fit for all construction stages

Section 5.3.4.1 presented the optimization results relative to the calibration of the simulation after construction stage 1. Parameters were recalibrated at every stage until the final construction stage (i.e. stage 5). At every new construction stage, the inclinometer data relative to that stage were added to the observations already available. Figure 5-15 showed

the visual fit comparison between inclinometer data and computed displacements when observations relative to stage 1 were used in the regression analysis. Figures 5-16, 5-17, 5-18 and 5-19 show the comparison between experimental and computed results for the remaining 4 stages (i.e. stage 2 to stage 5, respectively).

When stage 2 observations are used for the regression analysis (Figure 5-16) results do not change significantly. This indicates that the inclinometer readings relative to this construction stage do not provide significant extra information to improve the model calibration. When inclinometer data from stage 3 are added to the observations (Figure 5-17), the fit between the field and the computed results relative to this stage improves, especially in the upper soil layer. These results also improve the fit of stages 4 and 5. That is why observations from these last two construction stages (Figures 5-18 and 5-19) do not produce any change in the model. The calibrated model cannot be improved any further after stage 3.

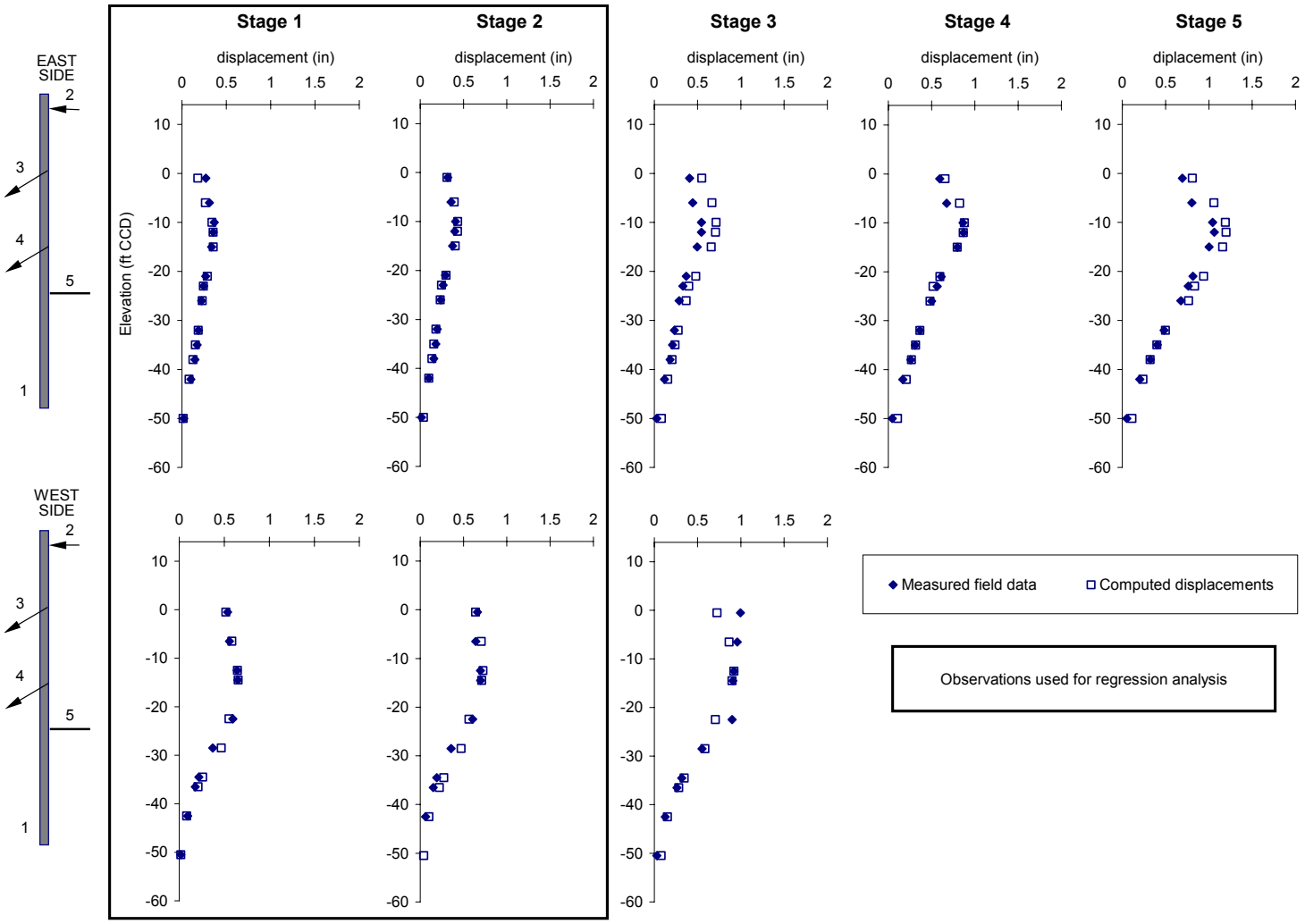

Figure 5-16 Measured vs. computed horizontal displacements: parameters optimized based on observations from stages 1 and 2

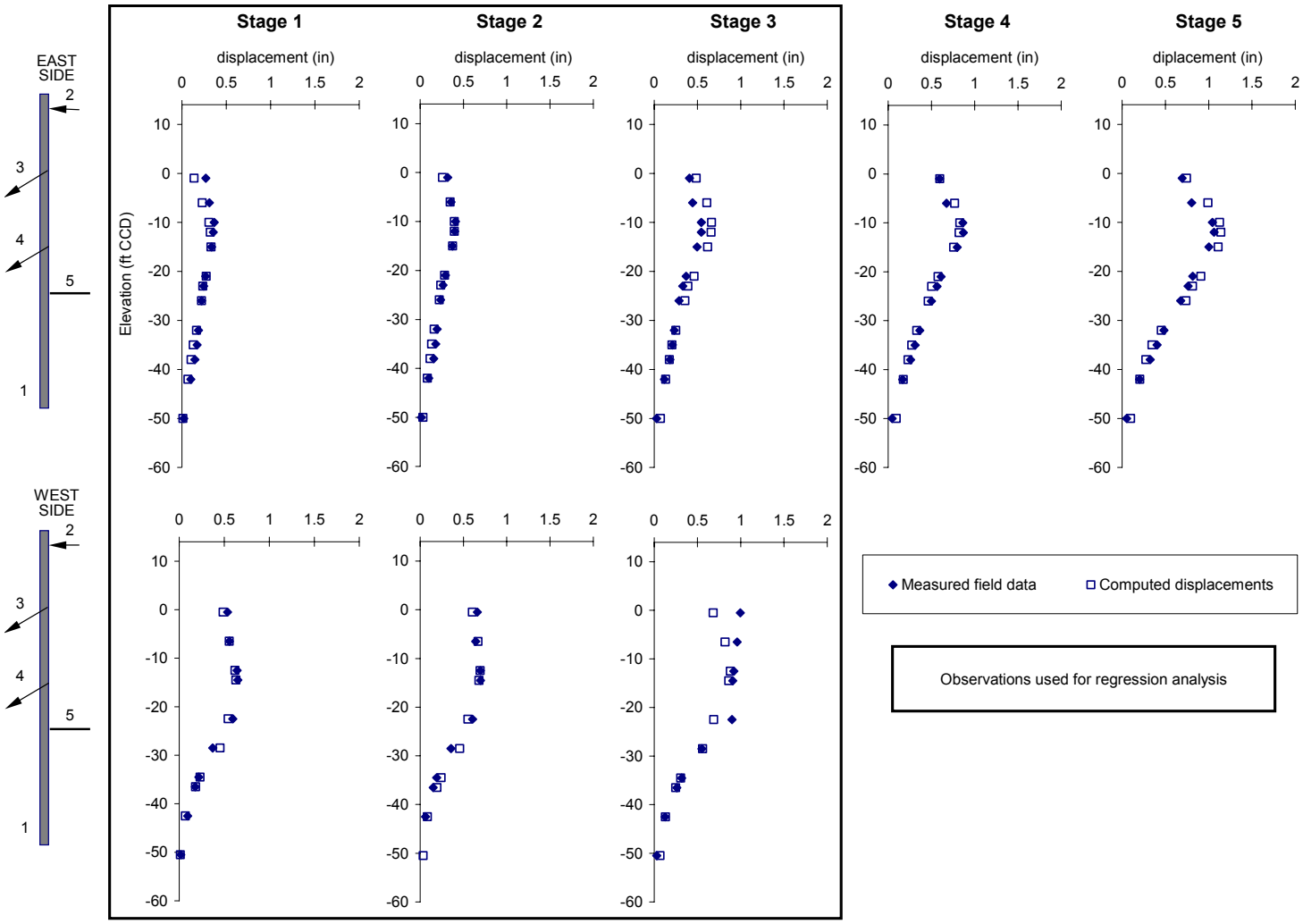

Figure 5-17 Measured vs. computed horizontal displacements: parameters optimized based on observations from stages 1, 2 and 3

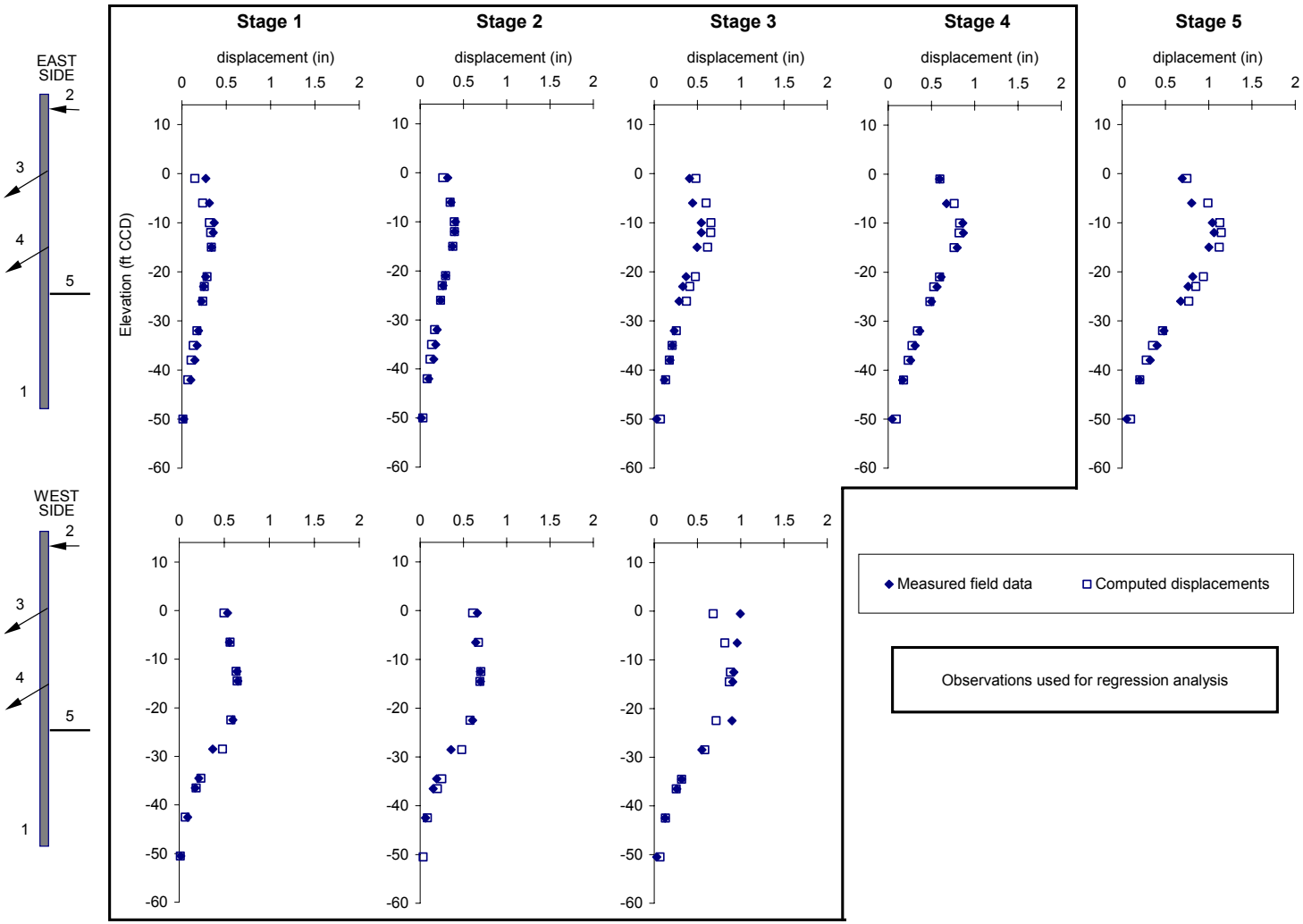

Figure 5-18 Measured vs. computed horizontal displacements: parameters optimized based on observations from stages 1, 2, 3 and 4

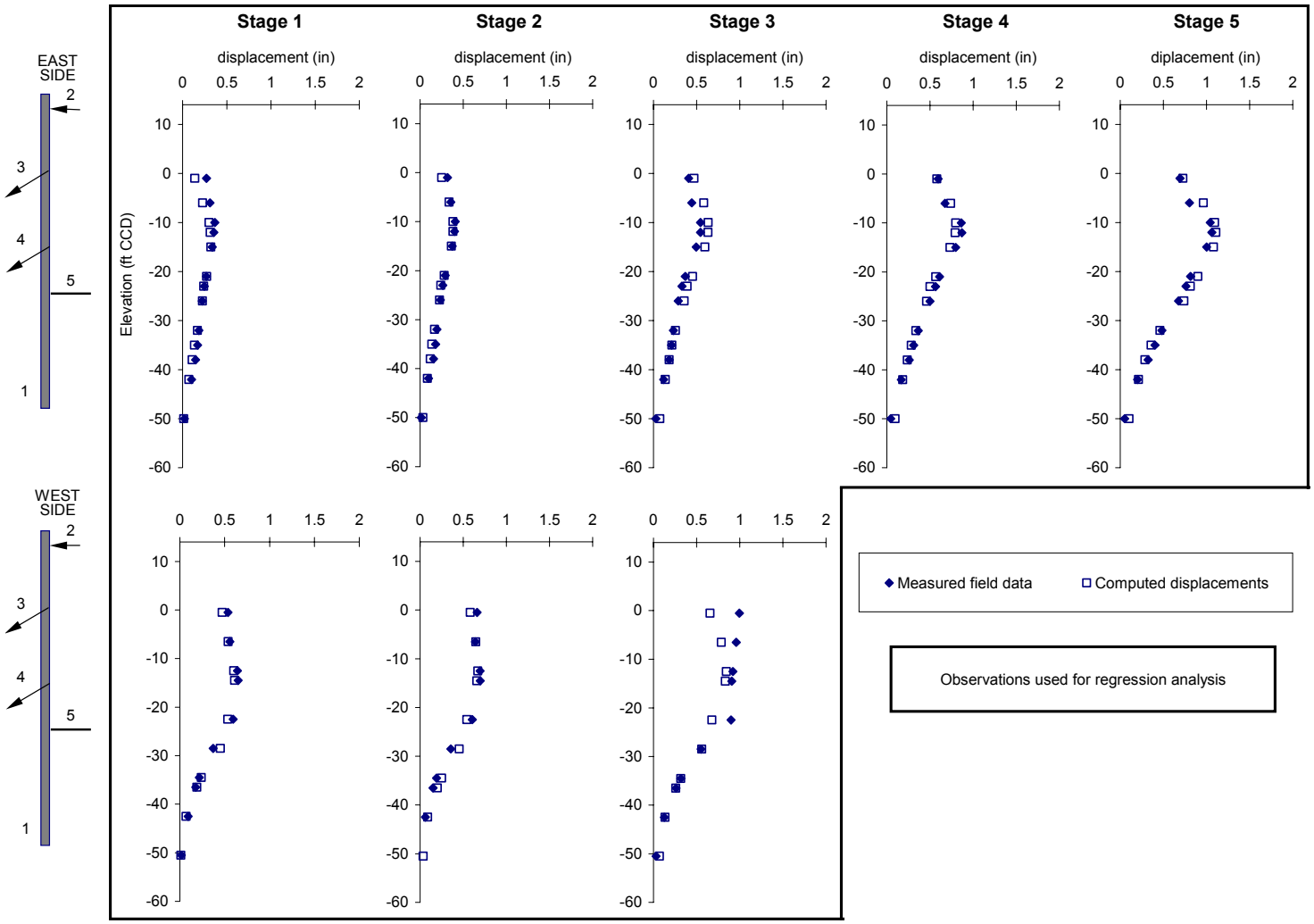

Figure 5-19 Measured vs. computed horizontal displacements: parameters optimized based on observations from all stages

Overall, the comparison between the measured field data and the computed horizontal displacements at the different optimization stages shows that the fit between the two sets of data is always remarkable. The inverse analysis performed after the first construction stage significantly improves the initial prediction of displacements and "recalibrates" the soil models in a way that allows them to capture the main behavior of the soil layers throughout construction. By the end of construction stage 3, the evolution of the horizontal movements at the inclinometer locations is predicted with great accuracy at all stages.

These results demonstrate that using inverse modeling techniques enhances the observational method practice. An engineer with detailed knowledge of finite element procedures and constitutive modeling, instead of performing a regression analysis, could modify the input soil parameters by trial-and-error. However, processing displacement data and using them to calibrate the results of the finite element model is an extremely time-consuming and highly subjective task. Figure 5-20 shows the comparison between the measured field data and the computed horizontal displacements in a simulation for which the "optimal" parameter values were estimated by trial-and-error. This research task was performed before developing the procedure described in this thesis. The fit between computed and observed data is relatively good, yet not every stage of construction is simulated with the same accuracy reached by the inverse analysis. Computed results match the maximum movements well, but they tend to overpredict the displacements of the stiffer layers.

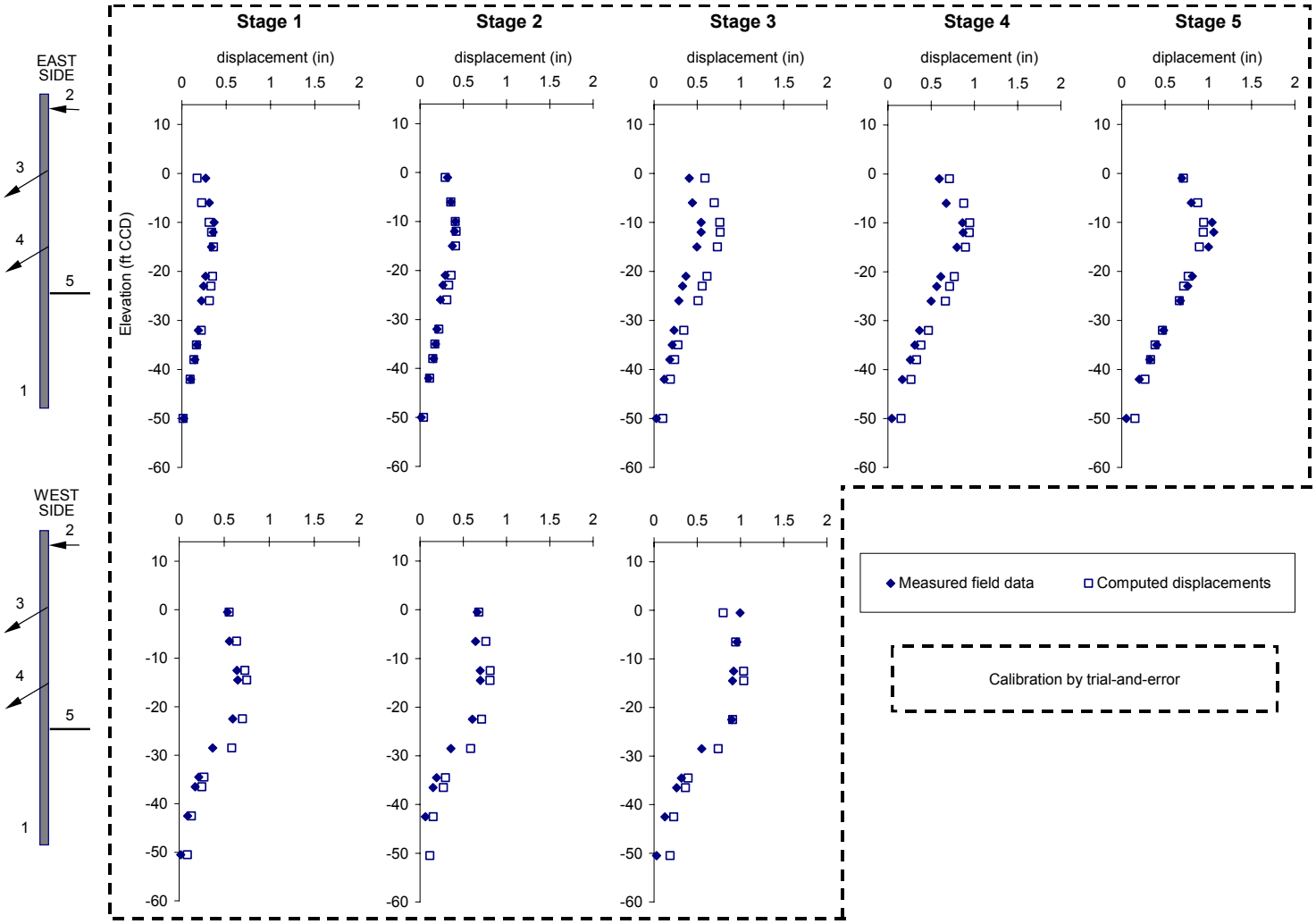

Figure 5-20 Measured vs. computed horizontal displacements: parameters estimated by trial and error based on all observations

5.3.4.3 Best-fit parameters

Table 5-13 shows the initial and optimized values of the 5 input parameters at the different optimization stages. Results show that, after construction stage 3, the values of the optimized input parameters do not change. This indicates that the observations at stages 4 and 5 "match" the computed results of the model calibrated at stage 3 and therefore further optimization of the model is neither possible nor necessary.

	E_1	E_2	E_3	E_4	E_5
Initial	4700		6000	8600	12900
Stage 1	6370		17960	42310	63465
Stage 2	6820		17530	44000	66000
Stage 3	7550		15670	53610	80415
Stage 4	7550		15670	53610	80415
Stage 5	7550		15670	53610	80415

Parameters optimized by inverse analysis
E_5 set to 1.5 E_4

Table 5-13 Best-fit values of input parameters at various optimization stages

In Figure 5-21 the variation of the input parameters at the various optimization stages is shown above a bar chart representing the progress of the excavation. The excavation depth is normalized with respect to the excavation width and plotted for the 5 construction stages. Results show that the maximum changes in parameter values occur at stage 1, when the observations relative to the installation of the secant-pile wall are used. Note that the

excavation was 74 ft wide, the secant pile wall was 60 ft deep and the maximum excavation depth was 39 ft below ground surface.

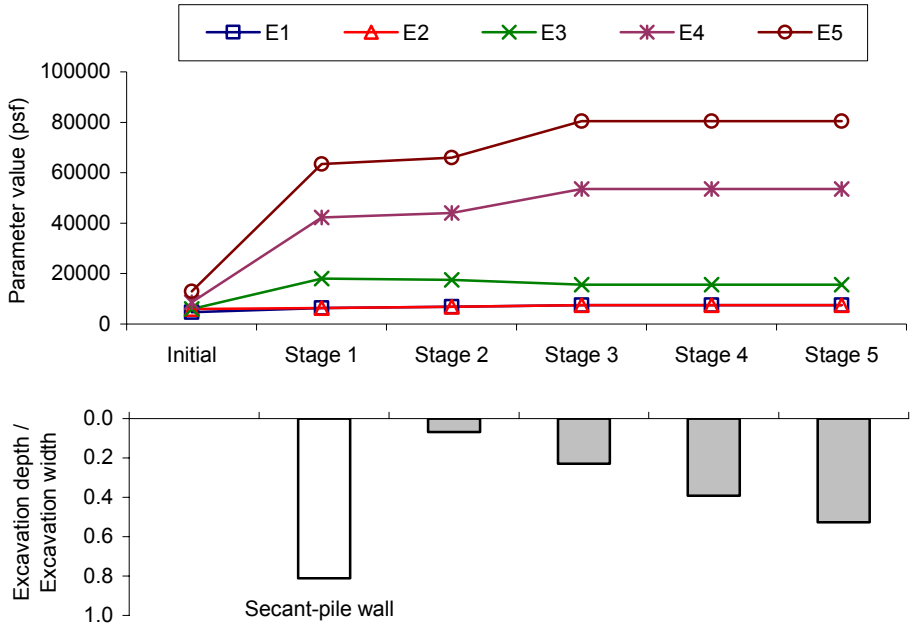

Figure 5-21 Best-fit parameter values and normalized excavation depth at different optimization stages

From the results presented in Table 5-13 and Figure 5-21 the following can be inferred:

1. The initial estimates of the stiffness parameters are significantly lower than the optimized values of the parameters. This is due to the fact that the initial values are based on triaxial compression test results, whereas most of the soil around the excavation experiences different stress paths (mainly undrained reduction of stresses).

2. The parameters that vary the most are the ones corresponding to the stiffer clay layers. The stiffer the clay, the more the laboratory test results are affected by sample disturbance and by the underestimation of stiffness values due to global measures of strains in a triaxial apparatus.

3. The simulated excavation is a 3D problem modeled in plane strain. When the excavated depth is small, most of the wall can be adequately modeled as plane strain and hence little changes in parameters are noted between stage 1 and 2. As the excavation deepens (stage 3), the ratio between excavation depth and excavation width increases and higher parameter values compensate for the lack of constraints in the out-of-plane direction.

4. The highest changes in parameter values occur at stage 1. The fit between computed and field displacement after stage 1 is extremely satisfactory. Thus, the calibrated parameters only need to change slightly at later stages. By the end of stage 3 the model essentially is calibrated.

5.3.4.4 Model statistics for all construction stages

The inverse analysis procedure produces very important by-products that allow one to quantify the effectiveness of the optimization procedure and assess the reliability of the predictions. Table 5-14 shows the values of a series of model fit statistics for the 5 optimization stages. Most of the statistics presented have been already defined elsewhere in this work, yet for convenience their expressions will be presented again in this section.

Results show that the calibration improved the fit between observations and computed results up to stage 3, after which there was no improvement.

Model statistic		Stage 1	Stage 2	Stage 3	Stage 4	Stage 5
Base objective function	$S(\underline{b})_{base\_i}$	2132	4597	9418	13652	21177
Initial objective funtion	$S(\underline{b})_{in\_i}$	2132	33.3	120	120.5	157.2
Final objective funtion	$S(\underline{b})_{fin\_i}$	7.57	29.8	97.6	120.5	157.2
Base error variance	$s^2_{base\_i}$	112.2	106.9	140.6	170.7	227.7
Final error variance	$s^2_{fin\_i}$	0.40	0.69	1.46	1.51	1.69
Relative fit improvement	RFI_i	99.6%	10.5%	18.7%	0.0%	0.0%
Total fit improvement	TFI_i	99.6%	99.4%	99.0%	99.1%	99.3%
Global objective function	OF_i	267.6	215.3	157.2	157.2	157.2
Predictive fit improvement	PFI_i	98.7%	99.0%	99.3%	99.3%	99.3%

Table 5-14 Model statistics of inverse analysis at various optimization stages

$$S(\underline{b})_{base\_i} = \left[\underline{y}_i - \underline{y}'(\underline{b})_{base\_i}\right]^T \underline{\omega}\left[\underline{y}_i - \underline{y}'(\underline{b})_{base\_i}\right] \tag{5.8}$$

$$S(\underline{b})_{in\_i} = \left[\underline{y}_i - \underline{y}'(\underline{b})_{in\_i}\right]^T \underline{\omega}\left[\underline{y}_i - \underline{y}'(\underline{b})_{in\_i}\right] \tag{5.9}$$

$$S(\underline{b})_{fin\_i} = \left[\underline{y}_i - \underline{y}'(\underline{b})_{fin\_i}\right]^T \underline{\omega}\left[\underline{y}_i - \underline{y}'(\underline{b})_{fin\_i}\right] \tag{5.10}$$

$$s^2_{base\_i} = \frac{S(\underline{b})_{base\_i}}{ND_i - NP} \tag{5.11}$$

$$s^2_{fin\_i} = \frac{S(\underline{b})_{fin\_i}}{ND_i - NP} \tag{5.12}$$

$$RFI_i = \frac{S(\underline{b})_{in\_i} - S(\underline{b})_{fin\_i}}{S(\underline{b})_{in\_i}} \tag{5.13}$$

$$TFI_i = \frac{S(\underline{b})_{base\_i} - S(\underline{b})_{fin\_i}}{S(\underline{b})_{base\_i}} \tag{5.14}$$

$$OF_i = \left[\underline{y}_{all} - \underline{y}'(\underline{b})_{all\_i}\right]^T \underline{\omega}\left[\underline{y}_{all} - \underline{y}'(\underline{b})_{all\_i}\right] \tag{5.15}$$

$$PFI_i = \frac{OF_{base} - OF_i}{OF_{base}} \tag{5.16}$$

where $\underline{b}$ is the vector of the estimated parameters, $\underline{y}_i$ is the vector of the observations used at stage i, $\underline{y}'(\underline{b})_{base\_i}$ is the vector of the results at stage i computed using the initial (base) estimates of the parameters, $\underline{\omega}$ is the weight matrix, $\underline{y}'(\underline{b})_{in\_i}$ is the vector of the results at stage i computed using the estimates of the parameters at the beginning of that stage, $\underline{y}'(\underline{b})_{fin\_i}$ is the vector of the results at stage i computed using the optimized estimates of the parameters at that stage, ND_i is the number of observations used at stage i, NP is the number of estimated parameters, $\underline{y}_{all}$ is the vector of all observations, $\underline{y}'(\underline{b})_{all\_i}$ is the vector

of all results computed using the optimized estimates of the parameters at stage i, and OF_{base} is the global objective function computed using the initial (base) estimates of the parameters.

Figure 5-22 shows the base and the final values of the error variance at the various stages. The graph allows one to compare the overall magnitude of weighted residuals relative to the initial estimates of the parameters with the fit resulting from the calibrated models. Results show that error variance values decrease by more than an order of magnitude at every stage. This indicates a significant improvement in the fit between observed and computed displacements. The final error variance values are always very close to 1.0. This indicates that the fit is consistent with the weighting of the observations, and thus with the measurement errors associated with the inclinometer data.

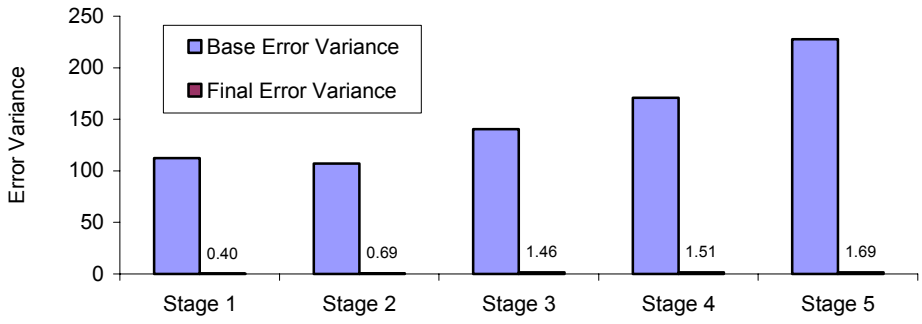

Figure 5-22 Error variance values at various optimization stages

Figure 5-23 shows the values of relative fit improvement, RFI, at the various stages and the values of the initial and final objective functions from which it is computed. The RFI indicates by what percentage the optimized results improved compared to the predictions

at the beginning of a given stage. Results show that stage 1 observations improved the predictions by 2 orders of magnitude (i.e. RFI equal 99%) and that, by the end of stage 3, the "recalibration" of the model is complete.

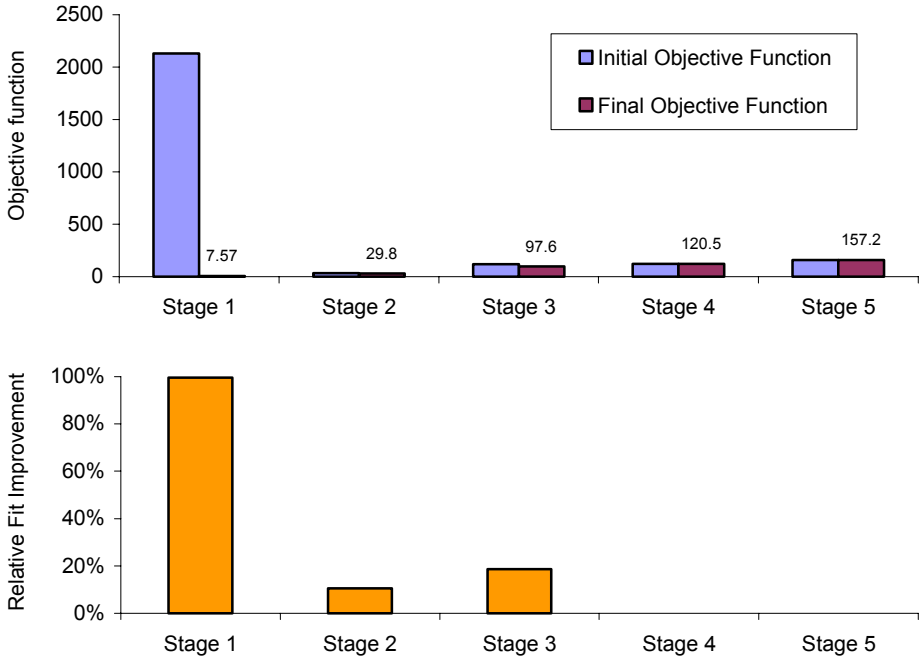

Figure 5-23 Objective function and relative fit improvement values

Figure 5-24 shows the values of the global objective function, OF_i, and the values of the predicted fit improvement, PFI_i, at the various stages. These statistics can be used to quantify the "predictive" capabilities of the analysis at the end of a given optimization stage. As one would expect, the global objective function values decrease as more observations become available (i.e. from stage 1 to stage 5). However, the PFI values indicate than most of the improvement "happens" at stage 1 and nothing is "gained" by including the

observations of stages 4 and 5. These results are extremely promising because they indicate that early stage observations are able to recalibrate the finite element simulation in a way that is beneficial to the predictions at later stages.

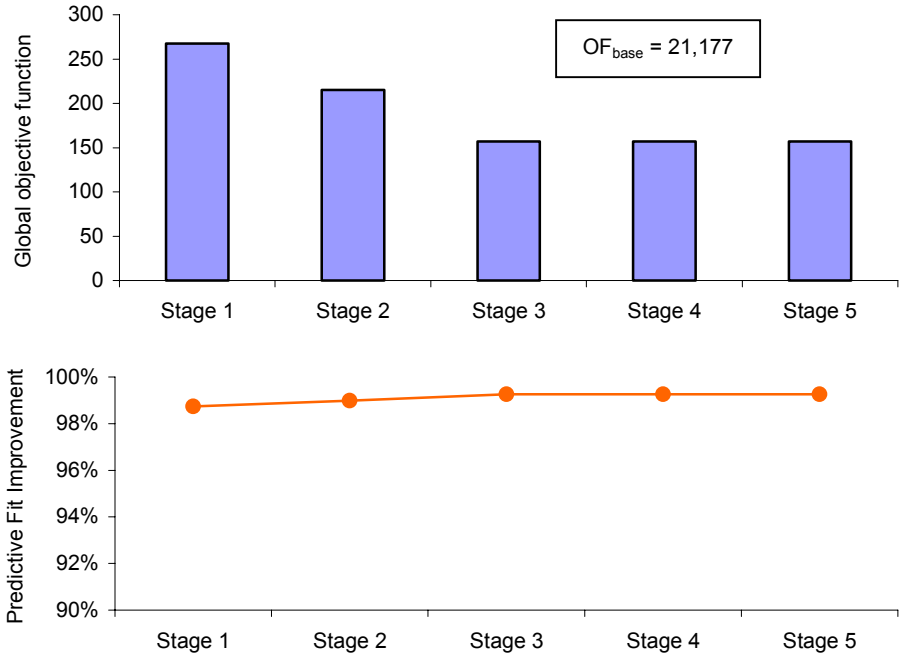

Figure 5-24 Global objective function and predictive fit improvement values

5.3.4.5 Comments on the calibrated model

In section 5.3.2.2 a procedure was presented to compare the initial stiffness-to-strength ratios, E_{50}/S_u, to typical values of undrained E_u/S_u ratios. Figure 5-25 shows the values of the initial and optimized E_{50}/S_u ratios of the 5 soil layers at different optimization stages. In Table 5-15 the values of the final equivalent undrained ratios, $(E_u/S_u)_{equivalent}$, are presented. Note that: (i) the stiffness E_{50} was computed from the values of parameter E_{50}^{ref} (see Table

5-13) according to Eq. 5.1 and considering the stress conditions in the middle of the layers on the two sides of the excavation at the inclinometer locations, and (ii) the equivalent undrained ratios, $(E_u/S_u)_{equivalent}$, were computed from the optimized values of E_{50}/S_u following the procedure described in section 5.3.2.2 and assuming $G_{50}=G_{in}/3$ and $\nu=0.2$.

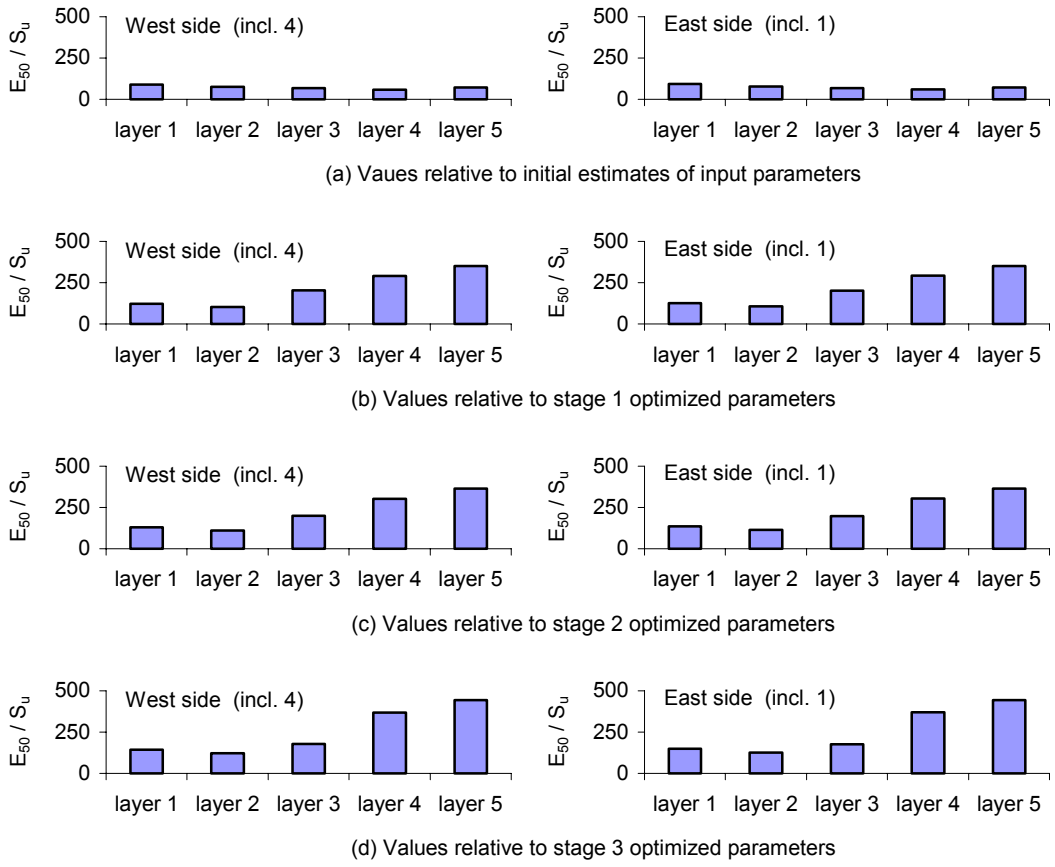

Figure 5-25 Initial and optimized E_{50}/S_u ratios of the different soil layers computed at different optimization stages: (a) initial, (b) stage 1, (c) stage 2 and (d) stage 3

		WEST			EAST		
	E_{50}^{ref} (psf)	E_{50} (psf)	E_{50}/S_u	$(E_u/S_u)_{eq}$	E_{50} (psf)	E_{50}/S_u	$(E_u/S_u)_{eq}$
layer 1	7550	51932	144	541	53860	150	561
layer 2	7550	63386	122	457	65264	126	471
layer 3	15670	178819	206	771	176931	203	763
layer 4	53610	868050	434	1628	874452	437	1640
layer 5	80415	1587844	529	1985	1587844	529	1985

Table 5-15 Stiffness-to-strength ratios for the best-fit values of the input parameters

Table 5-15 and Figure 5-25 showed that the optimized values of the stiffness-to-strength ratios increase with depth and are significantly higher than the initial values of the ratios. Note that the final values of $(E_u/S_u)_{equivalent}$ for layers 1, 2 and 3 (i.e. Bloldgett and Deerfield layers) are close to values reported by Finno and Chung (1992) for normally consolidated compressible Chicago clays (i.e. 400-600).

In Figure 5-26 the E_{50}/S_u ratios are plotted as a function of S_u/σ'_1. The values in the figure refer to the optimized values of the parameters (see Table 5-15). Results show that the value of E_{50}/S_u increases linearly with S_u/σ'_1. The following expression fits the data extremely well:

$$\frac{E_{50}}{S_u} = 800\frac{S_u}{\sigma'_1} \tag{5.17}$$

Eq. (5.17) can be conveniently used to estimate, for a given clay layer, the value of E_{50} from estimates of S_u and σ'_1, which are generally more easily available.

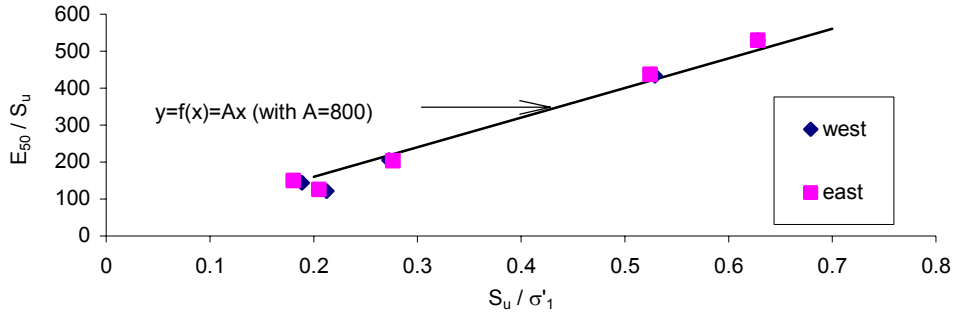

Figure 5-26 E_{50}/S_u vs. S_u/σ'_1 for the final calibrated model

In Figure 5-27 the optimized E_{50}/S_u ratios are plotted as a function of $(\sigma'_1-\sigma'_3)/2S_u$, an approximate measure of the relative shear stress of the layers. Results show that the value of E_{50}/S_u decreases as $(\sigma'_1-\sigma'_3)/2S_u$ increases, until the latter reaches the value of 1.0. Note that the slightly higher than 1.0 $(\sigma'_1-\sigma'_3)/2S_u$ values reported in the graph are possible because the undrained shear strength, S_u, is not an input parameter of the H-S model, thus its estimate does not influence the "exact" relative shear stress (whose maximum value is 1.0).

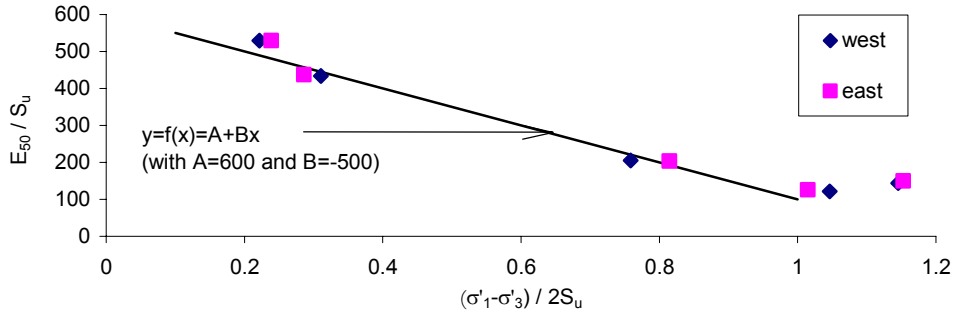

Figure 5-27 E_{50}/S_u vs. $(\sigma'_1-\sigma'_3)/S_u$ for the final calibrated model

A linear function can be used to interpolate the data:

$$\frac{E_{50}}{S_u} = 500 - 400\frac{\sigma_1 - \sigma_3}{S_u} \tag{5.18}$$

If we assume that, initially, the vertical and horizontal directions are principal directions the $(\sigma_1-\sigma_3)/S_u$ ratio can be written as:

$$\frac{\sigma_1 - \sigma_3}{S_u} = \left(1 - k_0\right)\frac{\sigma_v}{S_u} \tag{5.19}$$

where σ_v is the vertical effective stress and k_0 is the coefficient of earth pressure at rest.

Equations 5.18 and 5.19 can be combined to produce an equation to use for estimating the stiffness modulus E_{50} from values of S_u, k_0 and σ_v:

$$E_{50} = 500S_u - 400(1 - k_0)\sigma_v \tag{5.20}$$

5.4 SUMMARY

This chapter presented a numerical procedure that uses construction monitoring data to "recalibrate", by inverse analysis, the input parameters of a finite element model of a supported excavation. The inverse analysis methodology was developed and tested using data from a 39 ft deep excavation through soft clays in Chicago. The inverse analysis algorithm UCODE was used to optimize the PLAXIS plane-strain finite element

simulation of the excavation. Five clay layers, modeled using the Hardening-Soil model, were calibrated using inclinometer data that measured lateral movements of the soil behind the supporting walls. One stiffness parameter per layer was optimized in the regression analysis. The other model parameters were either kept constant at their initial value or related to the updated optimized parameters.

For the first three construction stages, the set of parameters converged to a new set of optimized values based on the observations available up to that stage. The improvement on the fit between the computed and measured response was always significant. When monitoring data relative to the first construction stage (i.e. installation of the wall) were used, the recalibrated model proved able to adequately "predict" the behavior of the soil for all construction stages. These results are significant in that a successful recalibration of the model at an early construction stage positively affected the predictions of the soil behavior throughout construction.

CHAPTER 6

6 ON HOW "MODELING VARIABLES" AFFECT THE INVERSE ANALYSIS OF A SUPPORTED EXCAVATION

6.1 INTRODUCTION

In Chapter 5 the finite element code PLAXIS was used to simulate the supported excavation associated with the renovation of the Chicago & State CTA subway station. Five compressible clay layers, all modeled using the Hardening-Soil model, were calibrated to find the best fit between computed horizontal displacements and field observations at different construction stages. The inverse analysis algorithm UCODE was used to optimize the input parameters of the 5 layers.

A series of "modeling assumptions" were necessary to set up the inverse analysis. The assumptions that led to the successful calibration of the problem described in chapter 5 were based on both geotechnical knowledge and on the results of studies described in Chapter 3 on the use of inverse analysis for geotechnical engineering purposes. In this chapter the effect of these assumptions on the inverse analysis results will be evaluated through a series of studies on the following "modeling variables:"

- Soil models and input parameters
- Stress history of the soil
- Observations

The simulation described in chapter 5 will be referred herein as the "base-case." Details about the definition of the finite element problem, the calculation phases and the model parameters of the base-case can be found in Appendix E.

6.2 SOIL MODELS AND INPUT PARAMETERS

The calibration of the base-case was achieved updating 3 Hardening-Soil model parameters (E_{50}^{ref}, E_{oed}^{ref} and E_{ur}^{ref}) at 5 clay layers. Of the three stiffness parameters, E_{50}^{ref} was the only one directly estimated by the optimization algorithm, while parameters E_{oed}^{ref} and E_{ur}^{ref} were related, at every regression iteration, to the updated value of E_{50}^{ref}. The base-case "parameterization" (see section 5.3.3.2) yielded satisfactory results that accurately matched the observed response at every construction stage. This section presents the results of a study that addresses the following two questions:

1. Is the base-case parameterization the only alternative for a successful calibration of the H-S model by inverse analysis?

2. Would it be possible to use a simpler model of the excavation (e.g., elastic-perfectly plastic soil model for clays) and successfully calibrate it to match the observed field response?

6.2.1 Parameterization of the Hardening-Soil model

The sensitivity analysis on the H-S input parameters presented in section 5.3.3.2 showed that the total number of parameters "relevant" to the results of the simulation is 10 (i.e. E_{50} and ϕ for layers 1 to 5). In the base-case, however, only 3 parameters were directly optimized by inverse analysis: $E_{1/2}=E_{50}^{ref}{}_{(layer\ 1)}=E_{50}^{ref}{}_{(layer\ 2)}$, $E_3=E_{50}^{ref}{}_{(layer\ 3)}$ and $E_4=E_{50}^{ref}{}_{(layer\ 4)}$. Parameter $E_5=E_{50}^{ref}{}_{(layer\ 5)}$ was assumed to be equal to 1.5 times E_4 and all the other parameters, including the failure parameter ϕ, were kept constant at their initial estimate. In this section the failure parameters of layers 1 to 5 will be included in the optimization to evaluate whether an alternative sets of parameter values are able to yield results that match the observations as accurately as the base-case.

Table 6-1 shows the four simulations presented in this section. In the first two cases the stiffness and failure parameters are optimized simultaneously. In the last two cases only the failure parameters are calibrated, while the value of the stiffness parameters are kept constant at their initial value. Note that, for all simulations, ϕ_1 is assumed to be equal to ϕ_2 (i.e. $\phi_{1/2}=\phi_1=\phi_2$) and ϕ_4 is assumed to be equal to ϕ_5 (i.e. $\phi_{4/5}=\phi_4=\phi_5$).

Simulation name	Parameters optimized	Observations used
E-ϕ-stage1	$E_{1/2}$, E_3, E_4, $\phi_{1/2}$, ϕ_3, $\phi_{4/5}$	Stage1 observations
E-ϕ-all	$E_{1/2}$, E_3, E_4, $\phi_{1/2}$, ϕ_3, $\phi_{4/5}$	All observations
ϕ-stage1	$\phi_{1/2}$, ϕ_3, $\phi_{4/5}$	Stage1 observations
ϕ-all	$\phi_{1/2}$, ϕ_3, $\phi_{4/5}$	All observations

Table 6-1 Simulations for study on parameterization of H-S model

None of the simulations was able to converge to an "optimal" solution. Indeed, in all four cases the regression analysis, for different reasons, could never be conducted to completion (i.e. convergence was never reached).

Figure 6-1 shows the regression progress for the E-ϕ-stage1 case, in which the observations used refer to construction stage 1 only. As expected, the objective function decreases as the regression progresses. However, most of the input parameters do not seem to converge towards definite and reasonable values. For instance, at iteration 4 the updated value of parameter ϕ_3 becomes higher than the value of $\phi_{4/5}$ and, at following iterations, the estimate of both parameters increases steadily. At iteration 6 the regression was stopped because the simulation could not be computed using the simultaneous updated estimates of ϕ and E for layer 3 (i.e. ϕ_3=50.7° and E_3=6240 psf), which PLAXIS deemes "not acceptable" (see section 4.4.4).

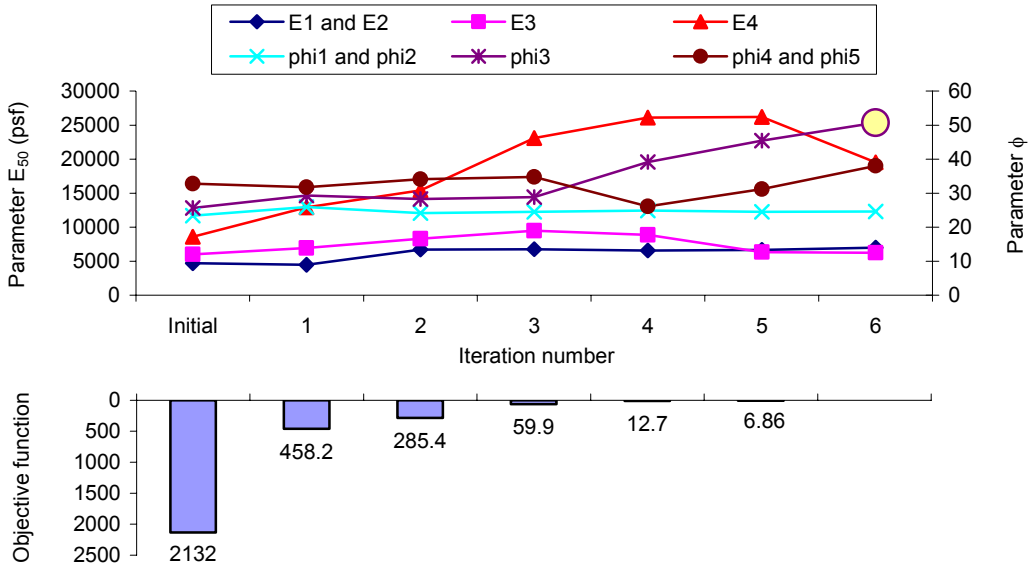

Figure 6-1 Parameters and objective function variation during regression of E-ϕ-stage1

Results did not improve when all observations were used to calibrate the model (i.e. simulation E-ϕ-all). Table 6-2 shows the values of the optimized parameters for the E-ϕ-all case. The regression was stopped at the first iteration because the very low and unreasonable estimate of parameter ϕ_3 (13.1°) causes the soil around the excavation to fail.

	$E_{1/2}$ (psf)	E_3 (psf)	E_4 (psf)	$\phi_{1/2}$	ϕ_3	$\phi_{4/5}$	S(b)
Initial	4700	6000	8600	23.4	25.6	32.8	2132
1	5118	9000	12300	24.38	**13.08**	34.02	

Table 6-2 Parameters and objective function variation during regression of E-ϕ-all

When inverse analysis was used to update the failure parameters only (i.e. simulations ϕ-stage1 and ϕ-all), the observed regression behavior was similar. Figure 6-2 shows the

regression progress for the ϕ-stage1 case. Even if the objective function value decreases as the regression progresses, the estimates of the parameters tend towards unreasonable values. For example, at iteration 4 the regression was stopped when the value of $\phi_{4/5}$ became higher than 60°. Figure 6-3 refers to the ϕ-all case, when the regression needed to be stopped at iteration 5 for the same reason.

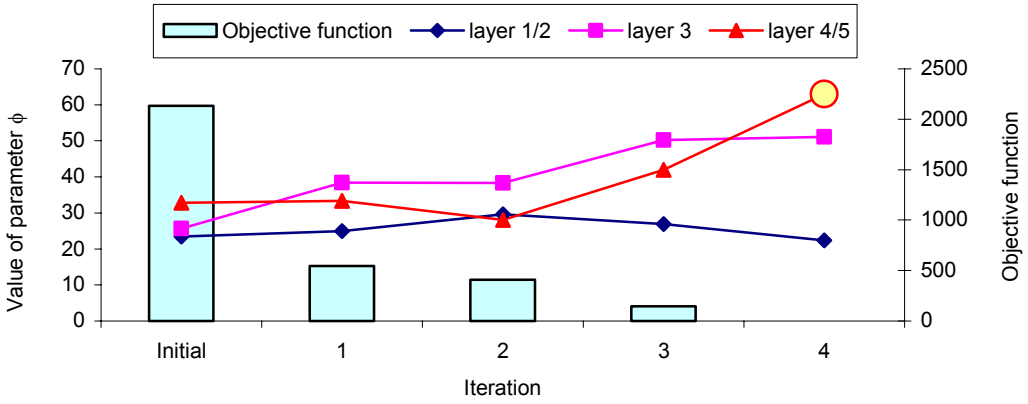

Figure 6-2 Parameters and objective function variation during regression for ϕ-stage1

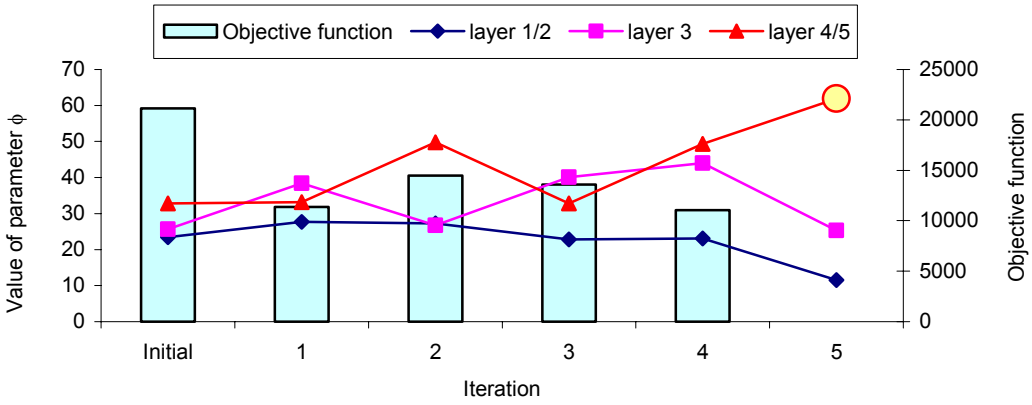

Figure 6-3 Parameters and objective function variation during regression for ϕ-all

Results of this study show that none of the proposed alternative formulations proved to be a "well posed" inverse analysis problem. This indicates that the base-case is, most likely, the only inverse analysis set-up alternative for the successful calibration of the finite element problem as defined in Appendix E (i.e. H-S model used to define the clay layers, pre-excavation construction activities explicitly modeled and horizontal displacement data used as observations).

6.2.2 Elastic-perfectly plastic model for clays

In the base-case the Hardening-Soil model is used to characterize the clay layers. However, when the model is calibrated by inverse analysis, the optimization algorithm only estimates 1 of the 10 model input parameters (i.e. E_{50}^{ref}). This section evaluates whether using a multi-yield surface elasto-plastic model is necessary to obtain accurate results or whether a simpler linear elastic perfectly-plastic model can also be effectively calibrated by inverse analysis. For this purpose the Mohr-Coulomb model is chosen to model the clay layers of the simulation.

The Mohr-Coulomb model is an elastic-perfectly plastic model. Details about the formulation of the M-C model and its implementation in PLAXIS can be found in the PLAXIS materials model manual. The model's input parameters are: the Young modulus, E, Poisson's ratio, ν, cohesion, c, friction angle, ϕ and dilatancy angle, ψ. The first two parameters define the stiffness of the material, the last 3 define the failure of the material.

Table 6-3 shows the initial values of the M-C input parameters for the five clay layers calibrated by inverse analysis. The initial estimates of the parameters are based on the initial estimates of the H-S model input parameters (see section 5.3.2.2). The failure parameters c, ϕ and ψ were assumed to have the same values of the corresponding H-S failure parameters, while the stiffness parameters E and ν were assumed to be equal to the H-S parameters E_{ur} (computed from E_{ur}^{ref} using Eq. 5.3) and ν_{ur}, respectively. The initial properties of all soil layers modeled using the M-C model can be found in Appendix F.

	E (psf)	ν	c	ϕ	ψ
Layers 1 and 2	100800	0.2	1	23.6	0
Layer 3	204600	0.2	1	25.8	0
Layer 4	298500	0.2	1	32.8	0
Layer 5	523200	0.2	1	32.8	0

Table 6-3 Initial values of M-C input parameters for clay layers 1 to 5

Figure 6-4 shows the comparison between computed and measured horizontal displacements for the initial estimates of the input parameters. Results show that the computed movements overpredict the measured displacements, suggesting that the initial values of the stiffness parameters are underestimated.

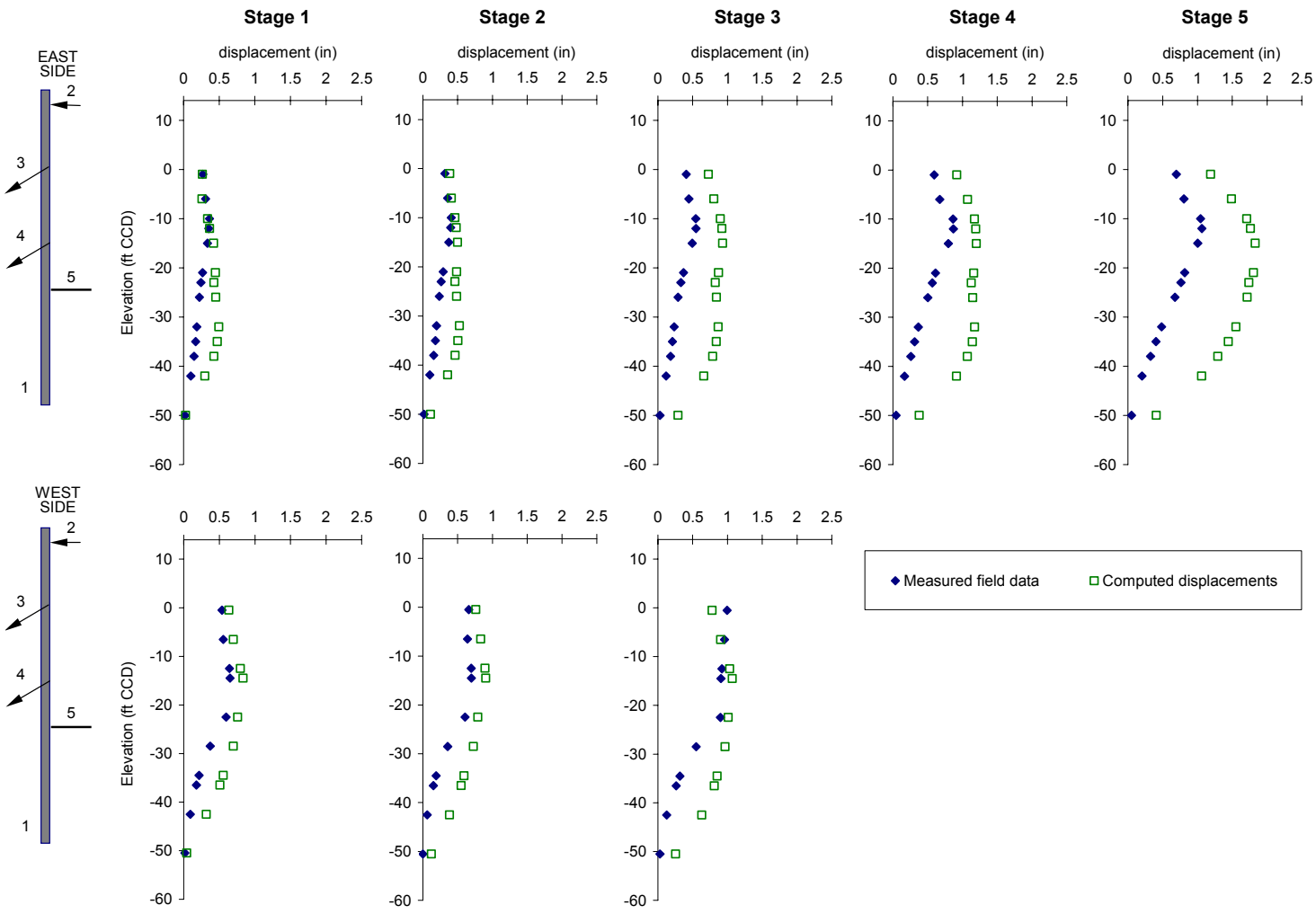

Figure 6-4 Measured vs. computed horizontal displacements for initial estimates of parameters

The M-C input parameters to optimize by inverse analysis are chosen in the same manner as described in section 5.2. The model parameters that one can expect to effectively estimate using an optimization algorithm are determined by: (i) the model's characteristics, (ii) the stress conditions in the soil around the excavation, and (iii) the type of observations used for the inverse analysis. The Mohr-Coulomb model has the same failure parameters of the H-S model. Results presented in section 4.4.4 indicate that changes in the failure parameters c and ψ do not significantly affect the results of the analysis. Results presented in section 6.2.1 indicate that it is not possible to satisfactorily calibrate the failure parameter ϕ in this inverse analysis problem of a supported excavation. Therefore, the M-C parameters considered for optimization are the two stiffness parameters E and ν. The number of soil layers to calibrate is 4 (layers 1 and 2 are assumed, as before, to have the same input parameters), thus the total number of model parameters considered is 8 (E and ν for layers 1/2, 3, 4 and 5). Table 6-4 shows the initial values of the 8 parameters and the results of a sensitivity analysis conducted to determine the final number of relevant and uncorrelated model parameters to optimize by inverse analysis.

	$E_{1/2}$	$\nu_{1/2}$	E_3	ν_3	E_4	ν_4	E_5	ν_5
Initial value	100800	0.2	204600	0.2	298500	0.2	523200	0.2
Compositre scaled sensitivity	5.46	0.69	3.87	0.87	8.45	1.39	5	0.95
Correlation coefficients	-0.11		0.76		0.99		0.98	

Table 6-4 Results of sensitivity analysis on M-C parameters E and ν for layers 1/2, 3, 4 and 5

The composite scaled sensitivity values show that the layers' Young modules, E_i, are the parameters to which results are most sensitive. The values of the correlation coefficients indicate a high correlation between the elastic parameters of layers 3, 4 and 5, suggesting that the two parameters are unlikely to be successfully estimated simultaneously at those layers. Based on these results it was decided to calibrate the following parameters: $E_{1/2}$, E_3, E_4 and E_5. Parameter $\nu_{1/2}$ was not included in the regression because it is the parameter with the lowest composite scaled sensitivity.

Table 6-5 shows the best-fit values of the parameters and the value of the objective function, $S(\underline{b})$, computed by the optimization algorithm when the regression was conducted using only stage 1 observations. The value of $S(\underline{b})$ decreases significantly, but the estimates of the parameters are unreasonable (E_4 is 50% higher than E_5). Figure 6-5 shows the comparison between computed and measured horizontal displacements for these estimates of the parameters. The regression analysis effectively minimizes the errors relative to these observations, but the computed response does not predict the measured displacements at the other stages.

	$E_{1/2}$ (psf)	E_3 (psf)	E_4 (psf)	E_5 (psf)	$S(\underline{b})$
Initial	100800	204600	298500	523200	521.4
Stage 1	162200	178700	1172000	736000	11.3

Table 6-5 Best-fit estimates of M-C parameters optimized (observations from stage 1 only)

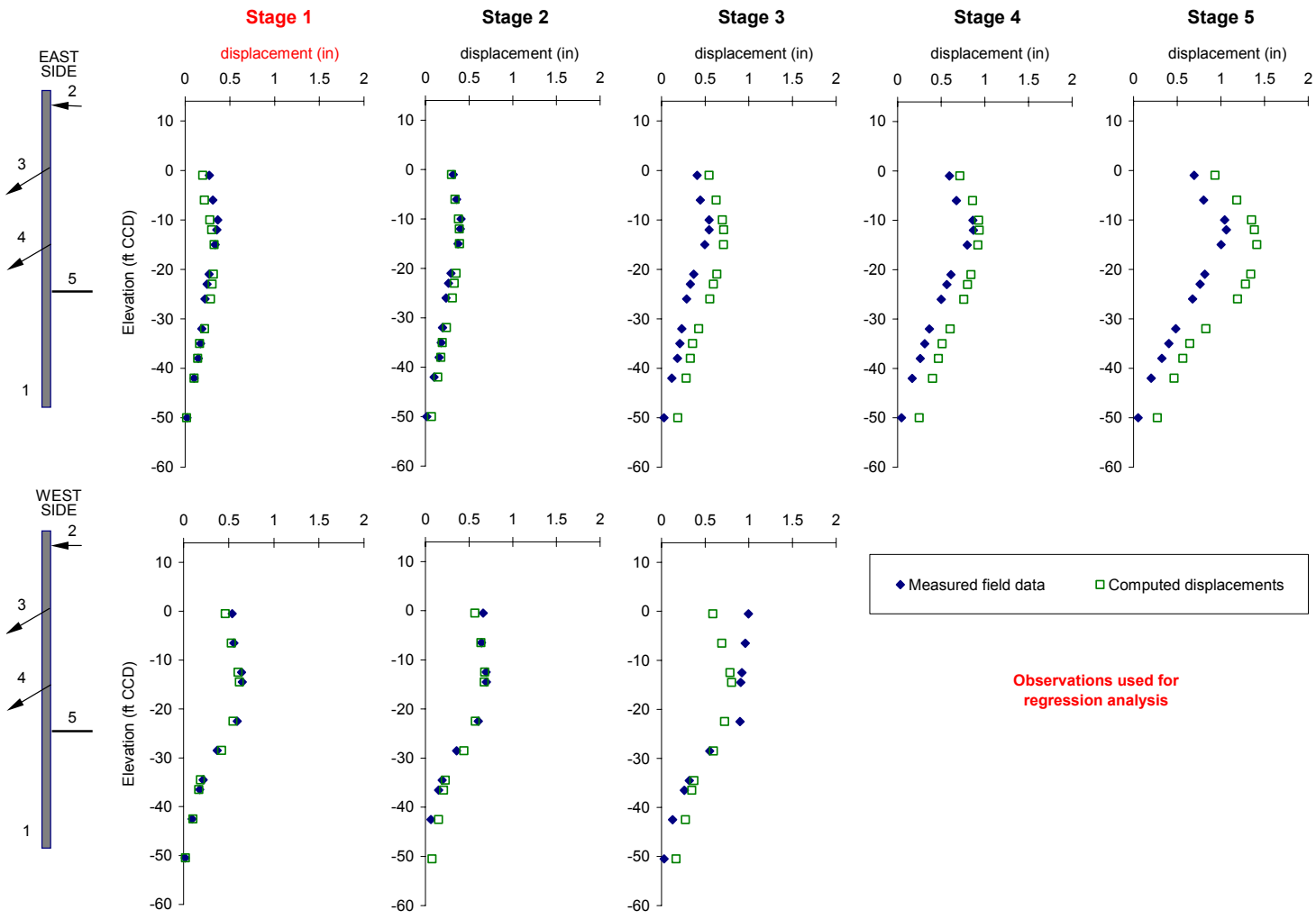

Figure 6-5 Measured vs. computed horizontal displacements for best-fit estimates of parameters from stage 1 observations

When all observations are used to calibrate the model, the regression converges to best-fit estimates of the parameters that are increasing with depth. In Table 6-6 the values of the parameters' estimates are shown. The table also shows the initial values of the parameters, the best-fit values of the parameters at stage 1 and the values of the global objective function, OF (Eq. 5.15), relative to these estimates.

	$E_{1/2}$ (psf)	E_3 (psf)	E_4 (psf)	E_5 (psf)	OF
Initial	100800	204600	298500	523200	14322
Stage 1	162200	178700	1172000	736000	2177
Stage 5	147000	247500	1255000	2484000	415

Table 6-6 Best-fit estimates of M-C parameters optimized

A comparison between the measured horizontal displacements and the simulation results, computed using final best-fit values of the parameters (i.e. stage 5), is shown in Figure 6-6. The overall fit between measured and computed displacements is remarkably good if one considers the simplicity of the model used to simulate the clay layers. The accuracy of the fit is not as good as the one achieved using the H-S model (i.e. base-case), yet the final value of the global objective function (see Table 6-6) is not far from the value of the objective function of the calibrated base-case, $OF_{\text{base case}}$ =157.2 (see Table 5.14).

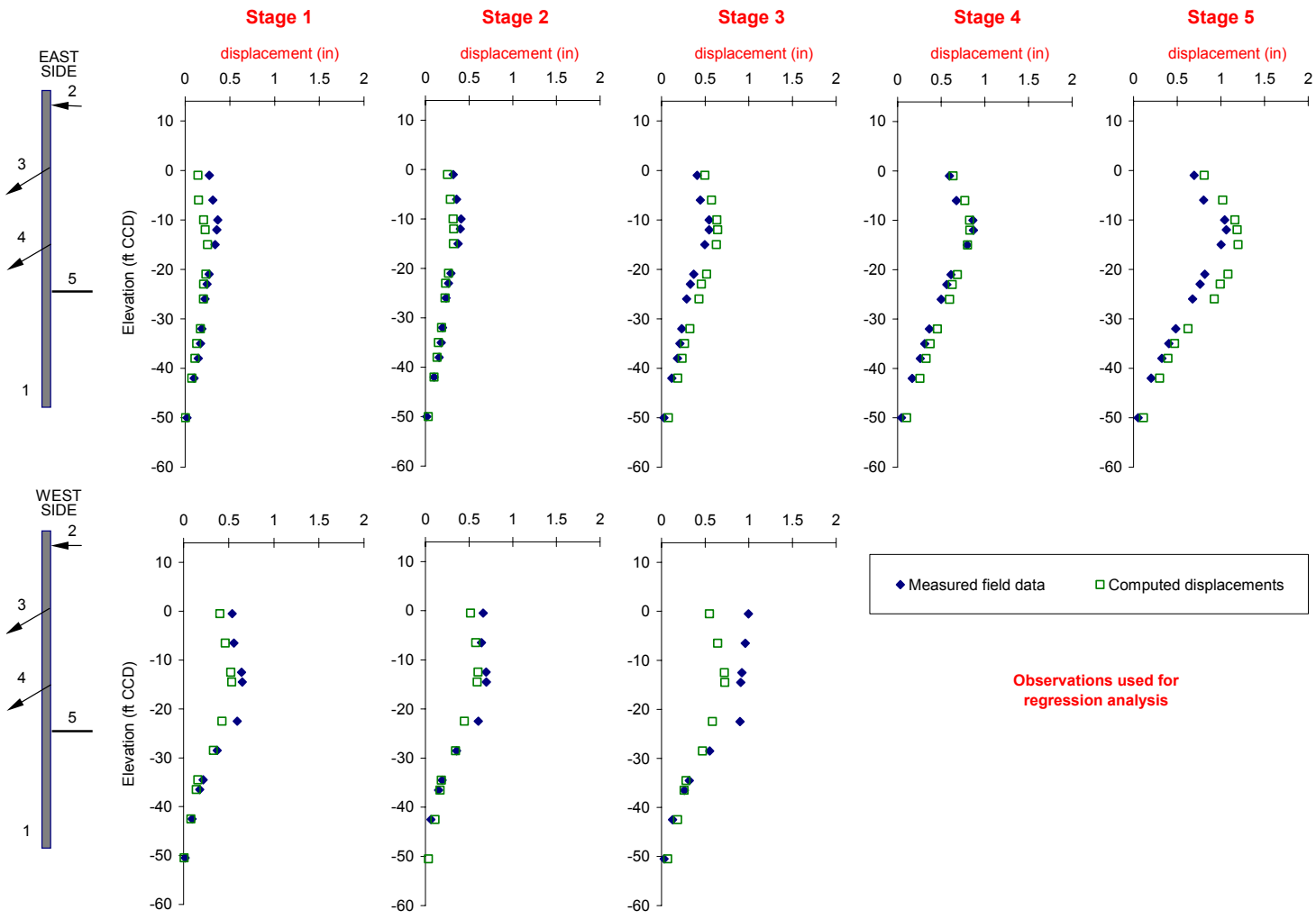

Figure 6-6 Measured vs. computed horizontal displacements for best-fit estimates of parameters from all observations

Figure 6-7 shows the values of the E/S_u ratios computed for the initial, stage1 and stage 5 estimates of the parameters. One would expect the values of the stiffness-to-strength ratios to increase with depth (i.e. from layer 1 to layer 5). The final estimates of the parameters (i.e. best-fit for stage 5) are the ones that yield the most reasonable E/S_u trend, yet the value of E/S_u at layer 3 is slightly lower than E/S_u at layer 2.

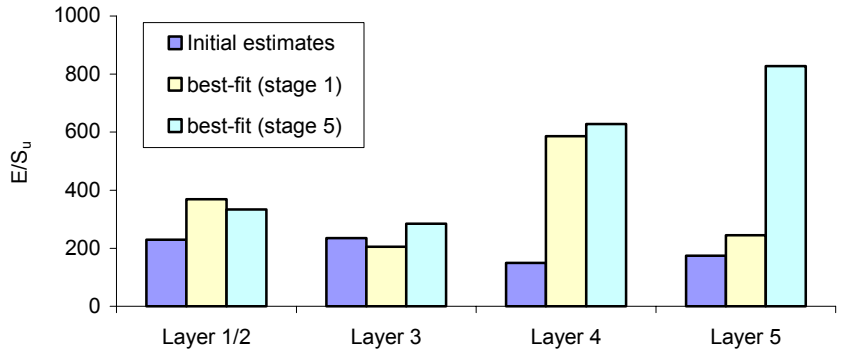

Figure 6-7 E/S_u ratios of M-C parameters optimized

In Figure 6-8 the best-fit estimates of Mohr-Coulomb parameter E are compared with the values of the base-case parameters E_{50} and E_{ur}, which are computed from the H-S parameters E_{50}^{ref} and E_{ur}^{ref} using Eq. 5.1 and 5.3, respectively. The comparison shows that M-C stiffness modulus E is always higher than the 50% secant modulus, E_{50}, and always lower than the unloading-reloading modulus, E_{ur}. These results are reasonable given that the value of parameter E, the only stiffness parameter of the M-C model, represents an average stiffness of the highly non-linear behavior of the clays. However, considering that the problem under study is an excavation (i.e. an unloading problem), one would have expected the values of E to be closer to the values of E_{ur} than to the values of E_{50}.

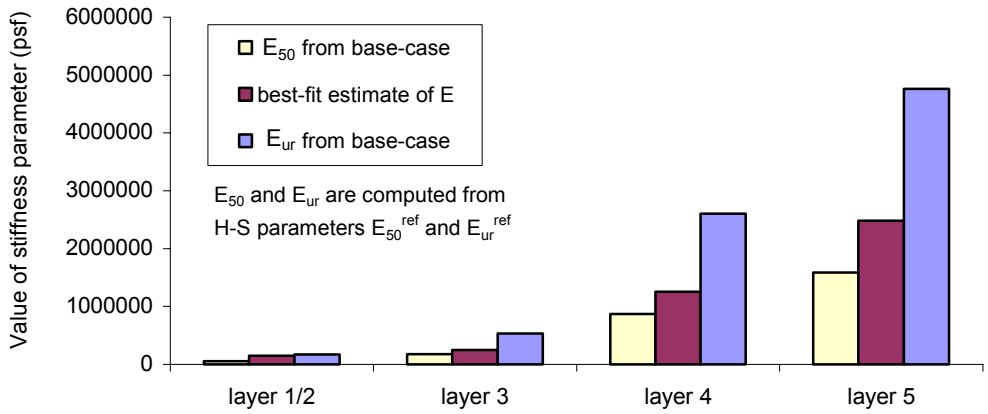

Figure 6-8 Comparison between best-fit estimates of M-C parameter E (stage 5) and base-case values of E_{ur} (computed from H-S parameter E_{ur}^{ref})

Figure 6-9 shows the comparison between the measured horizontal displacements and the displacements computed using the base-case values of E_{50} and E_{ur} (see Figure 6-8) as estimates of the M-C stiffness parameter E. On the east side, the computed displacements cannot match the measured profile for the first 2 stages but they clearly define an upper and lower "bound" for the measured data for the last 3 construction stages (i.e. stages 3, 4 and 5). On the west side, the simulation that yields the best results is the one for which E_{50} is used to estimate the values of M-C parameter E.

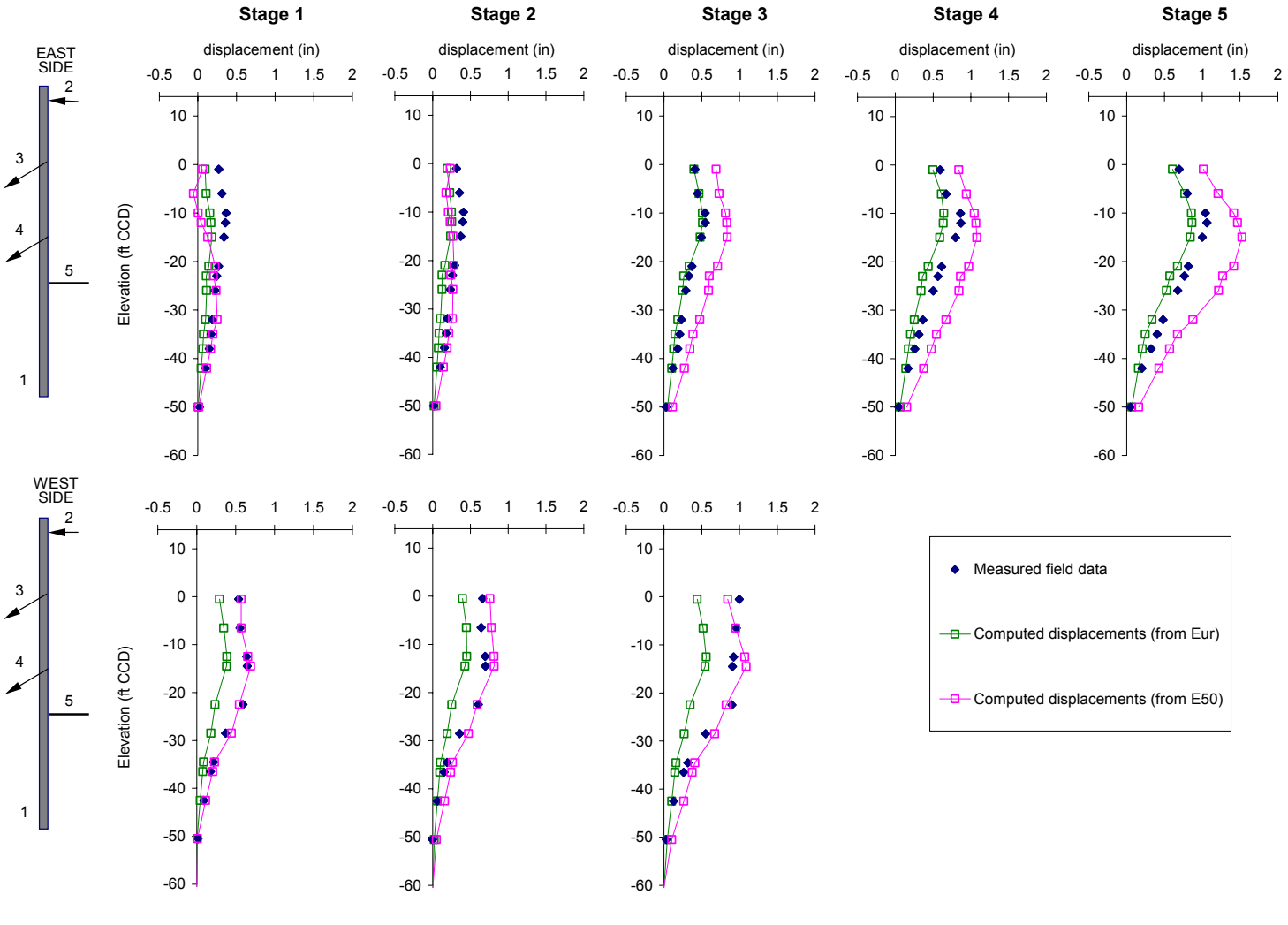

Figure 6-9 Measured vs. horizontal displacements computed using the base-case values of E_{50} and E_{ur} as estimates of M-C parameter E

Results of this study indicate that (i) using a simple elastic-perfectly plastic soil model (e.g., Mohr-Coulomb) to model the clay layers does not yield results that are as accurate as the ones achieved when the H-S model is used (i.e. base-case), (ii) when the Mohr-Coulomb model is calibrated based on observations from construction stage 1 the computed results relative to the other stages do not accurately match the measured behavior of the soil, yet (iii) when all observations are used, the inverse analysis is able to effectively calibrate the M-C model to produce a relatively good fit between computed and measured displacements throughout construction.

6.3 STRESS HISTORY OF SOIL AT THE EXCAVATION SITE

This section presents the results of a study evaluating the importance of "appropriately" considering the stress history of the soil at the Chicago & State excavation site. All pre-excavation activities, namely the construction of the tunnel tubes, the construction of the school and the installation of the supporting wall, were explicitly considered in the base-case simulation. These activities influence the stress conditions of the soil at the beginning of the excavation-part of the analysis. Note that the "pre-excavation" activities are quite common for excavations in mature urban areas. This section will show the effect that "proper modeling" of these structures has on the optimized results.

Table 6-7 summarizes the modeling approach used to consider the effect of the existing structures and wall construction in the base-case, as well as the other four simulations described in this section. Note that, when a construction activity was not modeled, the

corresponding structure was either wished in place or not included in the finite element mesh and k_0-conditions (i.e. gravity loads) were assumed to be representative of the initial stresses in the soil. The initial estimates of the input parameters are, for all simulations, the same used for the base-case (Table 5.2). The PLAXIS calculation phases and the relative shear stresses of the simulations at various calculation stages can be found in Appendix F.

	Structure			
Simulation name	Tunnel	School	Wall	Excavation
Base-case	construction modeled	construction modeled	construction modeled	stage-by-stage modeling
No-tunnel	wished-in-place	construction modeled	construction modeled	stage-by-stage modeling
No-school	wished-in-place	wished-in-place	construction modeled	stage-by-stage modeling
No-wall	wished-in-place	wished-in-place	wished-in-place	stage-by-stage modeling
Free-field	not included	not included	wished-in-place	stage-by-stage modeling

Table 6-7 Modeling approach used to include the tunnel, the school and the wall in the finite element simulation of the excavation

6.3.1 Tunnel construction not modeled (no-tunnel case)

In this simulation (i.e. no-tunnel case) the tunnel tubes are wished-in-place at the beginning of the analysis, while the construction of the school and the installation of the support walls are explicitly modeled. Figure 5-15 shows the comparison between the measured and computed horizontal displacements for the initial estimates of the input parameters.

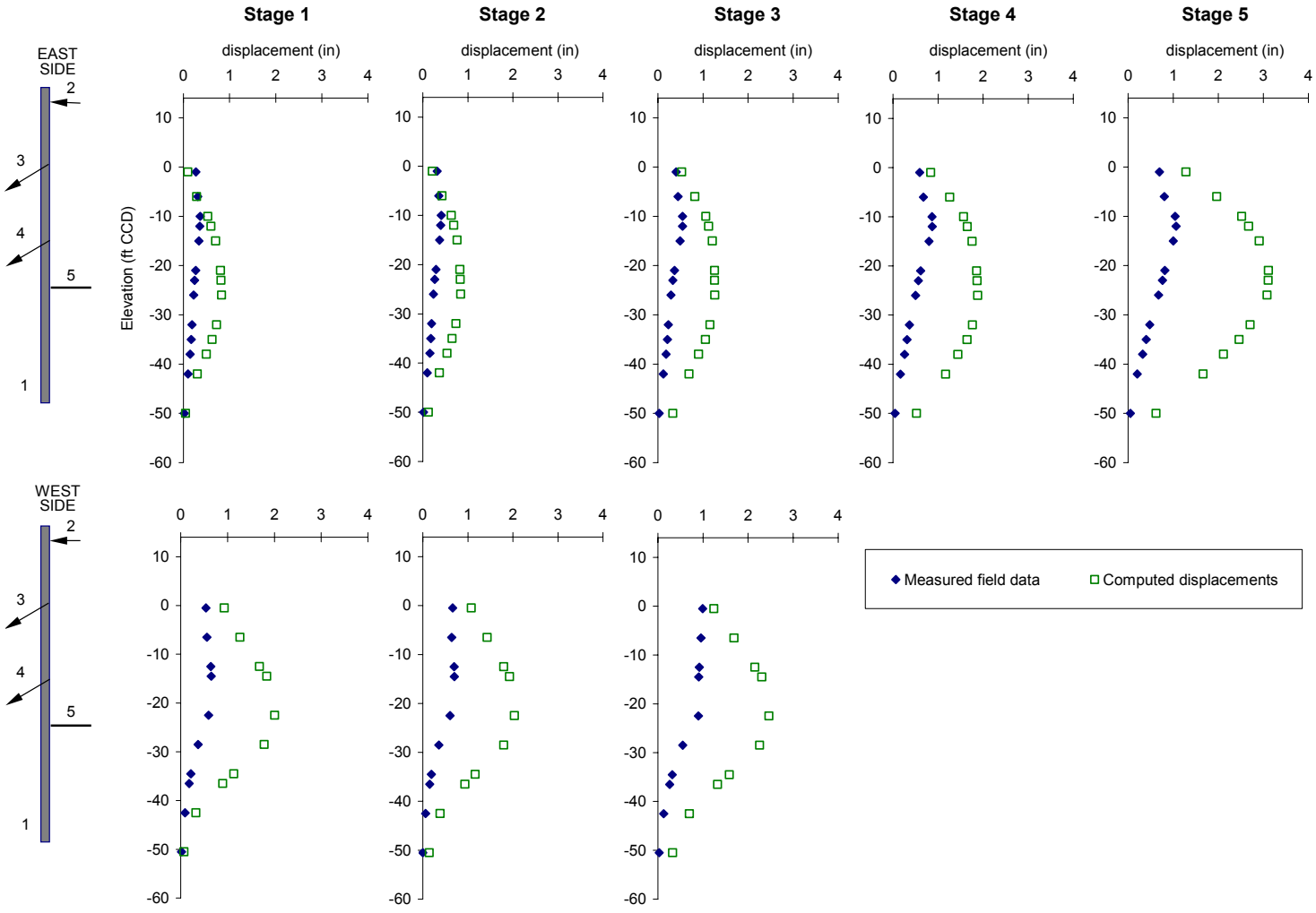

Figure 6-10 Measured vs. computed horizontal displacements for initial estimates of parameters (no-tunnel case)

The comparison shows that the finite element model significantly overpredicts the displacements at every construction stage. The maximum computed displacements are about three times the measured ones and are about 50% larger than the displacements computed when the initial estimates of the parameters were used in the base-case (see Figure 5-14).

Similarly to what has been done for the base-case, the model is initially calibrated using observations from stage 1. Figure 6-11 shows the comparison between measured and computed horizontal displacements when the parameters are optimized based on these observations. The comparison shows that the finite element results fit the stage 1 experimental data relatively well, with the exception of the displacements for layer 1 on the east side (i.e. shallower 4 observations). The calibrated model, however, does not "predict" the behavior of the soil for the remaining 4 stages with the same accuracy of the base-case model (see Figure 5-15). For instance, it significantly overpredicts the final displacements at all elevations (the maximum computed displacements are about 50% larger than the measured ones).

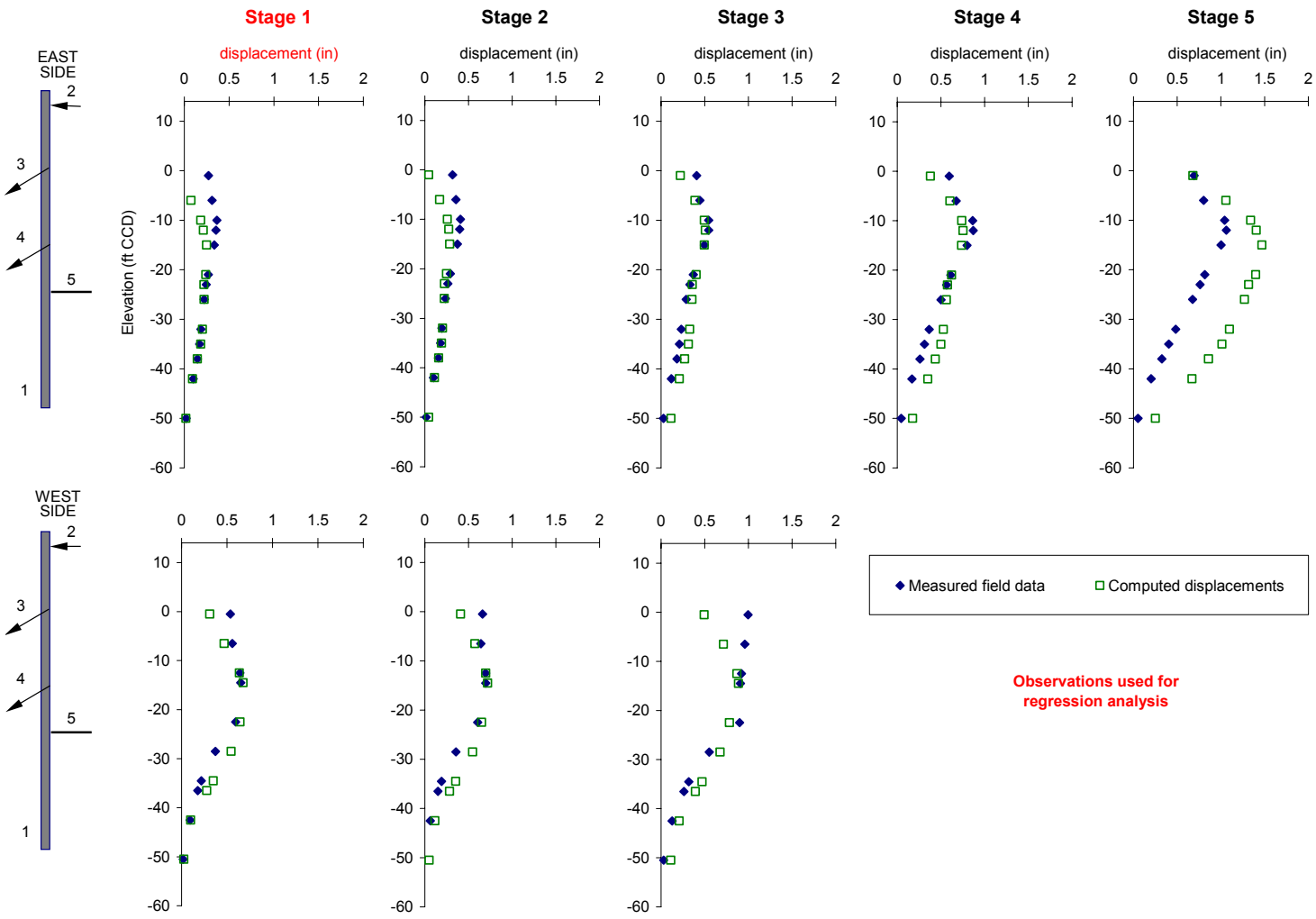

Figure 6-11 Measured vs. computed horizontal displacements: parameters optimized based on stage 1 observations (no-tunnel case)

Table 6-8 shows the values of the model parameters at the beginning of the simulation and the best-fit values of the parameters at the end of the optimization based on observations from stage 1. Figure 6-12 shows the values of the three parameters optimized and the value of the objective function at every regression iteration. The regression converged to the optimal solution after 11 iterations.

	$E_{1/2}$ (psf)	E_3 (psf)	E_4 (psf)
Initial	4700	6000	8600
Stage 1	9644	41770	32620

Table 6-8 Initial and optimized model parameters at stage 1

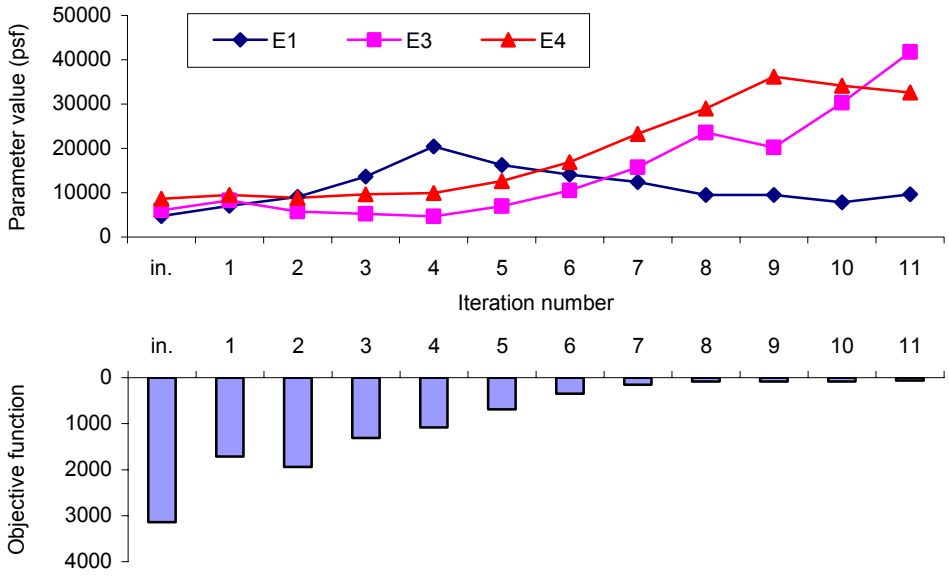

Figure 6-12 Variation of parameters and objective function values during the regression analysis based on observations from stage 1

The results of the regression analysis indicate that the model cannot be "uniquely and satisfactorily" optimized based only on observations from stage 1. Indeed: (i) during the last five iterations the value of the objective function does not appreciably decrease, while changes in the estimates of the parameters are still significant, and (ii) the final estimates of the three input parameters are not realistic because layer 3 becomes, at the end of the optimization, "stiffer" than layer 4. Note that the regression converged because the objective function changes were lower than the specified SOSR (see Table 5.9) for three consecutive iterations. This indicates that the accuracy of the fit shown in Figure 6-11 could be achieved with more than one set of parameter values. For instance, the value of parameter E_4 became smaller than the value of parameter E_3 at the last iteration. If we would have stopped the regression at iteration 8 or 9, the fit between computed and measured results would have been similar to the one showed in Figure 6-11 and the estimates of the input parameters would have been significantly different (more "reasonable" from a geotechnical point of view).

Figure 6-13 shows the comparison between the measured and computed horizontal displacements when parameters are optimized based on all observations. The fit is better than the one showed in Figure 6-11. However, the calibrated simulation is unable to accurately model the behavior of the soft clay during the initial construction phases (i.e. layers 1 and 2 at stages 1 and 2) and the behavior of the stiffer clays during the final construction phases (i.e. layers 3, 4 and 5 at stages 4 and 5).

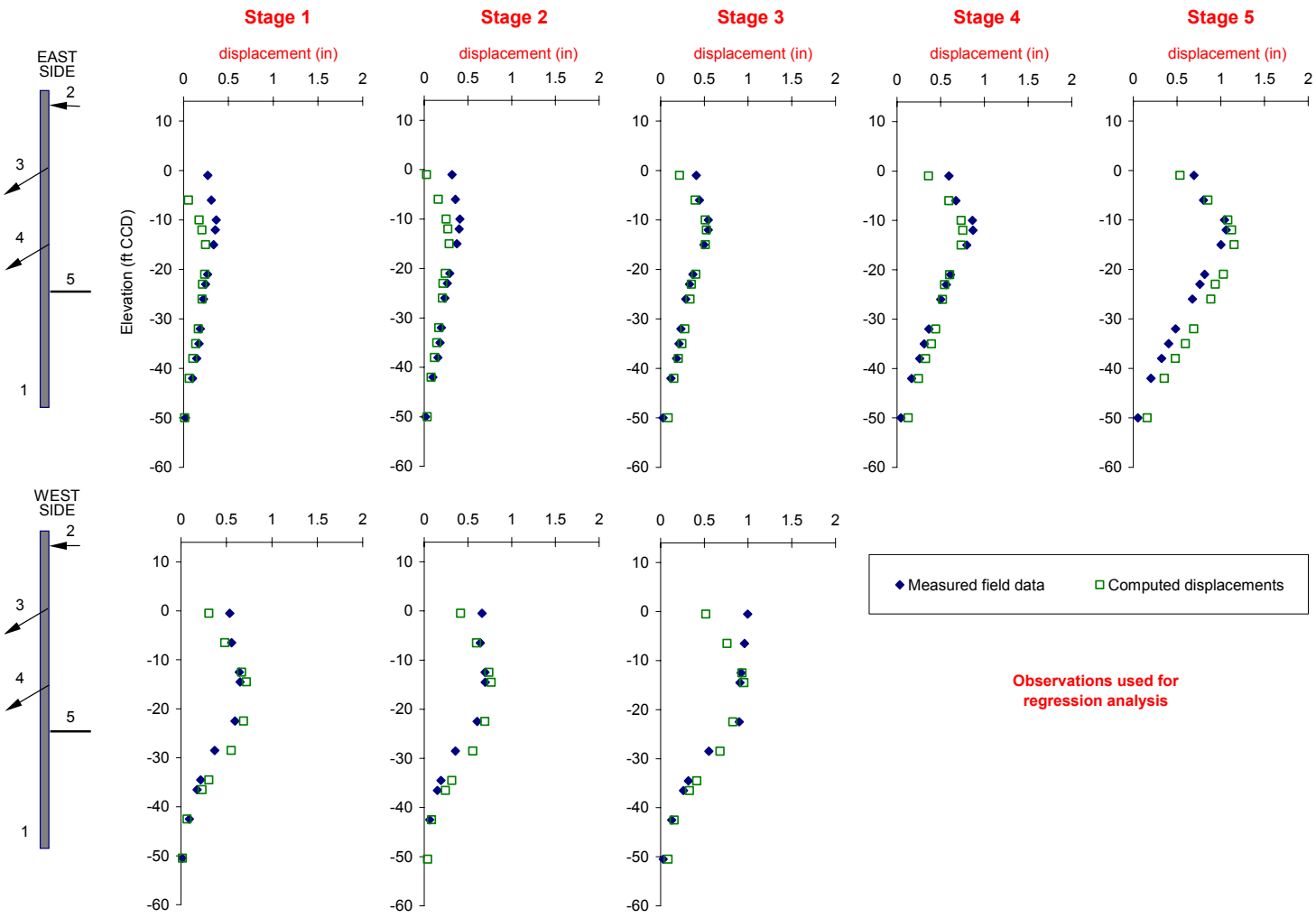

Figure 6-13 Measured vs. computed horizontal displacements: parameters optimized based on all observations (no-tunnel case)

Table 6-9 shows the initial values of the input parameters and their value at the end of the optimization. In Figure 6-14 these values are compared with the values of the optimized parameters from the base-case (see Table 5-13). The comparison shows that the best-fit estimates of parameters E_1 and E_4 are similar in the two cases, but the final values of parameter E_3 are significantly different in the two simulations.

	$E_{1/2}$ (psf)	E_3 (psf)	E_4 (psf)
Initial	4700	6000	8600
Stage 5	8380	31190	49300

Table 6-9 Initial and optimized model parameters at the end of the optimization

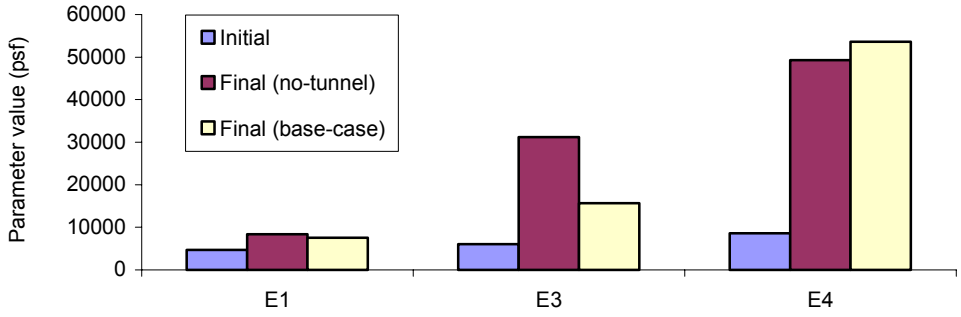

Figure 6-14 Comparison between optimized results with results of base-case optimized model

The different estimates of the input parameters in the two simulations are a direct result of the different stress conditions produced in the soil by the different approaches used to model the tunnel (explicitly considered in the base-case and wished in place in the no-tunnel case). Figure 6-15 shows the relative shear stresses in the soil at the end of the calculation phase simulating the tunnel construction.

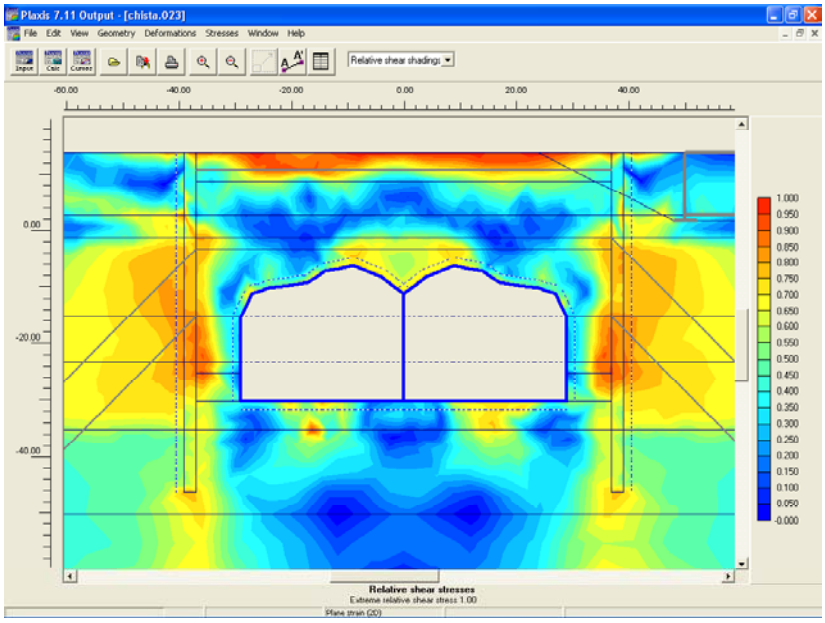

(a) base-case

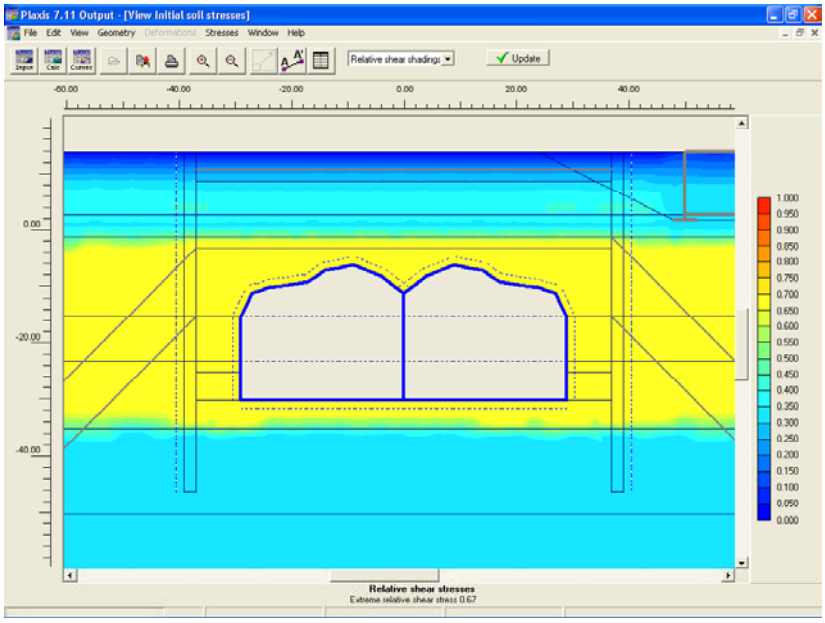

(b) no-tunnel

Figure 6-15 Relative shear stresses at the end of the tunnel construction for (a) base-case and (b) no-tunnel simulations

The relative shear, defined as the ratio between the current shear stress and shear stress at failure for the current value of mean normal stress, is a measure of the stress point's distance from failure. In the base-case the soil at the sides of the tunnel is very close to failure, as indicated by a red shading, as a result of the stress relief produced by the tunnel construction. Whereas, when the tunnel is not explicitly considered (i.e. no-tunnel case), the relative shear stress distribution is significantly different. Note that the shear stresses of a given clay layer are constant in the no-tunnel case. This occurs because this plot refers to the initial conditions of the simulation and the initial shear stresses are related to the values of parameters ϕ and k_0. Figure 6-16 shows the relative shear stresses in the soil for the two simulations after the wall installation (i.e. at the beginning of the excavation-part of the analysis). The difference between the two cases is not as significant as the one shown in Figure 6-15 (i.e. the end of the tunnel construction). Yet, the lighter shear stresses at the sides of the tunnel apparently are sufficient to produce a significant difference in the results of the two simulations.

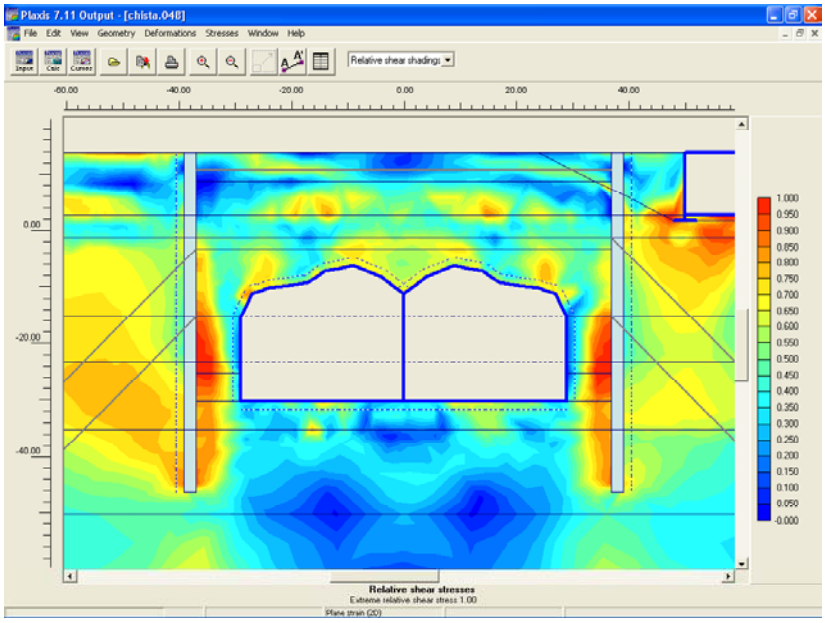

(a) base-case

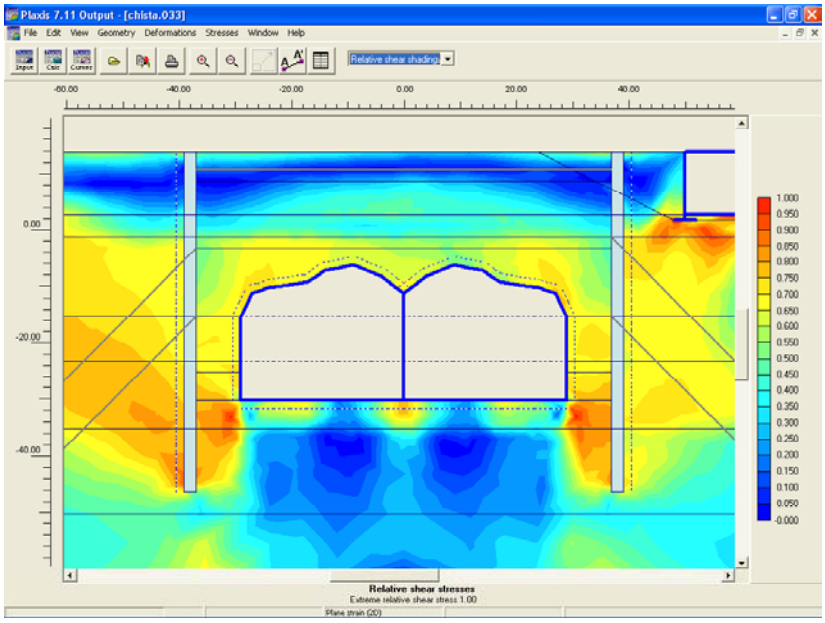

(b) no-tunnel

Figure 6-16 Relative shear stresses after wall installation for (a) base-case and (b) no-tunnel simulations

6.3.2 School construction not modeled (no-school case)

In this simulation (i.e. no-school case) both the tunnel and the school are wished-in-place at the beginning of the analysis, and only the installation of the support walls is explicitly modeled. Figure 6-17 shows the relative shear stresses at the beginning of the analysis. Note that the initial stress conditions only depend on the properties of the different soil layers because the installation of the tunnel and the school does not affect the surrounding soil.

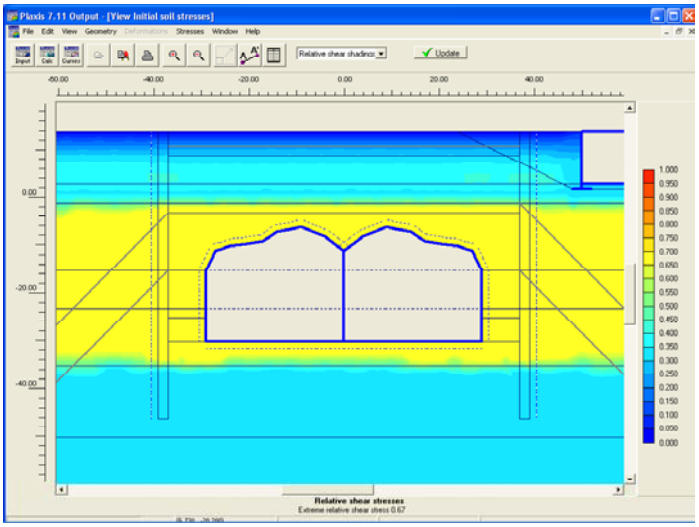

Figure 6-17 Relative shear stresses prior to wall installation (i.e. tunnel and school wished in place)

Figure 6-18 shows the comparison between the measured and computed horizontal displacements for the initial estimates of the input parameters. The comparison shows that the model is not able to capture the behavior of the soil in that: (i) the shape of the computed displacement profiles at the early construction stages is not consistent with the measured data, and (ii) the final movements are significantly overpredicted.

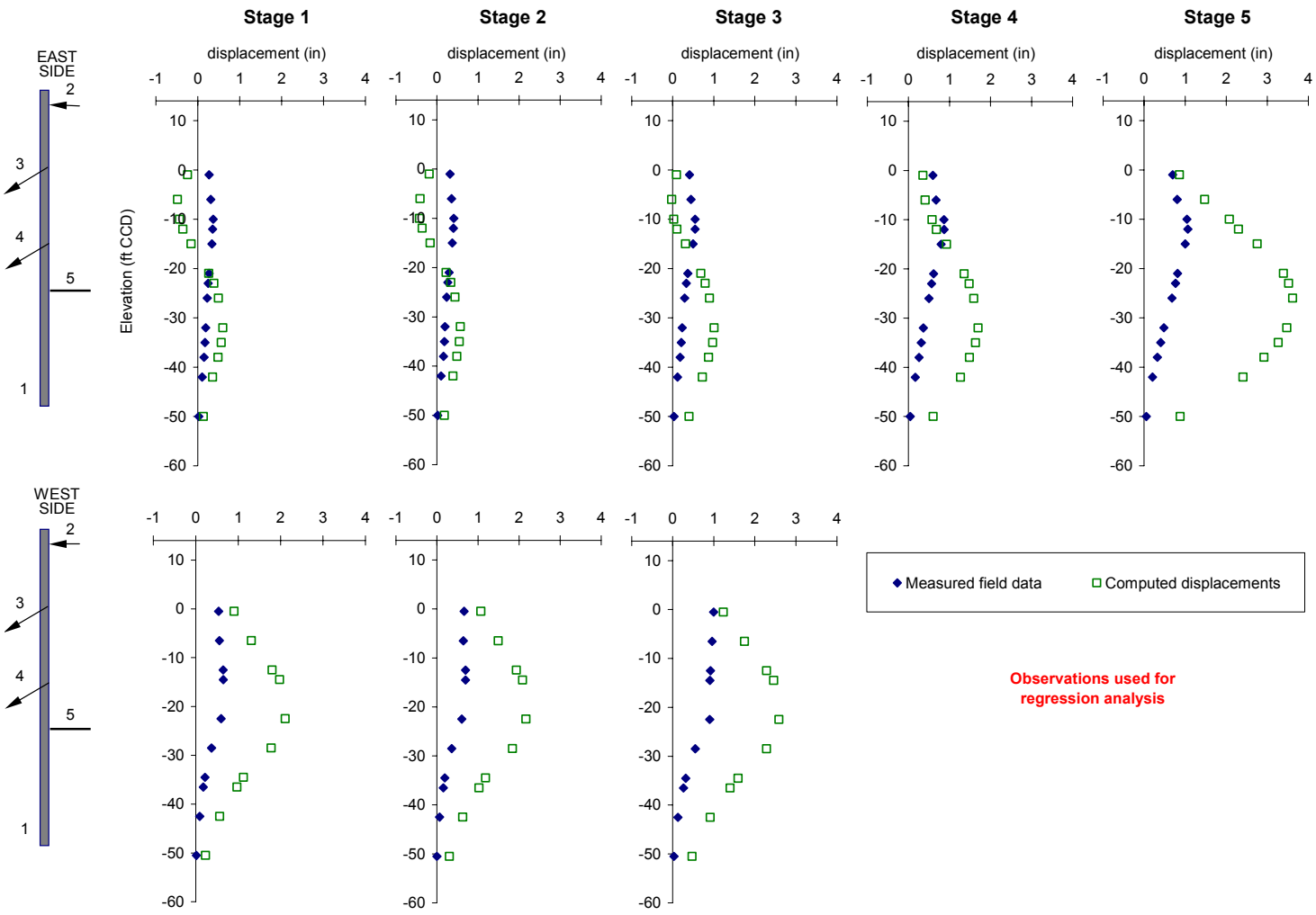

Figure 6-18 Measured vs. computed horizontal displacements for initial estimates of parameters (no-school case)

Differently from the previous simulations (i.e. base-case and no-tunnel case), the model could not be successfully calibrated using only the observations from early construction stages. When all observations were used, however, the regression analysis was able to converge to a new set of input parameters. Table 6-10 shows the values of the input parameters at the end of the optimization. Note that the best-fit values, which represent the "optimal" estimates of the parameters (i.e. they produce the lowest value of the objective function), are unacceptable from a geotechnical point of view because the estimates of the stiffness parameters do not increase with depth. On the contrary, the best-fit value of parameter $E_{1/2}$ is more than 10 times higher than the best-fit value of parameter E_3.

	$E_{1/2}$ (psf)	E_3 (psf)	E_4 (psf)
Final (no-school)	56280	4047	110000

Table 6-10 Initial and optimized model parameters at the end of the optimization

The fit between the measured data and the results computed using the updated estimates of the parameters is shown in Figure 6-19. The comparison clearly indicates that the calibrated model cannot match the displacements observed on the east side of the excavation.

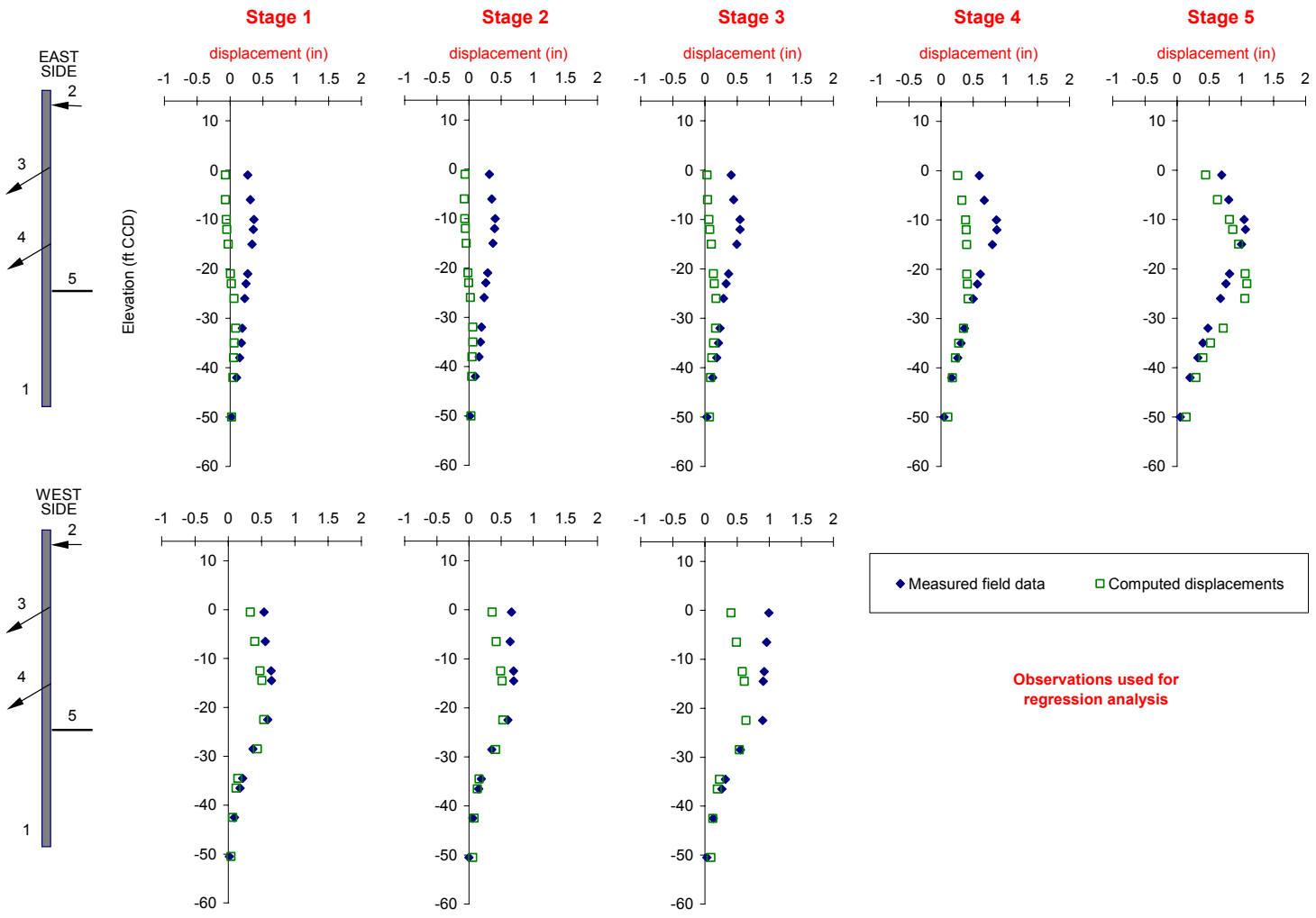

Figure 6-19 Measured vs. computed horizontal displacements: parameters optimized based on all observations (no-school case)

These results could have been expected given the characteristics of the simulation. Figure 6-20 shows the computed displacements in the soil at the end of stage 1 (i.e. wall installation). The plot, which refers to the initial estimates of the input parameters, shows that the computed movements of the upper clay layers on the school side of the east wall at stage 1 are "away from" the excavation, whereas the observations indicate movement toward the excavation. The predicted movements on the east side are a result of (i) the stabilizing slurry-type pressure used to simulate the installation of the support wall, (ii) the presence of the school and the tunnel, and (iii) the fact that these structures are wished in place, therefore the initial effective stresses in the soil layers beneath the structure are low. The direction of the movements cannot be reversed by model calibration. The regression analysis, however, to minimize the difference between computed and observed movements on the east side, yields a very high best-fit estimate of the stiffness parameter of the upper clays, $E_{1/2}$. Note how, at the end the calibration (see Figure 6-19), the movements of the upper clay layers on the school side are still away from the excavation but they magnitude is negligible. At the same time, when the initial values of the parameters are used (see Figure 6-18), the movements on the west side are overestimated. Therefore, the information provided to the regression by the observations from the two sides of the excavation is discordant. This explains the very low value of the best-fit estimate of parameter E_3, which compensates for the high estimate of parameter $E_{1/2}$.

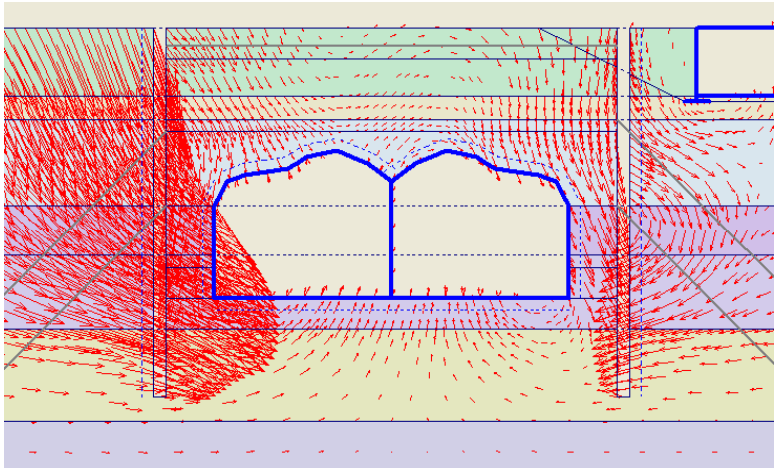

Figure 6-20 Computed displacements at stage 1 (i.e. wall installation) for initial estimate of parameters

Results of this study indicate that the no-school simulation cannot adequately represent the measured response of the soil at the excavation site. The solution to which the regression analysis converged is "unacceptable" from a geotechnical point of view because the best-fit values of the optimized parameters are unrealistic ($E_{1/2}>E_3$).

6.3.3 Wall installation not modeled (no-wall case)

In this simulation (i.e. no-wall case) the tunnel, the school and the wall are all wished-in-place at the beginning of the analysis. The wall, differently from what was done for the previous cases, is simulated using a beam element. The properties of the beam element, which is assumed to be equivalent to the "elastic wall" used in the other simulations, can be found in Appendix F.

Stage 1 observations cannot be included in the inverse analysis of this simulation because they refer to the installation of the wall, which is not modeled. Therefore, the construction stages for which the observations can be compared with the computed results are four, from stage 2 to stage 5. Figure 6-21 shows the fit between the measured and computed horizontal displacements for the initial estimates of the input parameters. Note that the inclinometer readings (i.e. observations) were re-zeroed so that the initial set of readings is the one at the end of the wall installation (i.e. stage 1 readings).

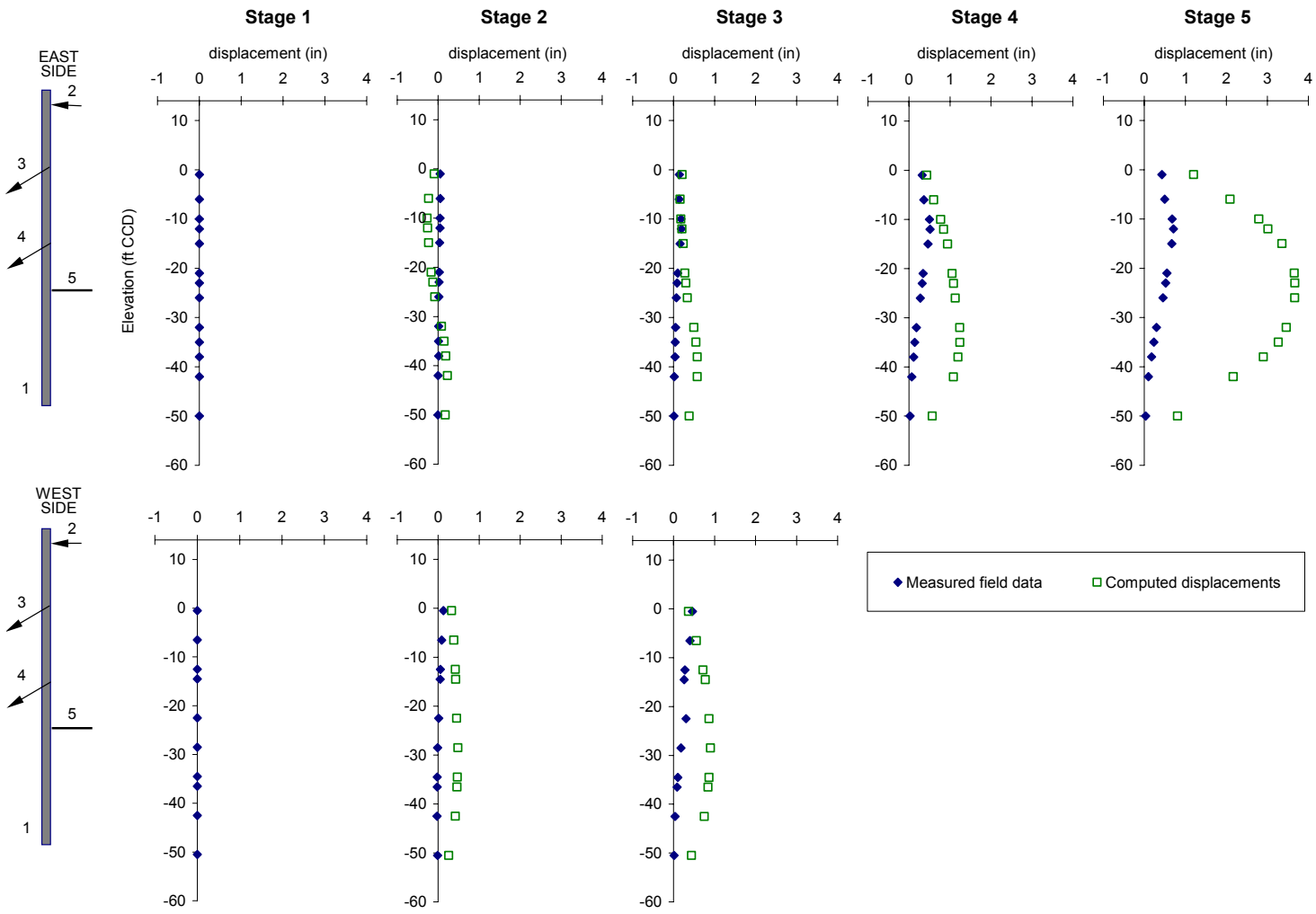

Figure 6-21 Measured vs. computed horizontal displacements for initial estimates of parameters (no-wall case)

Results show a behavior similar to the one observed for the no-school case (see Figure 6-20), in that the computed displacements of the upper clay layers on the east side are, for stage 2, away from the excavation. Figure 6-22 shows the deformed mesh at the end of stage 2. When the first 5 ft of soil are excavated, the pressure acting on the west wall is larger than the pressure acting on the east wall because the initial effective stresses in the upper soil layers on the east side are lower than the stresses on the west side (the school is wished-in-place). Therefore, given that, in this step, the clay layers are undrained (i.e. no volume changes occur), the soil on the east side moves away from the excavation.

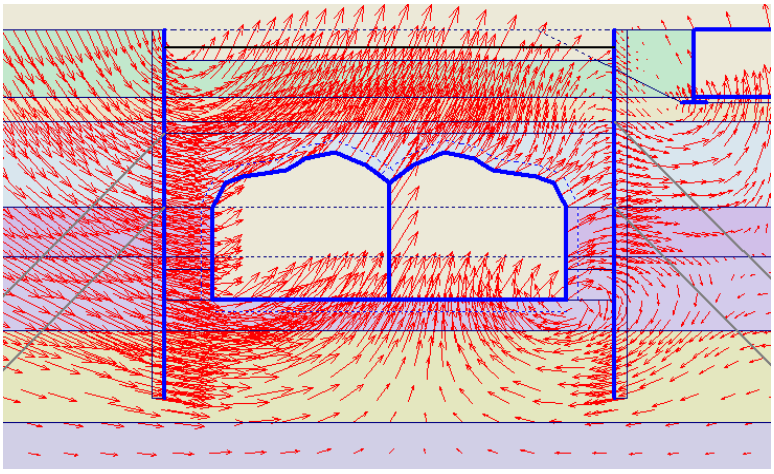

Figure 6-22 Deformed mesh (scaled 50 times) at the end of construction stage 2

Similarly to what happened for the no-school case, the model could not be successfully calibrated using only the observations from early construction stages. Figure 6-23 shows the comparison between the measured data and the computed results when all observations (i.e. stage 2 to stage 5) are used in the regression analysis.

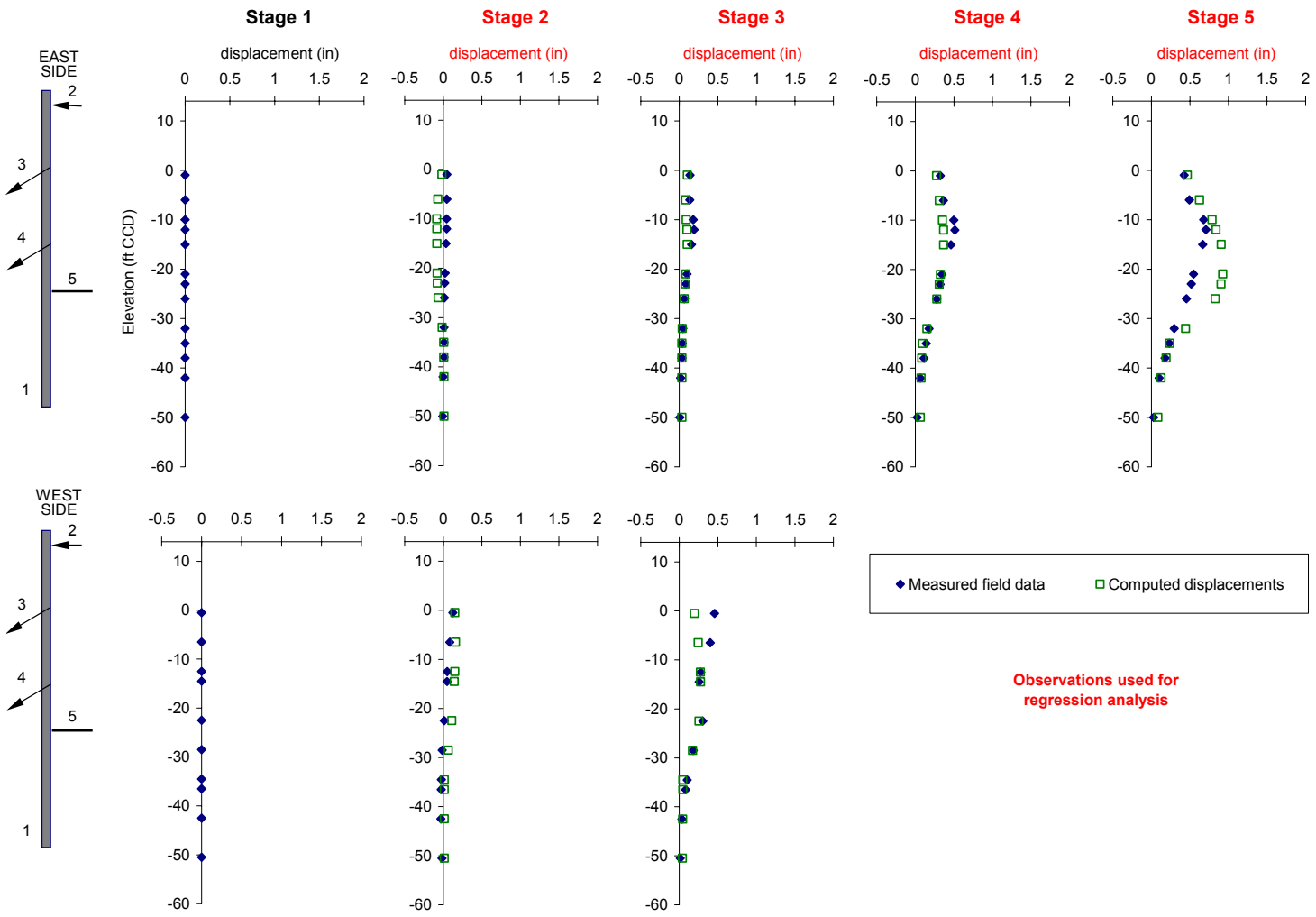

Figure 6-23 Measured vs. computed horizontal displacements: parameters optimized based on all observations (no-wall case)

Results of the final calibrated model fit the measured data relatively well. They clearly overpredict the final observed displacements, yet they satisfactorily capture the behavior of the soil for stages 2, 3 and 4. However, similarly to what happened for the no-school case, the final estimates of the parameters calibrated by inverse analysis are unrealistic. Table 6-11 shows the best-fit values of the three input parameters optimized. The value of parameter E_1 is larger than E_3 and the estimate of E_4 is about twenty times the best-fit value of E_4 for the base-case.

	$E_{1/2}$ (psf)	E_3 (psf)	E_4 (psf)
Final (no-wall)	18440	7850	1060000

Table 6-11 Initial and optimized model parameters at the end of the optimization

Results of this study indicate that the no-wall simulation, like the no-school case, cannot adequately represent the measured response of the soil at the excavation site because the optimal solution yields unrealistic estimates of the input parameters.

6.3.4 Free field conditions (free-field case)

In this simulation (i.e. free-field case) the tunnel and the school are not included in the simulation, while the wall, wished-in-place at the beginning of the analysis, is simulated using a beam element. Figure 6-24 shows the finite element mesh of the model. Note that, for consistency, the generated mesh is the same used for the previous simulations (see Appendix E1.6), where both the tunnel and the school were considered.

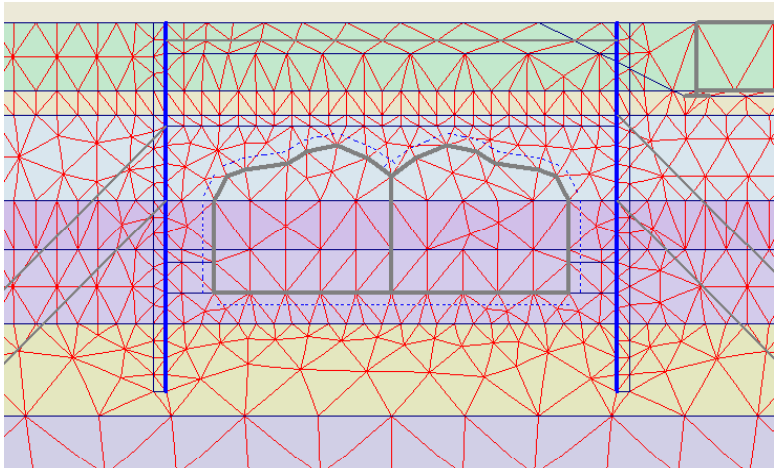

Figure 6-24 Finite element mesh of free-field model

Like for the no-wall case, the observation stages considered for the regression analysis are four (stage 2 to stage 5). Figure 6-25 shows the comparison between measured and computed horizontal displacements for the initial estimates of the input parameters. The comparison shows that the model results match the shape of the measured displacement profiles at every construction stage, yet the model significantly overpredicts the magnitude of the horizontal movements.

Figure 6-26 shows the comparison between measured and computed horizontal displacements at the end of the regression analysis, when all observations are used to calibrate the model. The fit is quite satisfactory, yet not as accurate as the one achieved for the base-case (see Figure 5.19).

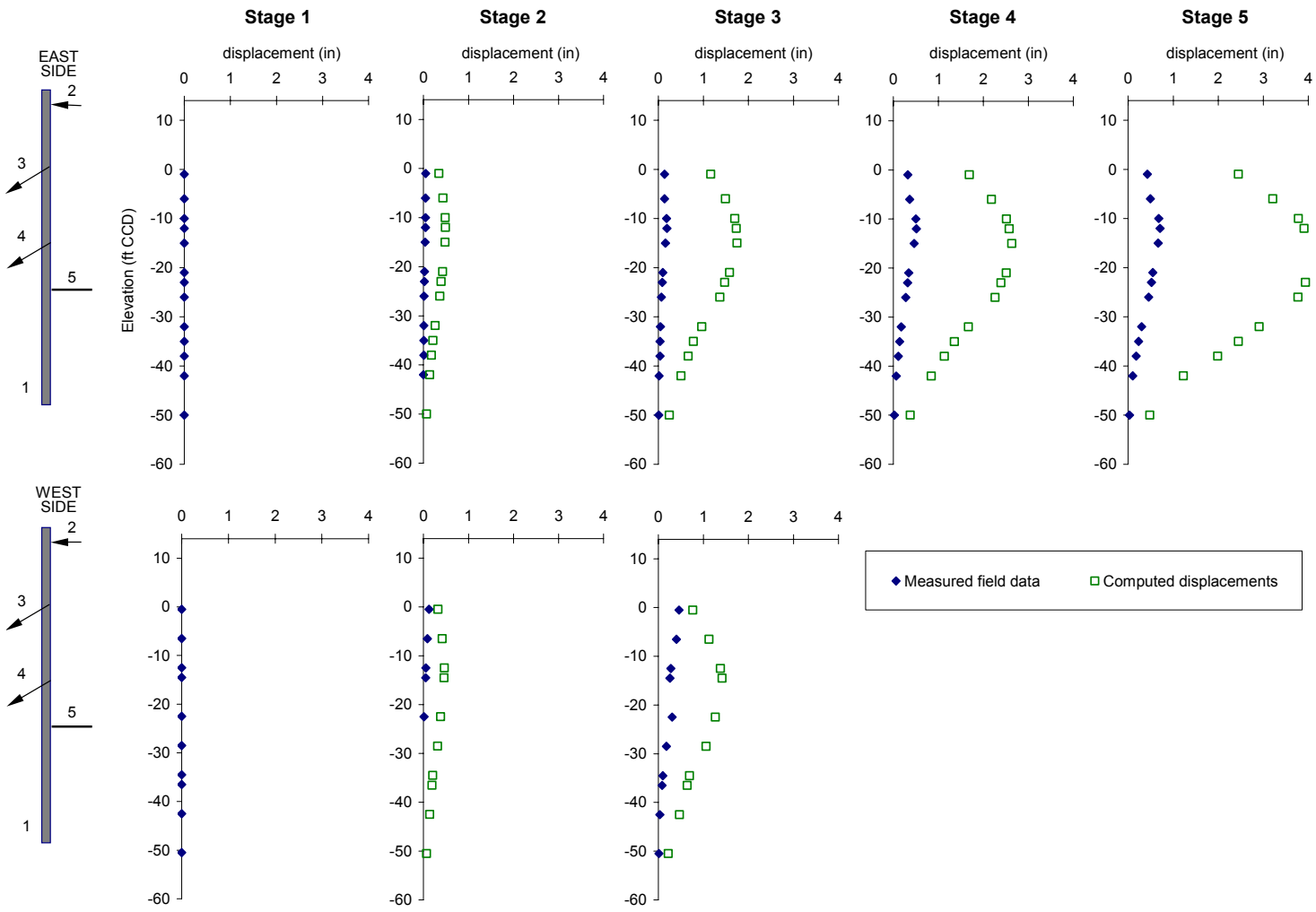

Figure 6-25 Measured vs. computed horizontal displacements for initial estimates of parameters (free-field case)

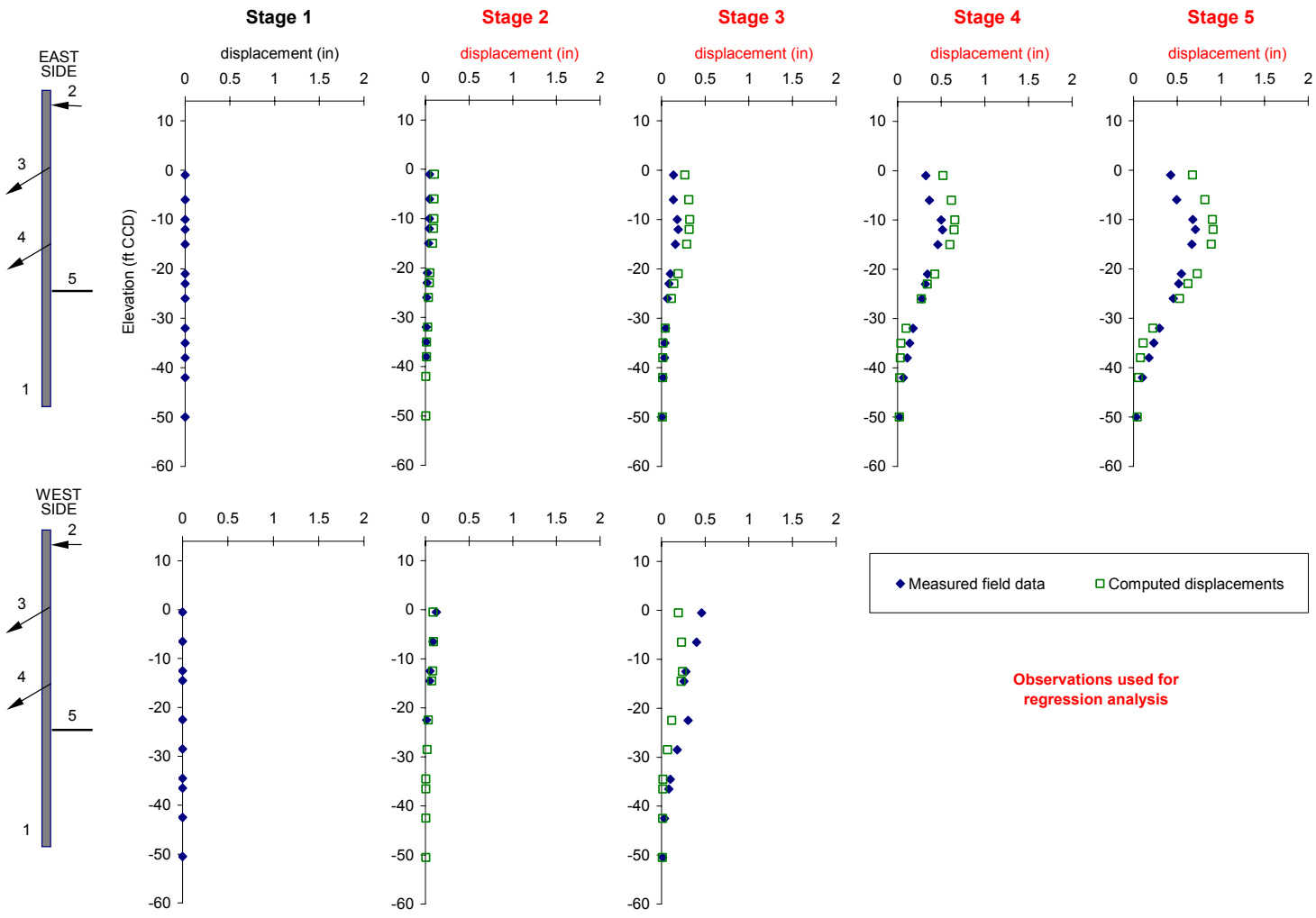

Figure 6-26 Measured vs. computed horizontal displacements: parameters optimized based on all observations (free-field case)

Table 6-12 shows the values of the best-fit model parameters at the end of the optimization. The values of the stiffness parameters are 1 or 2 orders of magnitude higher than the initial estimates of the parameters and significantly higher than the best-fit values of the base-case (see Table 5-13). Figure 6-27 compares, in a dimensionless plot, the parameter estimates of the free-field case and the base-case. Note the optimized estimate of parameter E_4 for the free-field case is more than 10 times the optimal value of E_4 for the base-case.

	$E_{1/2}$ (psf)	E_3 (psf)	E_4 (psf)
Final (free-field)	27780	69030	655260

Table 6-12 Optimized model parameters at the end of the optimization

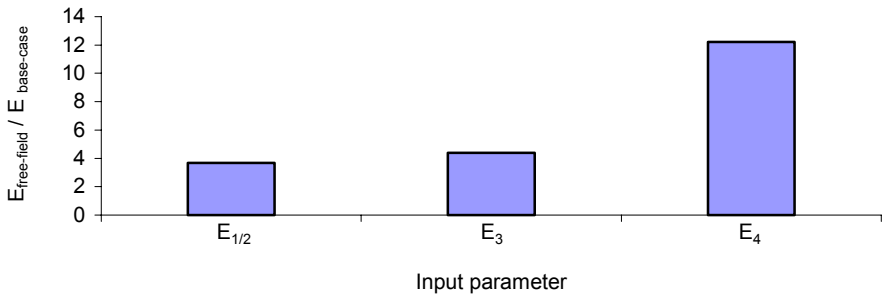

Figure 6-27 Dimensionless comparison between parameter estimates for free-field and base-case

The higher estimates of the optimized stiffness parameters can be explained considering that, in the free-field simulation, (i) the tunnel is not considered, thus the soil mass excavated is larger and the stress relief caused by the excavation is more significant, (ii) the

school is not considered, thus the soil pressure on the east side of the wall is higher, and (iii) the stresses at the start of the excavation are significantly different for the two cases.

6.3.5 Summary on the study on stress history

Results of the simulations discussed in this section showed the importance of "appropriately" considering the stress history of the soil at the excavation site. To accurately predict the movements in the soil around the excavation, one has to explicitly model the construction of the tunnel, the construction of the school and the installation of the secant-pile wall. Table 6-13 shows a summary of the final parameter estimates of the simulations discussed in this section.

	Best-fit parameter estimates (psf)		
Simulation name	$E_{1/2}$	E_3	E_4
Base-case	7550	15670	53610
No-tunnel	8380	31190	49300
No-school	56280	4047	110000
No-wall	18440	7850	1060000
Free-field	27780	69030	655260

Table 6-13 Best-fit parameter estimates of "case history" simulations

In the no-school and no-wall cases the estimate of parameter E_3 is lower than the estimate of $E_{1/2}$. In the free-field case the estimates of all parameters are extremely high. The no-tunnel case is the only simulation, beside the base-case, that produced reasonable parameter

estimates. However, the fit between computed and measured displacements for that simulation (see Figure 6-13) is not as accurate as the final fit of the base-case (see Figure 5-19). Moreover, when the no-tunnel model is calibrated using only observations from stage 1 (see Figure 6-11), the behavior of the soil for the remaining 4 stages is not "predicted" with the same accuracy of the base-case model (see Figure 5-15).

The calibration of the various simulations by inverse analysis also indicated that the convergence of the optimization algorithm to an "optimal solution" does not necessarily mean that the model is satisfactorily calibrated. A geotechnical evaluation of the optimized parameters is always necessary to verify the reliability of the solution. The following criteria must hold for the model to be considered "reliably" calibrated:

1. satisfactory fit between computed and observed results (i.e. errors are within desired and/or accepted accuracy);

2. reasonable values of the calibrated model parameters;

3. model calibration at early construction stages is able to predict the soil behavior at later construction stages.

Some of the simulations discussed in this section satisfy some of the above-specified criteria, but only the base-case simulation satisfies all of them.

6.4 OBSERVATIONS USED IN REGRESSION

Section 3.3.1 showed that the results of the calibration of a model by inverse analysis are affected, at times significantly, by the number and type of observations used in the regression. This section presents the results of a study on the type of observations used for the inverse analysis of the Chicago & State excavation problem.

In the base-case the observations used to define the regression analysis were retrieved from inclinometer readings on the two sides of the excavation at five different construction stages. The total number of observations used was 98 (see section 5.3.3.1). Settlement data, which were surveyed at various locations on the school adjacent to the excavation (see section 5.3.1), were not used as observations. For the simulations that will be presented in this section vertical displacements will be used as observations and their effect on the results of the analysis will be evaluated. Table 6-14 shows the names of the simulations and indicates whether horizontal and/or vertical observations are used.

	Observations used	
Simulation name	Horizontal displ.	Vertical displ.
base-case	yes	no
v-only	no	yes
v-h	yes	yes

Table 6-14 Simulations for study on type of observations used in the regression analysis

Figure 6-28 shows the location of the vertical observation points relative to the secant-pile wall and the school. Six observations per construction stage are used in the regression (30 total). Note that the settlement data in the figure are computed at the elevation of the school's foundations (+2ft CCD). The values and the weight of the vertical displacements used as observations can be found in Appendix F.

Figure 6-29 shows the comparison between computed vertical displacements and measured settlements for the initial estimates of the input parameters. Computed results (i) significantly overpredict the extent of the settlement trough (i.e. the magnitude of the vertical displacements away from the excavation), and (ii) predict heave during the installation of the wall (i.e. stage 1) up to 5-10 ft away from it.

In Figures 6-28, 6-29 and 6-30, the comparisons between computed and measured settlements are plotted for the base-case, the v-only case and the v-h case, respectively, and refers to the best-fit estimates of the parameters. Note that the optimization of the parameters by inverse analysis improves the results of all three simulations, especially at distances greater than 35 ft from the edge of the excavation.

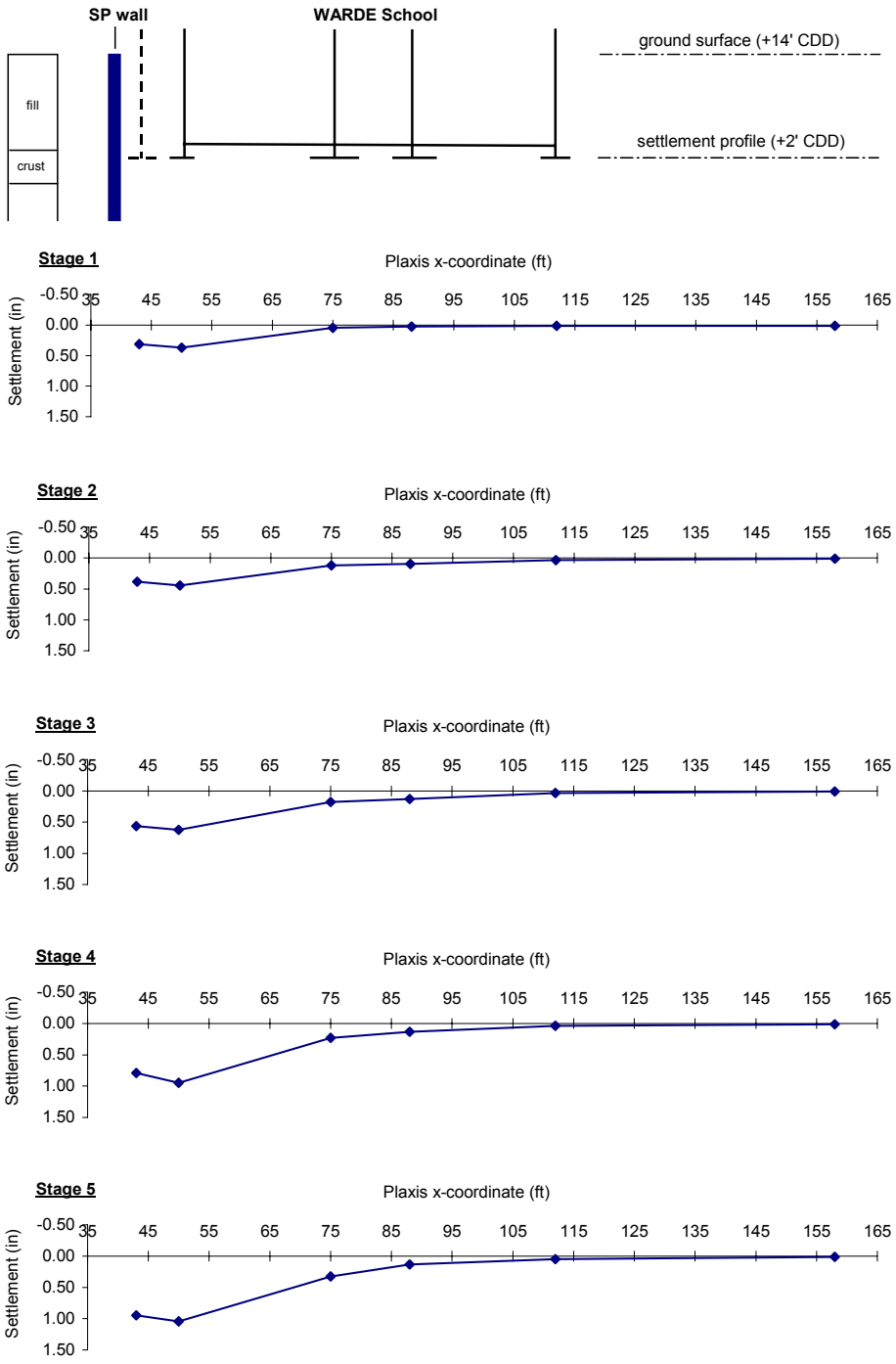

Figure 6-28 Settlement readings used as observations

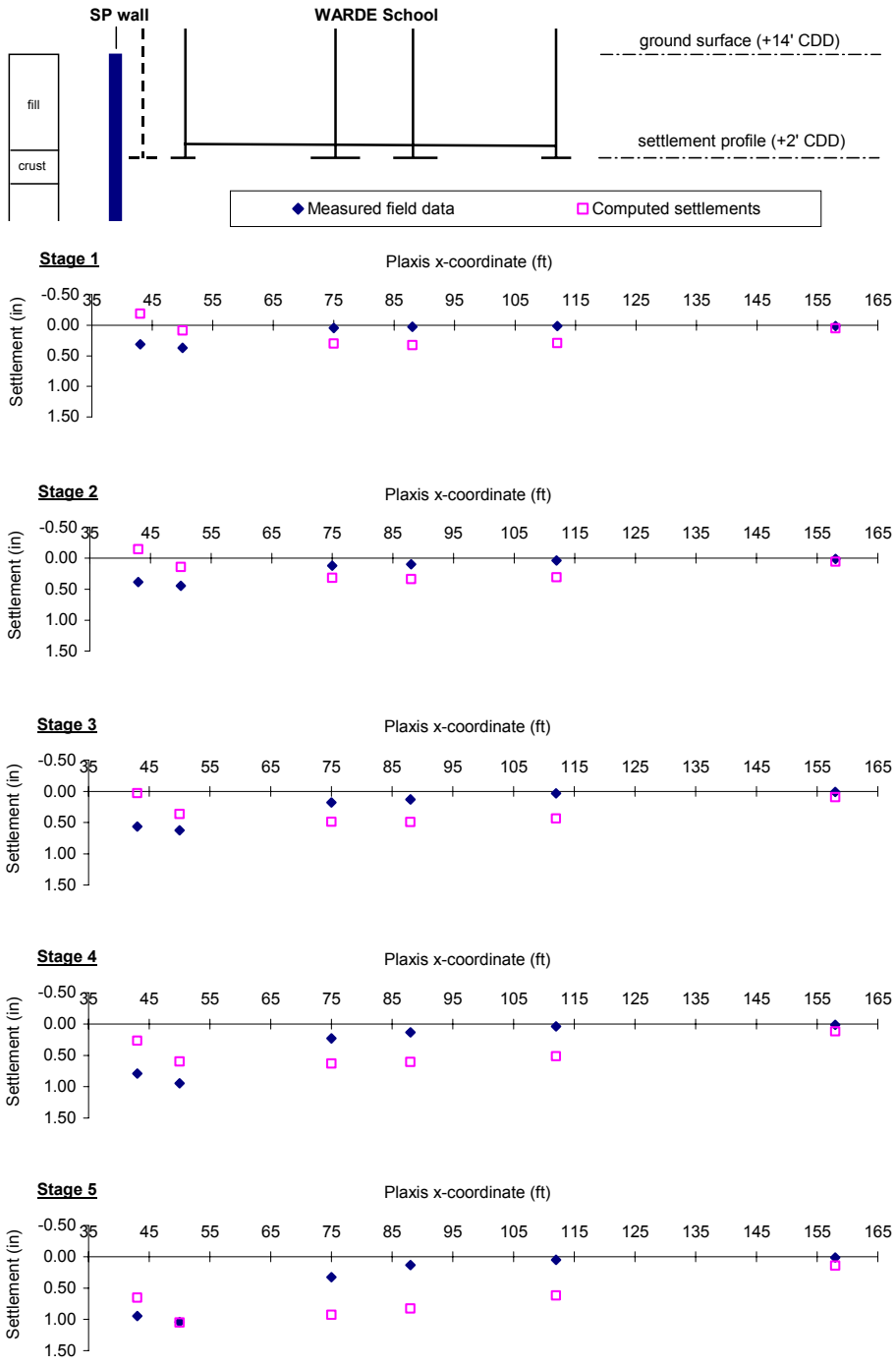

Figure 6-29 Measured vs. computed vertical displacements: initial estimates of input parameters

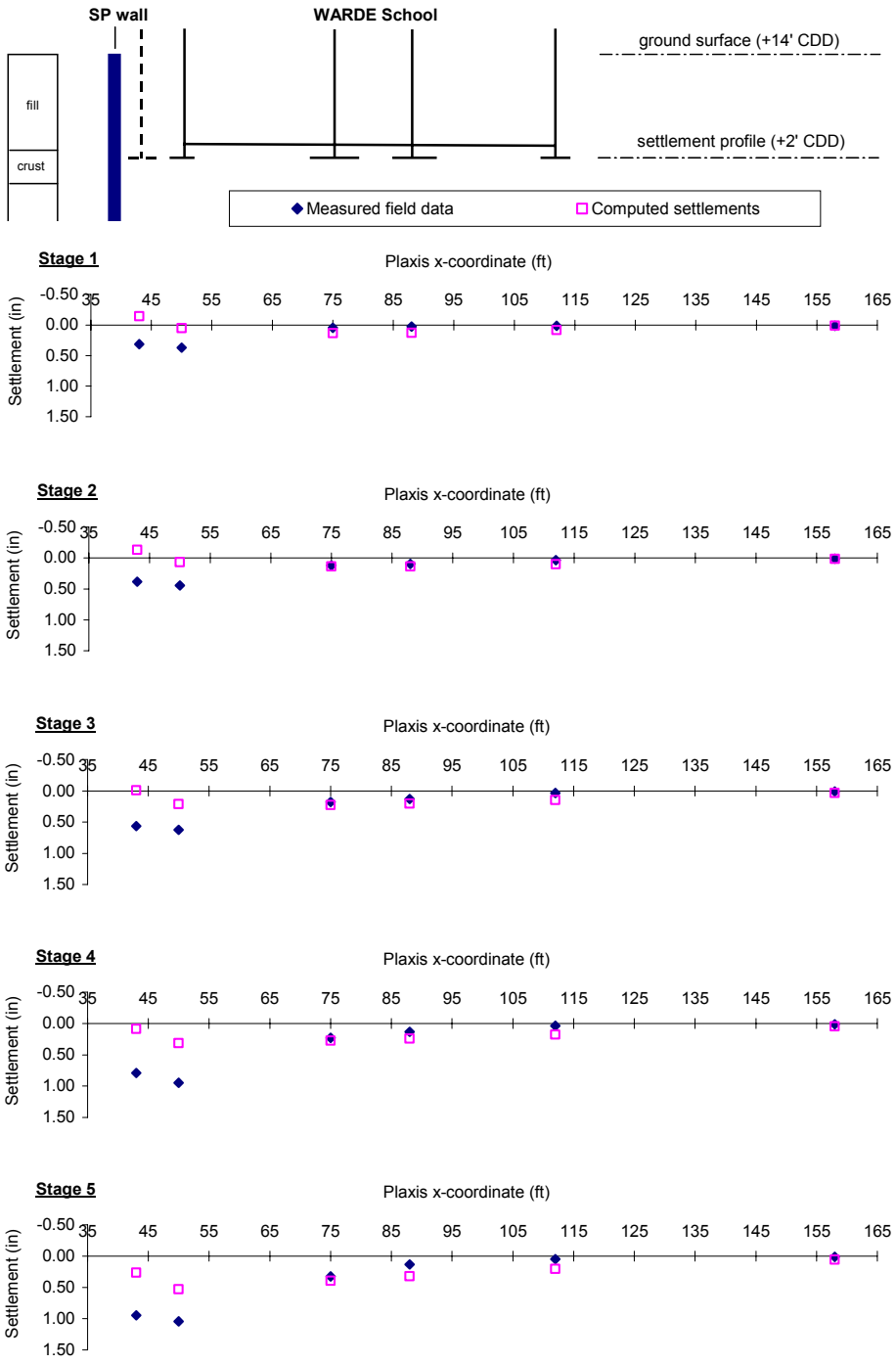

Figure 6-30 Measured vs. computed vertical displacements: final estimates of parameters for base-case

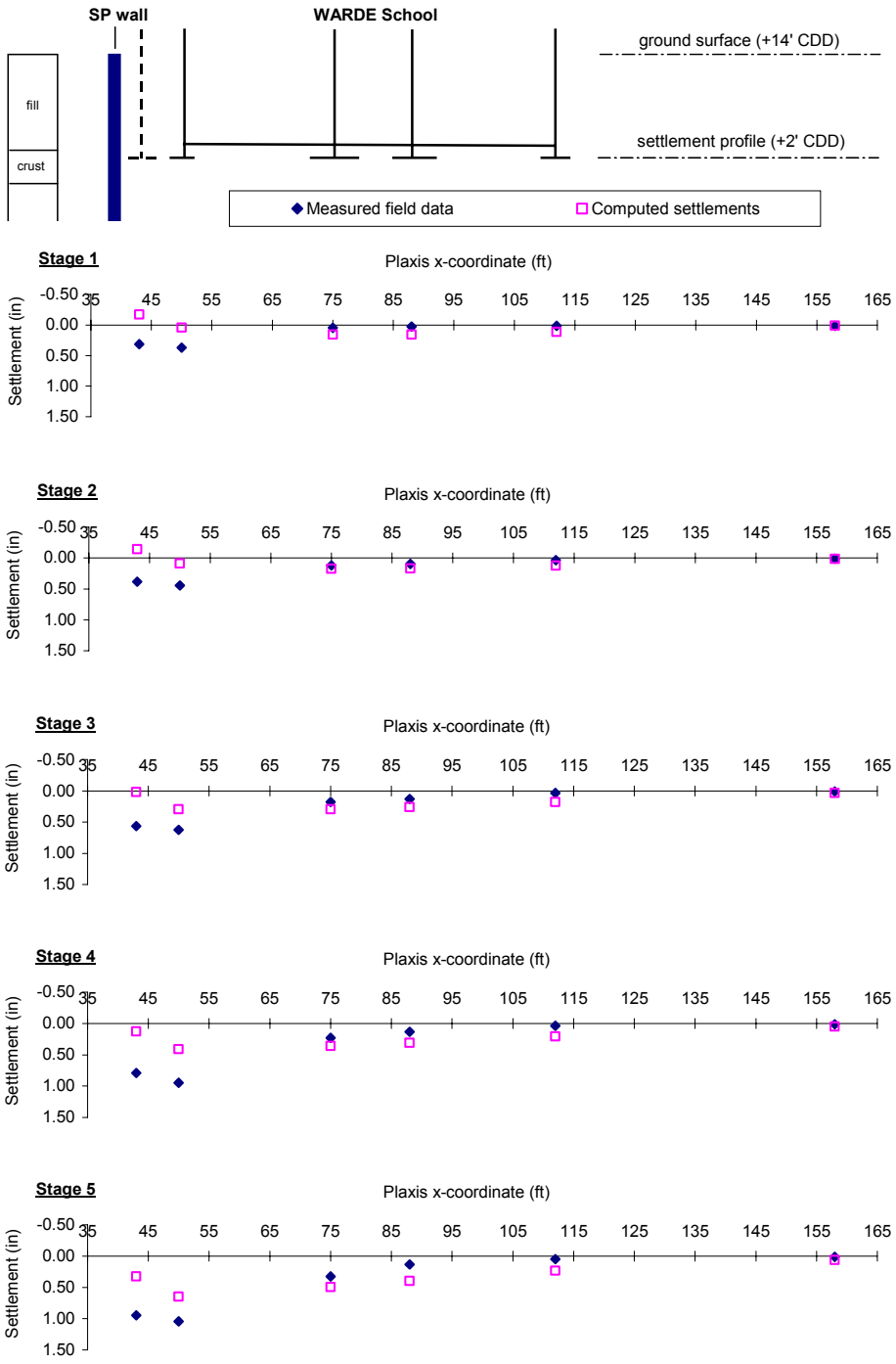

Figure 6-31 Measured vs. computed vertical displacements: final estimates of parameters for v-only case

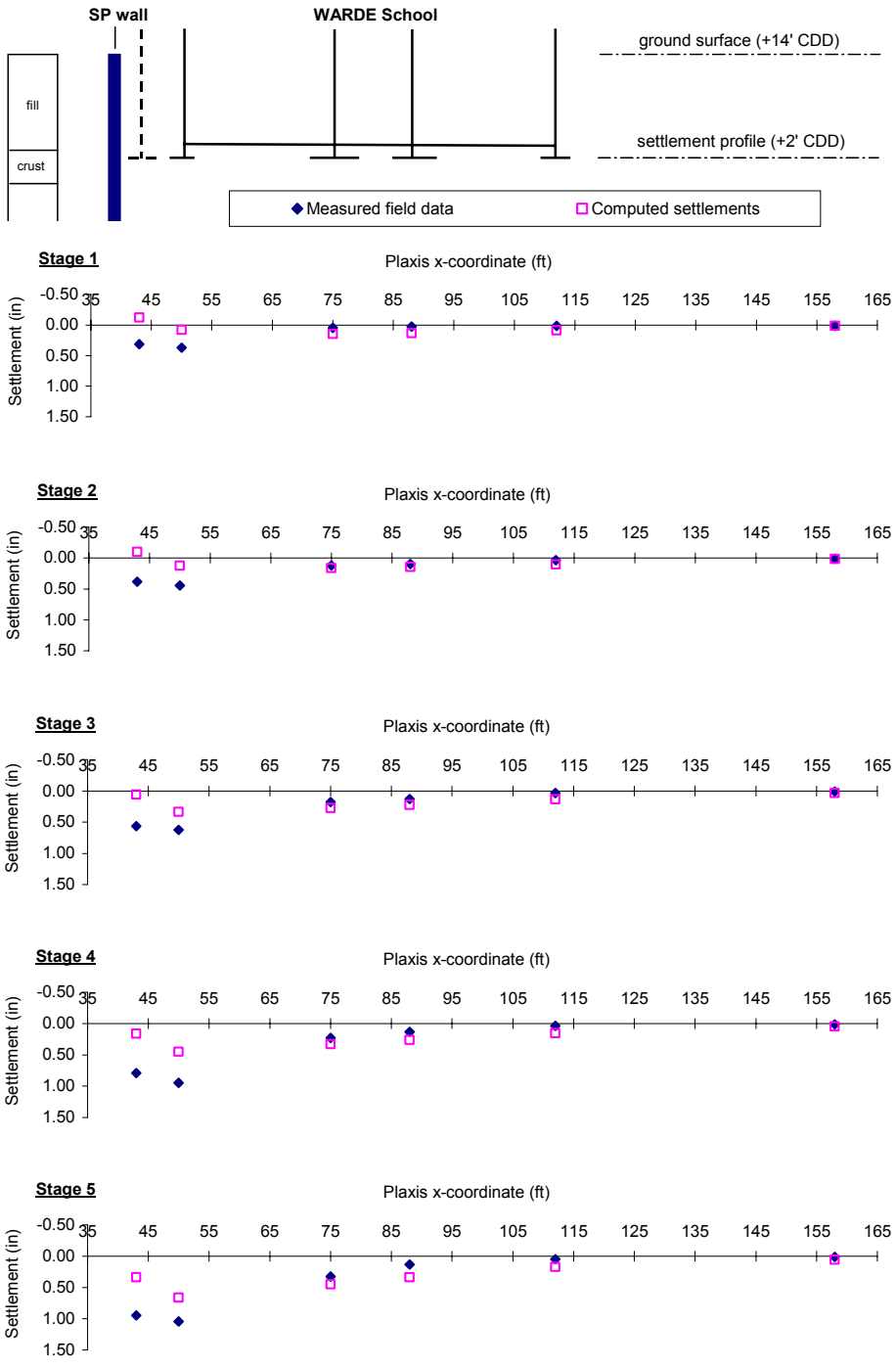

Figure 6-32 Measured vs. computed vertical displacements: final estimates of parameters for v-h case

In Figure 6-33 the area of the computed settlement troughs is compared with the area of the trough calculated from the measured observations (the areas are computed assuming a linear behavior between consecutive settlement points). Results show that the initial fit between the measured data and the computed results is poor at all construction stages, whereas the fit between the field data and the results of all three calibrated models is always satisfactory.

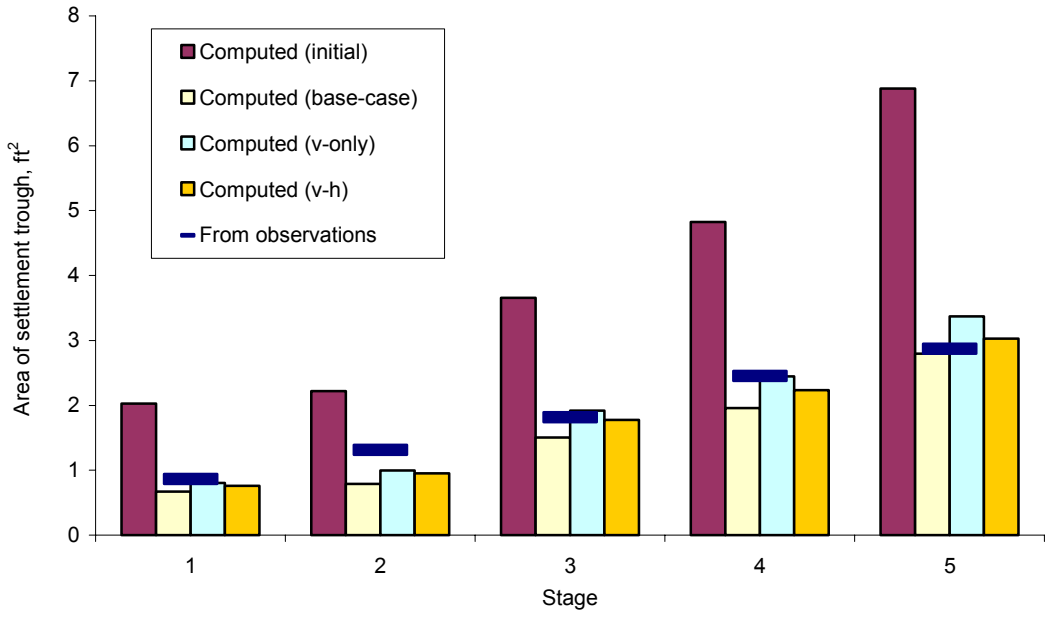

Figure 6-33 Comparison between computed and observed areas of settlement throughs

Figures 6-32 and 6-33 show the visual fit between measured and computed horizontal displacements for the v-only case and the v-h case, respectively. The fit is not as accurate as the one relative to the base-case (see Figure 5-19).

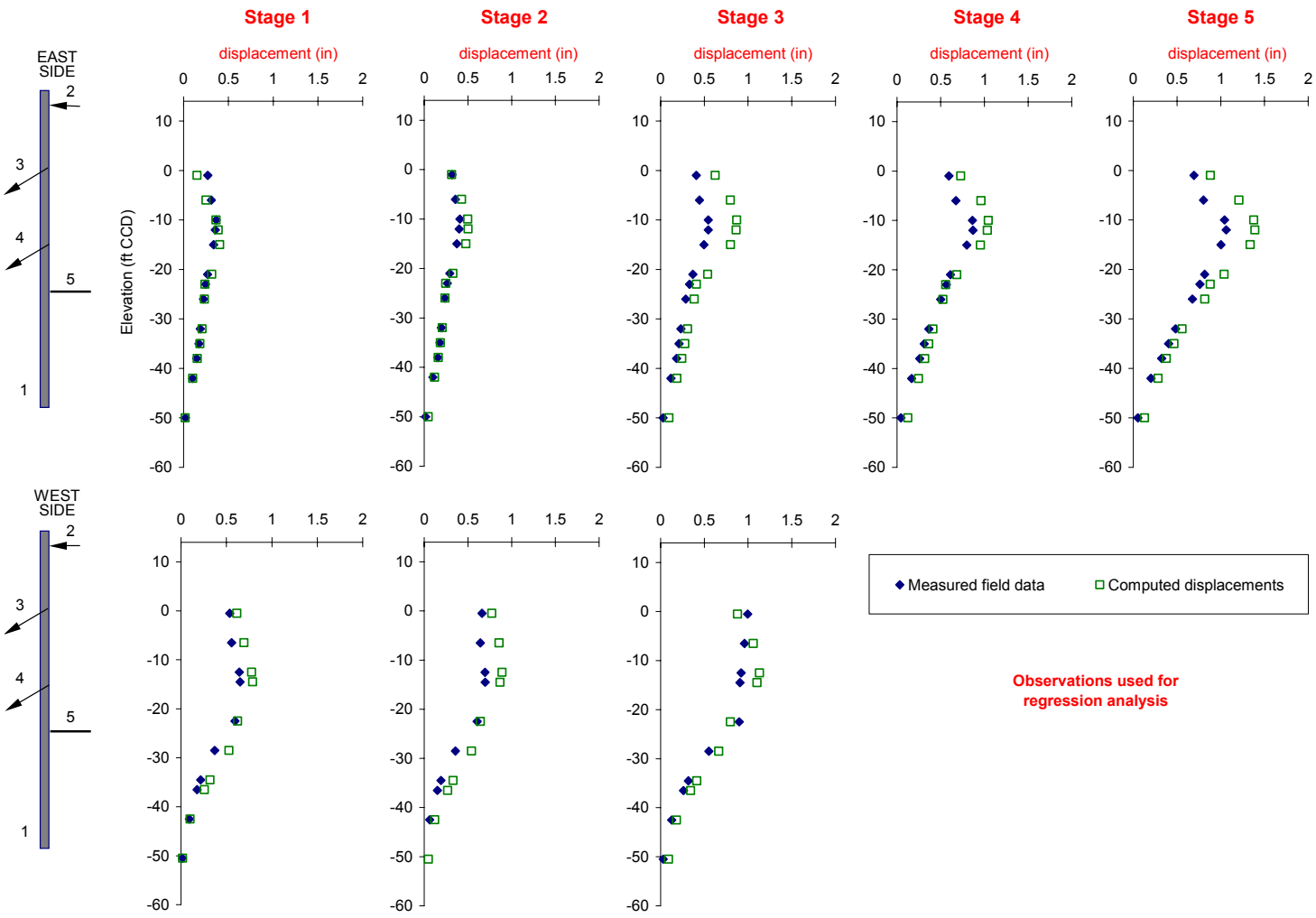

Figure 6-34 Measured vs. computed horizontal displacements for v-only case

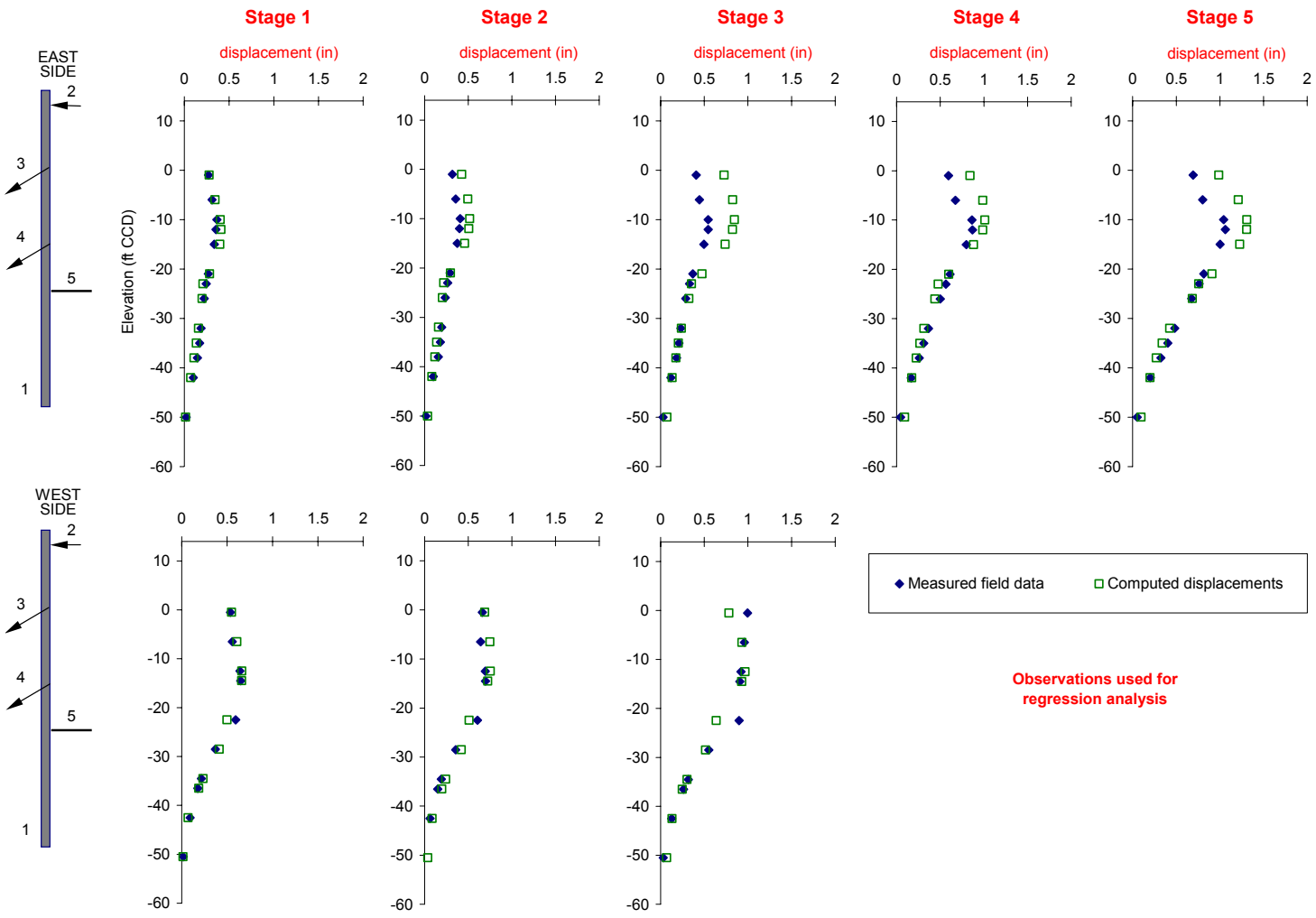

Figure 6-35 Measured vs. computed horizontal displacements for v-h case

The optimized parameter values for the three simulations are shown in Table 6-15. Note that the optimization yields three different but reasonable sets of parameter estimates.

	Best-fit parameter estimates (psf)		
Simulation name	$E_{1/2}$	E_3	E_4
Base-case	7550	15670	53610
v-only	4055	19810	34616
v-h	5133	23800	55506

Table 6-15 Best-fit parameter estimates and global objective function values

Results of this study show that the accuracy of the fit between computed and measured displacements is similar in all three simulations. In all three cases the total volume of soil settling underneath the school is predicted quite accurately, yet the vertical movements are always underpredicted close to the wall and overpredicted away from the wall. This indicates that using vertical observations (v-only and v-h cases) does not improve the calibrated model "ability" to predict the settlements induced by the excavation. Instead, it worsens the prediction of horizontal displacements on the sides of the excavation because (i) in the v-only case the horizontal displacements are not included as observations in the regression, and (ii) in the v-h case the overall weight of the horizontal observations is lowered by the presence of the vertical observations. In the latter case, the objective function includes "error contributions" from both horizontal and vertical displacements. Thus, the best-fit model is a result of the minimization of all errors, whereas the base-case optimized model minimizes the errors relative to the horizontal displacements only.

6.5 SUMMARY

This chapter presented the results of a number of studies evaluating the effect of various "modeling assumptions" on the inverse analysis of the Chicago and State excavation case study. The modeling variables considered in the studies were: (i) soil models and input parameters, (ii) stress history of the soil, and (iii) observations. Results of the various simulations discussed in this chapter were always compared to the results of the simulation discussed in Chapter 5 (i.e. base-case).

The study on the soil models and input parameters showed that a simple soil model (e.g., Mohr-Coulomb) could be successfully calibrated by inverse analysis to give a reasonably good fit between measured and computed horizontal displacements. Yet, it is necessary to model the clay layers using a more advanced plastic model (e.g., Hardening-Soil) to effectively update the design predictions based on data from early construction stages. For the latter case the base-case parameterization proved to be the best inverse analysis alternative.

The study on the stress history of the soil showed that correct modeling of the pre-excavation activities is crucial for the definition of a finite element problem that can accurately predict the horizontal movements of the soil around the excavation. Indeed, when the construction of the tunnel, the school and/or the wall was not modeled (i.e. the structures were either not considered or wished-in-place), the simulations could never be satisfactorily calibrated.

The study on the observations showed that the calibrated finite element model of the excavation can accurately predict the horizontal displacements of the soil around the excavation, yet it cannot predict the measured vertical movements with the same accuracy. Using vertical observations to calibrate the model worsen the analysis' results. This suggests that if a model is not able to predict an observed behavior (e.g., excavation induced settlements), the corresponding observations should not be included in the regression analysis.

Results of all studies showed that inverse analysis, posed as a parameter optimization problem, is very effective in minimizing the objective function of a given simulation, yet if the problem is not "well posed" the analysis, even when converging, yields unreasonable results.

7 SUMMARY AND CONCLUSIONS

7.1 SUMMARY

In this work inverse modeling techniques were used to optimize the calibration of soil models based on laboratory test results and field data. The model calibration by inverse analysis was conducted using UCODE, an optimization algorithm that works with any application software that can be executed in batch mode. UCODE was used in conjunction with the FE codes JFEST (chapters 3 and 4) and PLAXIS (chapters 4, 5 and 6) to calibrate different soil models from various data sets.

Chapter 2 introduced the concepts of inverse modeling and discussed of the possible uses of inverse analysis for geotechnical engineering purposes. The non-linear regression algorithm employed in UCODE (i.e. modified Gauss-Newton method) was presented in detail and various model fit and parameter statistics, generated during the regression, were introduced.

In Chapter 3 the input parameters of the Modified Cam-Clay model were optimized based on triaxial results from drained and undrained compression tests. Calibration by inverse modeling proved more effective than conventional estimation methods and the optimized values of the model input parameters yielded an extremely good fit between computed and experimental stress-strain data. Parametric studies were conducted on regression variables to evaluate their effect on the optimization results.

In Chapter 4 the results of triaxial tests on Chicago clay specimens were used to calibrate, by inverse analysis, four different soil models: the Duncan-Chang model, the Modified Cam-Clay model, the Anisotropic Modified Cam-Clay model, and the Hardening-Soil model. The laboratory data used for the calibration of the models referred to samples from four layers of compressible Chicago glacial clays: the Upper Blodgett, Lower Blodgett, Deerfield and Park Ridge layers. All four models were effectively calibrated by inverse analysis based on triaxial test results, yet the goodness of the fit between the experimental data and the computed results varied according to the model's ability to represent the stress-strain response of the soil specimen. The model that best simulated the triaxial compression tests that constituted this data set was the MCC model.

Chapter 5 presented a numerical procedure that improves the state-of-the-practice of controlling ground movements associated with supported excavations. The data set used to develop and test the procedure refers to a 39 ft deep supported excavation through soft clays in Chicago. The optimization of the finite element simulation of the excavation was

achieved through the calibration of five clay layers, all modeled using the Hardening-Soil model. The parameterization of the inverse analysis was based on various considerations, among which: (i) the sensitivity of the results to changes in the value of the parameters, and (ii) the need to define a well-posed inverse analysis problem. Three stiffness parameters per layer were updated during the analysis (and only one was directly optimized in the regression analysis) while the other model parameters were kept constant at their initial value.

Chapter 6 discussed of some of the modeling assumptions that led to the successful calibration of the problem described in Chapter 5. A series of studies evaluated (i) the effect of the model chosen to represent the clay behavior and its parameterization, (ii) the importance of accurately modeling the stress history of the soil at the excavation site, and (iii) the effects of the observations used to evaluate the fit between computed and measured response (i.e. objective function).

A "well-posed" optimization problem is the key to a successful and efficient use of inverse analysis techniques for geotechnical engineering purposes. The three main characteristics of a well-defined inverse analysis problem are:

- Effective numerical modeling. The numerical simulation of a geotechnical project must adequately reproduce the stress history of the soil at the site under study and the soil models used must be able to represent the behavior of the soil under the expected stress conditions. For instance, when, in the inverse analysis of the

Chicago and State excavation, the pre-excavation construction activities are inappropriately modeled, the results of the regression are unreasonable.

- Acceptable parameterization. The characteristics of the model, the expected stress conditions and the type of observations determine the parameters that can be effectively estimated by inverse analysis. For instance, the anisotropic parameters of the AMCC model, x and c, cannot be calibrated using observations from triaxial compression tests. Likewise, of the 10 H-S input parameters only 3, parameters ϕ, E_{50}^{ref} and m, were estimated by inverse analysis using triaxial compression test results.

- Appropriate choice of observations. The number and type of observations must carry enough information for the input parameters to be simultaneously and uniquely estimated by the regression and for the calibrated model to be "predictive" in nature. For instance, the calibration of the MCC model based on observations from drained compression tests does not produce a reasonable estimate of input parameter κ nor predicts the stress-strain response of an undrained test. Whereas, the optimization of the stiffness parameters of the H-S model based on horizontal displacement data from the early construction stages of an excavation positively affect the "predictions" of the soil behavior at all construction stages.

7.2 CONCLUSIONS

The inverse modeling procedure described in this work combines a finite element analysis and a parameter optimization algorithm to efficiently calibrate a soil model by minimizing the errors between experimental observations and model response.

Inverse analysis can be effectively used to calibrate a numerical soil model based on triaxial experimental results. Results of parametric studies conducted on a number of regression variables to evaluate their effect on the calibration of a Modified Cam-Clay model indicate that:

- observations for both drained and undrained tests are needed to successfully calibrate the four MCC input parameters simultaneously;

- an input parameter cannot be estimated if the observations used in the regression are not influenced by its changes;

- when a "reasonably" estimated parameter is excluded from the optimization the MCC model can still be successfully calibrated, whereas, if the initial estimate of a parameter is "unreasonable," changes in other parameters' values cannot compensate for the incorrect estimate;

- a well-posed problem is able to converge to a unique solution, even if the initial estimates of the input parameters are far from their optimal values;

- provided that the observations are "properly" chosen, a relatively low number of them produces the same results as does a large number;

- the weights assigned to the observations greatly influence the results of the optimization and appropriate weighting should include all the observations' uncertainty contributions.

With an inverse analysis procedure, monitoring data recorded at a construction site can be effectively used to control the construction process and, when enough movements occur within the "important" soil strata, predictions of movements can be updated based on the field performance data. The application of the inverse analysis methodology to data from a 39 ft deep excavation through soft clays in Chicago showed that:

- successful recalibration of the model at an early construction stage positively affect subsequent "predictions" of the soil behavior;

- the best-fit values of the stiffness parameters of the clay layers optimized in the analysis are significantly lower than the initial estimates of the parameters, which were based on results from triaxial compression tests;

- the optimized values of the stiffness parameters of a given clay layer can be related to the initial vertical effective stress and to the undrained shear strength of that layer (the optimal stiffness-to-strenght ratios increase with depth);

- the highest changes in parameter values occur at the first optimization stage and the calibrated parameters only need to change slightly at later stages.

A geotechnical evaluation of the results of an inverse analysis is necessary to verify the reliability of the best-fit solution, indeed regression convergence does not necessarily equate to a satisfactorily calibrated model. Results of a number of studies on the "assumptions" used to set up the inverse analysis of the Chicago & State excavation problem indicate that:

- only a well-posed problem is able to effectively minimize the objective function of a simulation while yielding reasonable estimates of the input parameters optimized;

- when the clay layers are modeled using a simple elastic-perfectly plastic model (Mohr-Coulomb) the optimization does not yield results as accurate as the ones achieved when a more advanced elasto-plastic model (Hardening-Soil) is used to represent the clays;

- the stiffness parameters control the soil response to the excavation activities at the Chicago & State project for both the M-C and the H-S model;

- the stress history of the soil at the excavation site must be appropriately modeled to accurately predict the movements in the soil around the excavation;

- using vertical displacements as observations does not improve the calibrated model ability to predict the settlements induced by the excavation.

REFERENCES

Auvinet G., Mellah R and Masrouri F. (2000). Stochastic finite element analyses in geomechanics. Applications of Statistics and Probability, Melchers & Stewart eds., Balkema, p. 79-85.

Bretz J.H. (1939). Geology of the Chicago region, Part I – General. Bulletin 65, Illinois State geological Survey, Urbana, IL.

Brinkgreve R.B.J. and Vermeer P.A. (1998). Finite Element Code for Soil and Rock Analysis. PLAXIS 7.0 manual. Balkema.

Carino C. (1998). Numerical simulation and analysis of structural systems with input uncertainties. Uncertainty modeling and analysis in civil engineering, edited by Ayyub, B.M., CRC Press LLC, p. 275-288.

Caspe M.S. (1966) Surface settlement adjacent to braced open cuts. Journal of the Soil Mechanics and Foundations Division, ASCE, Vol. 92, p. 51-59.

Chung C.K. and Finno R.J. (1992). Influence of Depositional Processes on the Geotechnical Parameters of Chicago Glacial Clays. Engineering Geology, Vol. 32, p. 225-242.

Clough G.W., Smith E.M. and Sweeney B.P. (1989). Movement control of excavation support systems by iterative design. Proceedings, Foundation Engineering: Current Principles and Practices, ASCE, Vol. 2, p. 869-884.

Dennis J.E., Gay D.M. and Welsch R.E. (1981). An adaptive nonlinear least-squares algorithm. ACM transaction on mathematical software, Vol. 7, No. 3, p. 348-368.

Dafalias Y.F. (1986). An anisotropic critical state soil plasticity model. Mechanics research communications, Vol. 13, p. 341-347.

Duncan J.M. and Chang Y-Y (1970). Nonlinear Analysis of Stress and Strain in Soils. Journal of the Soil Mechanics and Foundations Division, ASCE, Vol. 96, p. 1629-1653.

Finno R.J. (1983). Response of cohesive soil to advanced shield tunneling. PhD Thesis, Stanford University, CA.

Finno R.J. and Chung C.K. (1992). Stress-strain-strength responses of compressible Chicago glacial clays. Journal of Geotechnical Engineering, ASCE, Vol. 118, No. 10, p. 1607-1625.

Finno R.J. and Harahap I.S. (1991). Finite element analysis for the HDR-4 excavation. Journal of Geotechnical Engineering, ASCE, Vol. 117, No.8, p. 1045-1064.

Finno R.J., Bryson L.S. and Calvello M. (2002). Performance of a stiff support system in soft clay. Journal of Geotechnical and Geoenvironmental Engineering, ASCE, Vol. 128, No. 8, p. 660-671.

Focht, J.A. Jr and O'Neill. M.W. (1994). Lessons learned from missed predictions. Journal of Geotechnical Engineering, ASCE, Vol. 120, No. 10, p. 1653-1683.

Hill M.C. (1994). Five computer programs for testing weighted residuals and calculating linear confidence and prediction intervals on results from the ground-water parameter estimation computer program MODFLOWP. U.S. Goelogical Survey open-file report 93-481, 81pp.

Hill M.C. (1998). Methods and guidelines for effective model calibration. U.S. Geological Survey Water-Resources investigations report 98-4005, 90 pp.

Hill M.C., Cooley R.L. and Pollock D.W. (1998). A controlled experiment in ground-water flow model calibration using nonlinear regression. Ground Water, Vol. 36, p. 520-535.

Hsien P.G. and Ou C.Y. (1998). Shape of ground surface settlement profiles caused by excavation. Canadian Geotechnical Journal, Vol. 35, p. 1004-1017.

Jahangir M. (1997). Optimal groundwater management and inverse analysis using genetic algorithm and artificial neural network. PhD Thesis, Utah State University, Dept. of Civil and Environmental Engineering.

Keidser, Allen and Dan Rosjberg (1991). A comparison of four inverse approaches to groundwater flow and transport parameter identification, Water Resources Research, v. 27, no. 9, p. 2219-2232.

Kulhawy F.H. and Phoon K.K (1996). Engineering judgment in the evolution from deterministic to reliability-based foundation design. Proceeding of Uncertainty '96. Uncertainty in the geologic environment: from theory to practice, ASCE, Geotechnical special publication No. 58, pp 29-48.

Lambe T.W. and Whitman R.V. (1969). Soil mechanics. John Wiley and Sons. New York.

Morgenstern N. (1995). Managing risk in geotechnical engineering. Proc. 10th Pan American Conference on Soil Mechanics and Foundation Engineering, Vol. 4.

Otto G.H. (1942). An interpretation of the glacial stratigraphy of the city of Chicago. PhD Thesis, University of Chicago, Chicago, IL.

Ou C.Y. and Tang Y.G. (1994). Soil parameter determination for deep excavation analysis by optimization. Journal of the Chinise Institute of Engineers, Vol. 17, No.5, p. 671-688

Papalambros, P.Y. and Wilde, D.J. (1988). Principals of optimal design. Modeling and computations, Cambridge University Press, 416 p.

Peck R.B. (1969). Deep excavations and tunneling in soft ground. Proceedings 7th International Conference on Soil Mechanics and Foundation Engineering, State-of-the-Art Volume, p. 225-290.

Peck R.B. and Reed W.C. (1954). Engineering properties of Chicago subsoils. Bulletin No. 423, Engineering Experiment Station, University of Illinois, Urbana, IL.

Poeter E.P. and Hill M.C. (1998). Documentation of UCODE, a computer code for universal inverse modeling. U.S. Geological Survey Water-Resources investigations report 98-4080, 116 pp.

Poeter EP and Hill M.C. (1997). Inverse Methods: A Necessary Next Step in Groundwater Modeling, Ground Water, v. 35, no. 2, p. 250-260.

Roboski J. (2001). Soil Parameters for Constitutive Models of Compressible Chicago Glacial Clays. MS Thesis, Northwestern University, Evanston, IL.

Schanz T., Vermeer P.A. and Bonnier P.G. (1999). The Hardening Soil model - formulation and verification. Proceedings Plaxis Symposium "Beyond 2000 in Computational Geotechnics", Amsterdam, Balkema, p. 281-296.

Schweiger H.F. (1998). Results from two geotechnical benchmark problems. Proc. 4th Eur. Conf. on numerical methods in geotechnical engineering, NUMGE98, p. 645-654.

Terzaghi K. (1942). Shield tunnels of the Chicago subway. Journal of the Boston Society of Civil Engineers, Vol. 29, p. 163-209.

Terzaghi K. (1943). Liner-plate tunnels on the Chicago (Ill.) subway. Trans. ASCE, 108, p. 970-1007.

Viggiani G. and Atkinson J. (1995). Stiffness of fine grained soils at very small strains. Geotechnique, Vol. 45, p. 249-265.

Withman R.V. (1996). Organizing and evaluating uncertainty in geotechnical engineering. Proceeding of Uncertainty '96. Uncertainty in the geologic environment: from theory to practice, ASCE, Geotechnical special publication No. 58, p. 1-28.

Zentar R., Hicher P.Y. and Moulin G. (2001). Identification of soil parameters by inverse analysis. Computers and Geotechnics, Vol. 28, p. 129-144.